UNIVERSITAT POLITÈCNICA DE CATALUNYA BARCELONATECH

Evaluation of TH multi-scale coupling methods in BEPU analysis

by
Max Casamor Vidal

UNIVERSITAT POLITÈCNICA
DE CATALUNYA
BARCELONATECH

PhD Program in Nuclear and Ionizing Radiation Engineering

Evaluation of TH Multi-Scale Coupling Methods in BEPU Analysis

Doctoral thesis by:

Max Casamor Vidal

Thesis advisors:

Dr. Jordi Freixa Terradas

Dr. Francesc Reventós Puigjaner

Departament de Física

UPC - Universitat Politècnica de Catalunya

A thesis submitted for the degree of *Doctor* by the UPC

Barcelona, September 5, 2022

A la meva família i amics

ABSTRACT

The combined use of thermal-hydraulics system and sub-channel codes (TH-TH coupling) in transient analysis provides an integrated tool with the capability of modelling in detail both the core thermal-hydraulic conditions and the system behaviour. Different code coupling methods are often used in the nuclear industry to provide accuracy to the calculations while maintaining a sufficient degree of user accessibility. In some cases, and for specific scenarios, the coupling method can be simplified to the off-line transfer of the boundary conditions from plant models run by system codes to sub-channel codes (off-line coupling).

The off-line coupling approach has been considered valid to evaluate the safety margins for limiting parameters such as the minimum departure from nucleate boiling ratio, which relates the local power with the critical heat flux. The off-line coupling is fast and sufficiently accurate in most situations, however, boundary conditions at the inlet and the outlet of both solutions will present miss-matchings. In order to overcome the inconsistencies between system and sub-channel codes, advanced on-line coupling methods may be applied (e.g. semi-implicit coupling). These are methods that imply coherent boundary conditions between codes in all domain and are significantly more complex in mathematical terms. The selection of an appropriate coupling method between system and sub-channel codes is crucial. Recent sensitivity studies performed in sub-channel codes have shown a strong influence of the boundary condition's uncertainty on the major figures of merit.

The present study aims to evaluate the implications of the coupling methods in safety analysis evaluations in two transients with strong system effects. For this purpose, CTF (sub-channel code) and RELAP5 (system code) are coupled using two coupling techniques: the off-line coupling, where the boundary conditions are obtained from the RELAP5 model and imposed by table to CTF, and the semi-implicit coupling method, which has been applied to couple CTF and RELAP5, implementing the semi-implicit coupling methodology developed by Weaver in 2002.

The selected cases for the study are a complete loss of reactor coolant system forced flow and a pressurizer relief valve opening. The models used are, on one hand, a RELAP5 plant model that consists of a full plant model of a generic Westinghouse 3-loop nuclear power plant. On the other hand, a hybrid assembly sub-channel CTF core model has been developed using the same reference data as the RELAP5 model.

In recent years, the application of Best-Estimate Plus Uncertainty (BEPU) calculations has gained importance in the scientific community. This method, far from adding conservatism by forcing non-physical conditions to the calculations, tries to take the uncertainties of the calculations into the process. This is achieved by considering sources of uncertainty of the calculations that have an impact on results due to several causes: modelling inconsistencies, boundary conditions applied, or uncertainties of the physical models implemented in the code.

The BEPU method used in the present study is the GRS BEPU method, which implements Wilks' method using order statistics. This method permits the evaluation of the uncertainty of a scalar parameter with a limited number of runs regardless of the number of input parameters. Also, it allows the evaluation of sensitivity measures of the importance of input parameters deviation to the uncertainty of the results. One of the possible methods of such evaluation is the use of rank correlation coefficients.

BEPU analysis can be considered an additional tool for coupling methods comparisons. Results show that base cases and sensitivity analysis present good agreement between the coupling methods with some minor discrepancies. For the first case, the Spearman's rank correlation coefficients and distributions of the BEPU analysis present similar results for the two approaches. On the contrary, the second case shows differences in the evaluation of the figures of merit, which can be explained and correlated to the boundary conditions deviations between codes. This suggests that non-imposed

boundary condition values for the off-line coupling method is an important issue to take into account when applying this type of method for system-dependent transients that are extended in time.

PREFACE

The idea of obtaining a tool capable of performing core and system TH calculations with a great degree of detail came out when the UPC-ANT group had the possibility of using CTF provided by the Reactor Dynamics and Fuel Modeling Group (RDFMG) at North Carolina State University (NCSU). During the process of coupling CTF and RELAP5 using the semi-implicit method, the idea of performing a comparison on how the codes would perform by using the coupled code or the off-line approach (by table) came out.

The application of the off-line coupling approach is and has been considered valid to evaluate the safety margins for limiting parameters such as the minimum departure from nucleate boiling ratio (MDNBR), still assuming a certain degree of inconsistencies at the coupling boundaries between the system and the sub-channel codes. The present study aims to evaluate the differences among standard practices when coupling TH-TH codes by using a combination (coupling) of system codes and sub-channel codes. For this purpose, the system code RELAP5, developed by the Idaho National Laboratory (INL) has been coupled with CTF, a sub-channel thermal-hydraulics code developed and improved by the RDFMG at the North Carolina State University (NCSU).

ACKNOWLEDGMENTS

This PhD Thesis is the result of the efforts carried out by many people and the support received by many institutions. The coupling of CTF and RELAP5 TH codes has permitted the development of a tool capable of performing core system calculations with a great degree of detail. Also, it has permitted to carry out an evaluation of the differences in off-line and semi-implicit coupling methods to MDNBR. Not only the work performed but to learning the codes coding has been very important during this period.

First, I would like to thank the UPC and the Advanced Nuclear Technologies (UPC-ANT) group for letting me join the PhD program. Special thanks to Jordi Freixa and Francesc Reventós, who supervised the Thesis, for the guidance throughout this process and for letting me the opportunity to join other TH related projects. Also, this thesis would have not been possible without the help of UPC members: Lluís, Carme, Victor, Marina, Raimon, Kevin, Dani, Abdulrahman, Elisabet and Patricia.

I would like to thank the CSN to fund the research as well as to provide useful technical guidance, with special appreciation to Rafael Mendizábal and Miguel Sánchez-Perea. It is also worth mentioning the help of Chris Allison for providing helpful comments on code development, and also Tecnatom S.A. and the Associació Nuclear Ascó Vandellós II (ANAV), where learning the PWR NPP technology and operations has provided with useful knowledge applied in this Thesis.

I would also like to express gratitude to the CTF code development and maintenance team at North Carolina State University (NCSU), where thanks to the efforts of the Re-

actor Dynamics and Fuel Modeling Group (RDFMG) I could stay at NCSU and learn the basics of CTF programming. In particular, I would like to thank Maria Avramova and Kostadin Ivanov, and to recognize the help provided by the rest of the group: Taylor, Mario and Agustín as well as the NCSU staff.

CONTENTS

LIST OF TABLES

LIST OF FIGURES

ACRONYMS

ACC	Accumulator
AFW	Auxiliary Feed Water System
AM	Accident Management
ATWS	anticipated transient without scram
ANS	American Nuclear Society
ANT	Advanced Nuclear Technologies
AOOs	Anticipated Operational Occurrences
AQP	Advanced Qualification Process
BC	Boundary Condition
BEPU	Best-Estimate Plus Uncertainties
BE	Best-Estimate
BWR	Boiling Water Reactor
CASL	Consortium for Advanced Simulation of Light Water Reactors
CET	Core Exit Thermocouples
CFD	Computational Fluid Dynamics

CFR	Code of Federal Regulations
CHF	Critical Heat Flux
CRDM	Control Rod Drive Mechanism
CSAU	Code, Scaling, Applicability and Uncertainty
CSNI	Committee On The Safety Of Nuclear Installations
CSN	Consejo de Seguridad Nuclear
CVCS	Chemical and Volume Control System
DBA	Design Basis Accidents
DC	Downcomer
DNBR	Departure from Nucleate Boiling Ratio
DNB	Departure from Nucleate Boiling
DSA	Deterministic Safety Analysis
ECCS	Emergency Core Cooling System
ECI	Exterior Communications Interface
EJ	Expert Judgement
EOP	Emergency Operating Procedures
FDE	Finite Differential Equations
FFTBM	Fast Fourier Transform Based Method
FOM	Figures of Merit
FTC	Fuel Temperature Coefficient
GRS	Gesellschaft fur Anlagen-Und Reaktorsicherheit
HF	Calculated Heat Flux
HPIS	High Pressure Injection System
HS	Heat Structure

INEL Idaho National Engineering Laboratory

INL Idaho National Laboratory

ITF Integral Test Facilities

IUQ Inverse Uncertainty Quantification

IV Independent Variables

IPC Inter-Process Control

JAEA Japan Atomic Energy Agency

KAERI Korea Atomic Energy Research Institute

KIT Karlsruhe Institute of Technology

LHGR Linear Heat Generation Rate

LHS Left-Hand Side

LOCA Loss-Of-Coolant Accident

LPSI Low Pressure Safety Injeccion

LP Lower Plenum

LSTF Large Scale Test Facility

LWR Light Water Reactor

MARS Multi-dimensional Analysis of Reactor Safety

MCT Maximum Cladding Temperature

MDNBR Minimum Departure from Nucleate Boiling Ratio

MFW Main Feed Water

MSIV Main Steam Isolation Valve

MSLB Main Steam Line Break

MS Main Steam

MTC Moderator Temperature Coefficient

NCSU North Carolina State University

NC Natural Circulation

NEA Nuclear Energy Agency

NPP Nuclear Power Plant

NRC U.S. Nuclear Regulatory Comission

NV Nominal Value

OECD Organization For Economic Co-Operation

ONB Onset of Nucleate Boiling

OLC Off-line coupling

PCT Peak Cladding Temperature

PDF Probability Density Function

PVM Parallel Virtual Machine

PIRT Phenomena Identification and Ranking Table

PNL Pacific Northwest Laboratory

PORV Pressure Operated Relief Valve

PSA Probabilistic Safety Assessment

PSU Pennsylvania State University

PVST Power to Volume Scaling Tool

PWR Pressurized Water Reactor

RCCA Rod Cluster Control Assembly

RCP Reactor Coolant Pump

RCS Reactor Coolant System

RDFMG Reactor Dynamics and Fuel Management Group

RHR Residual Heat Removal System

RHS	Right-Hand Side
RPS	Reactor Protection System
RPV	Reactor Pressure Vessel
SBLOCA	Small Break LOCA
SCUP	Scaling-Up Methodology
SETF	Separated Effects Test Facilities
SET	Separated Effects Tests
SG	Steam Generator
SIMPLE	Semi-Implicit Method for Pressure-Linked Equations
SRP	Standard Review Plan
TH	Thermal-Hydraulics
TS	Technical Specifications
UPC	Universitat Politècnica de Catalunya
UR	Uncertainty Range
VERA-CS	Virtual Environment for Reactor Applications, Core Simulator

NOMENCLATURE

CTF conservation equations formulation

α	Volume fraction
ρ	Phase density
$\vec{V}$	Field velocity
l	Liquid film field
v	Vapor field
e	Entrained droplet field
Γ'''	Volumetric mass transfer due to phase change
η	Fraction of phase change between vapor and entrained droplets
Q'''_{wl}	Volumetric heat transfer from the wall to liquid phase
H_{fg}	Latent heat of vaporization
$\vec{\tau}'''$	Volumetric wall drag and form losses

RELAP5 conservation equations formulation:

P	Pressure
X_n	Noncondensable quality

U_g	Vapor specific internal energy
U_f	Liquid specific internal energy
v_g	Vapor velocity
v_f	Liquid velocity
h_v	Vapor enthalpy
h_l	Liquid enthalpy
ρ_v	Vapor density
ρ_l	Liquid density
α_g	Vapor volume fraction
α_l	Liquid volume fraction
ρ_b	Boron density
FWF	Wall drag coefficients liquid
FWG	Wall drag coefficients vapor
FIF	Interphase drag coefficients liquid
FIG	Interphase drag coefficients vapor
B_x	Body force in x coordinate direction
j	Junction index

SIC Coupling formulation:

CBJ	Coupling Boundary Junction
CBV	Coupling Boundary Volume
Vp	Volume Properties
Jp	Junction Properties

CHAPTER 1

INTRODUCTION

This chapter contains:

- The description of PWR NPP technology
- The definition of deterministic safety analysis
- A discussion of the main characteristics of TH codes
- The criteria for the selection of adequate base cases
- The state of the art of TH-TH coupling and BEPU methodologies
- The research aims and objectives of the Thesis

1.1 Pressurized water reactors (PWR)

Nuclear power reactors used in nuclear plants for power generation are designed, built and operated to produce heat energy through the fission chain reaction of ^{235}U and ^{239}Pu. A nuclear reactor is a device in which a chain reaction is maintained under control. The reactor core (mostly of a cylindrical shape) contains the fuel with fissile material (^{235}U or ^{239}Pu). The fission heat energy produced in the core is transferred from the core to a cooling medium. The fuel and coolant are separated by suitable cladding material, to prevent radioactive isotopes from reaching the coolant and to protect the fuel from being corroded or eroded by the coolant. Other main elements of the reactor core are

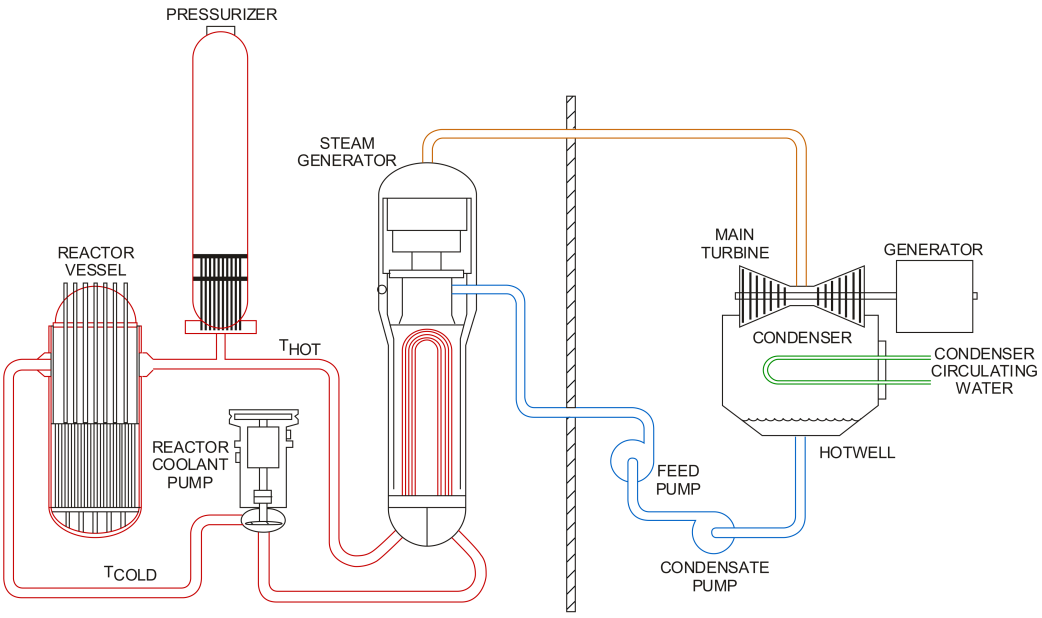

Figure 1.1: *Scheme of a general PWR NPP cycle (Source: U.S. NRC [1])*

the moderator and the neutron-absorbing materials. The moderator has the function of slowing down the neutrons emitted in the fission process to the thermal energy range at which they are more effective in producing further fissions to maintain the chain reaction. The neutron-absorbing materials are used in order to control or regulate the neutron flux and to compensate for the excess positive reactivity of the core fuel in order to have extended operating cycles between refuelling operations [2].

Pressurized water reactors (PWRs) were first conceived as a naval propulsion unit and have been operated for submarine applications in the USA since 1954 when the first nuclear submarine NAUTILUS was launched. The system was subsequently developed for civilian power application and led to the construction of Shippingport NPP, the first nuclear power plant prototype, with a net electrical output of 60 MWe. In this design, the reactor core is contained in a pressure vessel in which light water at high pressure is used as coolant and moderator, circulating through a closed primary circuit.

The PWR technology has evolved since and has been the most widely developed system among the proven types of reactors commercially available. As of 1st of July 2020, 31 countries were operating a total of 408 nuclear reactors. The annual electricity generation from nuclear power plants reached 2,657 TWh in 2019. The five nuclear-generating countries by rank (the USA, France, China, Russia and South Korea) generated 70 per cent of all nuclear electricity in the world in 2019. Two countries, the USA and France, accounted for 45 per cent of 2019 global nuclear production [3]. The operating experience with PWRs is extensive and it is certainly the most abundant of all available reactor systems in operation.

The 3-loop Westinghouse PWRs are divided into two independent circuits: the primary and the secondary circuits. The primary circuit consists of the reactor pressure vessel (RPV) containing the reactor core, the steam generators (SGs), the pressurizer, the reactor coolant pumps (RCPs) and the piping that connect the prior elements, forming a set of 3 loops (see Figure 1.1). The coolant flows through the reactor coolant system (RCS) loops transferring the heat produced in the reactor to the secondary circuit through the SGs, where steam is produced for the turbine-generator unit, where the generation of electrical power occurs. In this way, the SG tubes provide a barrier for the fission products between the primary and the secondary circuits.

In this work, a 3-loop Westinghouse PWR model has been used (as described in Chapter 6). A brief description of the systems, controls and protection systems is provided in this chapter for the general Westinghouse 3-loop nuclear power plant (NPP) design.

1.1.1 Reactor core

The main function of the nuclear fuel is to heat up the RCS coolant in order to transfer the energy to the secondary circuit. The fuel assemblies (as shown in Figure 1.2) are composed of 264 fuel rods, that contain the fuel pellets inside the fuel cladding. Also, each fuel assembly contains 24 guide thimble tubes and one instrumentation tube located at the central position. All the elements are displayed in a 17 x 17 array and are supported by two main structures: the top and bottom nozzles.

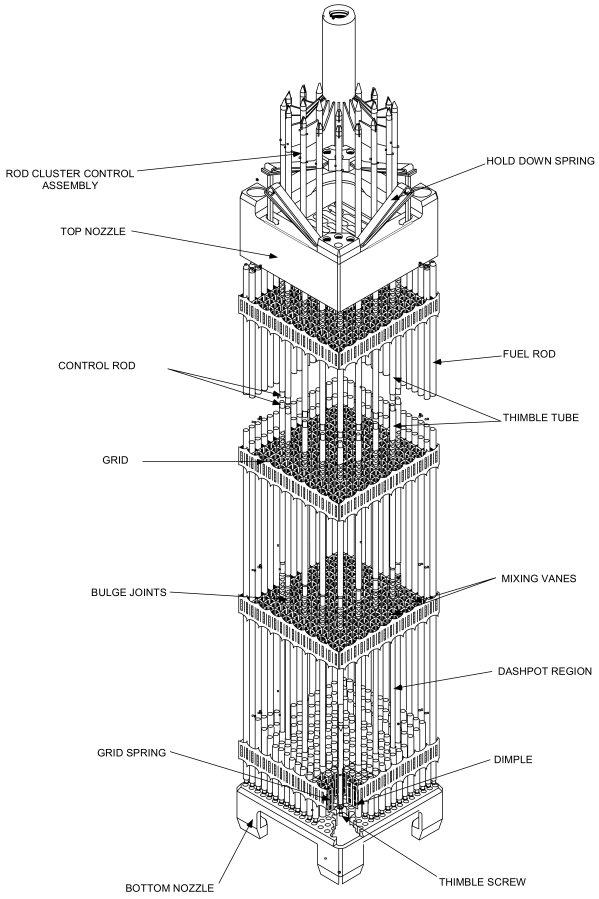

Figure 1.2: *Scheme of a PWR nuclear fuel (Source: U.S. NRC [1])*

The guide thimble tubes provide a means of insertion for a rod cluster control assembly (RCCA) in order to control reactivity. The instrumentation guide thimble provides a path for the insertion of intra-nuclear instrumentation. The fuel assemblies are vertically installed in the reactor vessel, with a geometrical disposition shown in Figure 1.3. The

assemblies are supported by the lower core plate and aligned by pins, while at the top they are kept in position by the upper core plate through the use of hold-down springs.

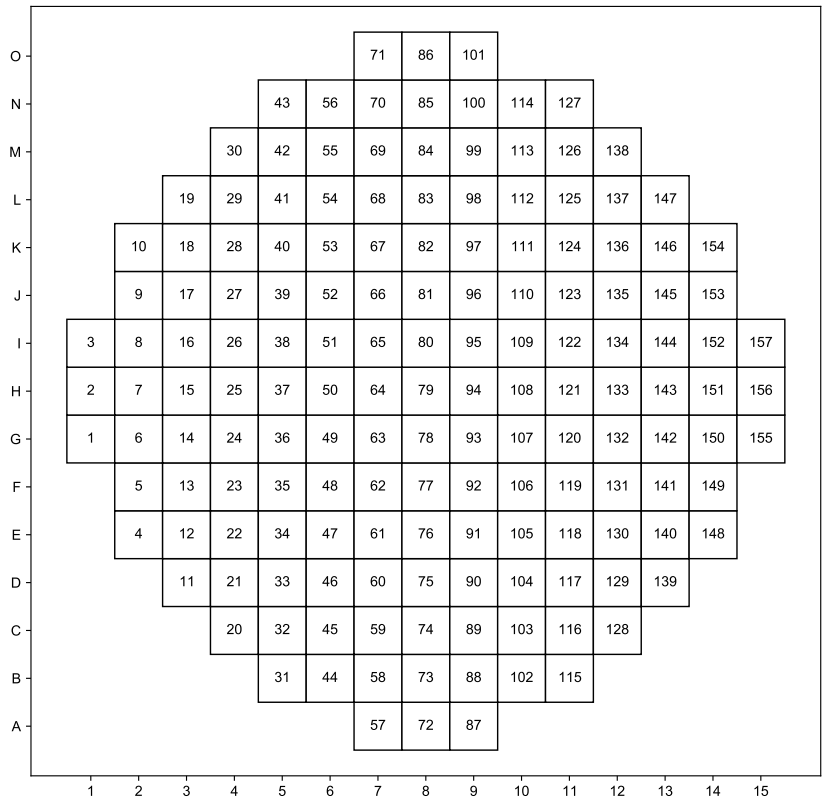

Figure 1.3: *Display of the nuclear fuel in PWR core.*

The fuel rods are composed of Zircaloy-4 sealed tubes filled with uranium dioxide ceramic pellets. The pellets are enriched uranium-dioxide powder sintered in a cylindrical shape. The pellets are axially compressed inside the fuel rods by an internal spring located at the top position. A gap is present between the pellets and the inner clad surface to accommodate fission gases during the cycle burn-up. The fuel rods are internally pressurized with helium during their manufacture, and they are supported laterally at intervals in their axial length by grids, that help maintain the fuel assembly geometry.

Two different types of grid assemblies are used: the first type of grids are used at the central length of the assembly, where higher neutron flux is expected and consists of welded zircaloy straps that hold mixing vanes to increase the local coolant mixing. The second type are the Inconel-718 grids, located at the ends of the fuel assemblies.

1.1.2 Reactor pressure vessel

The reactor vessel is made of a metallic cylinder, closed by a removable head assembly (Figure 1.4). It is connected to the RCS piping through 3 inlet and 3 outlet nozzles, located and distributed at the same horizontal plane above the top of the fuel assemblies. The RCS coolant enters the reactor vessel through the cold leg inlet nozzles and flows down through the downcomer between the vessel wall and the core barrel to the lower plenum. Then, it flows upwards through the core support structure, the fuel assemblies and the upper core plate, to exit through the hot legs nozzles.

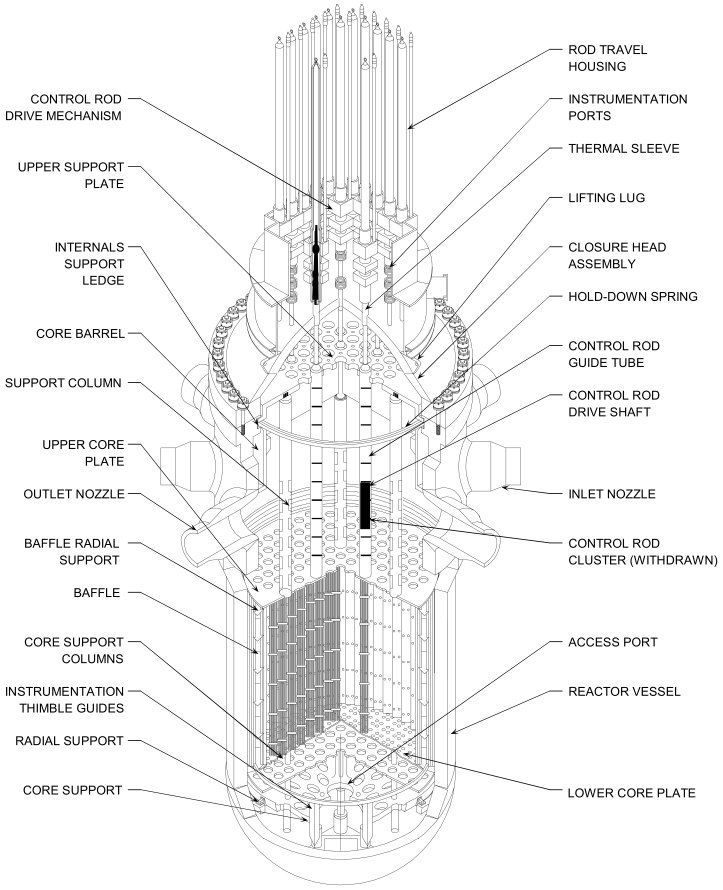

Figure 1.4: *Scheme of a general PWR vessel (Source: U.S. NRC [1])*

The position of the control rods is controlled through the use of the control rod drive mechanisms (CRDMs). Each CRDM controls the position of a single RCCA by the action of electromagnetic coils, which actuate a set of mechanical trinkets. The reactor trip is

accomplished when the coils are de-energized and the control rods are inserted into the core by gravity. The CRDMs are attached to the vessel head at the specified control rod positions of the core.

1.1.3 Reactor coolant system

The RCS is the system that groups the RPV, the piping, the pressurizer, the RCPs and the primary side of the SGs (see Figure 1.5). Each one of the 3 loops contains the connections with the RPV, one SG, one RCP and the connections to other systems such as residual heat removal system (RHR) and emergency core cooling system (ECCS). One of the hot legs is connected to the pressurizer through the pressurizer surge line.

The main functions of the RCS are, on one side, to extract the heat produced by the core to the SGs. On the other side, the RCS acts as a barrier by limiting the fission product release in case of a leak to the RCS coolant. Additionally, it provides the required conditions for the nuclear fuel in order to have the heat transfer conditions within limits by controlling the temperature, mass flow rate and pressure. Also, it provides a means of controlling the core reactivity by regulating the boron concentration of the coolant through the chemical and volume control system (CVCS) connections.

The pressurizer (see Figure 1.6), is designed to control the RCS pressure. It is connected to one of the hot legs through the surge line. It consists of a vertical cylindrical tank with hemispherical top and bottom heads, with steam and water being at saturation conditions by reaching a higher temperature than in the RCS at the same pressure.

The pressurizer is equipped with 4 types of pressure regulation elements: (a) the proportional and backup electrical heaters, located at the bottom of the pressurizer, are used to compensate for the thermal losses and to generate steam to increase pressure. (b) the spray nozzles, which are connected to a set of valves that regulate the amount of water injected from the cold legs to be sprayed to the steam portion of the pressurizer. The objective is to decrease the pressure of the RCS by partially condensing the steam in the pressurizer. (c) the relief and (d) the safety valves, located at the top of the pressurizer, used as a means to limitate pressure with their respective set-points.

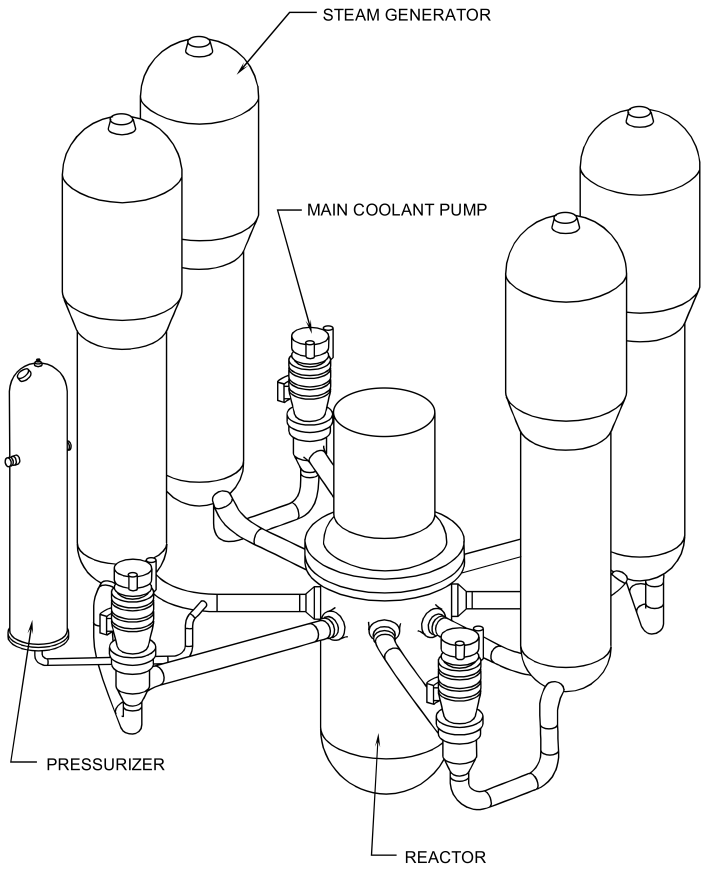

Figure 1.5: *Scheme of a general PWR RCS (Source: U.S. NRC [1])*

The outlet of the pressurizer safety and power-operated relief valves is connected to the pressurizer relief tank, which collects, condenses and stores the discharged fluid in form of steam. In case the system capacity is overridden, the tank is equipped with a rupture disk to discharge the collected fluid directly to the containment building.

The pressurizer level is controlled by the CVCS, which regulates the inlet flow to the RCS from the charging pumps while maintaining the discharge (outlet) constant. Among other functions, the CVCS regulates the boron concentration in the RCS coolant and it controls the fluid chemical conditions.

The last main RCS components are the RCPs, designed to provide forced-circulation flow through the core sufficient to ensure adequate heat transfer to maintain the thermal-hydraulic conditions related to the heat transfer process between the fuel clad and the coolant well below the design limits (e.g. the departure from nucleate boiling ratio (DNBR)).

The RCPs do not provide any safety function after a design basis accidents (DBA), but during the first seconds of the RCPs coastdown and prior to the reactor trip taking place, a sufficient amount of forced flow must be provided to the reactor core to avoid the degradation of the heat transfer conditions and possible fuel damage. This is the reason why each pump has an attached flywheel to the axis, which after a trip provides sufficient energy to the pump shaft to maintain adequate heat transfer capability in the short term.

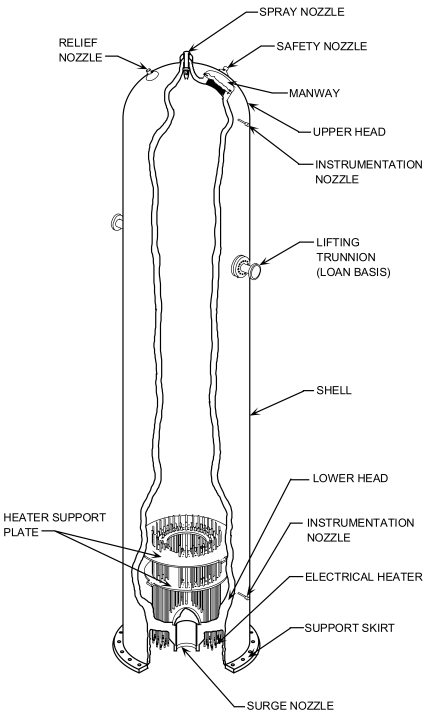

Figure 1.6: *Scheme of a general PWR PSZR (Source: U.S. NRC [1])*

1.1.4 Secondary systems

The function of the SGs is to produce saturated steam from the energy transferred from the RCS from the primary side to the secondary side (see Figure 1.7). The SGs are U-tube heat exchangers in which the RCS coolant flows through the tubes, and produces steam from the water injected at the secondary side by the main feed water (MFW) system. The RCS coolant enters the SGs through the inlet nozzle, then flows through the U-tubes to finally exit the SGs through the outlet nozzles.

The MFW coolant enters the SGs through the feedwater inlet connections and is distributed to the downcomer by the feedwater ring, which has J-tubes distributed along

the perimeter. The water flows downwards between the tube bundle wrapper and the shell first and then it flows through the tube bundle, producing a steam-water mixture. the mixture flows first through the swirl-vane moisture separators and second through the chevron separators before exiting the SGs through the outlet nozzle. The water removed from the mixture returns to the downcomer. The SGs level is measured at the downcomer for control and protection purposes.

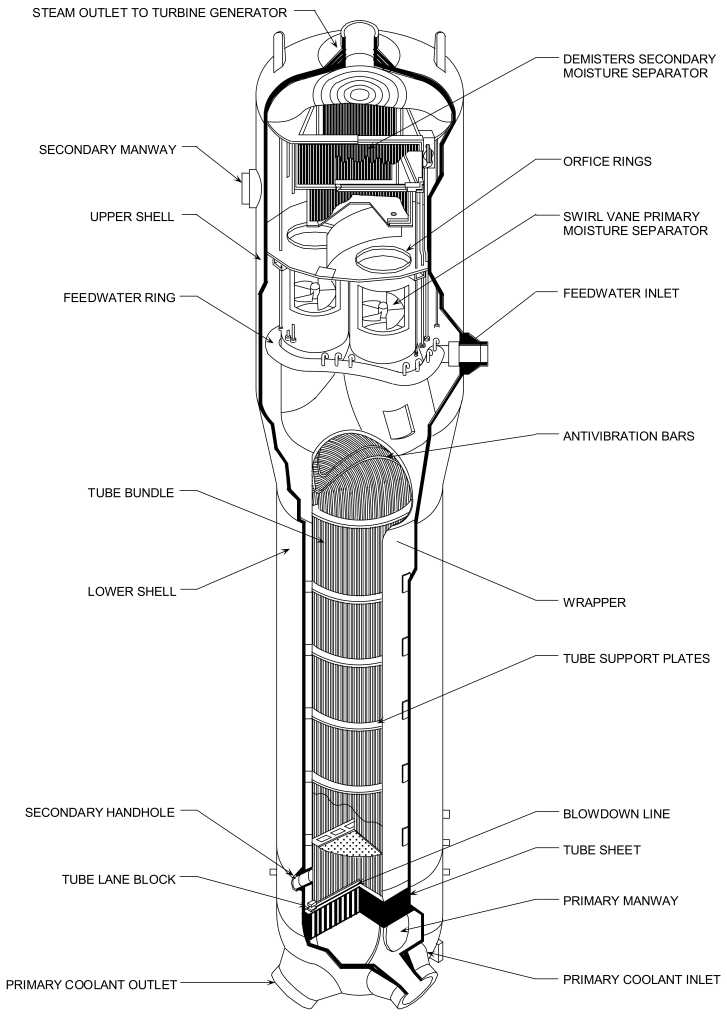

Figure 1.7: *Scheme of a general PWR SG (Source: U.S. NRC [1])*

The main steam system collects the SG steam flow to conduct it to the high-pressure turbine inlet and other secondary systems such as the bypass system, the main feedwater preheaters and the moisture separator reheaters. The main steam pipes are equipped with a set of safety valves and power-operated relief valves, to regulate RCS tempera-

ture at low reactor power. The lines are also connected to the main steam isolation valves (MSIVs), with the function of preventing the containment overpressurization and RCS overcooling produced by the leaking of more than one SG. Once the steam passes through the high-pressure turbine, it is reheated at the moisture separator reheaters with main steam before entering the low-pressure turbines.

The condenser receives the steam from the low-pressure turbines, with the purpose of condensing the steam to be injected back into the SGs. The condensate is collected from the condenser wells by the condensate pumps and passes through the low-temperature heaters, main feedwater turbine-driven pumps and high-temperature heaters before being injected into the SGs. The SGs level is controlled by regulating the speed of the main feedwater pumps and the position of the main feedwater control valves. In case of an accident or MFW malfunction, the auxiliary feed water system (AFW) system would inject coolant to the SGs to cool down the reactor to shut down conditions, extracting the residual heat from the core.

1.1.5 Safeguards systems

The ECCS, as shown in Figure 1.8, has the main function of providing core cooling (safety injection) to minimize fuel damage following a loss-of-coolant accident (LOCA). It is also designed to provide an additional shutdown margin following a steam line break accident by the means of injecting highly borated water. The system is divided into 3 subsystems:

- The 3 accumulators are pressurized tanks designed to act as passive components to discharge borated water into the cold legs. The amount of water is enough to fill the downcomer and the lower plenum of the RPV in case of a large-break LOCA prior to the beginning of the core reflood phase.
- The high-head injection system consists of a set of high pressure pumps that provide a means of high pressure and low flow injection to the RCS, in case of small to intermediate-sized LOCAs, with highly borated water.
- The low-head injection system consists of a set of low-pressure pumps that provide

high flow injection to the RCS, in case of large-sized LOCA, also with highly borated water. In the first stages of a LOCA, the system works in the injection mode by injecting the water from the refuelling waste storage tank. When the inventory is decreased, it is switched to the recirculation mode, in which the leaked containment inventory is collected by the low-head injection system to be cooled down and injected to the RPV again through the high and low-head injection systems.

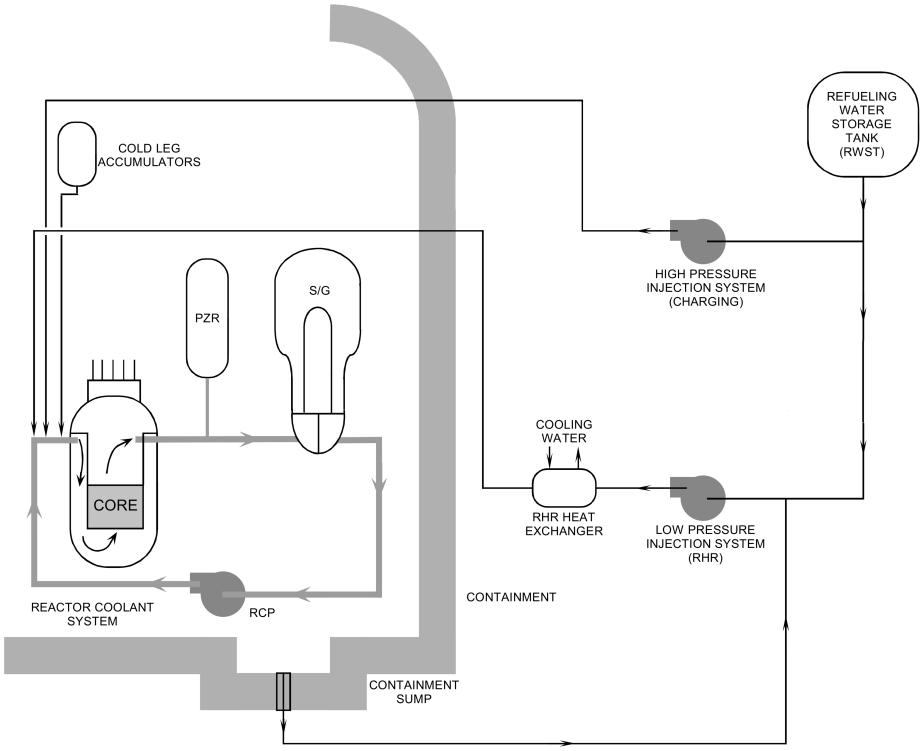

Figure 1.8: *Scheme of a general PWR ECCS (Source: U.S. NRC [1])*

1.2 Deterministic safety analysis and TH codes

The licensing process of NPPs is a key previous step to startup and a continuous process during the operation cycle to ensure that the nuclear safety standards and regulations set by the regulatory body of each country are met. In order to fulfil the licensing requirements, nuclear installations must identify the main internal and external events that potentially imply risks to the safety of the general public and the environment [4]. In addition, the consequences of the events that challenge NPP nuclear safety must be quantified and lie below the limits set by the safety regulations.

The regulatory safety limits are limits imposed on relevant parameters and are generally related to setting limits to ensure minimum radioactive releases during postulated accidents. They are set by each country's regulatory body, but they share common technical bases, and in many cases, they are or can be considered equivalent. Several efforts have been made to achieve harmonization between countries, either at the European level [5] or the international level (IAEA Safety Standards [6]).

One of the critical aspects of NPP safety analysis is to elaborate predictions on how the nuclear fuel and the whole system perform during the postulated transients and accidents. These predictions are calculated using computer codes explicitly designed for this purpose. The use of these codes often started a few decades ago and has undergone significant updates based on the increased knowledge of nuclear physics and thermal-hydraulics and in combination with code verification processes and the use of experimental data from integral test facilities (ITF).

The release of radioactive fission products is contained by a group of physical barriers: the fuel cladding, the reactor coolant pressure boundary and the containment building. These barriers must remain functional during normal operation and during the occurrence of a set of postulated accidental scenarios. From a licensing point of view, the IAEA [7] considers that NPPs should demonstrate through the use of deterministic safety analysis (DSA) that the barriers that protect from radioactive material releases will maintain their integrity to the extent required.

1.2.1 Nuclear safety

Nuclear safety is a concept applied to many aspects that involve the operation of commercial NPPs. Focusing on the design and operation of the systems, one of the most relevant concepts is safety functions. The safety functions are the fundamental functions that should be maintained by plant structures, systems and components to protect the fission product release barriers.

The general safety functions are subcriticality, as the capacity of the plant reactivity control systems to reach and maintain a subcritical condition, heat extraction, as the capacity of the plant systems to remove the residual heat after a reactor trip, and radioactivity confinement, as the capacity of the systems to maintain radioactive releases below the limits. The safety functions must be maintained during the whole duration of the postulated events and the systems that provide these functions must perform within their design parameters.

1.2.2 Initiating events

The functionality of the fission product release barriers is evaluated by measuring their capacity of maintaining their physical integrity during the postulated events. The postulated events are derived from the consideration that the plant response should be analyzed when system malfunctions or equipment failures occur. The number and type of postulated malfunctions or equipment failures are limited according to the type of analysis performed, as explained in Subsection 1.2.4.

The postulated events are categorized into 3 categories according to U.S. Nuclear Regulatory Comission (NRC) 10CFR [8]: normal operation, anticipated operational occurrences (AOOs) and postulated accidents. ANS Standard 51.1 [9] classifies the design basis accidents into 4 categories: I, II, III and IV, where each category includes a predefined set of accidents defined in the NRC RG-1.70 [4].

Each category of accident is assigned an estimated frequency of occurrence and specific limitations to its consequences, consisting of limitations on the effects produced

by the fission product barriers and the radioactive releases. These limitations are verified by code calculations through the use of acceptance criteria, defined for each condition to ensure that the consequences of the postulated accidents lie below the safety limits.

1.2.3 Acceptance criteria

The acceptance criteria are a set of limits imposed to judge the calculation results of an accident to verify the design and operation compliance with the regulations. There are mainly 3 types of acceptance criteria: safety, design and operation criteria. The first type is set to verify the performance of the safety barriers to perform the safety functions. The second type is set to verify that the structures, systems and components that play an important role in mitigating the accident consequences are working within their design limits. The third type is set to evaluate the capacity of the operator to perform the safety functions.

According to ANS Standard 51.1 [9], the acceptance criteria are set depending on the category of the accident. The accidents are divided into categories as a function of the frequency of expected occurrence. The accidents classified into categories with higher occurrence frequencies have more restrictive acceptance criteria than the accidents with less frequency and higher consequences. In the present work the focus is set on Condition II and III events, as explained in Section 1.3, because the two selected cases of interest fall into these categories. The general acceptance criteria for Condition II and III events are:

Condition II events:

- The incident should be terminated, at most, with the actuation of the reactor protection system (RPS).
- Should not cause any loss of function of any fission product barrier.
- Should not cause any Condition III or IV event.

Condition III events:

- The incident should not cause damage to more than a small fraction of the fuel elements in the core.
- The release of fission products may exceed 10CFR20 guidelines, but shall not be sufficient to restrict public use beyond the exclusion radius.
- Should not cause any Condition IV event.

The safety limit is considered to be the value for which a fission product barrier is known or assumed to fail to provide the defined safety function. The acceptance criteria limits concerning safety limits are shown in Figure 1.9. One of the objectives of the licensing process is to verify that the calculation results lie below the acceptance criteria limits. The safety margin is defined as the difference between results and the acceptance criteria and depends on the DSA method used, as defined in Subsection 1.2.4.

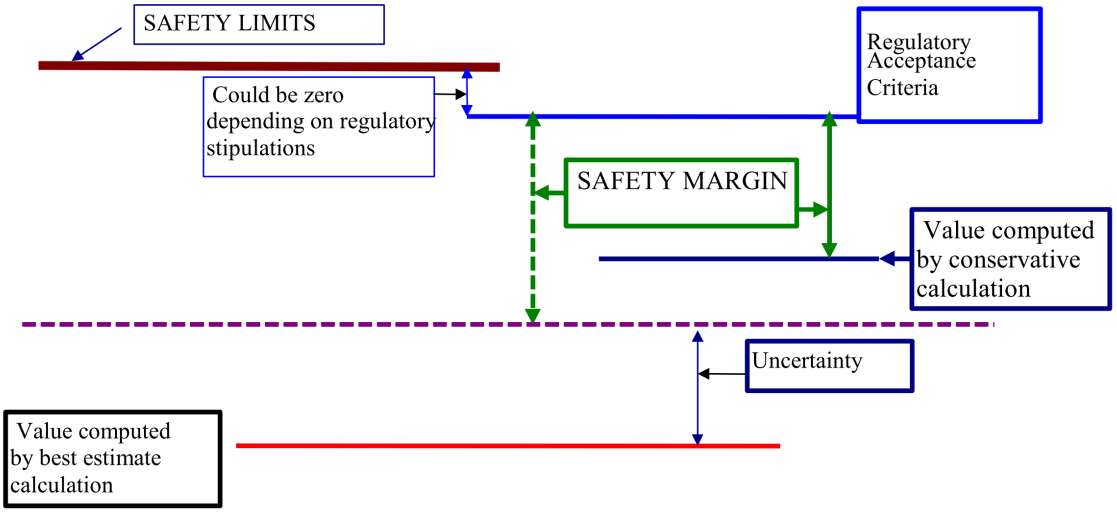

Figure 1.9: *Safety margins representation (Source: IAEA [10])*

1.2.4 Deterministic safety analysis

The main objectives of DSA are: on one hand, to help assess the plant against regulatory safety requirements. On the other hand, they are also used as an engineering tool capable of measuring the plant response or performance under any desired conditions [11].

According to IAEA, there are four different methodologies currently available to perform DSA (Options 1 to 3 are addressed in the following sections):

1. Conservative.
2. Best-estimate (BE) with conservative boundary conditions.
3. Best-estimate plus uncertainty (BEPU) evaluation.
4. BE with systems availability supplied through probabilistic assessment.

Where each methodology uses its specific codes and procedures [11]:

Option	Computer code	Availability of systems	Initial and boundary conditions
1	Conservative	Conservative assumptions	Conservative input data
2	BE	Conservative assumptions	Conservative input data
3	BE	Conservative assumptions	Realistic input data with uncertainties
4	BE	Probabilistic safety analysis based assumptions	Realistic input data with with uncertainties

Table 1.1: *Available calculation type options according to IAEA [11]*

1.2.4.1 Option 1: conservative calculations

One of the first regulatory requirements setting limitations for the accident consequences was power plant-specific. When the regulatory bodies moved from plant-specific to general requirements, the calculations were required to be conservative. When carrying out conservative calculations, some of the parameters related to the acceptance criteria of interest are forced with conservative values [12].

The decision of adopting those conservative values assumes that the effect on the acceptance criteria of interest will be also conservative (a result closer to the acceptance

criteria limit). The conservative values may include considerations of the initial boundary conditions (BCs), the capacity of the safety systems and the physical models.

In conservative calculations the plant controls are also set in a conservative way: if the actuation of control systems increase the margins to the safety limits, they should not be taken into account [13]. Operator actions are not credited in the short term, with the exception of a few cases, where it is required to demonstrate that the amount of time to evaluate the scenario and perform the correct actions is less than the calculated time to reach the limit of the acceptance criteria.

The performance or availability of safety systems is also subject to a conservative point of view: the simple failure criterion. It states that in the short term, as defined as 24 hours or the equivalent time to reach the coolant recirculation alignment following a LOCA accident, only an active failure can occur, aside from the failure that may cause the accidental scenario.

An active failure consists of the failure of an active component such as pumps, valves, relays, etc. to perform their defined safety functions. Also, in the long term, as defined as more than 24 hours or the equivalent time to reach the coolant recirculation alignment following a LOCA accident, an active or passive can occur, not having had any prior failure in the short term. A passive failure consists of the failure of a single passive component such as pipes, heat exchangers, etc. to perform their defined safety functions.

Conservative calculations may introduce modifications to the physical models used by the codes, considered then conservative codes, where some parameters are forced for conservative purposes in contradiction with the physical validity of the results (for example, constant low pressure is forced through an entire transient calculation).

1.2.4.2 Option 2: Best-estimate calculations

In the decade of 1980, the use of BE codes was allowed (10 CFR 50.46) for licensing purposes instead of using conservative code models, with the condition of quantifying the uncertainties of the calculations. BE computer codes are codes designed to repro-

duce the physical phenomena in an accurate and precise manner, so the obtained results are as close as possible to reality [12]. BE codes are traditionally designed to specifically model an aspect of transients and accidents (e.g. thermal-hydraulics, neutron transport, structural or fuel behaviour). The approach of thermal-hydraulics analysis related to nuclear systems can be performed at different modelling scale levels, i.e. system, sub-channel or computational fluid dynamics (CFD).

A relevant effort was put to obtain correlations and information to later develop specific models to simulate transients, by conducting experiments at ITFs that replicate the behaviour of the commercial NPP and separated-effects test facilities (SETFs), that replicate only specific phenomena occurring during the transients. The limitations applied by the regulatory bodies have been implemented through the use of acceptance criteria, which consist of setting limitations to plant parameters and calculation requisites.

1.2.4.3 Option 3: BEPU calculations

Option 3 consists of performing uncertainty analysis on calculations in which BE codes are used. There are many accepted methodologies related to BEPU analysis. The main steps consist of evaluating the input uncertainty and then quantifying the impact of the input uncertainty on the selected output parameters. The evaluation of uncertainties is performed in two different ways according to each method, either by the propagation of input uncertainties or by extrapolation of output uncertainties.

For the first case, probability density functions (PDFs) are defined for the values of input parameters, and later a number of cases are run with the input parameters values set according to the PDFs. For the second case, the uncertainty of the output values is directly obtained by comparison between calculation results and experimental data.

According to Figure 1.9, results computed by conservative calculations should be closer to safety limits than those computed by best-estimate calculations. Nonetheless, the addition of the uncertainty considerations described to the best-estimate calculations results in finding cases with specific combinations of uncertain parameters with their limiting values closer to the safety limits, but since the assumptions of BEPU calculations

are more realistic than conservative calculations, the resulting safety margins are more qualified and more useful within the licensing process than those resulting from the conservative calculations.

1.2.5 Thermal-hydraulics (TH) codes

System codes are used to model the plant behaviour. The components that are present in nuclear power plants or nuclear installations, such as pipes, heat exchangers, pumps, valves and controls, among others, are simulated using specific models and input data [14]. These codes use mostly 1-D formulation and occasionally 3-D formulation for certain specific components such as the reactor vessel [15]. However, system codes lack a proper consideration of the turbulence mixing due to viscous stress effects.

Sub-channel codes [16] are designed to model exclusively the reactor core and nuclear fuel bundles; they allow for 3-D calculations at a very detailed level and are used for predictions of nuclear fuel parameters such as cladding temperatures or departure from nucleate boiling (DNB) related parameters.

Finally, CFD codes may be required for an even more accurate representation of 3-D processes where viscous effects and the influence of detailed geometrical aspects dominate the mixing patterns. The major inconvenience is that, while system codes model all two-phase flow regime regions at the macroscopic level, CFD codes are currently limited to modelling dispersed bubbly or droplet flows and separate-phase flows [17].

1.3 Cases of interest

Two base cases have been selected to perform a BEPU analysis with two coupling methods. The cases have been chosen by taking into consideration two aspects: the limitations of the particular modelling approach with standalone CTF and RELAP5 codes, considering the same relevant acceptance criteria of interest. In this regard, the minimum departure from nucleate boiling ratio (MDNBR) has been selected to be the acceptance criteria of interest, since its evaluation requires the use of correlations with multiple local core parameters involved, as described in Subsection 1.3.2.

1.3.1 Base cases selection

The selection of the cases to run using the two coupling methods is based on the following considerations, which take into account the actual codes and coupling methods' limitations:

- The event must be initiated by system equipment failures or malfunctions. The evaluation of the coupling methodologies differences is achieved by selecting cases where the deviation of the plant parameters or equipment failures takes place in the system (system model) and the main effect or parameter to study takes place in the core (sub-channel model).
- The event must not produce substantial neutron flux distribution asymmetries. The model used for computing the reactor power change is the system code point kinetics model which supplies the total power to the sub-channel model, where it is applied proportionally over the core with fixed power distribution. If the case produces strong flux asymmetries within the core (for example due to local thermal-hydraulics core parameters asymmetries), the point kinetics model will not capture the asymmetrical effect in reactivity that will imply an asymmetrical power distribution, thus affecting in a relevant manner the calculation results.
- The event must not produce substantial inlet flow distribution asymmetries at the core inlet. The lower plenum is modelled using a single node in CTF, so the possible

differences in flow distribution at the core inlet would not be considered. Recent studies have shown that there is a strong influence of the inlet flow distribution patterns on the local core MDNBR conditions [18].

- The MDNBR must be one of the relevant parameters to be analyzed in the transient. The MDNBR depends strongly on local core parameters, and it is affected by a considerable amount of physical values. It is considered then a good indicator of the performance of coupled code calculations.

Considering the list of NUREG-800 Chapter 15 *Transient and Accident Analysis* [19] postulated equipment failures or malfunctions, in conjunction with the considerations above, the following two cases are selected:

(a) RCS depressurization due to pressurizer pressure operated relief valve (PORV) opening (*PORV Case*).

(b) RCS loss of forced flow due to all RCP trip (*RCP Case*).

1.3.2 Acceptance criteria of interest

According to NUREG-800 *Standard review plan for review of safety analysis reports for nuclear power plants* [19], in order to prevent fuel failures in Condition I and II events due to coolant overheating in pressurized water reactors (PWR), one of the acceptance criteria that must be met is that fuel rods must not reach DNB at any location of the core with a 95% probability at a 95% confidence level.

DNB is an effective limiting constraint on normal power operation or during transients in NPPs. DNB is defined by a thermal-hydraulic condition of coolant fluid at which the heat transfer between the fluid and the fuel rod decreases in a sharp manner. This is caused by the isolating effect of the steam blanket between the liquid part of the fluid and the fuel rod when the temperature increases. The main consequence of the heat transfer decrease is an increase in the clad and fuel temperatures, posing a risk to their integrity.

The DNB is expected to occur at the critical heat flux (CHF), that in turn is a function of the fluid and clad conditions and the geometry. CHF is evaluated by applying correlations

such as the W-3 correlation, available in CTF and described in Subsection 2.1.7. The limitation to prevent the DNB is implemented by setting a limit to the DNBR, defined as the ratio of the predicted CHF by correlations to the code calculated heat flux (HF) prediction at any core location.

The limitations on MDNBR are set for every fuel design. Since the CHF correlations are mathematical fits to the conducted tests, the values of the limits are provided by the fuel supplier [20]. Table 1.2 shows the criteria and MDNBR safety limits required by the Nuclear Energy Agency (NEA) countries in 2012:

Country	Criterion type	Value(s)	Basis	Relation to other criteria	Effect of recent changes	Type of methods and rational
Belgium	CHF/DNB	Depending on the correlation used	95/95, correlations: W3 (for low pressure), WRB-, HTP, ERB-, FC, ABBX-, ...depending on the fuel supplier	DNB operating limit	No change, verification required (new design, mixed cores)	Statistical
Canada	CHF		Correlations (e.g. Balint-Cheng)			
Czech Rep.	DNB	Depending on the correlation and TH models used	95/95 VVER440: variants of Czech correlation of PG type 95/95 VVER 1000: special Russian correlation CRT-1 for bundles with mixing vanes	3-D peaking at VVER440, DNB oper. limit at VVER1000	Verification required	Statistical
Finland	DNB/CPR	1.33/1.06	95/95/<0.1% of rods may experience DNB, correlations		No change (burn-up limit 40 GWd/t)	Statistical
France	CHF	1.17, 1.30	95/95, correlations (WRB-, W-3 for low pressure)	Operat. limits (e.g. axial offset)	No change, verif. required (new design, mixed core)	Statistical
Germany	DNB/CPR	1.15/1.09	95/95-correlations (PWR), <1 rod experience dryout -- THAM method (BWR), all correlations are FA specific	Addit. oper. crit.	Values change dep. on design	Statistical
Hungary	DNB	1.33	95/95, correlations (Bezrukov)	Pin power limit	Values change dep. on design	Statistical
Japan	DNB/CPR	1.17*/1.06*	95/95/<0.1% of rods may experience DNB, correlations (e.g. MIRC-1, NFI-1)	DNB/CPR oper. limit	No effect	Statistical
Korea (Rep. of)	DNB	Depending on the correlation used	95/95, correlations (KCE-1, NGF, WRB-1 etc.)	DNB oper. limit	No change, verif. required	Statistical
Netherlands	DNB	1.30	95/95, correlations (W-3)	DNB oper. limit		Statistical
Spain	DNB/CPR	Various	95/95, correlations provided by fuel vendors	DNB/CPR oper. limit	Values change dep. on design	Statistical
Sweden	DNB/CPR	1.17/1.06	95/95, correlations (VRB-1)<0.1% of rods may experience dryout	DNB/CPR oper. limit	Values change dep. on design	Statistical
Switzerland	DNB/CPR	1.15-1.45/1.09	95/95, correlations	DNB/CPR oper. limit	Values change dep. on design	Statistical
UK	DNB		95/95, correlations	DNB oper. limit		Statistical
USA	DNB	various	95/95, correlations	DNB oper. limit		Statistical

Table 1.2: *MDNBR safety limits for NEA countries (Source: NEA [20])*

1.3.3 RCP trip case description

The accidental decrease of the RCS coolant flow can be caused by malfunctions of the RCP of mechanical/electric nature or due to operator error [21]. Also, external electrical net disturbances can cause a frequency decrease of the buses that energize the RCPs that could lead to a speed decrease followed by a RCS coolant flow partial reduction. This accident is classified as a Condition III event. In this case, the simultaneous trip of all RCPs is considered, causing a RCS coolant flow to decrease governed by the RCPs coastdown as the energy of the inertia wheel is transferred to the coolant.

In this accident, the coolant flow decrease causes a degradation of the core heat transfer conditions that result in a coolant temperature increase that causes a pressure increase. The condition of reduced flow coincident with an elevated power level poses a challenge to the nuclear fuel, as the MDNBR decreases due to the temperature increase and flow reduction, while the power level remains elevated. In this case, the most probable first reactor trip setpoint to be reached is the low RCS flow setpoint.

1.3.4 PORV opening case description

The accidental depressurization of the RCS can be caused by the opening of a safety or PORV valves installed in the pressurizer [22]. The opening of the valve can be caused by electrical/mechanical malfunction or by operator error. The accident is classified as a Condition II event. The main effect following the opening of the valve is a pressure decrease in the RCS system caused by a loss of steam pressurizer inventory through the valve.

In this accident, the pressure decrease causes the addition of negative reactivity to the core produced by the moderator density feedback and a consequent power decrease. Until a reactor trip setpoint is reached and the control rods effectively trip the reactor, the conditions pose a challenge to the nuclear fuel, as the MDNBR decreases due to the pressure reduction and the elevated power level. In this case, the most probable first reactor trip setpoint to be reached is the low pressurizer pressure setpoint.

1.4 Multi-scale TH coupling methods state of the art

In this work, the combined use of a TH system code with a TH sub-channel code (TH-TH coupling) is considered, providing an integrated tool with the capability of modelling in detail the core thermal-hydraulic conditions and the system behaviour. The use of these tools is relevant in the study of events related to fuel overheating, where the core parameters are highly dependent on the system (plant) response. The use of coupled codes is expected to improve the reliability of licensing and is widely used in both research and the nuclear industry in order to take advantage of the individual capabilities that each code can offer [23]:

- Being able to solve different physical phenomena (multiphysics) at the same time.
- Being able to solve the problem at different scales (multiscale) at the same time.
- Use of a combination of previously validated and robust codes.

Three main scales are considered when modelling TH systems. TH codes are specifically designed for one of the scales, or, in some cases, they include the option of modelling a portion of the system on a specific smaller scale to obtain higher precision. The commonly accepted scales are the system scale, the sub-channel scale and CFD. The system scale is related to the ability to model the whole plant.

The codes that are capable to work at the system scale include the ability to model plant components such as pipes, heat exchangers, pumps, valves and their associated control systems. In most cases, they use rather coarse models for the core and simple reactivity models that determine the power distribution. In some cases, these codes may include 3-D components to model the reactor vessel.

The sub-channel scale is associated with the modelling of the reactor core or fuel bundles. In this case, the 3-D formulation is used, and they are able to achieve a great level of detail when predicting key parameters such as cladding temperature and DNB. CFD codes use finer 3-D nodalizations and more complex physical models. This causes the application of CFD methods to be limited in the simulations of two-phase flow systems,

due to the lack of 3-D data on the exchange of mass, momentum and energy between phases, which is very sparse in comparison to 1-D codes [24].

This section presents a review of the current development status of the multi-scale TH-TH codes coupling. The review focuses on two methods of system and sub-channel codes coupling, including the description of a variety of previous relevant works.

1.4.1 TH-TH Coupling methods

Many coupling methods are used in the nuclear field, consisting of a more or less profound integration of several codes. In some cases, for specific scenarios, the coupling method consists of obtaining the BCs from plant models run by system codes and imposing the time-dependent BCs by table (off-line coupling) to sub-channel codes. This approach has been considered valid, assuming that some boundary parameters would not match between system and sub-channel codes.

In a typical off-line coupling (OLC) scheme, the pressure would be imposed from the system code to the sub-channel code at the core outlet, while temperature and mass flow rate would be imposed at the core inlet. In this scheme, pressure at the inlet and temperature and mass flow rate at the outlet do not match between codes and reach higher deviations during transients.

In other cases, more complex coupling methods between system and sub-channel codes are achieved by compiling the codes together. In this case, the core is usually only modelled by the sub-channel code since a separate domain scheme is used. These methods imply coherent BCs between codes in all domain.

1.4.2 Relevant works

Many applications have been developed until the present day that include the combination of several validated codes. A brief presentation of some of the most relevant coupled codes is provided.

1.4.2.1 COBRA/TRAC

COBRA/TRAC program [25] is a code developed by Pacific Northwest Laboratory (PNL) in 1982 by merging COBRA-TF and TRAC-PD2 (TRAC/RELAP Advanced Computational Engine) into a single code. The TRAC-PD2 vessel module was substituted by the COBRA-TF code, using it as a vessel component. COBRA/TRAC predicts the thermal-hydraulic response in case of small and large break LOCAs. The pressure matrix equations of both codes are merged and solved simultaneously using a semi-implicit scheme. However, since COBRA was first integrated into the TRAC code, COBRA/TRAC code has not been maintained or updated with the new versions of COBRA or TRAC.

1.4.2.2 KAERI COBRA/RELAP5

COBRA/RELAP5 is a code developed by Korea Atomic Energy Research Institute (KAERI) in 1992, by coupling COBRA-TF and RELAP5/MOD3.2 [26] [27]. Both codes run in parallel on different processors and the exchange of information is carried out using Inter-Process Control (IPC) techniques. This is achieved by compiling the codes (both in Fortran 77), and in the UNIX system, and adopting the sophomore type IPC(1Z) IPC scheme. A supervisory program, COBLAP, is used to control timing and data transfer between COBRA-TF and RELAP5/MOD3. In COBRA/RELAP5, the system pressure matrix equations, set up in each code, are coupled via the momentum modelling at the interfaces and solved simultaneously.

1.4.2.3 KAERI MARS

KAERI continued developing the coupling between RELAP and COBRA-TF and in 1996 developed Multi-dimensional Analysis of Reactor Safety (MARS) [28]. MARS is a combination of COBRA-TF and RELAP5/MOD3.2.1.2, in which both codes are rewritten in Fortran 90 and restructured in a similar way using modular structures. The result is a code that runs using a serial computation model that includes 1-D (RELAP5) and 3-D (COBRA-TF) modules to simulate multi-dimensional two-phase flow transients. The

MARS code input deck defines both RELAP5 and COBRA-TF models in a single file.

1.4.2.4 RELAP5-3D/COBRA-TF

W.L. Weaver et al. developed a RELAP5-3D COBRA-TF coupled code using the semi-implicit numerical methodology [29]. This methodology, explained in Chapter 3, uses implicit velocities and pressures in the discretized conservation equations providing numerical stability for time-step sizes smaller than the material Courant limit. In this case, both codes are compiled separately, using the Parallel Virtual Machine (PVM) software package [30] for communication between the programs. To run both codes and control the data exchange, RELAP5-3D Executive Program [31] is used, which was developed also by W.L. Weaver as an interface to couple RELAP5-3D to other codes using the same semi-implicit numerical methodology.

1.4.2.5 MHI RELAP5/3D-CTF

RELAP5/3D-CTF coupling was developed by Soler-Martinez in 2011 [32] using a Fortran 77 version of RELAP5-3D and a Fortran 77 COBRA-TF version maintained by Reactor Dynamics and Fuel Management Group (RDFMG) at the Pennsylvania State University (PSU). In this case, Weaver's semi-implicit numerical methodology was used, as well as the RELAP5-3D Executive Program explained above. The difference from previous works is the coupling interfaces employed, which are designed to perform axial and lateral coupling between the two codes.

1.4.2.6 ATHLET/COBRA-TF

This work is a result of a collaboration between Karlsruhe Institute of Technology (KIT) and Gesellschaft fur Anlagen-und Reaktorsicherheit (GRS) to the NURESAFE project [33]. The ATHLET and COBRA-TF coupling is implemented within the SALOME platform, where the parallel coupling method is used. In this coupling, the core domain is modelled in both codes (overlapping domain), and certain inlet/outlet boundary conditions between

codes are transferred, in this case, the inlet mass flow rate, the inlet enthalpy and the outlet pressure.

1.4.2.7 TRACE/CTF

The TRACE/CTF coupling integrates multiscale and multiphysics coupling techniques [34]. The TRACE code is coupled to CTF implementing a semi-implicit coupling by using the Exterior Communications Interface (ECI) present in the TRACE source code and substantial modifications to the CTF source code. Nuclear kinetics is also coupled using an explicit coupling scheme, by coupling CTF to PARCS, internally present and coupled to TRACE code.

1.4.2.8 CTF and RELAP5-3D

In this coupling, RELAP5-3D [15] has been coupled to CTF and NESTLE [35] to model the neutronics and core thermal-hydraulics [36]. The platform 3KEYMASTER is used to couple the NESTLE model to the CTF model at the nodal level to balance run time with accuracy. The coupling scheme is: first, NESTLE provides node-dependent powers to CTF. Second, CTF provides node-dependent coolant densities and fuel temperatures to NESTLE. The overlapping domain is used for the core TH with CTF and RELAP5-3D. RELAP5-3D provides the BCs of the core and CTF provides a node-dependent coolant heating rate to the RELAP5-3D core component solution.

1.4.3 Conclusion

Much effort has been put by researchers and the nuclear industry to obtain codes that permit taking advantage of the coupled codes capabilities for hybrid scales. However, the use of consolidated coupled codes is not the only industry practice. Far from this, many users and organizations use the updated standalone version of the codes and perform off-line coupling techniques. This work provides a comparison and analysis of the differences between these two coupling approaches.

1.5 BEPU methods state of the art

In recent years, the application of best-estimate plus uncertainties (BEPU) calculations has gained importance in the scientific community. This method, far from adding conservatism by forcing non-physical conditions to the calculations, relies on best estimate calculations and takes the uncertainties of the calculations into the process by considering sources of uncertainty of the calculations that have an impact on results due to several causes: modelling inconsistencies, BCs applied, or uncertainties of the physical models implemented in the code.

1.5.1 BEPU methods

The idea of mixing the concepts of BE and uncertainties evaluation came out at the end of the 1990s when BE codes calculations were not given enough credit for licensing purposes. The idea to add the layer of the uncertainty evaluation to the BE calculations in contraposition to the conservative calculations, where the *unknown* uncertainty was taken into account by trying to obtain the *worst case scenario*, which came out as a reinforcement of the BE methods. This way, BEPU methods came out, being considered as an attribute of a calculation [12].

Several methods were developed around the same concept (BEPU), and its use was approved by the main institutions [37] [7] [11]. In contraposition to the interest of such methods in the research fields, only a few practical applications for licensing purposes included BEPU methods [38] [39] [40] [41]. In recent years, the BEPU methodologies are gaining presence in many areas, such as fuel performance methodology, transient analyses and LOCA analyses [42]. The benefit of applying a BEPU analysis is that it is the only method in which the licensing margin (distance between the calculated value and the licensing limit) can be obtained. Another advantage of BEPU is that by reducing the degree of conservatism we can provide more insights into the evolution of the accidental sequences. Moreover, on some occasions, it is not trivial to discern if a conservative assumption may derive to a non-conservative result [18].

1.5.2 Sources of uncertainty

Several sources of uncertainty are identified when performing BE calculations. The process of defining the problem, building the model, defining the BCs and running the TH codes implies many decisions and the use of tools that may include deviations from the real unknown values or the ideal physical models. Nevertheless, these uncertain sources do not imply that the calculations are invalid since a certain degree of simplification is required to be able to perform calculations with limited resources. According to IAEA [11] the sources of uncertainty can be classified into five groups (plus an additional group related to the aleatory/epistemic uncertainty):

(a) Code or model uncertainties: These are uncertainties associated with the code used and the physical models embedded in it, some examples are: approximation terms included in the field equations, material properties, and consideration of fully developed flow regimes.

(b) Representation uncertainties: the field equations are applied over control volumes, in some codes the control volumes are defined specifically for each field equation. The discretization of the physical problem is decided by the user taking into account the code limitations and the code developer's recommendations.

(c) Scaling uncertainty: in some cases, the codes are validated using data from experiments conducted in ITF or from SETF. These facilities are in most cases scaled-down mock-ups of commercial NPPs. The scaling is performed so the main parameters affecting the phenomena to study are maintained. Uncertainties related to scaling can be added because the applied scaling laws do not permit an ideal equivalent behaviour of the scaled-down installations.

(d) Plant uncertainty: initial and BCs are factors that affect calculation results. These values are generally controlled in NPPs by Technical Specifications (TS), which limit the critical parameters related to safety, and the availability and performance of the safety systems [43]. Other plant parameters may depend on the plant's operational status at the moment of the accident, such as core power. Such parameters are

considered a source of uncertainty in the calculations since the initial and BCs in the plants are not constant.

(e) User effect: the fact that different users create models to perform calculations in different ways, and the errors committed when building the models are considered also a source of uncertainties.

(f) Aleatory/epistemic uncertainty: Aleatory uncertainty is related to the inherent randomness of the system. Epistemic uncertainty is related to the uncertainty of the model applied. It is caused by the lack of knowledge related to the problem.

1.5.3 Uncertainty analysis methods

The main characteristics that define an uncertainty method are in the first term, (a) the type of characterization of the input uncertainty, as the uncertain parameters that are considered in the calculation come from different sources and their associated uncertainty. In the second term, as explained before, (b) the type of methodology to measure the influence of the input uncertainty on the output uncertainty, where the output uncertainty refers to the uncertainty of pre-selected output parameters as the *calculation results*.

The type of characterization of the input uncertainty will define if the method is either deterministic or probabilistic. In the deterministic methods, the input uncertainty is measured or accounted for by setting a range of values or PDFs assigned to each input value considered to be uncertain. Each range or PDF must be justified with a link to a realistic evaluation of the parameter's uncertainty. In the probabilistic methods, the input uncertainty is not obtained from ranges or PDFs, but the uncertainty ranges or bounding values are set according to available experimental data.

1.5.3.1 Probabilistic methods

Probabilistic methods make use of uncertain input parameters probability distributions. The probability distributions account for the variability of the parameter or its state of knowledge. The method used in this study falls into this category.

1.5.3.2 Deterministic methods

In the deterministic methods, the quantification of the input parameters uncertainty differs from the probabilistic methods. Instead of probability distributions, ranges or bounding values are defined for the input parameters based on experimental data. The conclusions obtained by this method are considered deterministic instead of probabilistic. The two main deterministic methods are the Atomic Energy Authority Winfrith (AEAW) [44] method and the Electricité de France (EDF)-Framatome deterministic realistic method (DRM) [45].

1.5.4 Propagation of input uncertainties

The study of the propagation of uncertainties consists of evaluating the effects on the results and their uncertainties as a consequence of the input uncertainties considered from all previously described sources. The propagation of input uncertainties is only discussed for probabilistic methods, since one of these methods, the GRS method [46], is chosen for the present work. The probabilistic methods can be considered as an extension to a BE calculation since they are performed as variations stemming from a base case, where the values considered uncertain are defined as the central values of the PDFs.

The sources of uncertainty must be identified and quantified, and the number of sources of uncertainty is restricted in some methods. Each input uncertain parameter is characterized by a probability density function and often with a range of applicability. In some cases, the ranges and PDFs of the uncertain parameters can not be determined due to the lack of knowledge of the physical processes or due to complex phenomena that may affect the input parameters, so they can be defined in a subjective manner (expert judgement). Figure 1.10 shows a representation of the sources of uncertainty applied in the BEPU calculation, via input deck or via source code. It also shows the propagation of the input uncertainty to the distribution of the BEPU results.

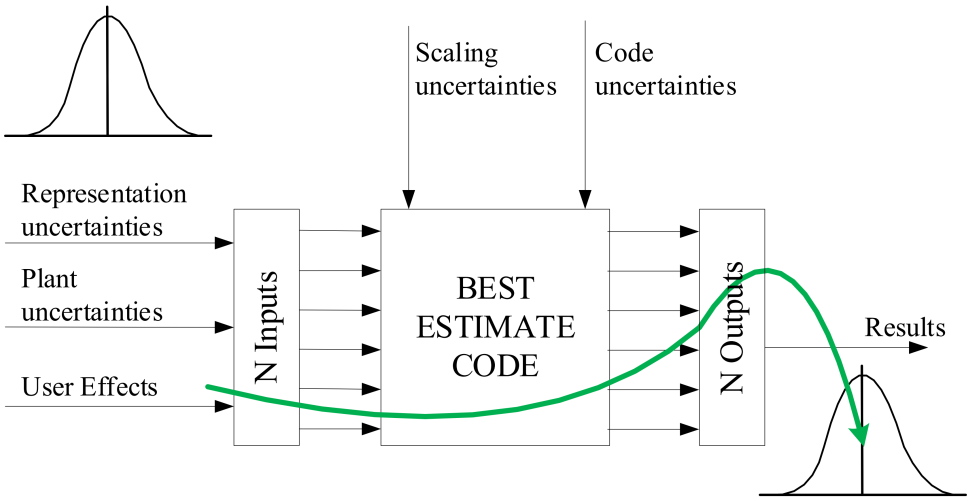

Figure 1.10: *Sources of uncertainties and uncertainty propagation*

1.5.5 Probabilistic BEPU methods state of the art

A brief description is provided for the main probabilistic BEPU methods: The CSAU method [44] [47] developed by the NRC, the GSUAM method [48] developed by Siemens (now Framatome ANP), the UMAE/CIAU methods [49] [50] developed by the University of Pisa (UNIPI), and the GRS method [46] developed by GRS.

1.5.5.1 CSAU method

In 1988 the NRC issued a revised rule for LOCA ECCS analysis to allow the use of BE codes. This option required the quantification of the uncertainty of the calculations. In parallel, the NRC developed the CSAU methodology, demonstrating that uncertainties with problems having complex phenomena can be quantified.

CSAU method focuses on quantifying code uncertainties. Considering a specific NPP model and transient, the method evaluates the accuracy of the calculations after the problem is scaled-up. The method considers three sources of uncertainties: code limitations uncertainties, scaling inaccuracies from the experimental data present in the code, and

uncertainties related to the initial conditions at the initiation of the scenario. The CSAU method consists of three parts (elements):

The first element, *requirements and code capabilities*, consists of an analysis to determine if the use of a code is consistent with the requirements of the scenario (if the code capabilities match the involved phenomena of the selected scenario). The code limitations are identified, as well as the processes and phenomena, that are identified and ranked according to the influence on the safety criteria. Only the uncertainty associated with the most relevant phenomena that affect the acceptance criteria is quantified since evaluating the uncertainty of all involved phenomena would need a too large amount of resources. The code is then selected by evaluating the ability to reproduce the ranked phenomena involved in the scenario and its associated uncertainty.

The second element, *assessment and ranking of parameters*, consists of a comparison between the code calculations and experimental data to assess the code capability to reproduce the main relevant scenario phenomena, the scale-up capability, as well as to determine the ranges for the input parameters in the sensitivity analysis. Bounding techniques may be used, and not always code calculations are required in this step.

The third element, *sensitivity and uncertainty analyses*, consists of obtaining the calculated uncertainty of the parameters of interest (e.g. the PCT). Relevant contributors to uncertainty are determined, collected and combined to provide the desired summary statement. The total uncertainty is expressed in terms of a probability or error band for the safety criteria.

1.5.5.2 GSUAM method

The GSUAM method was developed in 1998 and used to support the licensing process of the Angra II NPP. The GSUAM method (generic statistical uncertainty analysis methodology) objective is to evaluate the uncertainty of point values, such as the peak cladding temperature (PCT), not including the time-dependent quantification of the uncertainty of the results. The methodology considers that the main sources of uncertainty are: the code, the plant conditions and the fuel conditions.

In this methodology, the code is expected to be the element of most influence on the overall uncertainty. The uncertainty is obtained by comparison between the experimental data and the calculation results. The uncertainty of the input parameters is addressed by applying sensitivity studies, in order to obtain the ranges of the uncertain parameters. Finally, the uncertainties obtained from each one of the three sources of uncertainties are combined using statistical methods.

1.5.5.3 UMAE/CIAU method

The UMAE (Uncertainty Methodology based on Accuracy Extrapolation) was developed at the University of Pisa at the end of the 80s. Later it was used to develop CIAU (Code with Capability of Internal Assessment of Uncertainty) in 2000. The UMAE/CIAU method makes use of the *the propagation of code output errors* approach for uncertainty evaluation [41]. The method is based on the propagation of uncertainties rather than on the input parameter's uncertainty. This propagation is obtained by calculating the uncertainty of results by extrapolating the accuracy from related ITFs experiments to the NPPs full scale.

The method is based on the following procedure: first, the plant status is considered by characterization using six relevant quantities in addition to transient time: the upper plenum pressure, the primary loop mass inventory, the steam generator pressure, the cladding surface temperature at 2/3 of core active length, the core power and the steam generator down-comer collapsed liquid level. Second, the extrapolated error or uncertainty is associated with each plant's status.

Finally, a matrix of hypercubes and a vector of time intervals define the plant statuses. For each point of a result of a calculation plotted versus time, a rectangle is defined, to account for both the time and quantity uncertainties. This methodology states that any point of the curve can take any value within its rectangle with a defined probability, in relation to the definition of the edges of the rectangles.

1.5.5.4 Statistical (GRS) method

The GRS method is the method applied in the BEPU comparison and described in detail in Chapter 4. The GRS method implements Wilks' method using order statistics. It considers sources of uncertainty of the calculations that have an impact on results due to several causes: modelling inconsistencies, BCs applied, or uncertainties of the physical models implemented in the code.

To account for the uncertainty sources, certain selected input values and code parameters are replaced by PDFs. Each PDF represents the uncertainty of the input variable, and are defined by a distribution type (uniform, normal, lognormal, ...), mean, range or standard deviation depending on the source of the uncertainty for the defined input parameter.

Since no particular input values are defined for the problem run, the problem must be run a number of times using each time a specific set of input variables generated obtained by random sampling from the defined PDFs. A relevant characteristic of the GRS method is the possibility of the evaluation of sensitivity measures of the importance of input parameter parameters deviation to the uncertainty of the results.

1.6 Research aims and objectives

The present study aims to evaluate the differences among standard practices when coupling TH-TH codes by using a combination (coupling) of system and sub-channel codes. For this purpose, the system code RELAP5, developed by the Idaho National Laboratory (INL) [14] has been coupled with CTF, a sub-channel thermal-hydraulics code developed and improved by the RDFMG at the North Carolina State University (NCSU) [16].

This combination of codes has the advantage that while RELAP5 provides the capability of accurately modelling system components and controls, CTF code provides a basis for highly detailed TH analysis within the core. Two coupling methods have been used to couple RELAP5 and CTF: on the one hand, an off-line coupling (OLC method), in which the system code (RELAP5) provides the time-dependent values to CTF as input tables for the boundary volumes and junctions at the core inlet and outlet and other parameters such as power. On the other hand, Weaver's semi-implicit coupling method [29] has been applied to couple RELAP5 and CTF (SIC method). This type of coupling method provides consistent pressures and velocities for the coupled codes at the coupling volumes and junctions.

Base case comparisons and sensitivity analysis are processes often applied for comparisons of calculations with different characteristics: different codes, physical models applied, modelling alternatives, etc. Previous works have focused on the uncertainty propagation in multi-physics and multi-scale simulations [51] [52] [53]. Recent studies on the uncertainty of sub-channel code results have shown that there is a strong influence on the BCs [51] [54] [55], and that among the relevant parameters the inlet temperature can be the most important parameter across each of the figures of merit (FOM) [56]. In order to compare how BCs variations in multi-scale calculations are affecting results, a further step is taken by applying BEPU analysis for comparison purposes.

According to the IAEA [23], *"the coupled codes are applied to confirm the existence of safety margins in the operating plants and are used to predict the realistic phenomena in innovative or advanced reactors"*. The proposal is to assess the OLC and SIC methods by applying the BEPU analysis as a source of additional information. The objective is to

analyze the differences in the calculation results and evaluate the influence of model uncertainties for both coupling methods in multi-scale simulations. The question is whether these differences are relevant and if they are related to the BCs imposed by each method.

The study consists of 4 main steps executed for both coupling methods (OLC and SIC): First, a qualitative comparison is carried out for the selected base cases. Second, a sensitivity analysis is performed to evaluate the impact of the uncertain parameters. Third, a set of relevant figures of merit (FOM) related to MDNBR is selected, and a BEPU analysis is carried out. The Spearman's rank correlation coefficients are then used for comparison between methods, and fourth: the differences between coupling methods are correlated to the differences between BCs in the OLC method.

CHAPTER 2

CTF AND RELAP5 CODES

This chapter contains:

- A description of CTF and RELAP5 codes, including:
- The definition of the conservation equations
- The numerical solution methods
- The code iterations, convergence and time step size management
- Relevant works performed with CTF and RELAP5 codes

2.1 CTF sub-channel code

2.1.1 CTF overview

COBRA-TF (Coolant-Boiling in Rod Arrays - Two Fluids) is a TH simulation code designed for light water reactor (LWR) vessel analysis. The code was developed in 1980 by PNL. It has undergone many improvements since it was created, and recently it has been improved, updated and rebranded as CTF by the RDFMG in PSU. In 2015, the RDFMG moved to NCSU, where CTF is being used and maintained until the present day. Among the improvements introduced by RDFMG is the translation of the source code to Fortran 90, the improvement of the turbulent mixing, void drift and direct heating models and the implementation of new numerical solution schemes.

CTF is designed to perform LWR safety analysis under a range of conditions. It includes a set of TH models to accurately predict core parameters under normal operation and accidental conditions. The models included are flow regime-dependent and include two-phase heat transfer, inter-phase heat transfer and drag, droplet breakup, and quench-front tracking [16]. The code predicts in an accurate way in 3-D the void fraction, the pressure drop across channels and the flow distribution in fuel bundles.

The code has the capability of running full-core sub-channel calculations [57]. It has been also validated against several ITFs experiments and it is widely used for transient analysis, LOCA analysis, and other applications. Table 2.1 shows the finite differential equations (FDE) solved by CTF and the independent variables. The code documentation includes three main documents: the CTF Theory Manual [16], the CTF User's Manual [58] and the preprocessor manual [59], which can be used to build large sub-channel models in an agile manner.

2.1.2 CTF conservation equations

CTF uses a two-fluid model combined with a three-field (liquid film, liquid droplets, and vapour) modelling approach. The generalized conservation equations are defined and

	Continuity of non-condensable (CN)
	Continuity of continuous liquid (CL)
Finite	Continuity of entrained liquid (CE)
Difference	Continuity of vapor (CV)
Equations	Energy of vapor (EV)
	Energy of continuous and entrained liquid (EL)
Independent	$\alpha_v P_v, \alpha_v, \alpha_v h_v, (1-\alpha_v) h_l, \alpha_v P_e, P$
Variables	$\alpha_v + \alpha_e + \alpha_l = 1$

Table 2.1: *CTF FDE and IV*

later adapted to the Cartesian and sub-channel forms. Then they are discretized and applied to the model mesh before being solved by an iterative process.

The set of conservation equations is applied to each field, with the consideration that the liquid and the droplet fields are assumed to be in thermal equilibrium and consequently, one energy equation is shared. The CTF generalized conservation equations apply to each node in the model, producing the conservation of the mass, momentum and energy of each field. The conservation equations include terms that account for the dependency of the equations on mass exchange processes between phases.

The generalized conservation equations are: the mass conservation equation (Equation 2.1), the momentum conservation equation (Equation 2.7) and the energy conservation equation (Equation 2.17).

- Generalized mass equation (Equation 2.1):

$$\frac{\partial}{\partial t}(\alpha_k \rho_k) + \nabla \cdot (\alpha_k \rho_k \vec{V_k}) = L_k + M_e^T \tag{2.1}$$

The first term of the left-hand side (LHS) of Equation 2.1 represents the change of mass in the control volume with respect to time, while the second term represents the advection term due to the mass transport. The first term of the right-hand side (RHS) accounts for the mass change for phase k (evaporation/condensation and/or

entrainment/de-entrainment). The term L_k is expressed as:

$$L_v = \Gamma''' \tag{2.2}$$

$$L_l = -(1-\eta)\Gamma''' - S''' \tag{2.3}$$

$$L_e = -\eta\Gamma''' + S''' \tag{2.4}$$

Where Γ''' is the volumetric mass transfer due to phase change and η is the fraction of phase change between vapour and entrained droplets.

$$\eta_{evap} = \text{min}\left(1 - \frac{Q'''_{wl}}{\Gamma''' H_{fg}}, \frac{\alpha_e}{1-\alpha_v}\right) \tag{2.5}$$

$$\eta_{cond} = \frac{\alpha_e}{1-\alpha_v} \tag{2.6}$$

Equations 2.5 and 2.6 show the phase change fraction between vapor and entrained droplets in case of evaporation or condensation. The term M_e^T of Equation 2.1 accounts for the mass transfer in the mesh cell due to turbulent mixing and void drift.

- Generalized momentum equation (Equation 2.7):

$$\begin{aligned} &\frac{\partial}{\partial t}\left(\alpha_k \rho_k \vec{V}_k\right) + \frac{\partial}{\partial x}\left(\alpha_k \rho_k u_k \vec{V}_k\right) + \frac{\partial}{\partial y}\left(\alpha_k \rho_k v_k \vec{V}_k\right) + \frac{\partial}{\partial z}\left(\alpha_k \rho_k w_k \vec{V}_k\right) \\ &= \alpha_k \rho_k \vec{g} - \alpha_k \nabla P + \nabla \cdot \left[\alpha_k \left(\boldsymbol{\tau}_k^{ij} + \boldsymbol{T}_k^{ij}\right)\right] + \vec{M}_k^L + \vec{M}_k^\partial + \vec{M}_k^T \end{aligned} \tag{2.7}$$

The first term of the LHS of Equation 2.7 represents the change of momentum in the control volume with respect to time. The second to the fourth terms represent the advection of momentum in the three-dimensional Cartesian coordinates. The terms of the RHS account for the following respective effects: gravitational force, pressure force, viscous and turbulent shear stress, momentum source/sink due to phase change, interfacial drag forces and momentum transfer due to turbulent mixing.

The turbulent shear stress is not considered in CTF, and to account for the turbulent mixing, a simple turbulent diffusion approximation is used. The viscous stress is

decomposed in wall shear and fluid to fluid shear components (see Equations 2.8, 2.9 and 2.10):

$$\nabla \cdot (\alpha_e \boldsymbol{\tau}_e^{ij}) = \vec{\tau}_{we}''' \tag{2.8}$$

$$\nabla \cdot (\alpha_v \boldsymbol{\tau}_v^{ij}) = \vec{\tau}_{wv}''' + \nabla \cdot (\alpha_v \boldsymbol{\sigma}_v^{ij}) \tag{2.9}$$

$$\nabla \cdot (\alpha_l \boldsymbol{\tau}_l^{ij}) = \vec{\tau}_{wl}''' + \nabla \cdot (\alpha_l \boldsymbol{\sigma}_l^{ij}) \tag{2.10}$$

The terms $\vec{\tau}_{we}'''$, $\vec{\tau}_{wv}'''$, and $\vec{\tau}_{wl}'''$ account for the volumetric wall drag and form losses for the 3 fields (e, v and l). The term $\nabla \cdot (\alpha_k \boldsymbol{\sigma}_k^{ij})$ accounts for the wall drag and assuming that the droplet field makes no contact with the walls, this term is omitted in the case of the droplet field.

$$\vec{M}_v^L = \Gamma''' \vec{V} \tag{2.11}$$

$$\vec{M}_l^L = -\Gamma'''(1-\eta)\vec{V} - S'''\vec{V} \tag{2.12}$$

$$\vec{M}_e^L = -\Gamma'''\eta\vec{V} + S'''\vec{V} \tag{2.13}$$

The $\vec{M}_k^L$ term in Equations 2.11, 2.12 and 2.13 accounts for the momentum variation caused by phase change and entrainment/de-entrainment.

The interfacial drag term $\vec{M}_k^\partial$ is defined for each field:

$$\vec{M}_v^\partial = -\vec{\tau}_{i,vl}''' - \vec{\tau}_{i,ve}''' \tag{2.14}$$

$$\vec{M}_l^\partial = \vec{\tau}_{i,vl}''' \tag{2.15}$$

$$\vec{M}_e^\partial = \vec{\tau}_{i,ve}''' \tag{2.16}$$

- Generalized energy equation (Equation 2.17):

$$\begin{aligned} &\frac{\partial}{\partial t}(\alpha_k \rho_k h_k) + \nabla \cdot (\alpha_k \rho_k h_k \vec{V}_k) \\ &= -\nabla \cdot [\alpha_k (\vec{Q}_k + \vec{q}_k^T)] + \Gamma_k h_k^i + q_{wk}''' + \alpha \frac{\delta P}{\delta t} \end{aligned} \tag{2.17}$$

The LHS terms of the energy equation (Equation 2.17) are the change of energy over time and the gain/loss of energy for the considered control volume. The RHS

terms considered are k-phase conduction and turbulence heat flux, energy transfer due to phase change, volumetric wall heat transfer, and the pressure work term. The $\vec{q}_k^T$ term represents the energy exchange in the processes of turbulent mixing and void drift. These terms are only used in the lateral and orthogonal directions.

2.1.3 Modification of the conservation equations

The CTF conservation equations are adapted to provide a numerical solution for the volume meshing considered. The conservation equations are either expanded to the Cartesian form or the sub-channel form. While in the expansion to the Cartesian form each field of the conservation equations is explicitly written out, for the case of the expansion to the sub-channel form only the two flow directions are considered (axial and lateral).

Volumes are connected to lateral adjacent volumes through gaps. Lateral flow includes the orthogonal and transverse directions, and it is considered to have no direction once it leaves a gap. This way, one momentum equation for each field is discarded. This is considered since the reduced lateral flow in a fuel bundle transfers little momentum to lateral adjacent volumes.

Afterwards, the equations are discretized to be later applied to the mesh generated from the geometry definition entered by the user. Two staggered meshes are used to account for different fields and to improve stability and accuracy: scalar and momentum meshes. The scalar mesh (Figure 2.1) defines the scalar variables such as α, P and h, while the momentum mesh defines the fluid velocity field (Figure 2.2).

The momentum mesh is divided into two different momentum meshes, one for the axial direction and one for the lateral direction. After defining the discretized conservation equations they are reformulated to the finite-difference form in order to solve the equation system for the mesh considered.

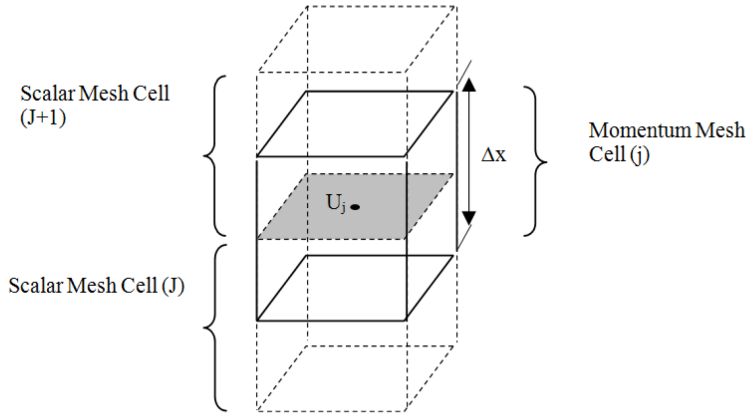

Figure 2.1: *CTF axial mesh cells (Source: CTF manual [16])*

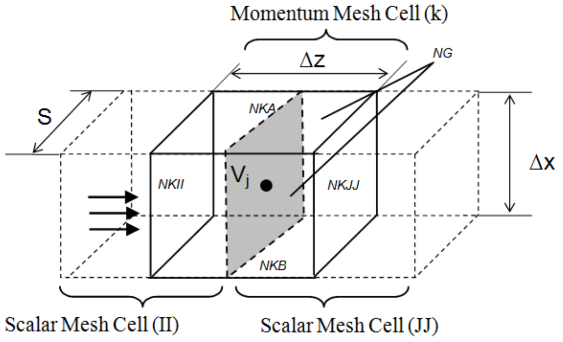

Figure 2.2: *CTF momentum mesh cells (Source: CTF manual [16])*

2.1.4 CTF numerical solution

CTF uses a form of the semi-implicit method for pressure-linked equations (SIMPLE) to solve the conservation equations. The SIMPLE algorithm consists of a series of steps based on the work by Patankar [60]:

1. Guess the pressure field, p^*: the pressure field is initialized by CTF using a user-entered value. CTF obtains the solution of the conservation equations of the next time-step using the previous time-step pressure field as a guess value for the new time-step.

2. Solve the momentum equations to obtain fluid velocities (u^*, v^*, and w^*): the trans-

verse momentum equations are solved firstly and the axial momentum equations are solved secondly.

3. Use the continuity equation to solve for the pressure field correction, p': the independent scalar and mass flow rates are solved using the previous time-step values and the effect of the pressure correction.

4. Calculate the corrected pressure field p by adding p' to p^*: the pressure field is obtained by adding p' to p^*. Back-substitution is performed in order to obtain the values for the other dependent variables.

5. Calculate the corrected velocity field (u, v, and w) using the corrected pressure field.

6. Solve remaining discretized equations that influence the flow field.

7. Use the corrected pressure (p) as the new guessed pressure (p^*).

2.1.5 Solution of the momentum, mass and energy equations

The transverse momentum equations are solved first and the axial momentum equations second. The liquid, droplet, and vapour transverse momentum equations are simultaneously solved for one gap at a time. The velocity field is first calculated using the previous pressure field, according to Step 1 in Section 2.1.4. Then the corrected pressure is obtained according to step 3, and it is used to correct the initial velocity field calculation. The continuity and energy equations are set as an equation system in which both the energy and mass are conserved (Equations 2.18 to 2.23).

$$C_g(\alpha_{mgas}, \alpha_v, \alpha_v h_v, (1-\alpha_v)h_l, \alpha_e, P_J, P_{i=1...nconn}) = 0 \tag{2.18}$$

$$C_l(\alpha_{mgas}, \alpha_v, \alpha_v h_v, (1-\alpha_v)h_l, \alpha_e, P_J, P_{i=1...nconn}) = 0 \tag{2.19}$$

$$E_v(\alpha_{mgas}, \alpha_v, \alpha_v h_v, (1-\alpha_v)h_l, \alpha_e, P_J, P_{i=1...nconn}) = 0 \tag{2.20}$$

$$E_l(\alpha_{mgas}, \alpha_v, \alpha_v h_v, (1-\alpha_v)h_l, \alpha_e, P_J, P_{i=1...nconn}) = 0 \tag{2.21}$$

$$C_e(\alpha_{mgas}, \alpha_v, \alpha_v h_v, (1-\alpha_v)h_l, \alpha_e, P_J, P_{i=1...nconn}) = 0 \tag{2.22}$$

$$C_v(\alpha_{mgas}, \alpha_v, \alpha_v h_v, (1-\alpha_v)h_l, \alpha_e, P_J, P_{i=1...nconn}) = 0 \tag{2.23}$$

The solution of Equations 2.18 to 2.23 does not only depend on the pressure of the J cell, P_J, it also depends on the pressures of the connected nodes to the node of interest ($P_{i=1..nconn}$). This is why the equations for all nodes in the system must be solved simultaneously.

In vector notation, the conservation equations are expressed as (where $\vec{f}$ represents the conservation equations and $\vec{x}$ represents the solution vector):

$$\vec{f}(\vec{x}) = \vec{0} \tag{2.24}$$

Equation 2.24 can be expressed as:

$$\vec{f}(\vec{x}) = \vec{f}(\vec{x}_0) + D\vec{f}(\vec{x}_0)(\vec{x} - \vec{x_0}) = 0 \tag{2.25}$$

Where $\vec{f}$ is the vector representing the mass and energy equations, $\vec{x}$ is the vector representing the value of the independent variable at the current time-step, and the $\vec{x_0}$ is the vector representing the value of the independent variables at the previous time-step and $D\vec{f}$ (Equation 2.26) is the Jacobian (rate of change of the functions with respect to the variables).

$$D\vec{f} = \begin{bmatrix} \frac{\partial}{\partial\alpha_v}C_l & \frac{\partial}{\partial\alpha_v h_v}C_l & \frac{\partial}{\partial(1-\alpha_v)h_l}C_l & \frac{\partial}{\partial\alpha_e}C_l & \frac{\partial}{\partial P_J}C_l & \frac{\partial}{\partial P_{i=1}}C_l & ... & \frac{\partial}{\partial P_{nconn}}C_l \\ \frac{\partial}{\partial\alpha_v}E_v & \frac{\partial}{\partial\alpha_v h_v}E_v & \frac{\partial}{\partial(1-\alpha_v)h_l}E_v & \frac{\partial}{\partial\alpha_e}E_v & \frac{\partial}{\partial P_J}E_v & \frac{\partial}{\partial P_{i=1}}E_v & ... & \frac{\partial}{\partial P_{nconn}}E_v \\ \frac{\partial}{\partial\alpha_v}E_l & \frac{\partial}{\partial\alpha_v h_v}E_l & \frac{\partial}{\partial(1-\alpha_v)h_l}E_l & \frac{\partial}{\partial\alpha_e}E_l & \frac{\partial}{\partial P_J}E_l & \frac{\partial}{\partial P_{i=1}}E_l & ... & \frac{\partial}{\partial P_{nconn}}E_l \\ \frac{\partial}{\partial\alpha_v}C_e & \frac{\partial}{\partial\alpha_v h_v}C_e & \frac{\partial}{\partial(1-\alpha_v)h_l}C_e & \frac{\partial}{\partial\alpha_e}C_e & \frac{\partial}{\partial P_J}C_e & \frac{\partial}{\partial P_{i=1}}C_e & ... & \frac{\partial}{\partial P_{nconn}}C_e \\ \frac{\partial}{\partial\alpha_v}C_v & \frac{\partial}{\partial\alpha_v h_v}C_v & \frac{\partial}{\partial(1-\alpha_v)h_l}C_v & \frac{\partial}{\partial\alpha_e}C_v & \frac{\partial}{\partial P_J}C_v & \frac{\partial}{\partial P_{i=1}}C_v & ... & \frac{\partial}{\partial P_{nconn}}C_v \end{bmatrix} \tag{2.26}$$

In Equation 2.24, the term $\vec{f}(\vec{x})$ must be zero in order to maintain the mass and energy conservation in the domain. Also, if changing the variables $\Delta\vec{x} = \vec{x} - \vec{x}_0$, Equation 2.24

results in:

$$D\vec{f}(\vec{x}_0)\Delta\vec{x} = -\vec{f}(\vec{x}_0) \tag{2.27}$$

The RHS of Equation 2.27 contains the conservation equations considering the previous time-step values ($\vec{x}_0$) for the variables. In the case of steady-state, these values would imply that $-\vec{f}(\vec{x}_0) = 0$, since the mass/energy balance would be maintained under the same circumstances, but in the case of transient, the velocities would have changed, then the term $-\vec{f}(\vec{x}_0)$ would contain residual values. Prior to obtaining the solution to the pressure matrix, a Jacobian ($D\vec{f}(\vec{x}_0)$) and a set of residual values ($-\vec{f}(\vec{x}_0)$) are set for each cell in the mesh.

2.1.6 Solution of the pressure matrix and back-substitution

The Jacobian matrix ($D\vec{f}(\vec{x}_0)$) is reduced by using Gaussian elimination. After this, the pressure equation for each node in the domain is obtained at the bottom row of each matrix (see Equation 2.28). The pressure equations are extracted from Equation 2.28, with the form of Equation 2.29:

$$\begin{bmatrix}
\frac{\partial}{\partial\alpha_{mgas}}C_{cg} & \frac{\partial}{\partial\alpha_v}C_{cg} & \frac{\partial}{\partial\alpha_v h_v}C_{cg} & \frac{\partial}{\partial(1-\alpha_v)h_l}C_{cg} & \frac{\partial}{\partial\alpha_e}C_{cg} & \frac{\partial}{\partial P_J}C_{cg} & \frac{\partial}{\partial P_{i=1}}C_{cg} & \frac{\partial}{\partial P_{nc}}C_l \\
\frac{\partial}{\partial\alpha_{mgas}}C_l & \frac{\partial}{\partial\alpha_v}C_l & \frac{\partial}{\partial\alpha_v h_v}C_l & \frac{\partial}{\partial(1-\alpha_v)h_l}C_l & \frac{\partial}{\partial\alpha_e}C_l & \frac{\partial}{\partial P_J}C_l & \frac{\partial}{\partial P_{i=1}}C_l & \frac{\partial}{\partial P_{nc}}C_l \\
\frac{\partial}{\partial\alpha_{mgas}}C_v & \frac{\partial}{\partial\alpha_v}C_v & \frac{\partial}{\partial\alpha_v h_v}C_v & \frac{\partial}{\partial(1-\alpha_v)h_l}C_v & \frac{\partial}{\partial\alpha_e}C_v & \frac{\partial}{\partial P_J}C_v & \frac{\partial}{\partial P_{i=1}}C_v & \frac{\partial}{\partial P_{nc}}C_v \\
\frac{\partial}{\partial\alpha_{mgas}}C_e & \frac{\partial}{\partial\alpha_v}C_e & \frac{\partial}{\partial\alpha_v h_v}C_e & \frac{\partial}{\partial(1-\alpha_v)h_l}C_e & \frac{\partial}{\partial\alpha_e}C_e & \frac{\partial}{\partial P_J}C_e & \frac{\partial}{\partial P_{i=1}}C_e & \frac{\partial}{\partial P_{nc}}C_e \\
\frac{\partial}{\partial\alpha_{mgas}}E_l & \frac{\partial}{\partial\alpha_v}E_l & \frac{\partial}{\partial\alpha_v h_v}E_l & \frac{\partial}{\partial(1-\alpha_v)h_l}E_l & \frac{\partial}{\partial\alpha_e}E_l & \frac{\partial}{\partial P_J}E_l & \frac{\partial}{\partial P_{i=1}}E_l & \frac{\partial}{\partial P_{nn}}E_l \\
\frac{\partial}{\partial\alpha_{mgas}}E_v & \frac{\partial}{\partial\alpha_v}E_v & \frac{\partial}{\partial\alpha_v h_v}E_v & \frac{\partial}{\partial(1-\alpha_v)h_l}E_v & \frac{\partial}{\partial\alpha_e}E_v & \frac{\partial}{\partial P_J}E_v & \frac{\partial}{\partial P_{i=1}}E_v & \frac{\partial}{\partial P_{nc}}E_v
\end{bmatrix} \tag{2.28}$$

$$\begin{bmatrix} \partial\alpha_{mgas} \\ \partial\alpha_v \\ \partial\alpha_v h_v \\ \partial(1-\alpha_v)h_l \\ \partial\alpha_e \\ \partial P_J \\ \partial P_{i=1} \\ \partial P_{i=nconn} \end{bmatrix} = - \begin{bmatrix} E_{CG} \\ E_{CL} \\ E_{CV} \\ E_{CE} \\ E_{EL} \\ E_{EV} \end{bmatrix} \tag{2.28}$$

$$dP_J = a_5 + \sum_{i=1}^{nconn} (g_{5,i} dP_i) \tag{2.29}$$

The pressure equations are combined forming a single pressure matrix, with the unknown dP_J, which accounts for the pressure changes over a time-step for each node J. Once the dP_J are obtained, back-substitution is used to calculate the other new time-step variables using Equation 2.30 with the form of Equations 2.31 to 2.34. Also, the velocities are updated using the momentum equations.

$$\begin{bmatrix} 1 & -c_1 & -d_1 & -e_1 & -f_1 & -g_{1,1} & ... & -g_{1,nconn} \\ 0 & 1 & -d_2 & -e_2 & -f_2 & -g_{2,1} & ... & -g_{2,nconn} \\ 0 & 0 & 1 & -e_3 & -f_3 & -g_{3,1} & ... & -g_{3,nconn} \\ 0 & 0 & 0 & 1 & -f_4 & -g_{4,1} & ... & -g_{4,nconn} \\ 0 & 0 & 0 & 0 & 1 & -g_{5,1} & ... & -g_{5,nconn} \end{bmatrix} \begin{bmatrix} d\alpha_v \\ d\alpha_v h_v \\ d(1-\alpha_v)h_l \\ d\alpha_e \\ dP_J \\ dP_{i=1} \\ ... \\ dP_{nconn} \end{bmatrix} = \begin{bmatrix} a_1 \\ a_2 \\ a_3 \\ a_4 \\ a_5 \end{bmatrix} \tag{2.30}$$

$$d\alpha_e = a_4 + f_4 dP_J + \sum_{i=1}^{nconn} (g_{4,i} dP_i) \tag{2.31}$$

$$d[(1-\alpha_v)h_l] = a_3 + e_3 d\alpha_e + f_3 dP_J + \sum_{i=1}^{nconn} (g_{3,i} dP_i) \tag{2.32}$$

$$d(\alpha_v h_v) = a_2 + d_2 d[(1-\alpha_v)h_l] + e_2 d\alpha_e + f_2 dP_J + \sum_{i=1}^{nconn} (g_{2,i} dP_i) \tag{2.33}$$

$$d\alpha_v = a_1 + c_1 d(\alpha_v h_v) + d_1 d[(1-\alpha_v)h_l] + e_1 d\alpha_e + f_1 dP_J + \sum_{i=1}^{nconn} (g_{1,i} dP_i) \tag{2.34}$$

2.1.7 Iterations, convergence and time-step size

The CTF iterations can be divided into two steps. First, the *inner iteration* consists of solving the pressure correction equations. This process of solving the equations in a matrix form requires special high-dimensional linear solver methods such as direct Gaussian elimination or the iterative Krylov methods. Second, the *outer iteration* consists of the sequential execution of steps 1 to 6 described in Section 2.1.4.

At the end of the outer iteration, the calculation convergence is checked against a set of convergence criteria. If the convergence criteria are not met the time-step is reduced and the outer iteration is repeated. The processes related to time-step size control are described in more detail since they are closely related to the coupling of CTF and RELAP5 performed in this work.

Time-step control in CTF is achieved by controlling a series of variables when defining the time-step value, these variables are the Courant limit, the pressure change, the iteration count, the void fraction change, and the total error.

- The time-step related to the courant limit (considering mesh size and flow velocity) is calculated using equation 2.35:

$$\Delta t < \left| \frac{\Delta X}{U} \right| \tag{2.35}$$

- The time-step correction due to pressure change is obtained by applying Equation 2.36, where $dP_{max,0}$ is the maximum pressure change at the previous time-step and $dP_{max,i}$ is the maximum pressure change at the current time-step.

$$\Delta t_P = \Delta t_o \frac{\partial P_{max,0}}{\partial P_{max,i}} \tag{2.36}$$

- The time-step correction due to void fraction change is obtained by applying Equation 2.37, where the old time-step is multiplied by 0.5 and divided by the maximum void fraction change ($\Delta \alpha_{v,max}$):

$$\Delta t_{\text{void}} = \Delta t_o * \frac{0.5}{\Delta \alpha_{v,max}} \tag{2.37}$$

- For a number of outer iterations > 5, the ratio of 5 to the number of iterations is multiplied by the time-step size. If the number of inner iterations is larger than 70% of the maximum allowed number of inner iterations, the time-step size is multiplied by the ratio of 70% of the maximum allowed number of inner iterations. If neither of these cases is true, the time-step size is increased by 5%.
- For a maximum pressure change > 0.1 at the previous time step, the new time-step size is multiplied by the ratio of 0.1 to the maximum previous time-step pressure change.

2.1.8 W-3 correlation

The selected correlation to evaluate the CHF in CTF is the W-3 correlation, developed by Tong [61] [62]. This correlation is widely used to evaluate the CHF in PWR fuel arrays [63].

The CHF is defined as:

$$\begin{aligned}\frac{q_{w3,D''_{heated,u}}}{10^6} &= [(2.022 - 0.0004302p) + (0.1722 - 0.0000984p) \\ &\exp[(18.177 - 0.004129p)x_e]][(0.1484 - 1.596x_e + 0.1729x_e|x_e|)\frac{G}{10^6} \\ &+ 1.037](1.157 - 0.869x_e)[0.2664 + 0.8357\exp(-3.151D_{heated})] \\ &[0.8258 + 0.000794(h_f - h_{in})]\end{aligned} \tag{2.38}$$

Where

- $q''_{w3,D_{heated},u}$ is the critical heat flux based on heated diameter [$BTU/hr \cdot ft^2$]
- p is pressure [$psia$]
- x_e is the local steam thermodynamic quality

- D_{heated} is the heated hydraulic diameter [in]
- h_{in} is the inlet enthalpy [BTU/lbm]
- G is the mass flux [$\frac{lbm}{hr \cdot ft^2}$]

The applicability of W-3 correlation is related to the following parameters ranges:

- p = 800 to 2300 [$psia$]
- $\frac{G}{10^6}$ = 1.0 to 5.0 [$lbm/hr \cdot ft^2$]
- D_{heated} = 0.2 to 0.7 [in]
- x_e = -0.15 to 0.15
- L = 10 to 144 [in]

Tong used the hydraulic diameter instead of the heated hydraulic diameter in the original form of Equation 2.38. The influence of unheated surfaces was taken into account by adding the following cold wall factor:

$$\frac{q''_{w3,cold\ wall,u}}{q''_{w3,D_{heated},u}} = 1.0 - Ru[13.76 - 1.372e^{1.78x_e} - 4.732(\frac{G}{10^6})^{-0.0535} - 0.0619(\frac{p}{10^3})^{0.14} - 8.509(D_{heated})^{0.107}] \quad (2.39)$$

Where:

$$Ru = 1 - \frac{D_h}{D_{heated}} \quad (2.40)$$

CTF takes into account the cold wall factor for the W-3 correlation. This factor is used in conjunction with the form of Equation 2.38 using the heated hydraulic diameter, as prescribed by Tong. Equation 2.39 is intended for use with constant axial heat distributions. The Tong F-factor is used to modify $q''_{chf,cold\ wall,nu}$ in case of non-uniform axial heat flux profiles:

$$q''_{chf,cold\ wall,nu} = \frac{q''_{w3,cold\ wall,u}}{F} \tag{2.41}$$

Tong used a theoretical basis to develop the F-Factor by analyzing a control volume over the boundary layer. His assessment takes upstream heating into account, resulting in an integration from the axial location where boiling starts to the current location being analyzed.

The Tong F-Factor is obtained by applying Equation 2.42:

$$F = \frac{C \int_0^l q''(z') \exp([-C * (l - z')]\, dz'}{q'' * l\, [1 - \exp(-C * l)]} \tag{2.42}$$

Where l is the axial location where CHF is being calculated.

The C term is a factor that accounts for flow quality and mass flux, as defined as follows:

$$C = 0.15 \frac{(1.0 - x_{DNB})^4 .31}{(G/10^6)^{0.478}} \tag{2.43}$$

2.2 RELAP5 system code

2.2.1 RELAP5 overview

The RELAP5 code is a program developed by Idaho National Laboratory (INL) and funded by NRC [14]. It is designed for BE transient simulation of LWR coolant systems during postulated accidents. The RELAP5 hydrodynamic model is a one-dimensional, transient, two-fluid model for two-phase steam-water mixture flow that can contain noncondensable components in the steam phase and/or a soluble component in the water phase. The two-fluid equations consist of two phasic continuity equations, two phasic momentum equations, two phasic energy equations, a continuity equation of noncondensable gases and a field equation for the conservation of the solute (as shown in Table 2.2).

	Density of non-condensable
Finite	Energy of vapor
Difference	Energy of liquid
Equations	Difference density equations
	Sum density equation
Independent	$X_n, U_g, U_f, \alpha_g, P$
Variables	$\alpha_g + \alpha_l = 1$

Table 2.2: *RELAP5 FDE and IV*

RELAP5 is based on a nonhomogeneous and nonequilibrium model for the two-phase system that is solved using a partially implicit numerical scheme to permit an economical calculation of system transients. Different models of components found in plant systems can be simulated, such as pumps, valves, pipes, heat structures, reactor point kinetics, electric heaters, jet pumps, turbines, separators, accumulators, and control system components.

Also, special process models are included for effects such as form loss, flow at an abrupt area change, branching, choked flow, boron tracking, and noncondensable gas transport. RELAP5 is used generally to model the entire plant system, using a rela-

tively coarse model for the core, then providing less accurate results of the local limiting conditions. RELAP5 critical heat flux condition prediction is based on look-up tables for various geometries: pipes, vertical parallel plates, vertical and horizontal tube bundles and horizontal flat plates.

The code documentation includes: the description of the code structure, system models and solution methods [14], the code input deck requeriments [64], and the programmers manual [64].

2.2.2 RELAP5 conservation equations

RELAP5 uses a two-fluid model for two-phase flow consisting of a steam-water mixture. The steam phase can contain noncondensable gases and the liquid phase can contain one soluble component. The conservation equations set for the two-fluid model are composed of two continuity equations, two momentum equations, and two energy equations. One equation is presented for each phase (g and f):

- Mass continuity equations (Equations 2.44 and 2.45):

  The equations are taken from the one-dimensional phasic mass equations in Reference [65]:

  $$\frac{\partial}{\partial t}(\alpha_g \rho_g) + \frac{1}{A}\frac{\partial}{\partial x}(\alpha_g \rho_g v_g A) = \Gamma_g \tag{2.44}$$

  $$\frac{\partial}{\partial t}(\alpha_f \rho_f) + \frac{1}{A}\frac{\partial}{\partial x}(\alpha_f \rho_f v_f A) = \Gamma_f \tag{2.45}$$

  The first term of the LHS of Equations 2.44 and 2.45 represents the change of mass in the volume with respect to time, and the second term represents the advection term due to the mass transport. The RHS terms $\Gamma_{g,f}$ account for the mass change for phase g or f (evaporation/condensation). The term $\Gamma_{g,f}$ are expressed as:

  $$\Gamma_f = -\Gamma_g \tag{2.46}$$

  The mass that changes phase is the same in the gas and liquid phase with no mass gain. The interfacial mass transfer model divides the mass transfer at the

vapour/liquid interface depending on two possible locations: an exchange at the interface in the bulk fluid (Γ_{ig}) or at the boundary layer near the walls (Γ_w):

$$\Gamma_g = \Gamma_{ig} + \Gamma_w \tag{2.47}$$

- Momentum conservation equations (Equations 2.48 and 2.49):

  The momentum effects are less relevant than mass and energy conservation in reactor safety analyses. Since nuclear reactor flows are dominated by large sources and sinks of momentum (i.e. pumps, abrupt area change) A less exact formulation is considered acceptable for the momentum conservation equations. The momentum conservation equations are taken from the one-dimensional phasic momentum equations in Reference [65]:

$$\begin{aligned}\alpha_g\rho_g A\frac{\partial v_g}{\partial x} + \frac{1}{2}\alpha_g\rho_g A\frac{\partial v_g^2}{\partial x} &= -\alpha_g A\frac{P}{\partial x} + \alpha_g\rho_g B_x A - (\alpha_g\rho_g A)FWG(v_g) \\ &+\Gamma_g A(v_{gI} - vg) - (\alpha_g\rho_g A)FIG(v_{gI} - vg) \\ &- C\alpha_g\alpha_f\rho_m A\left[\frac{\partial v_g - dv_f}{\partial t} + v_f\frac{\partial v_g}{\partial x} + v_g\frac{\partial v_f}{\partial x}\right]\end{aligned} \tag{2.48}$$

$$\begin{aligned}\alpha_f\rho_f A\frac{\partial v_f}{\partial x} + \frac{1}{2}\alpha_f\rho_f A\frac{\partial v_f^2}{\partial x} &= -\alpha_f A\frac{P}{\partial x} + \alpha_f\rho_f B_x A - (\alpha_f\rho_f A)FWF(v_f) \\ &+\Gamma_f A(v_{fI} - vf) - (\alpha_f\rho_f A)FIF(v_{fI} - vf) \\ &- C\alpha_f\alpha_g\rho_m A\left[\frac{\partial v_f - dv_g}{\partial t} + v_g\frac{\partial v_f}{\partial x} + v_f\frac{\partial v_g}{\partial x}\right]\end{aligned} \tag{2.49}$$

  The following simplifications have been taken into account:

  - the Reynolds stresses are neglected
  - the phasic pressures are assumed equal
  - the interfacial pressure is assumed to be equal to the phasic pressures (except for stratified flow)
  - the covariance terms are universally neglected
  - interfacial momentum storage is neglected

- phasic viscous stresses are neglected
- the interface force terms consist of both pressure and viscous stresses
- the normal wall forces are assumed adequately modelled by the variable area momentum flux formulation

The first term of the RHS of Equations 2.48 and 2.49 represent, respectively, the pressure gradient, the body force, wall friction, momentum transfer due to interface mass transfer, interface frictional drag, and force due to virtual mass. The terms FWG and FWF are part of the wall frictional drag, which are linear in velocity, and are products of the friction coefficient, the frictional reference area per unit volume, and the magnitude of the fluid bulk velocity. The terms FIG and FIF are part of the interface frictional drag; two different models (drift flux and drag coefficient) are used for the interface friction drag.

- Energy conservation equations (Equations 2.50 and 2.51):

The equations are taken from the one-dimensional phasic thermal energy equations in Reference [65]:

$$\frac{\partial}{\partial t}(\alpha_g \rho_g U_g) + \frac{1}{A}\frac{\partial}{\partial x}(\alpha_g \rho_g U_g v_g A) = -P\frac{\partial \alpha_g}{\partial t} - \frac{P}{A}\frac{\partial}{\partial x}(\alpha_g v_g A) + Q_{wg} + Q_{ig} + \Gamma_{ig} h_g^* + \Gamma_w h_g^{'} + DISS_g \quad (2.50)$$

$$\frac{\partial}{\partial t}(\alpha_f \rho_f U_f) + \frac{1}{A}\frac{\partial}{\partial x}(\alpha_f \rho_f U_f v_f A) = -P\frac{\partial \alpha_f}{\partial t} - \frac{P}{A}\frac{\partial}{\partial x}(\alpha_f v_f A) + Q_{wf} + Q_{if} + \Gamma_{if} h_f^* + \Gamma_w h_f^{'} + DISS_f \quad (2.51)$$

The following simplifications have been taken into account:

- the Reynolds heat flux is neglected
- the covariance terms are universally neglected
- interfacial energy storage is neglected
- internal phasic heat transfer is neglected

The first term of the LHS of Equations 2.50 and 2.51 represents the change of energy in the volume with respect to time, and the second term represents the

advection term due to the energy transport. Q_{wg} and Q_{wf} represent the phasic wall heat transfer rates per unit volume. These phasic wall heat transfer rates satisfy the following :

$$Q = Q_{wg} + Q_{wf} \tag{2.52}$$

Where Q is the total wall heat transfer rate to the fluid per unit volume.

The phasic enthalpies associated with bulk interface mass transfer (h_g, h_f) and with the thermal boundary layer ($h_g^{'}$, $h_f^{'}$) in Equations 2.50 and 2.51 are defined in order to satisfy the energy change when changing from liquid to vapour and vice-versa. Q_{ig}, Q_{if} are defined as the interface heat transfer terms and include heat transfer from the fluid states to the interface due to interface energy exchange in the bulk and the thermal boundary layer near the wall.

The vapour generation and condensation rates are established from energy balance considerations at the interface between the bulk and the thermal boundary layer. The dissipation terms considered in the energy conservation equation are the phasic energy dissipation for the wall friction and pump effects, included in the terms $DISS_g$ and $DISS_f$ (Equations 2.53 and 2.54). The term $DISS$ in Equation 2.55 represents the energy dissipation:

$$DISS_g = \alpha_g \rho_g FWG v_g^2 \tag{2.53}$$

$$DISS_f = \alpha_f \rho_f FWF v_f^2 \tag{2.54}$$

$$DISS = DISS_g + DISS_f \tag{2.55}$$

2.2.3 Semi-implicit scheme difference equations

The numerical scheme makes use of the equations that result from expanding the time derivative in the basic density and energy differential equations (expanded form). The semi-implicit numerical solution scheme is based on replacing the system of differential equations with a system of finite-difference equations partially implicit in time. In all cases, the implicit terms are formulated to be linear in the dependent variables at the new time.

An additional feature of the scheme is that implicitness is selected such that the field equations can be reduced to a single difference equation per fluid control volume in terms of the hydrodynamic pressure. Then, for a model with N control volumes, a system of $N * N$ equations must be solved at each time-step.

The difference equations are defined for every control volume by imposing that the mass and energy balance is maintained. This is achieved by equating the addition or subtraction through the control volume boundaries to the rate of change and source terms. By using this model, the mass and energy must be defined at the centre of the control volumes and the velocities must be defined at the boundaries. This results in a staggering spatial mesh with the volume properties defined at the centre of the mass/energy control volumes and the junction (j) properties defined at the centre of the momentum control volumes (see Figure 2.3).

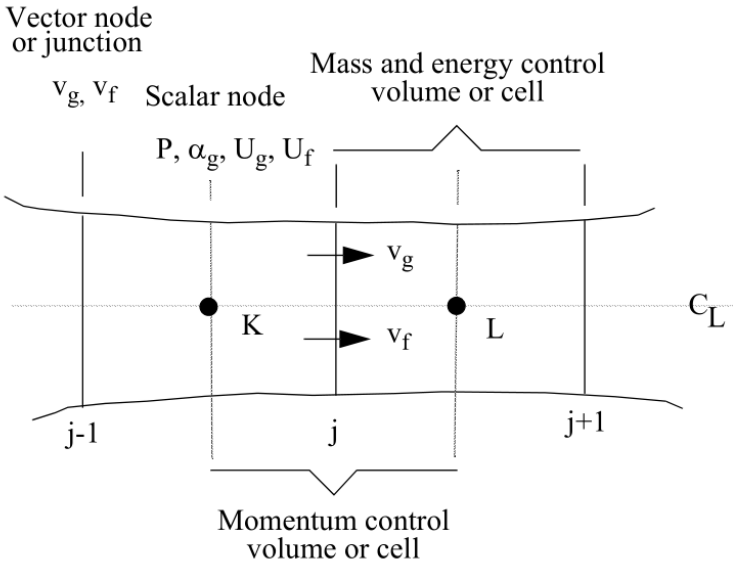

Figure 2.3: *RELAP5 control volume (Source: RELAP5 manual [15])*

2.2.4 Semi-implicit numerical solution scheme

The solution scheme is presented with the consideration that two phases are present in both old-time (n) and new-time (n+1) for a specific control volume. The expanded density and energy difference equations are displayed in the following order:

1. Noncondensable density equation
2. Vapor energy equation
3. Liquid energy equation
4. Difference density equation
5. Sum density equation

The energy and density variables are then expressed as differences between the old-time (n) and new-time (n+1) values, in order:

1. $\tilde{X}_{n,L}^{n+1} - X_{n,L}^{n}$
2. $\tilde{U}_{g,L}^{n+1} - U_{g,L}^{n}$
3. $\tilde{U}_{f,L}^{n+1} - U_{f,L}^{n}$
4. $\tilde{\alpha}_{g,L}^{n+1} - \alpha_{g,L}^{n}$
5. $P_{L}^{n+1} - P_{L}^{n}$

Considering that volume L in Figure 2.3 is connected to two volumes, Equation 2.56 represents the full set of conservation equations in matrix form in RELAP5:

$$Ax = \tilde{b} + \tilde{g}^1 v_{g,j+1}^{n+1} + \tilde{g}^2 v_{g,j}^{n+1} + \tilde{f}^1 v_{\tilde{f},j+1}^{n+1} + f^2 v_{f,j}^{n+1} \tag{2.56}$$

Where $\tilde{A}$, $\tilde{x}$, $\tilde{b}$, $\tilde{g}^1$, $\tilde{g}^2$, $\tilde{f}^1$ and $\tilde{f}^2$ are:

$$\tilde{A} = \begin{bmatrix} A_{11} & A_{12} & 0 & A_{14} & A_{15} \\ A_{21} & A_{22} & A_{23} & A_{24} & A_{25} \\ A_{31} & A_{32} & A_{33} & A_{34} & A_{35} \\ A_{41} & A_{42} & A_{43} & A_{44} & A_{45} \\ A_{51} & A_{52} & A_{53} & A_{54} & A_{55} \end{bmatrix} \tag{2.57}$$

$$\tilde{x} = \begin{bmatrix} \tilde{X}_{n,L}^{n+1} - X_{n,L}^{n} \\ \tilde{U}_{g,L}^{n+1} - U_{g,L}^{n} \\ \tilde{U}_{f,L}^{n+1} - U_{f,L}^{n} \\ \tilde{\alpha}_{g,L}^{n+1} - \alpha_{g,L}^{n} \\ P_{L}^{n+1} - P_{L}^{n} \end{bmatrix} \tag{2.58}$$

$$\tilde{b} = \begin{bmatrix} 0 \\ b_{21} \\ b_{31} \\ b_{41} \\ 0 \end{bmatrix} \quad (2.59) \qquad \tilde{g}^1 = \begin{bmatrix} g_{11} \\ g_{21} \\ 0 \\ g_{41} \\ g_{51} \end{bmatrix} \quad (2.60) \qquad \tilde{g}^2 = \begin{bmatrix} g_{11} \\ g_{21} \\ 0 \\ g_{41} \\ g_{51} \end{bmatrix} \quad (2.61) \qquad \tilde{f}^1 = \begin{bmatrix} 0 \\ 0 \\ f_{31} \\ f_{41} \\ f_{51} \end{bmatrix} \quad (2.62) \qquad \tilde{f}^2 = \begin{bmatrix} 0 \\ 0 \\ f_{31} \\ f_{41} \\ f_{51} \end{bmatrix} \quad (2.63)$$

The matrix $\tilde{A}$ is a 5 x 5 matrix where each row contains the conservation equations, the vector $\tilde{x}$ contains the ordered variables, and vectors $\tilde{b}$, $\tilde{g}^1$, $\tilde{g}^2$, $\tilde{f}^1$ and $\tilde{f}^2$ contain old-time values. The $A_{i,x}$, $b_{i,x}$ and $f_{i,x}$ equations are defined in Reference [14].

2.2.5 Solution of the pressure matrix and back-substitution

Since matrix A and vectors b, g^1, g^2, f^1, f^2 in Equation 2.56 contain only old-time values, if both sides of the equation are multiplied by the bottom row of the inverse of the matrix A, A_5^{-1}, it becomes the pressure equation:

$$\delta P_L^{n+1} = A_5^{-1}(b + g^1 v_{g,j+1}^{n+1} + g^2 v_{g,j}^{n+1} + f^1 v_{f,j+1}^{n+1} + f^2 v_{f,j}^{n+1}) \quad (2.64)$$

Where:

$$v_{g,j}^{n+1} = \tilde{v}_{g,j}^{n+1} + \frac{\partial v_g}{\partial \Delta P}(\delta P_{K,j}^{n+1} - \delta P_{L,j}^{n+1}) \quad (2.65)$$

$$v_{f,j}^{n+1} = \tilde{v}_{f,j}^{n+1} + \frac{\partial v_f}{\partial \Delta P}(\delta P_{K,j}^{n+1} - \delta P_{L,j}^{n+1}) \quad (2.66)$$

A system matrix is then set using the pressure equation (Equation 2.64) for each volume, so the changes in pressures are expressed in terms of the velocities at the junctions between the volumes. Then, with the momentum equations (Equation 2.65 and Equation 2.66) the change in pressures at the volumes and velocities at the junctions in all domain are obtained. Using the new-time velocities in Equation 2.56, the provisional time variables $\tilde{X}_{n,L}^{n+1}$, $\tilde{U}_{g,L}^{n+1}$, $\tilde{U}_{f,L}^{n+1}$, $\tilde{\alpha}_{g,L}^{n+1}$ are also obtained. To compute the new values,$X_{n,L}^{n+1}$,

$U_{g,L}^{n+1}$, $U_{f,L}^{n+1}$ and $\alpha_{g,L}^{n+1}$, the unexpanded form of energy and mass difference equations is used (as described in Reference [14]).

2.2.6 Iterations, convergence and time-step size

RELAP5 checks the Courant limit to control the time-step before a hydrodynamic advancement takes place. As a consequence, the time-step may be reduced, but it does not cause a time-step to be repeated. The Courant limit is calculated using Equation 2.67, where $V_{K,L}$ is the volume of upstream volume, volume K or volume L (m3), A_j is the area of junction j (m^2) and v_j is the velocity at junction j (m/s).

$$\Delta t_c = \frac{V_{K,L}}{A_j v_j} \tag{2.67}$$

A specific Courant limit is calculated at each junction separately for liquid and vapour. The Courant limit is calculated at the beginning of the time-step using old-time phasic velocities. The Courant limit is calculated as the minimum time-step for all junctions:

$$\Delta t_c = min(\sum_{j}^{njuns} (\Delta t_c)_{fj}, \sum_{j}^{njuns} (\Delta t_c)_{gj}) \tag{2.68}$$

2.3 Relevant works performed with CTF and RELAP5

This section describes two relevant works using CTF and RELAP5 that provide a good example of the codes applicability and capabilities. The first case is related to MDNBR calculations in a full-core model using CTF. The second case is related to plant calculations with the objective of qualifying integral plant models using RELAP5.

2.3.1 BEPU analysis of MDNBR with VERA-CS in response to MSLB event in PWR

In this work, the core calculations are performed to simulate the core behaviour of a typical Westinghouse 4-loop PWR in response to a main steam line break (MSLB) accident [56]. The simulation was performed by using VERA-CS (Virtual Environment for Reactor Applications, Core Simulator), which consists of a coupled neutron transport and thermal-hydraulics sub-channel code under development by the Consortium for Advanced Simulation of Light Water Reactors (CASL).

The code includes three main components: MPACT (reactor physics and neutron transport), COBRA-TF (thermal-hydraulics), and ORIGEN (isotopic depletion). The VERA-CS validation process included testing the core physics [66], including the full-core modelling of the Watts Bar Nuclear Unit 1 fuel cycles [67], and startup core modelling for the Westinghouse AP1000 NPP [66].

The model was a typical 17x17 PWR fuel assembly with 264 fuel rods, 24 guide tubes, and 1 instrumentation tube. The BCs to apply to VERA-CS were determined by using a system code, while the core inlet flow and temperature distributions were obtained using a CFD code. The study included BEPU analysis for the cases of either with or without loss of off-site power in coincidence with the accident, resulting in high or low flow cases. The objective of the study was to provide the MDNBR, calculated by using the W-3 correlation, at the 95/95 (95% probability with 95% confidence level) tolerance limit.

The sensitivity analysis was performed for 59 cases by using Pearson's correlation coefficients. Results show that there was a margin with respect to the MDNBR safety limit, being the case of available off-site power being more restrictive. This work provides

an example where CTF can be used to provide a TH simulation of a full core response to transients with nonhomogeneous inlet flow distributions, in combination with detailed core power profiles.

2.3.2 Advanced qualification process of NPP models with RELAP5

This work provides insight into the qualification process and configuration control of extensive and detailed NPP models in RELAP5 [68]. The plant models are large models in the way of having more than 600 hydrodynamic volumes and more than 1500 control variables and logical trips. Aside from detailed nodalizations of the core, RCS, pressurizer and the SGs, many auxiliary systems are modelled (safety injection systems, main steam lines, main and auxiliary feed-water systems). All the systems are controlled by implementing the sometimes complex plant controls through the extrapolation to RELAP5 of the plant control logic diagrams.

The nodalization of the plant model is developed as an engineering task with the input from the available design information (drawings, equipment data sheets and descriptive documents). The Advanced Qualification Process (AQP) begins with applying the recommendations related to the validation of the input models (OECD/CSNI [69]) and the transient analysis (IAEA [70]). Another step in the qualification process is the comparison of the NPP model to experimental facility results, by applying the K_v scaling methods [71] [72].

The concept of plant configuration is applied to the version control of the input decks since only the important plant modifications produce new plant model versions. When assessing a new configuration of the plant model, the process is divided into the following steps: prepare the qualification matrix, execute assessment calculations, perform the comparison and the final evaluation [73].

The use of such models in the NPPs provides several applications that are beneficial, either for the purpose of safety [74] or plant availability [75]. In this sense, many studies related to plant malfunctions have been carried out, making use of the extended capabilities of the plant model, provided the fact that all the main control systems were modelled

and to some degree also verified. The application of the models can be performed in different fields aside from safety analysis, such as engineering, operation and training.

Examples of these works are: an assessment of the model for the case of a turbine trip from 100% power [76], an assessment of the model in case of a main feedwater turbine trip [77], a study of the anticipated transient without scram (ATWS) related transients with sensitivity analysis [78], an assessment of station black-out transients related to the Emergency Operating Procedures (EOP) [79], and an evaluation of a pressurizer PORV opening [80].

CHAPTER 3

SIC AND OLC METHODOLOGIES

This chapter contains:

- Considerations on the problem domain definition when coupling codes
- Considerations on the numerical solution methods for coupled codes
- The description of the semi-implicit coupling method SIC)
- The description of the off-line coupling method (OLC)

3.1 TH codes coupling methods

This section contains an explanation of the coupling methodologies used in this study. Also, some considerations about the many possibilities that can be chosen in different aspects such as the domain representation or the numerical solution methods when coupling TH codes are discussed. Finally, the selection and application of the coupling methodologies used is justified in accordance with the previously described work objectives.

The coupling of computer codes is considered beneficial to safety analysis [23]. The advantages include being able to solve different physical phenomena or different scales at the same time with the robustness of validated codes. Many applications have been developed until the present day that include the combination of several validated codes [27] [25] [33] [29]. When coupling system and sub-channel codes, different coupling methods are available, having different benefits and limitations.

The coupled code execution method may vary depending on the coupling method considered and the programming involved. On one hand, the codes can be executed independently, using I/O data methods to inform the codes (as input data) or to obtain information from the codes (as output data) as external data tables (off-line coupling). On the other hand, the codes can be merged so the points of data exchange are embedded in the advancement schemes (on-line coupling), having several degrees of code merging (while in some methods the merging of the codes is minimal, in some methods the codes are completely restructured to be inserted to the main code as a callable subroutine). This option has been applied in general mostly for coupling TH system codes with 3-D neutronics or TH system codes with containment codes [23].

One of the main disadvantages of merging codes is that once the codes are merged it is not possible to benefit from the future development of new code versions. This is the reason why when possible, a solution is to add coupling interfaces to the updated versions of the codes so the modification of the source code is minimal or unnecessary when coupling to other codes. In most cases, the built-in coupling interfaces perform the same function as entering the BCs obtained by other codes by input tables.

One important aspect to take into account when coupling TH codes is the coupling domain scheme. When coupling two TH codes (a system and a sub-channel code), a decision must be made as if whether the two codes are used to model the region of interest (in this case the core) or if each code is used to model a separate region of the problem domain. In general, each type of domain scheme is associated with the specific coupling method applied, as explained in the following subsection.

3.1.1 Overlapping vs. separate domain schemes

Figures 3.1a and 3.1b show a simplified model consisting of a single vertical pipe where the overlapping and separate domain coupling schemes have been applied. Assuming that the problem domain is a pipe consisting of 10 nodes and the region of interest consists of the 4 central nodes, the CTF and RELAP5 models differ depending on the applied coupling scheme. While in both cases CTF is used to model the central portion of the pipe (the 4 central nodes), in the case of the separate domain scheme, RELAP5 models the whole domain except for the central region, and in the case of the overlapping domain, RELAP5 models the whole domain.

The use of an overlapping domain scheme permits the extraction of results from the system code without the need of modifying either the code or the model for coupling purposes. On the contrary, when applying a separate domain scheme, where each code models a portion of the domain, special methods must be applied to ensure consistency in the values at the coupling volumes and junctions for both codes. When the codes are to be executed independently, the overlapping domain schemes are usually addressed, while the separate domain schemes are related to more complex coupling methods such as the semi-implicit coupling method.

3.1.2 Numerical solution methods: Implicit and semi-implicit schemes

The numerical solution methods are used to solve time-dependent partial differential equation systems, applied often to two-phase flow problems when modelling NPPs. Implicit and semi-implicit schemes are of interest in relation to code coupling. Iterations are

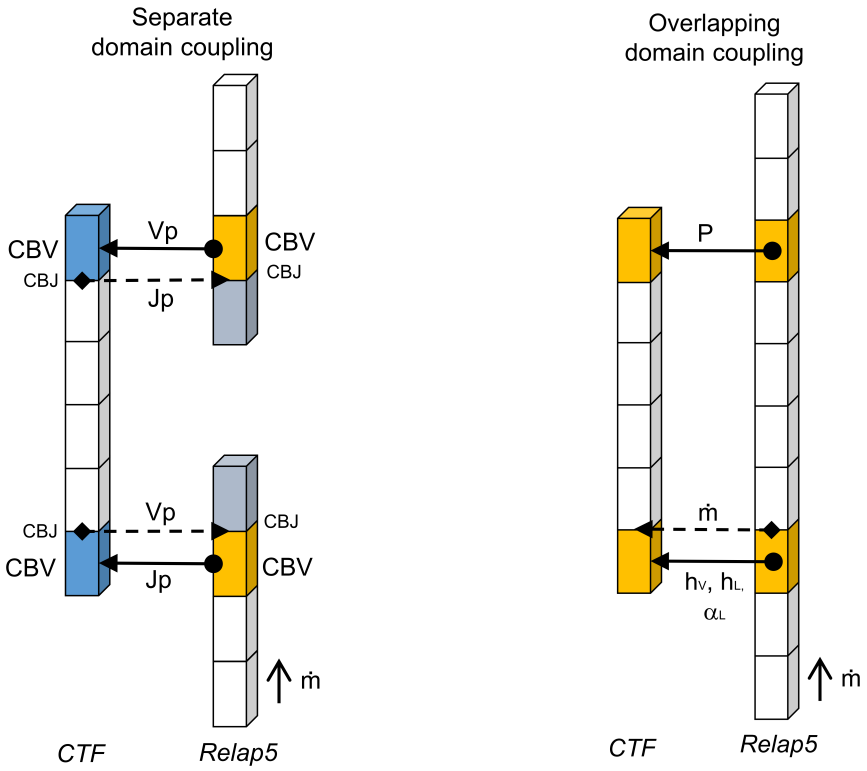

(a) *Separate domain*

(b) *Overlapping domain*

Figure 3.1: *Coupling domain schemes comparison*

often required in order to obtain the convergence of the solution. Most of the numerical solution methods are based on the finite-volume and finite-difference methods based on the Implicit Continuous Eulerian (ICE) method [81].

A numerical scheme is a set of algorithms designed to solve a set of non-linear partial differential equations. Finite-difference methods are usually applied to solve differential equations by approximating derivatives with finite differences. The implicit methods solve the equations applied to the discretized model for both the present time-step and the next one. While they can afford large time steps, they may have convergence issues. In some cases, they may be used for steady-state calculations or relatively slow transients. The semi-implicit methods are considered reliable in two-phase flow transients since they increase the convergence of the implicit methods while maintaining stability. This is achieved by reading the values of some parameters (e.g. velocities) from the previous time-steps [82].

3.2 Description of the semi-implicit coupling method (SIC)

The SIC method has been applied to couple CTF and RELAP5, by implementing the semi-implicit coupling methodology developed by W.L. Weaver [29] [83]. This section describes the coupling methodology, being the resulting coupled program (CTF-RELAP5) later described in Chapter 3.

The generic problem domain, represented in Figure 3.2a by the shaded area, is divided into two computational domains (right and left), each domain being modelled with one of the coupled codes. The connections between them (from now on the coupling volumes) are represented by volumes 1 and 2 for the left and by I and II for the right computational domains respectively.

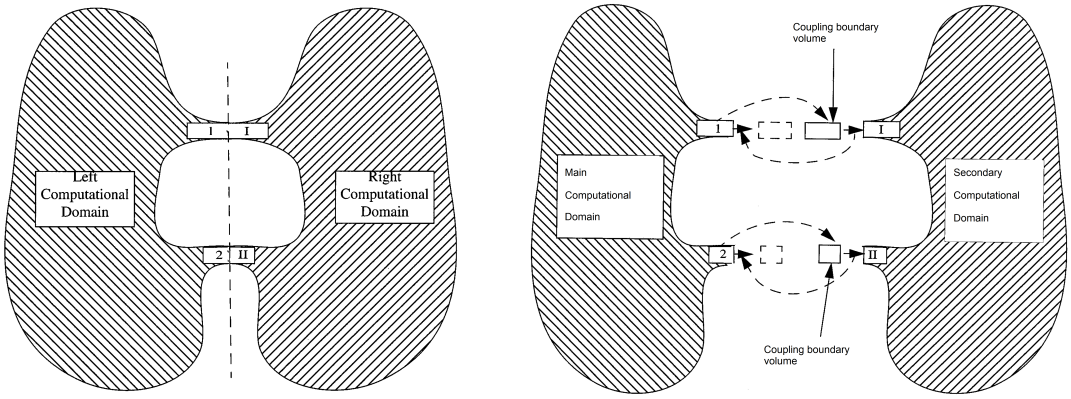

(a) *Schematic of SIC domains* (b) *Schematic of SIC data exchange*

Figure 3.2: *SIC schemes (Source: [29])*

The semi-implicit coupling methodology considers having also two separate computational domains (primary and secondary) as shown in Figure 3.2b. In this case, the coupling volumes are connected to the coupling boundary volumes through the use of coupling junctions. This scheme allows for the data exchange needed according to the methodology.

The reference coupling scheme model in which this methodology is applied is the overlapping domain scheme, as described in Subsection 3.1.1. The final CTF and RELAP5 models used in this methodology are described in detail in Chapter 6.

This methodology is based on the two following requirements for a successful implementation. First, the new-time pressures in the coupling volumes must be consistent with the velocities at the coupling junctions. This way, the Courant limit does not correspond to the sonic Courant but to the material Courant limit, decreasing the time-step dramatically. Second, the convected quantities across the coupling junctions must be equal to maintain the system's energy and mass balance. In this coupling method, the velocities are used velocities implicitly and the convected quantities such as void fraction and density are used explicitly.

This being considered, the step-by-step execution of the two codes can not be sequential because some information has to be shared between the codes before the time-step completion. The hierarchy of the codes considered is a primary/secondary program-level approach. In the particular case of this study, the primary code function has been assigned to RELAP5 and the secondary code function to CTF. RELAP5 and CTF have been then compiled as a single running instance with the purpose of being able to exchange information in an agile manner [84], as described in Chapter 5.

In the selected methodology, obtaining consistent parameters at the coupling boundaries is achieved by the following steps: First, the primary process sends to the secondary process the pressure in the master coupling volumes as a function of the convected quantities across the coupling junctions, then the secondary process computes the convected quantities in the coupling junctions and pressure in the secondary coupling volumes and the rest of the secondary domain. Using the convected quantities in the coupling junctions the primary process computes the pressure in the primary coupling volumes and in the primary domain.

In order to compute RELAP5 coupling volumes pressure as a function of the convected quantities across the coupling junctions, RELAP5 numerical solution scheme is modified in the coupling volumes. First, the pressure equation in RELAP5 (Equation 3.1) is modified only at the coupling volumes by expressing $g^1 v_{g,j+1}^{n+1} + f^1 v_{f,j+1}^{n+1}$ as in Equation 3.2, being $j+1$ the coupling junction.

$$Ax = \tilde{b} + \tilde{g}^1 v_{g,j+1}^{n+1} + \tilde{g}^2 v_{g,j}^{n+1} + \tilde{f}^1 v_{\tilde{f},j+1}^{n+1} + f^2 v_{f,j}^{n+1} \tag{3.1}$$

$$g^1 v_{g,j+1}^{n+1} + f^1 v_{f,j+1}^{n+1} = \frac{\Delta t}{V} \begin{bmatrix} n_{g,j+1}^{n+1} \\ u_{g,j+1}^{n+1} + P^n w_{g,j+1}^{n+1} \\ u_{f,j+1}^{n+1} + P^n w_{f,j+1}^{n+1} \\ m_{f,j+1}^{n+1} - m_{g,j+1}^{n+1} \\ m_{f,j+1}^{n+1} + m_{g,j+1}^{n+1} \end{bmatrix} \tag{3.2}$$

Where the convected quantities across the coupling junctions are:

- $n_{g,j+1}^{n+1}$ is the flow rate of non-condensable gas (kg s-1)
- $u_{g,j+1}^{n+1}$ is the flow rate of vapor internal energy (J s-1)
- $u_{f,j+1}^{n+1}$ is the volumetric rate of vapor (ms-1)
- $w_{g,j+1}^{n+1}$ is the flow rate of liquid internal energy (J s-1)
- $w_{f,j+1}^{n+1}$ is the volumetric rate of liquid (ms-1)
- $m_{g,j+1}^{n+1}$ is the mass flow rate of vapor (kg s-1)
- $m_{f,j+1}^{n+1}$ is the mass flow rate of liguid (kg s-1)

By substituting Equation 3.2 into Equation 3.1 for the coupling volumes, the system pressure matrix is obtained as described in Subsection 2.2.5 , expressed as a function of the convected quantities across the coupling junctions, with the form presented in Equation 3.3, where $k = 1, 2, ...Nv$, being Nv the number of volumes in the master domain and NC being the number of coupling volumes:

$$\begin{aligned} \delta P_k^{n+1} = a_k &+ \sum_{j=1}^{NC} b_{k,j} n_{g,j}^{n+1} + \sum_{j=1}^{NC} c_{k,j} u_{g,j}^{n+1} + \sum_{j=1}^{NC} d_{k,j} u_{f,j}^{n+1} \\ &+ \sum_{j=1}^{NC} e_{k,j} m_{g,j}^{n+1} + \sum_{j=1}^{NC} f_{k,j} m_{f,j}^{n+1} + \sum_{j=1}^{NC} g_{k,j} w_{g,j}^{n+1} + \sum_{j=1}^{NC} h_{k,j} w_{f,j}^{n+1} \end{aligned} \tag{3.3}$$

In Equation 3.3, coefficients a through h allow defining the pressure change as a function of the convected quantities across the coupling junctions. These coefficients are then sent to CTF, which are used to compute the mass, energy and volume flow rates in the coupling junctions to be sent to RELAP5. Once RELAP5 computes the velocities in the coupling junctions using the flow rates received by CTF, the new pressures in the RELAP5 domain will be obtained and the time-step advancement calculations will proceed in both codes. The semi-implicit coupling scheme is implemented by a series of steps executed sequentially (shown in Table 3.1), that implement intra-step information exchange and the partial execution of each code time advancement scheme.

Step 1	RELAP5 sends CTF the properties of the CBV attached to the CBJ at the beginning of the time-step, corresponding to the old-time volume quantities.
Step 2	Using RELAP5 CBV information, CTF computes the convected quantities between the CTF CBV and the next connection to the model using upwind differencing.
Step 3	The convected quantities (Jp) are then sent to RELAP5.
Step 4	RELAP5 receives the convected quantities to compute the pressure change in all RELAP5 domain as a function of the convected quantities in the coupling junctions
Step 5	This relation is expressed in terms of a set of coefficients $(a_{k,j}...h_{k,j})$ relating the dP in RELAP5 volumes and the convected quantities. The coefficients are sent to CTF.
Step 6	CTF modifies the pressure matrix to add the effect of coupling volumes and the convected quantities to the solution in all CTF domain.
Step 7	The convected quantities and the pressure change in all CTF domain are computed.
Step 8	The convected quantities are then sent to RELAP5 (Vp).
Step 9	RELAP5 uses the received convected quantities to compute the dP in all RELAP5 domain, and then the rest of the time-step calculations continue.

Table 3.1: *Main SIC methodology steps. CBJ are the coupling boundary junctions, CBV are the coupling boundary volumes, Vp are the volume properties and Jp the junction properties.*

3.3 Description of the off-line coupling method (OLC)

The OLC method has been applied to couple CTF and RELAP5 by implementing the off-line coupling methodology presented in other studies [33] [85]. This section describes the coupling methodology, consisting first on the extraction of data from RELAP5 and then the introduction of the processed data to the CTF input deck. In this case, the reference model coupling scheme in which this methodology is applied is the overlapping domain scheme, as described in Subsection 3.1.1. Also, the final CTF and RELAP5 models used in this methodology are described in detail in Chapter 6.

The coupling method consists of performing two separate runs using the standalone versions of both codes. First, RELAP5 is run and the following parameters are extracted in the form of a time trend:

- Outlet pressure
- Inlet mass flow rate
- Inlet liquid and vapour enthalpy
- Inlet void fraction
- Core power

The data is processed and then imposed to CTF as BC by table. Figure 3.1 represents the BC transmission from RELAP5 to CTF. One advantage of this method is that there is no need to modify the codes and so the robustness and stability remain unaltered. This is a relevant consideration for this type of code, which are in continuous development.

However, it is important to bear in mind that using this method some parameters may present inconsistencies. For instance, the inlet pressure in the core is calculated by CTF and may differ from the inlet pressure calculated by RELAP5. Also, the outlet mass flow rate calculated by CTF may differ from the outlet mass flow rate calculated by RELAP5.

CHAPTER 4

BEPU METHODOLOGY

This chapter contains:

- A brief description of the GRS BEPU method
- The determination of the uncertain parameters considered
- The description of the analysis of input uncertainties propagation

4.1 GRS method description

The BEPU method used in the present study is the GRS BEPU method [46], which implements Wilks' method using order statistics. The GRS method considers sources of uncertainty of the calculations that have an impact on results due to several causes: modelling inconsistencies, BCs applied, or uncertainties of the physical models implemented in the code.

To account for the uncertainty sources, certain selected input values and code parameters are replaced by PDFs. Each PDF represents the uncertainty of the input variable, and it is defined by a distribution type (uniform, normal, lognormal, ...), and its associated mean, range or standard deviation. The distribution type depends on the source of the uncertainty for the defined input parameter. Since no particular input values are defined for the problem run, the problem must be run a number of times using each time a specific set of input variables. The input values are obtained by random sampling from the defined PDFs.

Wilks' method [86] [87] [88] provides a basis for calculating the necessary minimum sample size for one and two-sided tolerance limits for given confidence. The application of Wilks' method implies that there is a correspondence between the minimum number of runs and the coverage and confidence of the results when comparing to either one or two-sided tolerance limits and the order considered [89]. The number of runs or sample size N is provided by Wilks' formula for either one (Equation 4.1) or two-sided (Equation 4.2) tolerance limits, being rank r, higher tolerance P, and higher confidence $(1-\alpha)$:

$$I_{1-P}(r, N-r+1) \geq 1-\alpha \tag{4.1}$$

$$I_{P}(N-2r+1, 2r) \leq \alpha \tag{4.2}$$

By using a number of runs higher than those defined by Equations 4.2 and 4.2, it can be accepted that the considered most limiting result of all runs will not be exceeded with a probability P of the output distribution values, in comparison to the acceptance criterion. The rank r determines the order statistic used, then for $r = 1$ the higher value will be the one considered, for $r = 2$ the higher value will be the second one, etc.

For $r = 1$, Equations 4.1 and 4.2 are simplified as:

$$\alpha \geq P^N \tag{4.3}$$

$$\alpha \geq NP^{N-1} - (N-1)P^N \tag{4.4}$$

Table 4.1 shows the minimum sample sizes (N) that meet the requirements for specific rank (r), tolerance (P) and confidence ($1-\alpha$) for either one-sided ($1s$) or two-sided ($2s$) tolerance limits. As it can be seen, higher rank, tolerance (P) and confidence ($1-\alpha$) increase the number of minimum runs for the BEPU analysis.

	95%/95%		95%/99%		99%/95%		99%/99%	
r	1s	2s	1s	2s	1s	2s	1s	2s
1	59	93	90	130	299	473	459	662
2	93	153	130	198	473	773	662	1001
3	124	208	165	259	628	1049	838	1307

Table 4.1: *Sample size number for Wilks' method (Source: [90])*

The minimum number of runs applied to the BEPU analyses in the present study is obtained by applying the one-sided second-order Wilks' formula, with the following parameters: 95% of coverage and 95% confidence (95/95), resulting in 93 runs. By executing this number of runs and considering rank=2 it allows for discarding the run with the most limiting value for our scalar FOM (in this case the MDNBR).

Figure 4.1 shows a representation of the transmission of input uncertainties to results. At the top of the figure, a single BE calculation is represented. In this case, a single set of input values is used, that when applied to the system model and the code using *submodels* or *physical models* produce a single time-trend of the parameter of interest, in this case, the temperature.

At the bottom of the Figure, a BEPU calculation is represented. In this case, instead of a single set of input values, N sets of input values are considered, one for each run. Each set is obtained by random sampling using the pre-defined PDF for each input parameter. All cases are run by the code similarly to the single best-estimate case run. In this case, the results are multiple time trends of the same parameter of interest. One way

to represent results is to plot the bands: the bands are two-time trends where only the higher and lower value of all time trends for every time-step are considered. A number of higher or lower values should be discarded based on the rank r as previously discarded. Then the representation permits visualizing the limits at each time-step where the result will fall with a defined tolerance P and confidence $1 - \alpha$.

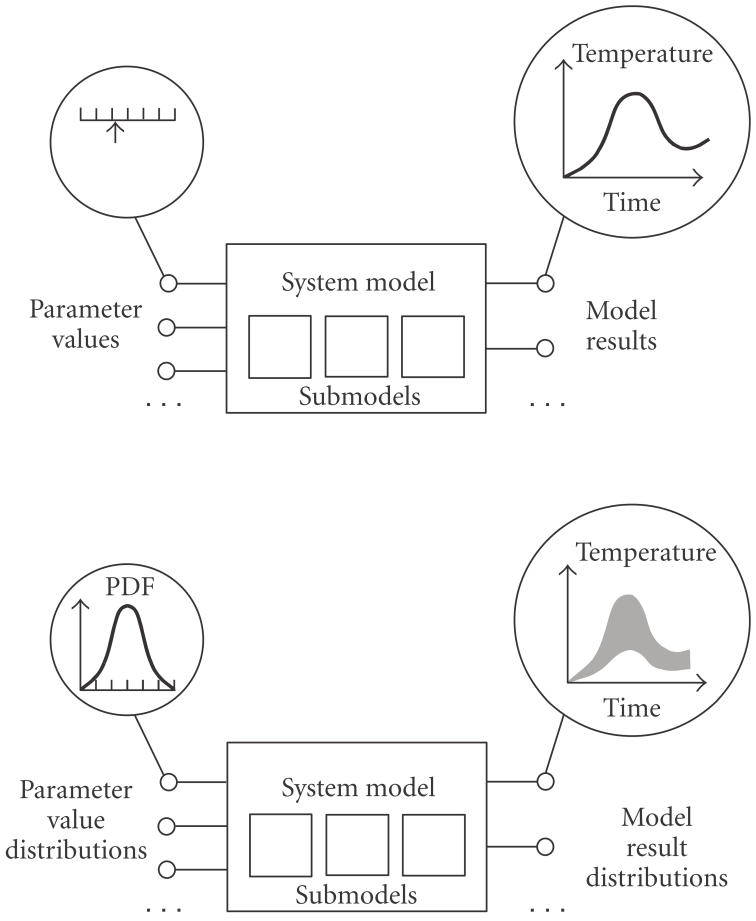

Figure 4.1: *Consideration of input parameter value ranges in the GRS method. (Source: [46])*

Even though this type of representation is common in the scientific community, it is important to bear in mind that this method can solely assess the probability of occurrence of a single scalar and not the complete time trend. The uncertainty bands provide more insights into the analysis but are not part of it or have no statistical significance.

A relevant characteristic of the GRS method is the possibility of the evaluation using

sensitivity measures of the importance of input parameter deviation to the uncertainty of the results. One of the possible methods of such evaluation is the use of rank correlation coefficients. These evaluations are performed by using actual results obtained from calculations rather than approximations (e.g. experimental values) used by other methods [46]. Also, the evaluations of sensitivity measures are valid in both scalar or time dependant values of interest, such as MDNBR or pressure respectively.

4.2 Application of the GRS BEPU method

4.2.1 Procedure

This subsection describes the procedure used in order to perform the BEPU analysis using the GRS method. A BEPU analysis has been performed for each one of the cases (RCP trip and PORV opening) and each coupling method (SIC and OLC methods). The steps followed in each BEPU analysis are:

1. Selection of the cases and running the base case calculations for each coupling method.
2. Selection of the input uncertain parameters for each case.
3. Determination of the PDFs for each uncertain parameter.
4. Perform the sensitivity analysis for the selected uncertain parameters.
5. Determination of the % of coverage, % confidence and the minimum number of runs.
6. Obtain a set of input parameters from a random sampling of the PDFs.
7. Generate each input deck (RELAP5 and CTF) and execute each case.
8. Obtain Spearman's rank correlation coefficients for the defined parameters of interest.

4.2.2 Considerations

The objective of this study is not to perform a BEPU analysis for licensing purposes but rather to evaluate the influence of the coupling methods. Therefore, some considerations need to be addressed:

- The GRS BEPU method focuses on one single output parameter, the tolerance and confidence can only be ensured for a single output value. In both RCP trip and

PORV opening cases, the output parameter of interest is the MDNBR, but since one of the objectives is to compare the results of two coupling methods, the distributions of other relevant results are also quantitatively and qualitatively used for comparison purposes only.

- The process of obtaining the PDFs of the uncertain input parameters in licensing studies need extended data research and evaluations such as in the works with References [91] and [92]. The OECD/NEA PREMIUM project [93] benchmarked the available inverse uncertainty quantification (IUQ) methods and observed strong user effects due to a lack of best practices guidance. As a follow-up, the OECD SAPIUM project [94] was designed to provide a systematic approach for input uncertainty quantification, and a guideline for good practices was generated. In this study, the PDFs of the uncertain input parameters have been obtained either by reference to other works or by expert judgement.

- Regarding the validation of the GRS BEPU method, several efforts have been put to carry out validations of the BEPU method as a whole, through the use of benchmark activities in modelling experiments [95] or regarding scaling considerations [84].

4.2.3 Selection of input uncertain parameters

According to IAEA [23], when performing a BEPU analysis, it is necessary to investigate the uncertainty of the results and the sensitivity of most of the effective parameters. In this study, several RELAP5 (system) and CTF (core) uncertain input parameters have been considered when performing the BEPU analysis. The selection process of the parameters has been done considering two factors: first, considering general plant and core parameters that affect the DNB phenomena and second, considering those specific relevant parameters that are related to each case (RCP trip and PORV opening).

The list of uncertain input parameters considered for the PORV opening case and the RCP trip case is provided in Table 4.2. NV stands for the nominal value, which is the value that has been taken into account for the base case calculations. UR stands for the uncertainty range considered, which is centred on the NV. A different number of

parameters have been considered for the RCP and PORV cases: 7 RELAP5 and 8 CTF uncertain parameters in the RCP case, and 9 RELAP5 and 8 CTF uncertain parameters in the PORV case. In Table 4.2, FTC stands for fuel temperature coefficient, MTC stands for moderator temperature coefficient, HTC stands for heat transfer coefficient and VD model stands for void drift model. Changes in parameters 8 (PORV valve discharge coefficient) and (pressurizer level) have been considered to have non or negligible effect in the RCP case calculations.

RCP	PORV	Parameter	NV	UR	Ref.
		RELAP5 model parameters			
1	1	Pressure	15.516 MPa	$\pm$1.0%	[96]
2	2	Core power	100.0 %	$\pm$2.0%	[56]
3	3	Mass flow rate	13522.0 kg/s	$\pm$3.0%	[96]
4	4	FTC factor	1.0	$\pm$10.0%	EJ
5	5	Reactor trip time	2.0 s	$\pm$0.50 s	EJ
6	6	MTC factor	1.0	$\pm$10.0%	EJ
7	7	Pumps moment of inertia	2612.7 kg*m^2	$\pm$10.0%	EJ
-	8	Pressurizer valve discharge coeff.	1.0	$\pm$10.0%	EJ
-	9	Pressurizer level	55.0 %	$\pm$10.0%	EJ
		CTF model parameters			
8	10	Pellet to clad gap HTC	17034.9 W/m^{2}C	$\pm$66.66%	[56]
9	11	Fuel % of theoretical density	95.0 %	$\pm$1.684%	[56]
10	12	Fraction of power directly to coolant	0.02	$\pm$10.0%	[56]
11	13	Fuel pellet diameter	0.8192 cm	$\pm$0.977%	[56]
12	14	Clad outer diameter	0.95 cm	$\pm$0.421%	[56]
13	15	Clad thickness	0.057 cm	$\pm$0.421%	[56]
14	16	Gap horizontal pressure loss coeff.	0.5	$\pm$10.0%	EJ
15	17	Dist. weighting factor VD model	1.4	$\pm$10.0%	[56]

Table 4.2: *RCP and PORV cases uncertain BEPU parameters. NV: nominal value, UR: uncertainty range, EJ: expert judgement. All parameters are considered to have uniform distributions.*

The ranges and distributions for uncertain parameters have been taken from [56] and [96]. EJ stands for expert judgement, where the values have been imposed by the authors with the limitation of not having relevant references for those parameters. For the present study, all distributions have been considered uniform, as in References [56] and [96]. This is a common practice in BEPU analyses when there is a lack of knowledge of the distribution of uncertain parameters.

A sensitivity analysis has been performed and applied to the uncertain parameters prior to the BEPU analysis. This is considered useful for two reasons: on one side, it provides a coherent approach to evaluate the change of the parameters of interest for each coupling method, and on the other side, it provides a means of checking that the range of parameter variations is producing acceptable calculations. As described in Section 7.4, the sensitivity is performed by running 3 cases at the upper and 3 in the lower uncertainty ranges for each parameter.

4.2.4 Selection of BEPU FOM

A set of relevant FOMs has been selected: FOMs are scalars computed from calculation results, being selected based on the assumption that they have a relation to the calculation of the CHF and that provide relevant information about the comparison between the BEPU analyses. The main FOM considered in the present study is the MDNBR, and the additional FOM are:

- HF: heat flux at the MDNBR location
- CHF: critical heat flux at the MDNBR location
- CT: clad temperature at the MDNBR location
- VF: void fraction at the MDNBR location
- MCT: maximum cladding temperature

CHF is calculated using the W-3 correlation available in CTF, as described in Subsection 2.1.8.

4.2.5 Analysis of input uncertainties propagation

The input uncertainties propagation is evaluated by correlating the input values to the defined FOM. The correlation coefficients are used to quantitatively analyze the contribution of the uncertainty of each input parameter to each FOM. The coefficients obtained are Spearman's rank correlation coefficients, chosen to capture the possible monotonic relationships between the variables. In order to verify that the use of Spearman's rank correlation coefficients is adequate, the scatter plots of MDNBR versus each uncertain parameter are generated and no non-monotonic relationships are observed.

CHAPTER 5

DESCRIPTION OF THE CTF-RELAP5 SIC CODE

This chapter contains:

- The description of the CTF-RELAP5 code semi-implicit coupling scheme
- The description of the CTF-RELAP5 code structure
- A brief description of the CTF-RELAP5 code verification

5.1 Application of the SIC scheme

This section describes the application of the SIC scheme to couple CTF and RELAP5. The method used is an adaptation of the procedure used by A. Soler [97], which consists of the implementation of the SIC method developed by W.L. Weaver [31]. The methodology used is described in Chapter 3.

5.1.1 SIC scheme description

The SIC method is performed by executing a series of sequential steps with intra-step information exchange and the partial execution of each code through a time-advancement scheme. The steps are divided into two types of steps, according to the nature of the actions performed: while the internal code actions are those actions performed internally by each code using stored data within the code and with no data exchange, the external code actions are those related to data exchange between codes. The main programmed steps of the method are presented in Table 3.1.

In the next subsections, the most relevant SIC steps are described (steps 5, 6 and 7), the main structure of the program is presented and the formulation of the most relevant calculations is provided. Since the SIC method uses RELAP5 as the main program and CTF as the secondary program, the original solution process for RELAP5 is presented before the formulation related to the code modifications.

Figure 5.1 represents a simplified coupled model in CTF and RELAP5 used in this chapter to describe the data exchange of the method, having the same number of coupling volumes and junctions as the actual CTF and RELAP5 models used. In the figure, the vertical channel modelled by CTF represents the core, while the C-shaped channel represents the system portion of the NPP connected to the core. The actual RELAP5 and CTF models used in the SIC scheme are described in Chapter 6 and presented in Figure 6.10. The equivalence between the simplified model (represented in Figure 5.1) and the models used (represented in Figure 6.10) is presented in Table 5.1.

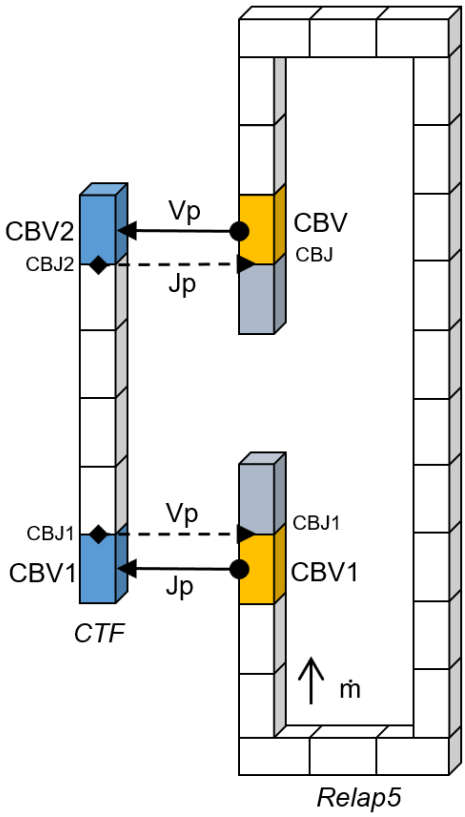

Figure 5.1: *Schematic of semi-implicit coupling methodology data exchange*

RELAP5 CBV1:	Volume 136
RELAP5 CBV2:	Volume 139
CTF CBV1:	Channel 1 Node 1
CTF CBV2:	Channel 482 Node 11
RELAP5 CJ1:	Junction 256
RELAP5 CJ2:	Junction 258
CTF CJ1:	Vertical connection 1
CTF CJ2:	Vertical connection 482

Table 5.1: *Coupling volumes/junctions correspondance between the simplified model (Figure 5.1) and the actual model used in the calculations (Figure 6.10)*

5.1.2 RELAP5 original semi-implicit solution scheme

The formulation of the RELAP5 original semi-implicit solution scheme is modified in order to obtain the dependencies between pressure and the convected quantities. In this subsection the formulation previously described in Section 2.2 is expanded to the programming level, to being linked later to the modifications needed. The following formulation described is based on the momentum, mass and energy control volumes previously defined in Figure 2.3, where two staggered meshes are used, the scalar and the momentum mesh. The scalar mesh defines the scalar variables (P, α_g, U_g, U_f), and the momentum mesh defines the fluid velocity field (v_g, v_f).

The RELAP5 full set of conservation equations (as described in Chapter 2) for volume L in matrix form is:

$$\delta P_L^{n+1} = \mathbf{A_5^{-1}}(\mathbf{b} + \mathbf{g^1} v_{g,j+1}^{n+1} + \mathbf{g^2} v_{g,j}^{n+1} + \mathbf{f^1} v_{f,j+1}^{n+1} + \mathbf{f^2} v_{f,j}^{n+1}) \tag{5.1}$$

The momentum equations for the junction j are:

$$v_{g,j}^{n+1} = \tilde{v}_{g,j}^{n+1} + \frac{\partial v_g}{\partial \Delta P}(\delta P_{K,j}^{n+1} - \delta P_{L,j}^{n+1}) \tag{5.2}$$

$$v_{f,j}^{n+1} = \tilde{v}_{f,j}^{n+1} + \frac{\partial v_f}{\partial \Delta P}(\delta P_{K,j}^{n+1} - \delta P_{L,j}^{n+1}) \tag{5.3}$$

Substituting Equations 5.2 and 5.3 into Equation 5.1 results in:

$$\begin{aligned} \delta P_L^{n+1} = \mathbf{A_5^{-1}}(\mathbf{b}+ & \\ & + \mathbf{g^1}(\tilde{v}_{g,j+1}^{n+1} + \frac{\partial v_g}{\partial \Delta P}(\delta P_L^{n+1} - \delta P_M^{n+1})) \\ & + \mathbf{g^2}(\tilde{v}_{g,j}^{n+1} + \frac{\partial v_g}{\partial \Delta P}(\delta P_K^{n+1} - \delta P_L^{n+1})) \\ & + \mathbf{f^1}(\tilde{v}_{f,j+1}^{n+1} + \frac{\partial v_f}{\partial \Delta P}(\delta P_L^{n+1} - \delta P_M^{n+1})) \\ & + \mathbf{f^2}(\tilde{v}_{f,j}^{n+1} + \frac{\partial v_f}{\partial \Delta P}(\delta P_K^{n+1} - \delta P_L^{n+1}))) \end{aligned} \tag{5.4}$$

The terms $\frac{\partial v_f}{\partial \Delta P}$ and $\frac{\partial v_g}{\partial \Delta P}$ for volumes K and L are then expressed as: `vgdpk`, `vfdpk`, `vgdpl` and `vfdpl` (terms being dependant only on the junction parameters), resulting in:

$$\begin{aligned}\delta P_L^{n+1} = \mathbf{A_5^{-1}b}+ \\ &+ \mathbf{A_5^{-1}g^1}(\tilde{v}_{g,j+1}^{n+1} + \texttt{vgdpk(j+1)} * \delta P_L^{n+1} - \texttt{vgdpl(j+1)} * \delta P_M^{n+1}) \\ &+ \mathbf{A_5^{-1}g^2}(\tilde{v}_{g,j}^{n+1} + \texttt{vgdpk(j)} * \delta P_K^{n+1} - \texttt{vgdpl(j)} * \delta P_L^{n+1}) \\ &+ \mathbf{A_5^{-1}f^1}(\tilde{v}_{f,j+1}^{n+1} + \texttt{vfdpk(j+1)} * \delta P_L^{n+1} - \texttt{vfdpl(j+1)} * \delta P_M^{n+1}) \\ &+ \mathbf{A_5^{-1}f^2}(\tilde{v}_{f,j}^{n+1} + \texttt{vfdpk(j)} * \delta P_K^{n+1} - \texttt{vfdpl(j)} * \delta P_L^{n+1}) \end{aligned} \quad (5.5)$$

The terms `tkg`, `tlg`, `tkf` and `tlf` are introduced (terms being dependant only on the volume parameters):

$$\begin{aligned}\mathbf{A_5^{-1}g^1} &= \texttt{tkg(L)} \\ \mathbf{A_5^{-1}g^2} &= \texttt{tlg(L)} \\ \mathbf{A_5^{-1}f^1} &= \texttt{tkf(L)} \\ \mathbf{A_5^{-1}f^2} &= \texttt{tlf(L)} \end{aligned} \quad (5.6)$$

Substituting:

$$\begin{aligned}\delta P_L^{n+1} = \mathbf{A_5^{-1}b}+ \\ &+ \texttt{tkg(L)}(\tilde{v}_{g,j+1}^{n+1} + \texttt{vgdpk(j+1)} * \delta P_L^{n+1} - \texttt{vgdpl(j+1)} * \delta P_M^{n+1}) \\ &+ \texttt{tlg(L)}(\tilde{v}_{g,j}^{n+1} + \texttt{vgdpk(j)} * \delta P_K^{n+1} - \texttt{vgdpl(j)} * \delta P_L^{n+1}) \\ &+ \texttt{tkf(L)}(\tilde{v}_{f,j+1}^{n+1} + \texttt{vfdpk(j+1)} * \delta P_L^{n+1} - \texttt{vfdpl(j+1)} * \delta P_M^{n+1}) \\ &+ \texttt{tlf(L)}(\tilde{v}_{f,j}^{n+1} + \texttt{vfdpk(j)} * \delta P_K^{n+1} - \texttt{vfdpl(j)} * \delta P_L^{n+1}) \end{aligned} \quad (5.7)$$

Substituting the terms $\tilde{v}_{g,j}^{n+1}$ by `velgj` and `velfg`:

$$\begin{aligned}\delta P_L^{n+1} = \mathbf{A_5^{-1}b}+ \\ &+ \texttt{tkg(L)}(\texttt{velgj(j+1)} + \texttt{vgdpk(j+1)} * \delta P_L^{n+1} - \texttt{vgdpl(j+1)} * \delta P_M^{n+1}) \\ &+ \texttt{tlg(L)}(\texttt{velgj(j)} + \texttt{vgdpk(j)} * \delta P_K^{n+1} - \texttt{vgdpl (j)} * \delta P_L^{n+1}) \\ &+ \texttt{tkf(L)}(\texttt{velfj(j+1)} + \texttt{vfdpk(j+1)} * \delta P_L^{n+1} - \texttt{vfdpl(j+1)} * \delta P_M^{n+1}) \\ &+ \texttt{tlf(L)}(\texttt{velfj(j)} + \texttt{vfdpk(j)} * \delta P_K^{n+1} - \texttt{vfdpl (j)} * \delta P_L^{n+1}) \end{aligned} \quad (5.8)$$

For volume L, the pressure matrix can be expressed as an equation of the type:

$$[A][B] = [C] \tag{5.9}$$

Being:

$$[A] = [\texttt{-tlf(L)vfdpk(j)-tlg(L)vgdpk(j)},$$
$$\texttt{1+tlf(L)vfdpl(j)+tlg(L)vgdpl(j)-tkf(L)vfdpk(j+1)-tkg(L) vgdpk(j+1)}, \tag{5.10}$$
$$\texttt{tkf(L)vfdpl(j+1)+tkg(L)vgdpl(j+1)}]$$

$$[B] = \begin{bmatrix} \delta P_K^{n+1} \\ \delta \mathbf{P_L^{n+1}} \\ \delta P_M^{n+1} \end{bmatrix} \tag{5.11}$$

$$[C] = [\mathbf{A_5^{-1}b} + \texttt{tlg(L)*velgj(j)+tlf(L)*velfj(j)} + \texttt{tkg(L)*velgj(j+1)+tkf(L)*velfj(j+1)}] \tag{5.12}$$

Matrix A terms can be defined as $\mathbf{lk(j)}$, $\mathbf{ll(j)} + \mathbf{kk(j+1)}$ and $\mathbf{kl(j+1)}$, and are respectively related to the upstream volume (before volume K), the present volume (volume K) and the downstream volume (volume L). The pressure matrix for a whole hydrodynamic system is built by the addition of matrices represented in Equation 5.9, resulting in an equation system with the following matrices sizes, being Nn the number of volumes:

- Matrix A size: $N_n * N_n$ (noted as `coefp` in RELAP5)
- Matrix B size: $N_n * 1$
- Matrix C size: $1 * N_n$ (noted as `sourcp` in RELAP5)

5.1.3 Step 5: RELAP5 coefficients calculation

The objective of step 5 is to express the pressure change in the current time-step in all RELAP5 domain as a function of the convected quantities received from CTF in step 4. The relationship between the dPs and the convected quantities is expressed by a set of

coefficients defined for each coupling volume. Considering a RELAP5 hydraulic system with a number of coupling junctions, the addition of the $[D]$ and $[E]$ terms to the original pressure matrix permits to account for the pressure change as a function of the convected quantities:

$$[A] * [B] = [C] + [D] * [E] \tag{5.13}$$

$$\begin{bmatrix} coefp_{1,1} & ... & coefp_{1,N_n} \\ ... & ... & ... \\ coefp_{N_n,1} & ... & coefp_{N_n,N_n} \end{bmatrix} \begin{bmatrix} \delta P_1 \\ ... \\ \delta P_{N_n} \end{bmatrix} = \begin{bmatrix} sourcp_1 \\ ... \\ sourcp_{N_n} \end{bmatrix} + \Big[\mathsf{D}\Big] * \Big[\mathsf{E}\Big] \tag{5.14}$$

The $[D]$ and $[E]$ matrices are composed of the vectors $form_{i,j}$ and $conv_i$:

$$\Big[\mathsf{D}\Big] = \begin{bmatrix} [form_{1,1}] & ... & [form_{1,N_j}] \\ ... & ... & ... \\ [form_{N_n,1}] & ... & [form_{N_n,N_j}] \end{bmatrix} \tag{5.15}$$

$$\Big[\mathsf{E}\Big] = \begin{bmatrix} [conv_1] \\ ... \\ [conv_{N_j}] \end{bmatrix} \tag{5.16}$$

Where the vectors $form_{i,j}$ and $conv_i$ are (being the convected quantities for each coupling junction defined in Section 3.2):

$$\Big[conv_{N_j}\Big]^{-1} = \Big[\begin{array}{ccccccc} n_{g,N_j}^{n+1} & u_{g,N_j}^{n+1} & u_{f,N_j}^{n+1} & m_{g,N_j}^{n+1} & m_{f,N_j}^{n+1} & w_{g,N_j}^{n+1} & w_{f,N_j}^{n+1} \end{array}\Big] \tag{5.17}$$

$$\Big[form_{N_n,N_j}\Big] = \frac{\Delta t}{V_{N_n}} \Big[\begin{array}{ccccccc} A_{5,1}^{-1} & A_{5,2}^{-1} & A_{5,3}^{-1} & A_{5,5}^{-1} - A_{5,4}^{-1} & A_{5,4}^{-1} + A_{5,5}^{-1} & A_{5,2}^{-1} P_{N_n} & A_{5,3}^{-1} P_{N_n} \end{array}\Big] \tag{5.18}$$

Where the number of volumes and coupling junctions are:

- Nn: number of volumes in the RELAP5 (primary) domain
- Nj: number of coupling junctions between the primary and secondary domains
- $j+1$ is the coupling junction

Matrix $[A]$ is reduced to $[Id]$, then the values of the coefficients that relate dP with the convected quantities are obtained ($[a_k, b_{k,j}, c_{k,j}, d_{k,j}, e_{k,j}, f_{k,j}, g_{k,j}, h_{k,j}]$), where k is the RELAP5 domain volume index and j is the coupling junction index.

5.1.4 Steps 6 and 7: CTF calculation of the convected quantities and pressure change (dP)

Steps 6 and 7 are performed by a series of substeps. First, the momentum equation is solved in CTF for each volume. The new-time velocities are obtained by using currently known values by solving the discretized form of the momentum equation, where the junction flows and volume pressures are related to each other.

The CTF energy and momentum equations (where P_J is the pressure in the volume and $P_{i=1...nconn}$ are the pressures in the connected volumes) are:

$$C_n(\alpha_v, \alpha_v h_v, (1-\alpha_v)h_l, \alpha_e, P_J, P_{i=1...nconn}) = 0 \tag{5.19}$$

$$C_l(\alpha_v, \alpha_v h_v, (1-\alpha_v)h_l, \alpha_e, P_J, P_{i=1...nconn}) = 0 \tag{5.20}$$

$$E_v(\alpha_v, \alpha_v h_v, (1-\alpha_v)h_l, \alpha_e, P_J, P_{i=1...nconn}) = 0 \tag{5.21}$$

$$E_l(\alpha_v, \alpha_v h_v, (1-\alpha_v)h_l, \alpha_e, P_J, P_{i=1...nconn}) = 0 \tag{5.22}$$

$$C_e(\alpha_v, \alpha_v h_v, (1-\alpha_v)h_l, \alpha_e, P_J, P_{i=1...nconn}) = 0 \tag{5.23}$$

$$C_v(\alpha_v, \alpha_v h_v, (1-\alpha_v)h_l, \alpha_e, P_J, P_{i=1...nconn}) = 0 \tag{5.24}$$

In vector notation:

$$\vec{f}(\vec{x}) = \vec{0} \tag{5.25}$$

Where $\vec{f}$ is the vector representing the mass and energy equations and $\vec{x}$ is the vector representing the values of the independent variables at the current time-step:

$$\vec{x} = \begin{bmatrix} \alpha_v \\ \alpha_v h_v \\ (1-\alpha_v)h_l \\ \alpha_e \\ P_J \\ P_{i=1} \\ \cdots \\ P_{nconn} \end{bmatrix} \tag{5.26}$$

The change of the independent variables over one time-step can be expressed as:

$$\vec{f}(\vec{x}) = \vec{f}(\vec{x}_0) + D\vec{f}(\vec{x}_0)(\vec{x} - \vec{x_0}) = 0 \tag{5.27}$$

Where $\vec{x_0}$ is the vector representing the value of the independent variable at the previous time-step.

Replacing Equation 5.27 with $\Delta\vec{x} = \vec{x} - \vec{x}_0$:

$$D\vec{f}(\vec{x}_0)\Delta\vec{x} = -\vec{f}(\vec{x}_0) \tag{5.28}$$

Where $D\vec{f}(\vec{x}_0)$ and $-\vec{f}(\vec{x}_0)$ are:

$$D\vec{f}(\vec{x}_0) = \begin{bmatrix} \frac{\partial C_n}{\partial \alpha_v} & \frac{\partial C_n}{\partial \alpha_v h_v} & \frac{\partial C_n}{\partial (1-\alpha_v)h_l} & \frac{\partial C_n}{\partial \alpha_e} & \frac{\partial C_n}{\partial P_J} & \frac{\partial C_n}{\partial P_{i=1}} & \cdots & \frac{\partial C_n}{\partial P_{nconn}} \\ \frac{\partial C_l}{\partial \alpha_v} & \frac{\partial C_l}{\partial \alpha_v h_v} & \frac{\partial C_l}{\partial (1-\alpha_v)h_l} & \frac{\partial C_l}{\partial \alpha_e} & \frac{\partial C_l}{\partial P_J} & \frac{\partial C_l}{\partial P_{i=1}} & \cdots & \frac{\partial C_l}{\partial P_{nconn}} \\ \frac{\partial E_v}{\partial \alpha_v} & \frac{\partial E_v}{\partial \alpha_v h_v} & \frac{\partial E_v}{\partial (1-\alpha_v)h_l} & \frac{\partial E_v}{\partial \alpha_e} & \frac{\partial E_v}{\partial P_J} & \frac{\partial E_v}{\partial P_{i=1}} & \cdots & \frac{\partial E_v}{\partial P_{nconn}} \\ \frac{\partial E_l}{\partial \alpha_v} & \frac{\partial E_l}{\partial \alpha_v h_v} & \frac{\partial E_l}{\partial (1-\alpha_v)h_l} & \frac{\partial E_l}{\partial \alpha_e} & \frac{\partial E_l}{\partial P_J} & \frac{\partial E_l}{\partial P_{i=1}} & \cdots & \frac{\partial E_l}{\partial P_{nconn}} \\ \frac{\partial C_e}{\partial \alpha_v} & \frac{\partial C_e}{\partial \alpha_v h_v} & \frac{\partial C_e}{\partial (1-\alpha_v)h_l} & \frac{\partial C_e}{\partial \alpha_e} & \frac{\partial C_e}{\partial P_J} & \frac{\partial C_e}{\partial P_{i=1}} & \cdots & \frac{\partial C_e}{\partial P_{nconn}} \\ \frac{\partial C_v}{\partial \alpha_v} & \frac{\partial C_v}{\partial \alpha_v h_v} & \frac{\partial C_v}{\partial (1-\alpha_v)h_l} & \frac{\partial C_v}{\partial \alpha_e} & \frac{\partial C_v}{\partial P_J} & \frac{\partial C_v}{\partial P_{i=1}} & \cdots & \frac{\partial C_v}{\partial P_{nconn}} \end{bmatrix} \tag{5.29}$$

$$-\vec{f}(\vec{x}_0) = \begin{bmatrix} E_{C_n} \\ E_{C_l} \\ E_{E_v} \\ E_{E_l} \\ E_{C_e} \\ E_{C_v} \end{bmatrix} \tag{5.30}$$

Being:

- $D\vec{f}(\vec{x}_0)$ the Jacobian of the system of equations evaluated for the set of independent variables, composed of analytical derivatives of each equation with respect to linear variation of the independent variables.
- $\Delta\vec{x}$ the change of the independent variables over one time-step.
- $-\vec{f}(\vec{x}_0)$ the negative of the residual errors to zero each equation value.

CTF uses Equation 5.28 to solve the momentum equation at each volume, estimating the new-time velocities from the known values at the present time-step. By the discretization of the momentum equation, a system of equations is obtained, which relates volume pressures to the junction flows.

Equation 5.28 is then adapted to the coupling methodology by, in the case of facing a coupling junction, being expanded with the terms $RCJ(1..6)$ and P_{CJ}:

$$\begin{bmatrix} \frac{\partial C_n}{\partial \alpha_v} & \frac{\partial C_n}{\partial \alpha_v h_v} & \frac{\partial C_n}{\partial (1-\alpha_v) h_l} & \frac{\partial C_n}{\partial \alpha_e} & \frac{\partial C_n}{\partial P_J} & \frac{\partial C_n}{\partial P_{i=1}} & \cdots & \frac{\partial C_n}{\partial P_{nconn}} & RJC(1) \\ \frac{\partial C_l}{\partial \alpha_v} & \frac{\partial C_l}{\partial \alpha_v h_v} & \frac{\partial C_l}{\partial (1-\alpha_v) h_l} & \frac{\partial C_l}{\partial \alpha_e} & \frac{\partial C_l}{\partial P_J} & \frac{\partial C_l}{\partial P_{i=1}} & \cdots & \frac{\partial C_l}{\partial P_{nconn}} & RJC(2) \\ \frac{\partial E_v}{\partial \alpha_v} & \frac{\partial E_v}{\partial \alpha_v h_v} & \frac{\partial E_v}{\partial (1-\alpha_v) h_l} & \frac{\partial E_v}{\partial \alpha_e} & \frac{\partial E_v}{\partial P_J} & \frac{\partial E_v}{\partial P_{i=1}} & \cdots & \frac{\partial E_v}{\partial P_{nconn}} & RJC(3) \\ \frac{\partial E_l}{\partial \alpha_v} & \frac{\partial E_l}{\partial \alpha_v h_v} & \frac{\partial E_l}{\partial (1-\alpha_v) h_l} & \frac{\partial E_l}{\partial \alpha_e} & \frac{\partial E_l}{\partial P_J} & \frac{\partial E_l}{\partial P_{i=1}} & \cdots & \frac{\partial E_l}{\partial P_{nconn}} & RJC(4) \\ \frac{\partial C_e}{\partial \alpha_v} & \frac{\partial C_e}{\partial \alpha_v h_v} & \frac{\partial C_e}{\partial (1-\alpha_v) h_l} & \frac{\partial C_e}{\partial \alpha_e} & \frac{\partial C_e}{\partial P_J} & \frac{\partial C_e}{\partial P_{i=1}} & \cdots & \frac{\partial C_e}{\partial P_{nconn}} & RJC(5) \\ \frac{\partial C_v}{\partial \alpha_v} & \frac{\partial C_v}{\partial \alpha_v h_v} & \frac{\partial C_v}{\partial (1-\alpha_v) h_l} & \frac{\partial C_v}{\partial \alpha_e} & \frac{\partial C_v}{\partial P_J} & \frac{\partial C_v}{\partial P_{i=1}} & \cdots & \frac{\partial C_v}{\partial P_{nconn}} & RJC(6) \end{bmatrix} \begin{bmatrix} \partial \alpha_v \\ \partial \alpha_v h_v \\ \partial (1-\alpha_v) h_l \\ \partial \alpha_e \\ \partial P_J \\ \partial P_{i=1} \\ \cdots \\ \partial P_{nconn} \\ \partial P_{CJ} \end{bmatrix} = - \begin{bmatrix} E_{C_n} \\ E_{C_l} \\ E_{E_v} \\ E_{E_l} \\ E_{C_e} \\ E_{C_v} \end{bmatrix} \tag{5.31}$$

The original Jacobian matrix is modified for every volume, where $ncon$ represents the number of connections of the volumes to other volumes. In the case of a volume being connected to a coupling junction, the Jacobian matrix is expanded to take into account the connection (CJ) with the associated pressure P_{CJ}. Also, $RJC(1..6)$ represent the junction coefficients that include the effects of the coupling junctions.

The junction coefficients $RJC(1..6)$ are calculated by CTF, but since they are not necessary at the top or bottom of the sub-channels, in the standalone version they are overwritten. Before that, they are read and stored by the program to be used for the matrix expansion with the coupling junctions. This way, the pressures of all CTF domain are related through the application of the Jacobian matrices.

The following expressions relate the pressure differences of connected volumes to the mass flow rates across the junctions:

$$\dot{m}_l(i,j) = \dot{m}_l(i,j)_0 + \frac{\partial \dot{m}_l(i,j)}{\partial p}[p(i,j) - p(i,j-1)] \tag{5.32}$$

$$\dot{m}_e(i,j) = \dot{m}_e(i,j)_0 + \frac{\partial \dot{m}_e(i,j)}{\partial p}[p(i,j) - p(i,j-1)] \tag{5.33}$$

$$\dot{m}_g(i,j) = \dot{m}_g(i,j)_0 + \frac{\partial \dot{m}_g(i,j)}{\partial p}[p(i,j) - p(i,j-1)] \tag{5.34}$$

The CTF pressure matrix for the coupled system (Equation 5.36) results from the expansion of the original matrix (Equation 5.35). In this step of the coupling scheme, the CTF pressure matrix must be expanded to add the effect of the pressure and flow effects to the solution in all CTF domain. While the junction pressure effects have been already calculated (noted as K terms), the flow effects (L terms) are to be calculated.

The CTF original pressure matrix is:

$$\begin{bmatrix} J_{1,1} & ... & J_{1,N_n} \\ ... & ... & ... \\ J_{N_n,1} & ... & J_{N_n,N_n} \end{bmatrix} \begin{bmatrix} \delta P_1 \\ ... \\ \delta P_{N_n} \end{bmatrix} = \begin{bmatrix} b_1 \\ ... \\ b_{N_n} \end{bmatrix} \tag{5.35}$$

The CTF modified pressure matrix results:

$$\begin{bmatrix} J_{1,1} & ... & J_{1,Nnode} & K_{1,I} & ... & K_{1,Njun} \\ ... & ... & ... & ... & ... & ... \\ J_{Nnode,1} & ... & J_{Nnode,Nnode} & K_{Nnode,I} & ... & K_{Nnode,Njun} \\ L_{1,1} & ... & L_{1,N_n} & L_{1,I} & ... & L_{1,Njun} \\ ... & ... & ... & ... & ... & ... \\ L_{Nnode,1} & ... & L_{Nnode,Nnode} & L_{Nnode,I} & ... & L_{Nnode,Njun} \end{bmatrix} \begin{bmatrix} \delta P_1 \\ ... \\ \delta P_{Nnode} \\ \delta P_I \\ ... \\ \delta P_{Njun} \end{bmatrix} = \begin{bmatrix} b_1 \\ ... \\ b_{Nnode} \\ a_1 \\ ... \\ a_{Nnode} \end{bmatrix} \tag{5.36}$$

For a coupling scheme with two coupling junctions at the top and bottom of the hydrodynamic system, the coupled pressure matrix can be simplified as:

$$\begin{bmatrix} J_{1,1} & ... & J_{1,Nnode} & K_{1,I} & K_{1,Njun} \\ ... & ... & ... & ... & ... \\ J_{Nnode,1} & ... & J_{Nnode,Nnode} & K_{Nnode,I} & K_{Nnode,Njun} \\ -\lambda\beta_{CBV1-J1} & 0 & -\lambda\beta_{CBV1-J2} & 1+\lambda\beta_{CBV1-J1} & \lambda\beta_{CBV1-J2} \\ -\lambda\beta_{CBV2-J1} & 0 & -\lambda\beta_{CBV2-J2} & \lambda\beta_{CBV2-J1} & 1+\lambda\beta_{CBV2-J2} \end{bmatrix} \begin{bmatrix} \delta P_1 \\ ... \\ \delta P_{Nnode} \\ \delta P_{CBV1} \\ \delta P_{CBV2} \end{bmatrix} = \begin{bmatrix} b_1 \\ ... \\ b_{Nnode} \\ \alpha_{CBV1} \\ \alpha_{CBV2} \end{bmatrix} \tag{5.37}$$

Where the coefficients α_k and β_k are:

$$\alpha_k = A_k + \sum_{i=1}^{7} \sum_{j=1}^{NC} B_{k,j} * RFLOW(i,j) \tag{5.38}$$

$$\beta_k = \sum_{i=1}^{7} B_{k,j} * DRFLOWDP(i,j) \tag{5.39}$$

Being $RFLOW(i,j)$ the flows sent from RELAP5 and $DRFLOWDP(i,j)$ the flow derivatives that are coincident with the RELAP5 coefficients previously calculated. The next step is to solve the CTF pressure matrix. The solution for the coupling volumes will be later used to calculate the junction flows.

5.2 Coupled code coding

5.2.1 CTF-RELAP5 Program requeriments

The new program consists of the integration of CTF and RELAP5 codes, by maintaining the original code capabilities and the input/output decks format. In this case, RELAP5, written in Fortran 77, and CTF, written in Fortran 90, have been compiled together in a single-thread executable.

The integration has been carried out by merging the RELAP5 routines into CTF. The coupled code follows the CTF original structure with calls to RELAP5 portions of code organized as subroutines. In addition, a Fortran 90 module called `ctfrelap` has been created to store all the common variables and subroutines related to the coupling, in order to reduce to the minimum the addition of new code lines to CTF and RELAP5. Also, aside from modifying some parts of the RELAP5 code, some RELAP5 routines have been created to perform specific tasks related to the coupling data exchange.

In the case of the work developed by W.L. Weaver [29] used as a reference, the use of PVM allowed the parallel execution of certain portions of the coupled scheme. In this case, the execution of the portions of CTF and RELAP5 is in all cases sequential, since the program is designed to run in a single thread. Also, the ability of CTF to run in parallel for multiple channels [98] is not available for the coupled code.

5.2.2 Input/output format

The coupled code reads the original CTF and RELAP5 input decks and also generates the output decks with the original format, so it can be read by using the usual external software such as AptPlot® or specific Python tools. In addition, the coupled code reads a specific input deck with the following information:

- Problem time domain: The execution of the cases is divided into periods with different time-step selection values. Also, the ending of the calculation is defined.

- Time-step limits: The minimum and maximum time steps allowed for each time domain are defined.
- Output writing: The frequency of output data writing for CTF and RELAP5 is defined.
- Coupling volumes and junctions: The coupling volumes and junctions of RELAP5 and CTF are defined:

    ◦ RELAP5: The coupling junctions must be defined as time-dependent junctions. The coupling volumes at the limit of the model must be defined as time-dependent volumes, while the volume attached to the coupling junction (the actual coupling volume) must be defined as a single volume.

    ◦ CTF: Two volumes must be defined as coupling volumes, one at the top and one at the bottom of the model. The definition of the volumes must include the section, the channel and the node number.

5.2.3 Time-step selection

The time-step used for each time-advancement calculation is set to the minimum value of the minimum time steps calculated by CTF and RELAP5, as described in Sections 2.1 and 2.2.

5.2.4 File structure

The file structure of the CTF-RELAP5 program is described by Figures 5.2 and 5.3. The figures show the main subroutines of the codes, the points of information exchange between programs and the step and time advancements.

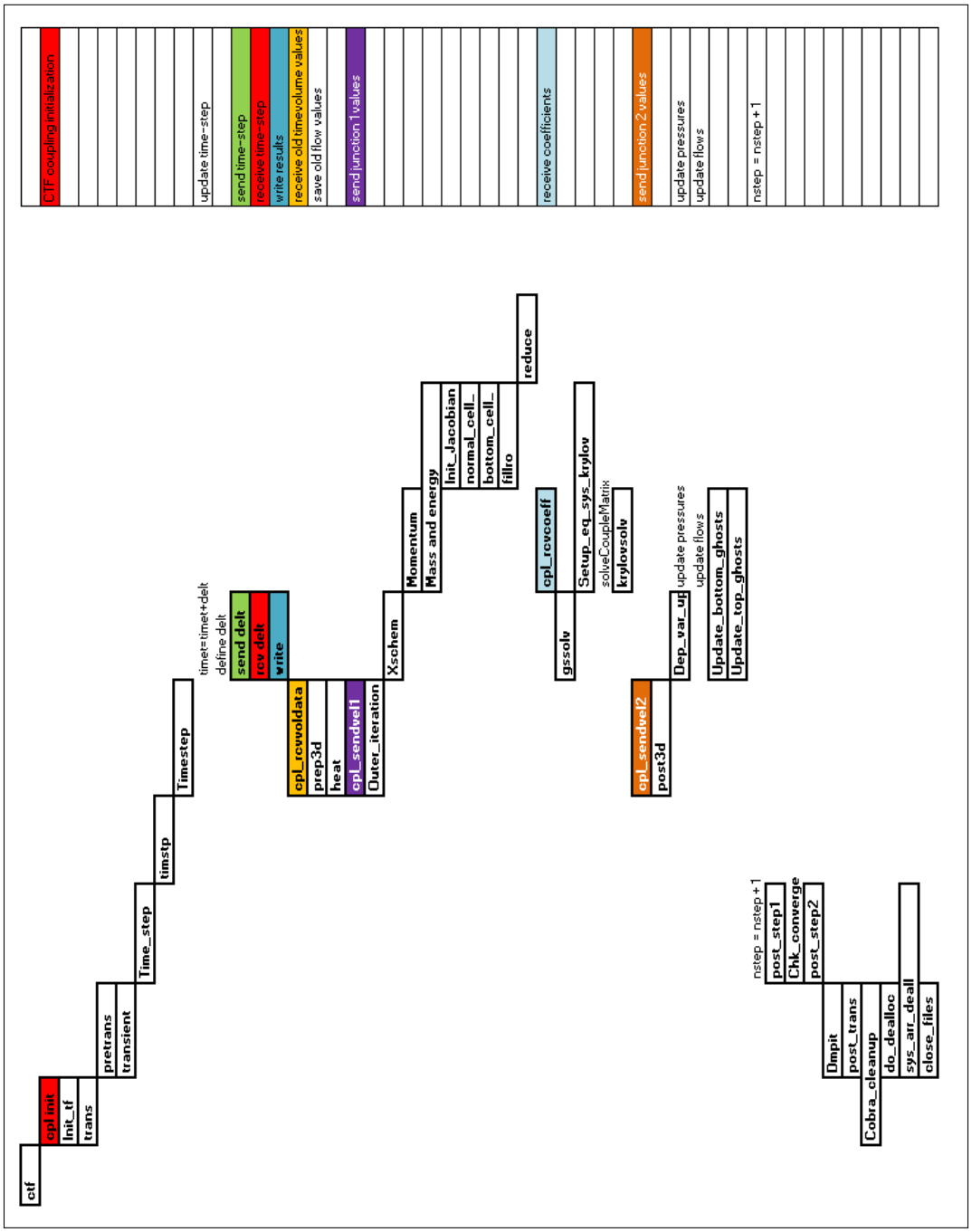

Figure 5.2: *RELAP5 routines coupling scheme, showing the main subroutines of RELAP5 relevant to coupling, the points of information exchange between programs and the step and time advancements.*

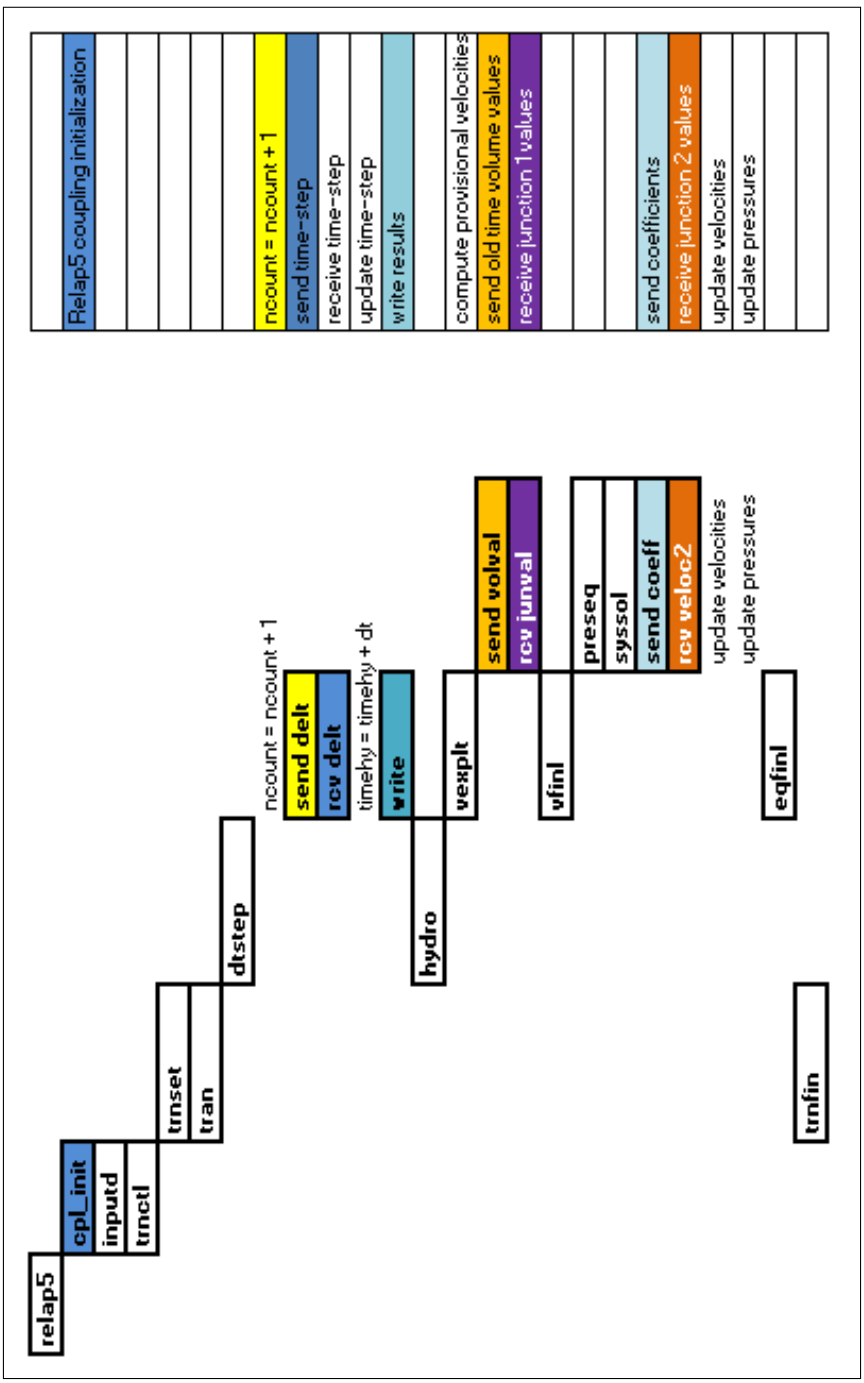

Figure 5.3: *CTF routines coupling scheme, showing the main subroutines of CTF relevant to coupling, the points of information exchange between programs and the step and time advancements.*

5.2.5 Exchange of fluid properties between codes

As described in the CTF-RELAP5 file structure, several points of data exchange are defined, two related to junction values and one related to volume values. The description of the data exchange between codes is presented in Tables 5.2, 5.3 and 5.4. The data of CTF and RELAP5 must be converted from SI units to BU units and vice-versa since the codes are using different units for physical properties. Two other groups of data are exchanged between the codes, aside from the values present in the tables:

- Power: The RELAP5 point kinetics model computes the reactor thermal power as a function of the core reactivity. In the coupling scheme, it is used to send CTF the reactor power at every time-step. In this case, the fuel and moderator reactivity effects have been taken into account in RELAP5 as described in Section 6.1.
- Boron concentration: The boron concentration is sent and imposed from RELAP5 to CTF for the inlet coupling volumes and from CTF to RELAP5 for the outlet coupling volumes.

Property	Description
ng	Junction mass flow rate of non-condensable gas (kg/s)
ug	Junction flow rate of vapor internal energy (J/s)
uf	Junction flow rate of liquid internal energy (J/s)
mg	Junction flow rate of vapor (kg/s)
mf	Junction flow rate of liquid (kg/s)
wg	Junction volumetric flow rate of vapor (m3/s)
wf	Junction volumetric flow rate of liquid (m3/s)

Table 5.2: *CTF-RELAP5 exchanged coupling junction data 1*

Property	Description
voidgj	Junction Vapor fraction (-)
rhogj	Junction Vapor density (kg/m3)
ugj	Junction Vapor specific internal energy (J/kg)
qualaj	Junction Mass quality of non-condensable gas (-)
velgj	Junction Vapor velocity (m/s)
voidfj	Junction Liquid fraction (-)
rhofj	Junction Liquid density (kg/m3)
ufj	Junction Liquid specific internal energy (J/kg)
velfj	Junction Liquid velocity (m/s)
qualanj1 to 5	Junction Mass quality of first to fifth non-condensable gas (-)

Table 5.3: *CTF-RELAP5 exchanged coupling junction data 2*

Property	Description
p	Pressure (Pa)
voidg	Vapor fraction (-)
voidf	Liquid fraction (-)
ug	Vapor specific internal energy (J/kg)
uf	Liquid specific internal energy (J/kg)
quala	Mass quality of non-condensable gas (-)
rhog	Vapor density (kg/m3)
rhof	Liquid density (kg/m3)
tempg	Vapor temperature (K)
tempf	Liquid temperature (K)
qualan1 to 5	Mass quality of first to fifth non-condensable gas (-)

Table 5.4: *CTF-RELAP5 exchanged coupling volume data*

5.3 CTF-RELAP5 code verification

The next steps introduce the verification of the coupled code. A simplified model has been developed to verify that pressures, massflows and fluid properties are consistent when coupling CTF and RELAP5. For this purpose, two transient scenarios have been executed. This section includes the description of the model, the transient scenarios and comments on the results. The verification tests carried out show consistent results for CTF and RELAP5 codes.

5.3.1 Verification model and transient scenarios

A simple verification model has been built for carrying out the verification of the CTF-RELAP5 SIC (as shown in Figure 5.4). It consists of three sections: the inlet section, the central section and the outlet section. Both the inlet and the outlet sections are modelled in RELAP5, while the central section is modelled in CTF. Both the inlet and outlet sections include time-dependent volumes and time-dependent junctions to impose the conditions for the transients. The inlet volume imposes the liquid enthalpy and the mass flow rate, while the outlet volume imposes the system pressure.

The main parameters of the model are presented in Table 5.5. The model has been built with the objective of having a similar geometry with a fuel assembly and a limited number of nodes. The steady-state conditions of the model are:

- Outlet pressure: 15.52 MPa
- Inlet temperature: 580.0 K
- Inlet mass flow rate: 0.348 kg/(s*cm^2)

The conditions for the transients are designed to be as close as possible to the base cases performed: a pressure decrease and a mass flow rate decrease.

- Transient A: Outlet pressure decreases from 15.52 MPa to 13 MPa.
- Transient B: Mass flow rate decreases from 0.348 to 0.210 kg/(s*cm^2).

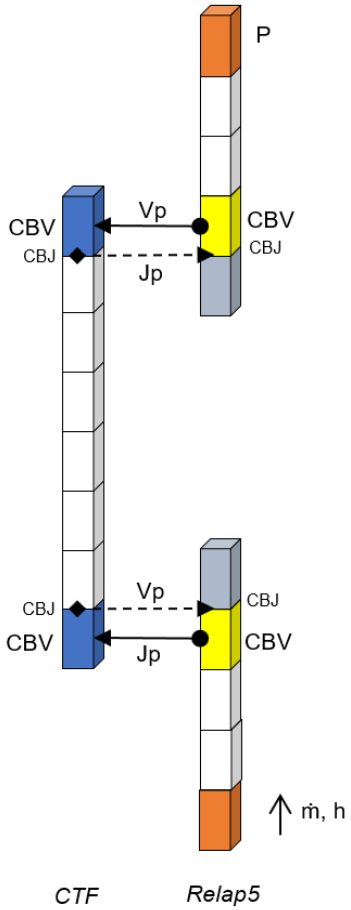

Figure 5.4: *CTF-RELAP5 verification model*

Flow Area	0.02415 m^2
Channels	1
CTF section number of nodes	8
RELAP5 sections number of nodes	5
CTF section height	3.7925 m
RELAP5 sections height	1.7238 m
Number of Rods	0
CTF grids located	as shown in Figure 6.3

Table 5.5: *Main parameters of the verification model*

5.3.2 Results and comments

Figures 5.5 to 5.8 show the mass flow rates and pressures for CTF and RELAP5 for Transients A and B. The steady-state results present consistent values between the RELAP5 model (R_in, R_out) and CTF model (C_1 ... C_7).

- Transient A: Figures 5.5 and 5.6 show that, while pressure decreases due to the BCs applied, some minor flow oscillations are observed. Also, some oscillations are observed in the pressure plot. It is important to note that despite the oscillations the values of pressure and mass flow rates are consistent between the coupled codes.

- Transient B: As seen in Figures 5.7 and 5.8, a good agreement of the mass flow rates are observed as the mass flow rate decreases. In the case of pressures, some oscillations are observed during the transient, with low amplitude, and recovering to final and consistent values. In this case, the pressures between RELAP5 and CTF present a small degree of inconsistency during the transient.

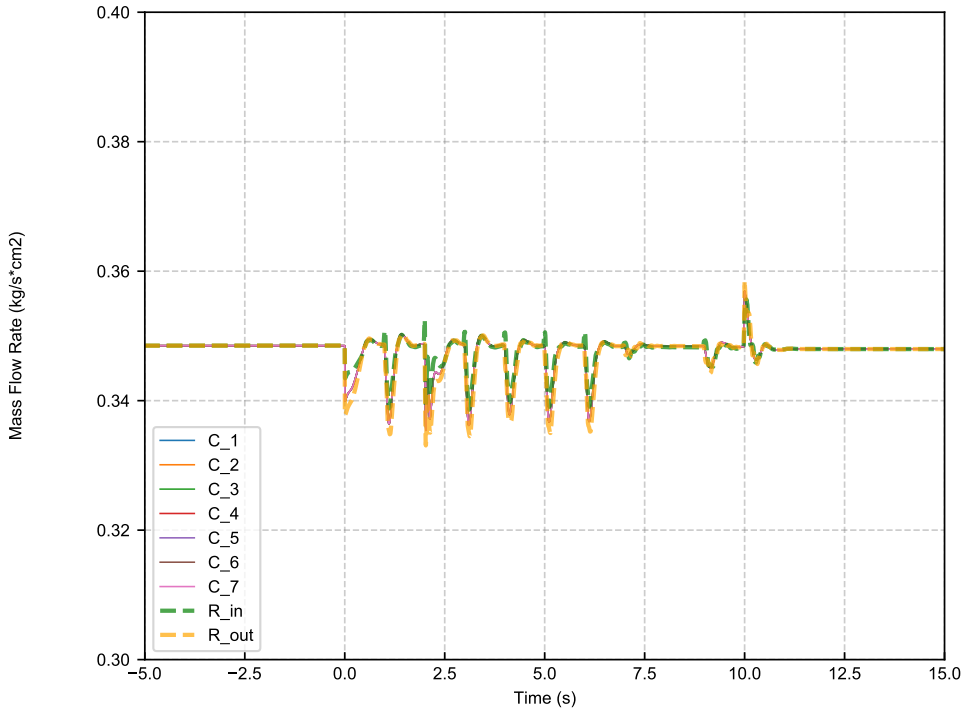

Figure 5.5: *Transient A: Mass flow rates*

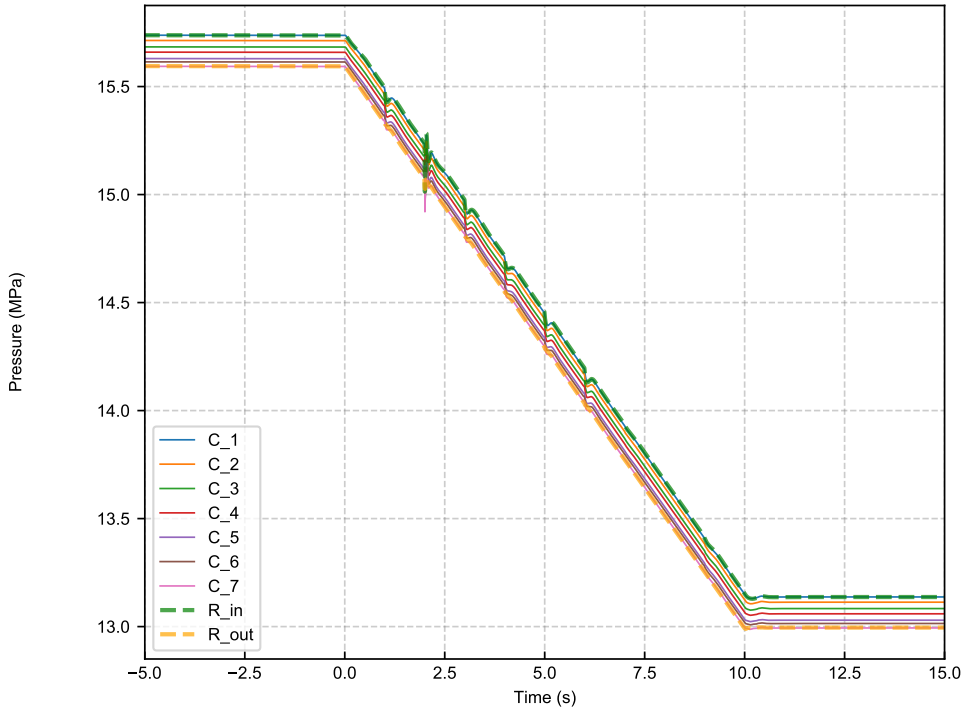

Figure 5.6: *Transient A: Pressures*

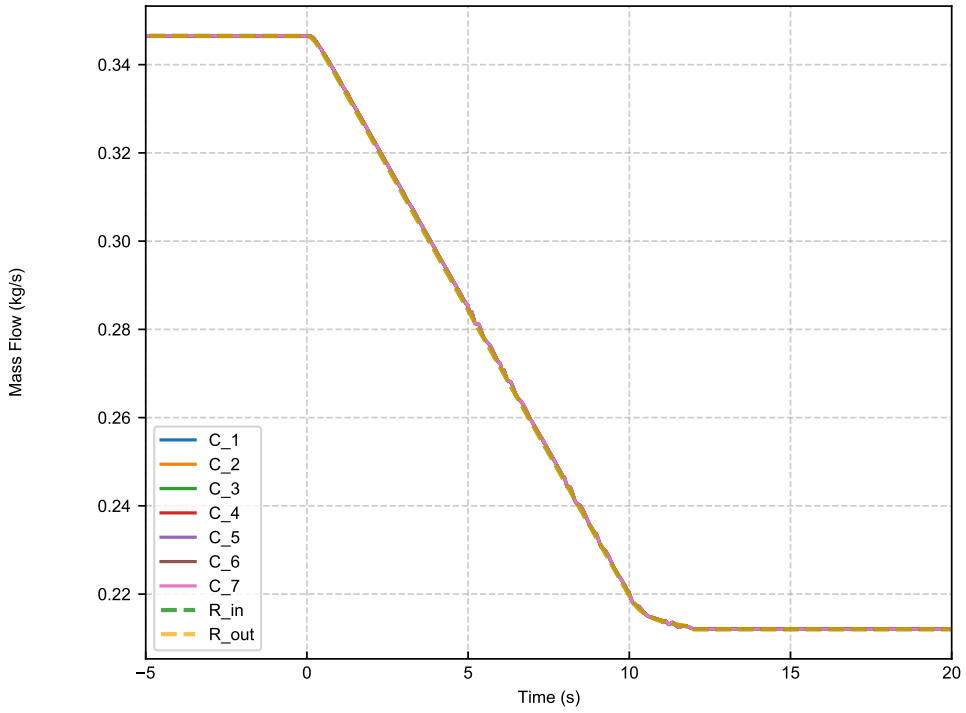

Figure 5.7: *Transient B: Mass flow rates*

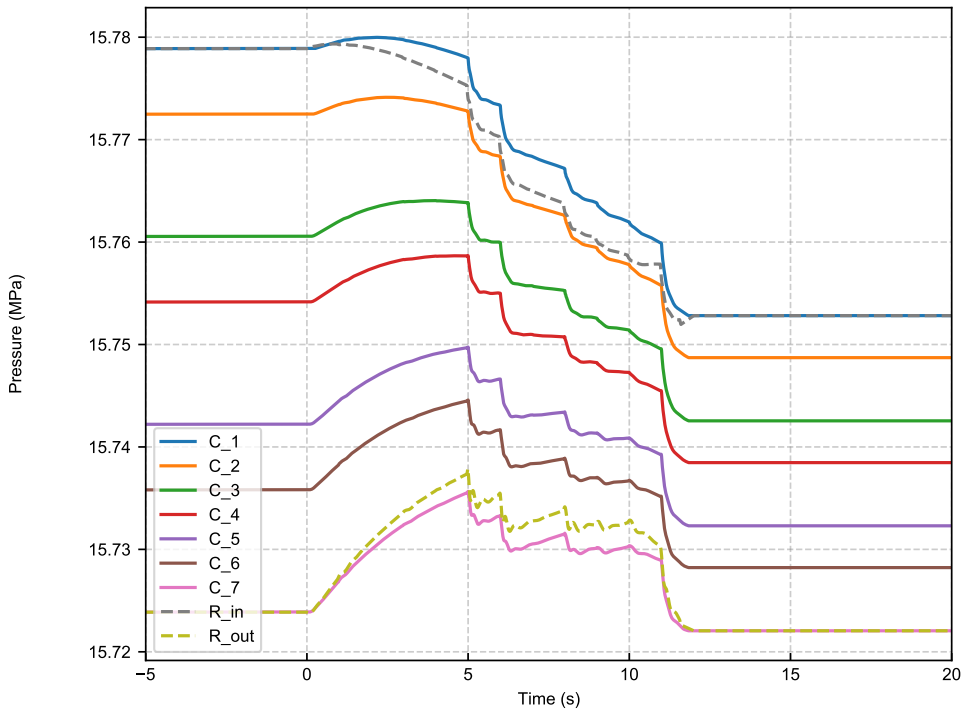

Figure 5.8: *Transient B: Pressures*

CHAPTER 6

DESCRIPTION OF THE CORE AND SYSTEM MODELS

This chapter contains:

- The RELAP5 plant model description
- The CTF assembly and sub-channel core models description
- The CTF hybrid core model description

6.1 RELAP5 plant model description

The RELAP5 plant model used in this study consists of an adaptation from an original full-plant model of a generic Westinghouse 3-loop NPP. The adaptation has been performed by taking into account the requirements of the SIC and OLC methods described in Sections 3.2 and 3.3. First, the original model used in the OLC method is described, and second, the changes to adapt the model to the SIC method are listed.

6.1.1 Original RELAP5 plant model

The original RELAP5 plant model consists of a full plant model of a generic Westinghouse 3-loop NPP, derived from a model previously used in many studies [99] [100] [101], which has undergone many improvements since it was created by UPC Advanced Nuclear Technologies (UPC-ANT) group. The improvements include the core modelling as parallel channels with transverse connections, an improved nodalization of the SGs, the improved nodalization of the upper plenum and the improved modelling of the core thermocouples. Some of the works conducted by UPC-ANT were specifically related to the qualification of the model [68] [102].

6.1.1.1 System nodalization

The RELAP5 model simulates the main NPP systems: the primary and secondary circuits, the ECCS, the main and auxiliary feedwater systems, the steam supply systems, the plant controls and the reactor protection system in an extensive and accurate manner. The model uses 549 hydrodynamic volumes, 1454 control variables and 672 variables and logical trips. Table 6.1 describes the main parameters of the model and Figure 6.1 shows the original plant model nodalization, with a simplified representation of the main hydrodynamic components, excluding the reactor vessel.

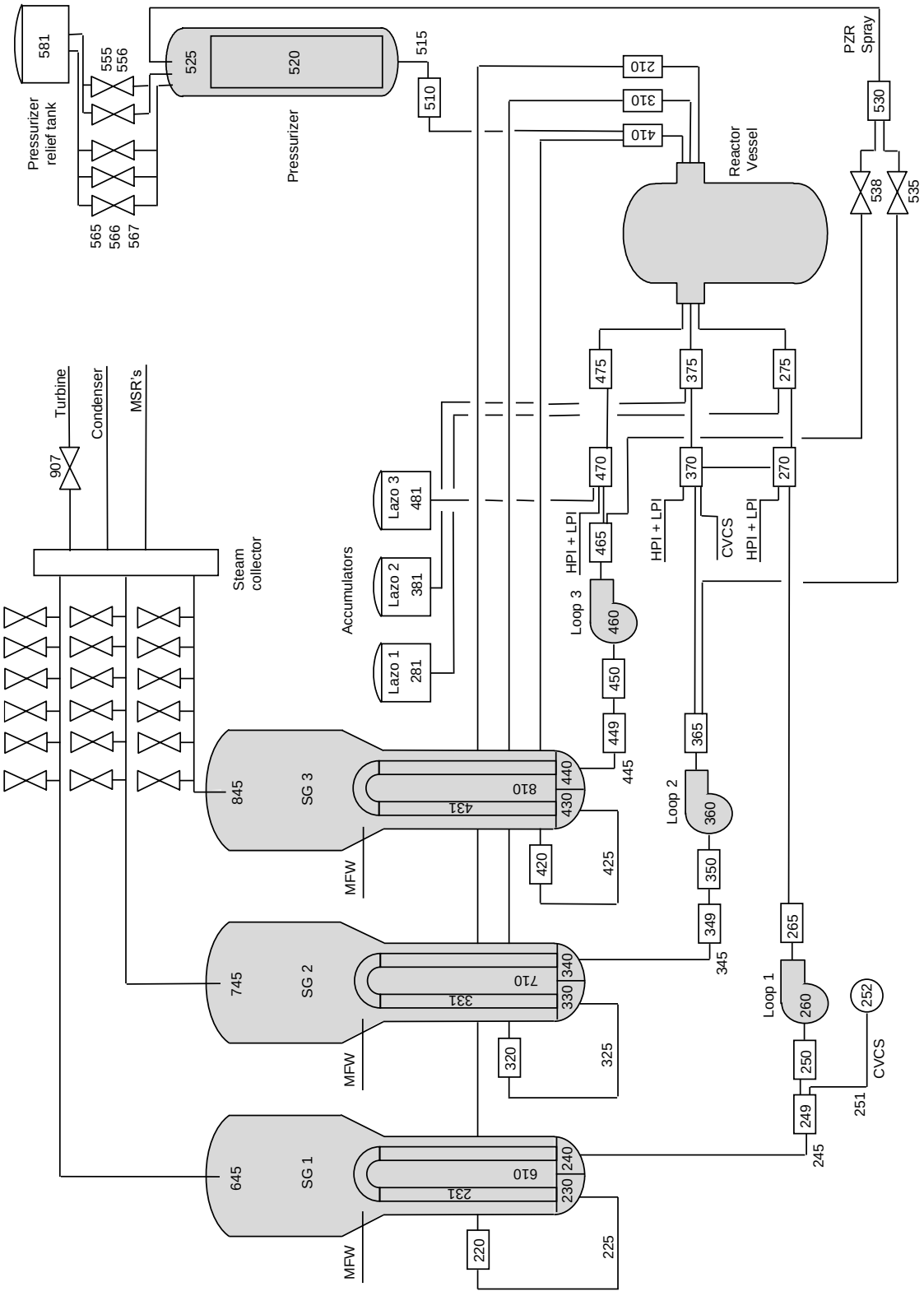

Figure 6.1: *Original RELAP5 model plant nodalization*

System	Loops	3
System	Thermal power	2940 MW
System	Nominal pressure	15.52 MPa
System	Average temperature	580.05 K
System	Core mass flow rate	13789.0 kg/s
System	Pressurizer level	60%
System	Steam pressure	6.5 MPa
System	Feedwater mass flow rate	1675.0 kg/s
System	SG level	50%
Core	Fuel elements	157
Core	Number of fuel rods	264 (17x17)
Core	Number of guide tubes	24
Core	Number of instrumentation tubes	1
Core	Fuel pellet diameter	8.192 mm
Core	Clad outer diameter	9.5 mm
Core	Clad thickness	0.57 mm
Core	Fuel active lenght	3.7925 m

Table 6.1: *Original RELAP5 model vessel nodalization*

6.1.1.2 Core nodalization

The nodalization of the core model present in the original RELAP5 model is shown in Figure 6.2. The core is modelled by 4 parallel channels with 19 axial nodes per channel (multi-pipe approach), which permits adequate modelling of the active and passive heat structures [102].

The vessel is built from a set of connected volumes to account for the main parts: the cold legs (275, 375, 475) are connected to a set of volumes (275, 375, 475) that represent the downcomer, the bottom of the downcomer volumes are connected to volumes 110 and 112 that represent the lower plenum of the vessel. Volume 112 is connected to the four pipes (121 to 123) representing the core. The top of the core pipes is connected to a set of elements (140, 150, 155, 158, 160) that represent the upper plenum and the

vessel head, having connections to the hot legs (210, 310, 410). The active portion of the core is modelled by four vertical parallel pipes that include cross-flow junctions, in order to account for the transverse mass transport between channels. The axial nodes have the same geometrical vertical properties (height and length) for every one of the four channels.

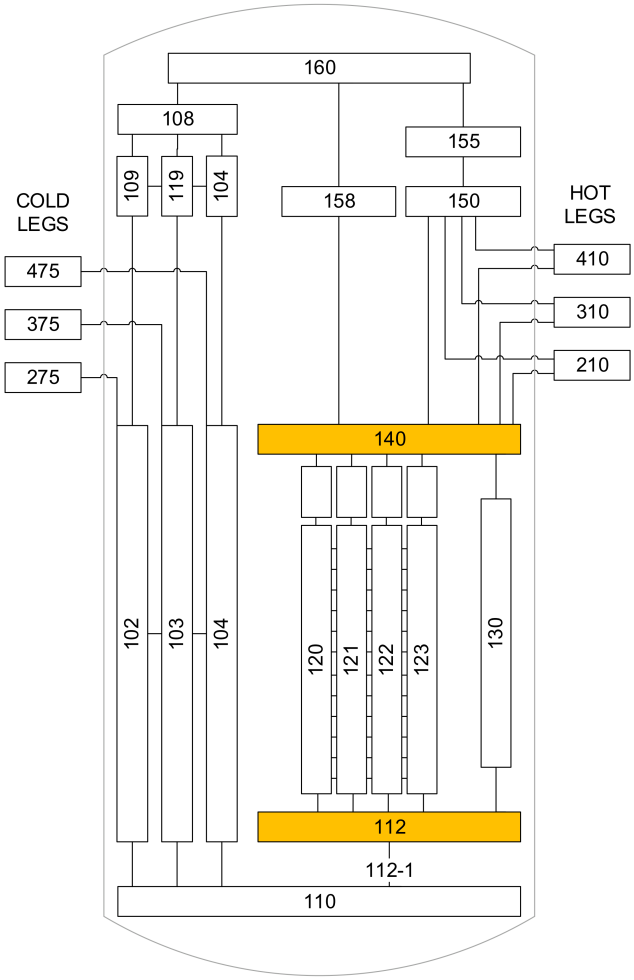

Figure 6.2: *Original RELAP5 model excluding the vessel*

The cross-flow junctions are defined to connect all axial nodes from every channel at the same height. Figure 6.3 shows a representation of the fuel element of reference for the RELAP5 and CTF core models, where the length of the axial nodes has been set to preserve the distances between the fuel mixing vanes.

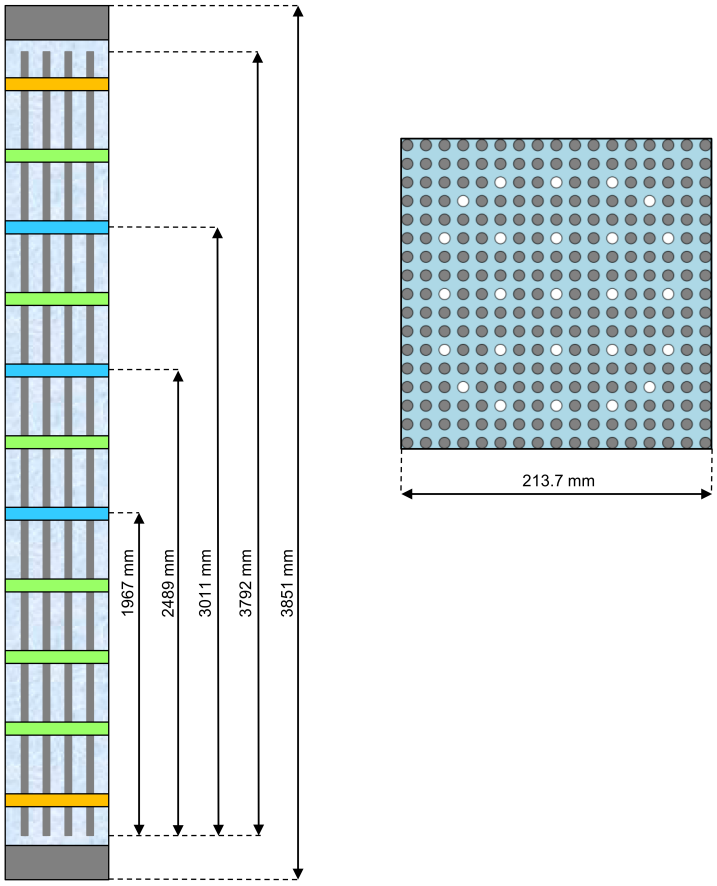

Figure 6.3: *Representation of a fuel element for RELAP5 and CTF core models*

The core power is distributed amongst the heat structures in contact with each vertical parallel pipe of the model. The radial distribution is done by radially dividing the core into power zones, so each power zone represents a fraction of the core with a similar power factor. The fuel assemblies are then grouped according to their linear heat generation rate (LHGR) into four groups (Low, Average, Hot 1 and Hot 2 zones as shown in Figure 6.4), having the average power factors described in Table 6.2.

Zone	Elements	Power Factor	Area fraction
Low	37	0.424	0.234
Average	57	1.097	0.362
Hot 1	43	1.242	0.276
Hot 2	20	1.324	0.128

Table 6.2: *Core power zones data*

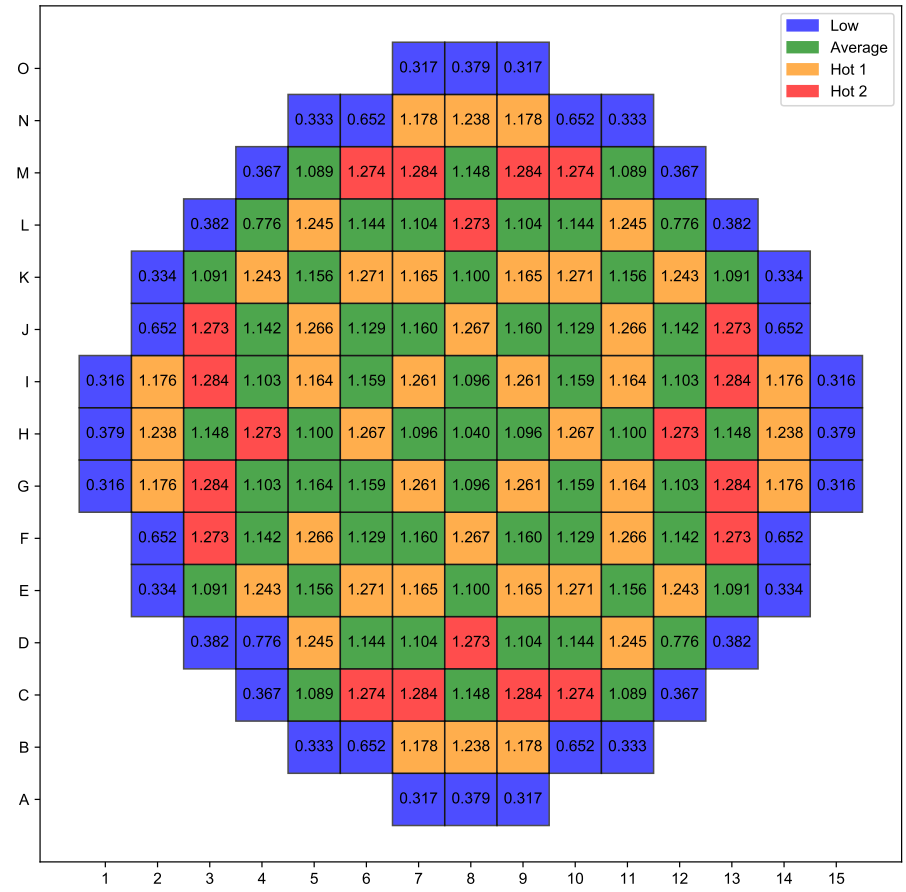

Figure 6.4: *Core average power factors and assembly power grouping*

The heat structures connected to the core channels represent the proportional amount of nuclear fuel in each core power zone. The pipes area is set also according to the area of the group of represented fuel assemblies. The Hot 1 zone has also a heat structure that represents the hot rod, with a power factor of 1.583. The axial power distribution for each zone is shown in Figure 6.5.

It is important to note that the division of the core in 4 parallel channels is not related to any simplification of the spatial core power distribution; it is the result of a process of grouping the regions of the core with similar power density. This way, the channel representing the region with the highest power density is connected to the heat structure that represents the fuel rod with the highest power. It is in this heat structure where the most restrictive results are expected, as it represents the hot pin.

However, the results obtained from this core model are not used in the present study,

since the original RELAP5 model with the core included is only used with the purpose of extracting the boundary condition values to impose on the CTF model as described in Section 3.3 for the OLC method.

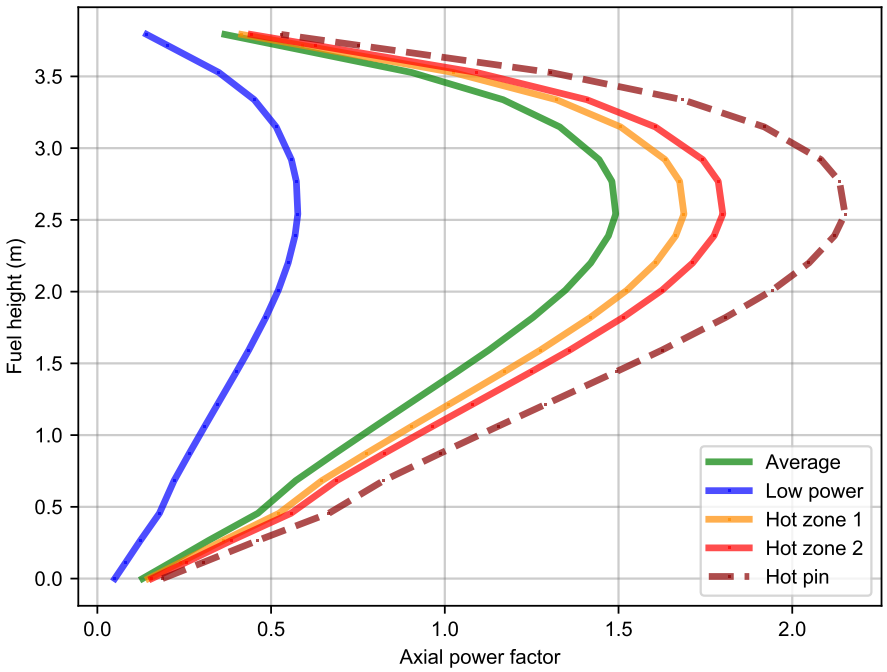

Figure 6.5: *Axial power distributions for power grouping*

6.1.1.3 Point kinetics model

The core power behaviour is obtained from the point kinetics model option included in RELAP5. This model considers that power is independent of space and it can be divided into space and time functions. As described in Section 1.3, the selected cases do not produce substantial neutron flux distribution asymmetries, so the use of the point kinetics model is considered valid.

The point kinetics model provides a power value that can be distributed across the reactor core via axial functions applied to the selected heat structures. The power considers immediate fission and decay fission products as power sources, being the immediate fission energy the result of the kinetic energy of the fission products and the energy provided by neutrons during the moderation. The decay power is computed by the values given by the American Nuclear Society (ANS) [103].

The point kinetics model considers the effect on the reactivity of the following sources:

- **Moderator temperature coefficient of reactivity (MTC)**

  The effect on reactivity due to changes in the moderator temperature is computed by applying this coefficient, which accounts for the change in reactivity due to changes in the moderator temperature. The changes in the moderator temperature affect the capacity of the moderator to slow down neutrons because of moderator density changes. Also, the moderator density changes affect the neutron capture of the moderator due to the change in the probability of resonance absorption. The point kinetics model uses the liquid density of the core vertical channels to compute the reactivity due to the moderator temperature coefficient (MTC) from input deck tables.

- **Fuel temperature coefficient of reactivity or Doppler coefficient (FTC)**

  The effect on reactivity due to changes in the fuel temperature is caused by the change of neutron resonance escape probability. The neutron capture cross-section shape is dependent on the relative kinetic energy of the incident neutron and the velocity of the target nucleus. A fuel temperature increase causes a broadening of the resonance capture cross-sections of the fertile material. This effect produces a higher neutron absorption rate, affecting reactivity. The point kinetics model uses the core heat structures temperature to compute the reactivity due to the fuel temperature coefficient (FTC) from input deck tables.

- **Differential boron coefficient**

  Boric acid is an absorber dissolved in the moderator with the function to control reactivity by absorbing neutrons. The boron concentration is decreased as the cycle advances in order to compensate for the decrease of fuel reactivity due to burn-up. The amount of reactivity that can be compensated with the boric acid is high in comparison to the reactivity that the control rods can compensate for, but the ability to change the boric acid concentration is limited because of the limited capacity of the CVCS.

  The point kinetics model takes into account the reactivity associated with the boric

acid concentration, through the use of the defined differential boron coefficient. The reactivity is obtained from the boron concentration and the liquid density of the core vertical channels.

- **Control rods**

  The negative reactivity added by the control rods is dependent on the control rods position. The control rods are modelled by a series of control variables and trips described in Section 6.1.1.4. The control rods reactivity is then obtained by an input deck table as a function of the control rods position, assuming the design bank overlap and the initial position.

6.1.1.4 System controls

In this section the main plant controls that are modelled with RELAP5 are briefly described:

- RCS pressure control
- pressurizer level control
- rod control
- main feedwater control
- turbine control

The control systems present in the model are used to obtain a desired steady-state in combination with other ways of imposing desired parameters to reach steady-state values with the purpose of consuming less computational time before the transient phase. The actuation of the control systems can be activated or blocked by the user, depending on the case assumptions.

According to NUREG-800, when selecting the conditions of a case calculation, the actuation of the control systems must be only taken into account if the effect consists of a decrease of the safety margin that is the object of study, if the safety margin is increased

as a result of the actuation of the control systems, the actuation of the systems must be blocked. In Chapter 7 the conditions of the cases of interest and the considerations over the plant controls availability are defined.

- **RCS pressure control**

  In a PWR the pressure of the RCS is controlled by a set of elements that are installed in the pressurizer. Those elements are the PORV valves, the safety valves, the spray valves and the electric heaters. The PORV valves are actuated by the control system when the pressurizer pressure reaches a set-point value.

  The safety valves are mechanically actuated by an internal mechanism when the pressure reaches a defined pressure value. The spray valves regulate the amount of subcooled water injected from the cold legs to the top of the pressurizer through spray nozzles. The effect of the cold water injection is a partial condensation of the pressurizer saturated steam, causing a pressure decrease due to the volume contraction.

  The last component is a set of electric heaters that regulate pressure by increasing the amount of steam in the pressurizer by heating the water fraction. The effect of the steam expansion is a pressurizer pressure increase. The pressurizer heaters are divided into three banks, one proportional and two backup banks.

  The main difference between the proportional and the backup banks is that the power of the proportional bank is regulated and the status of the backup banks is connected or disconnected. This way, the proportional banks compensate for the ambient heat losses and maintain the saturation conditions of the pressurizer at nominal conditions, and the backup heaters are connected when a low-pressure setpoint is reached. Figure 6.6 shows the setpoints of the pressure control elements as a function of pressure.

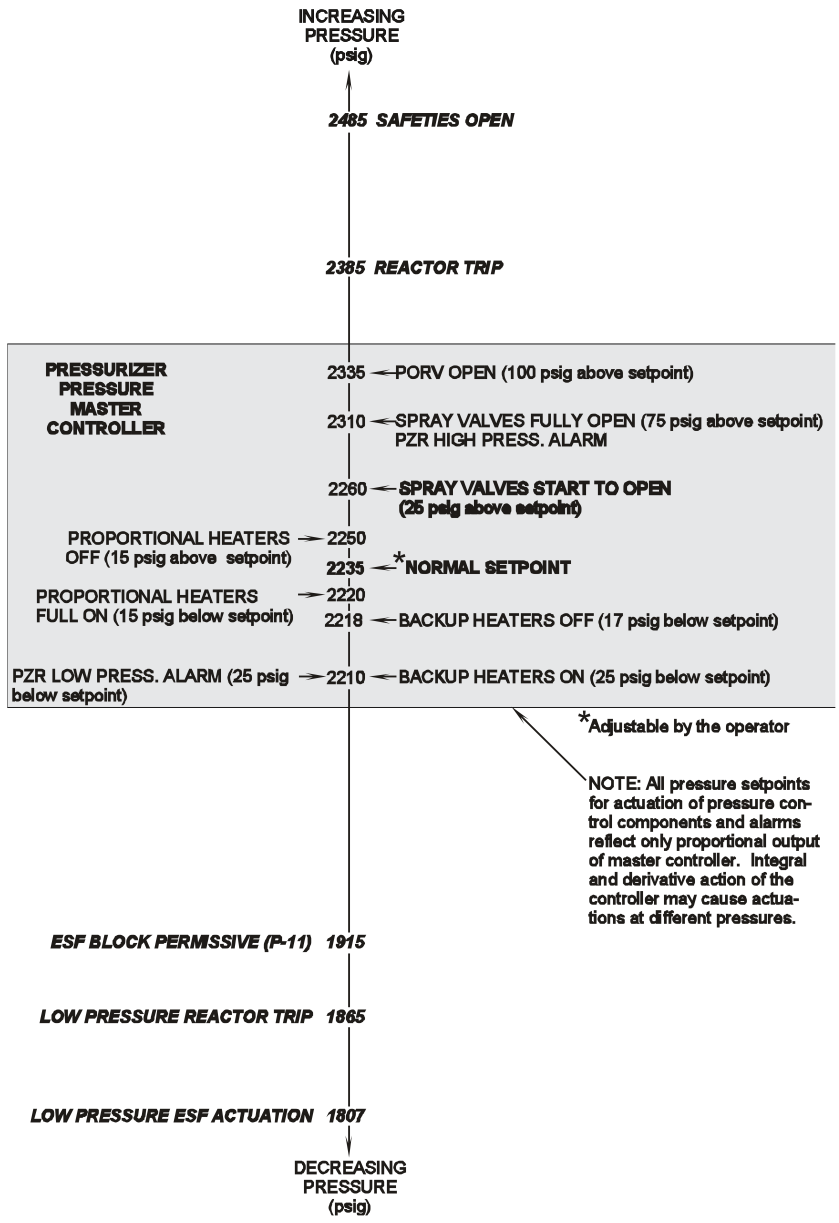

Figure 6.6: *RCS pressure control set-points (Source: U.S. NRC [1])*

- **Pressurizer level control**

  The pressurizer level control regulates the RCS inventory by actuating the CVCS charging line makeup valve. The RCS inventory balance is affected by three flow paths that are active in normal plant operation: the charging line, the discharge line and the RCP seals injection line. The last two are considered constant since they depend mainly on the RCS pressure: the CVCS discharge line has a set of orifices to control the letdown mass flow, but in normal operation, the alignment of

the orifices is not modified.

The mass flow injected to the RCS through the RCP seals is also constant, since it depends on the RCS pressure and the CVCS charging pumps header pressure. The mass flow injected through the charging line is controlled by a regulation valve as a function of the pressurizer level. The programmed pressurizer level depends on the average temperature to account for the RCS coolant expansion at different reactor power levels (see Figure 6.7).

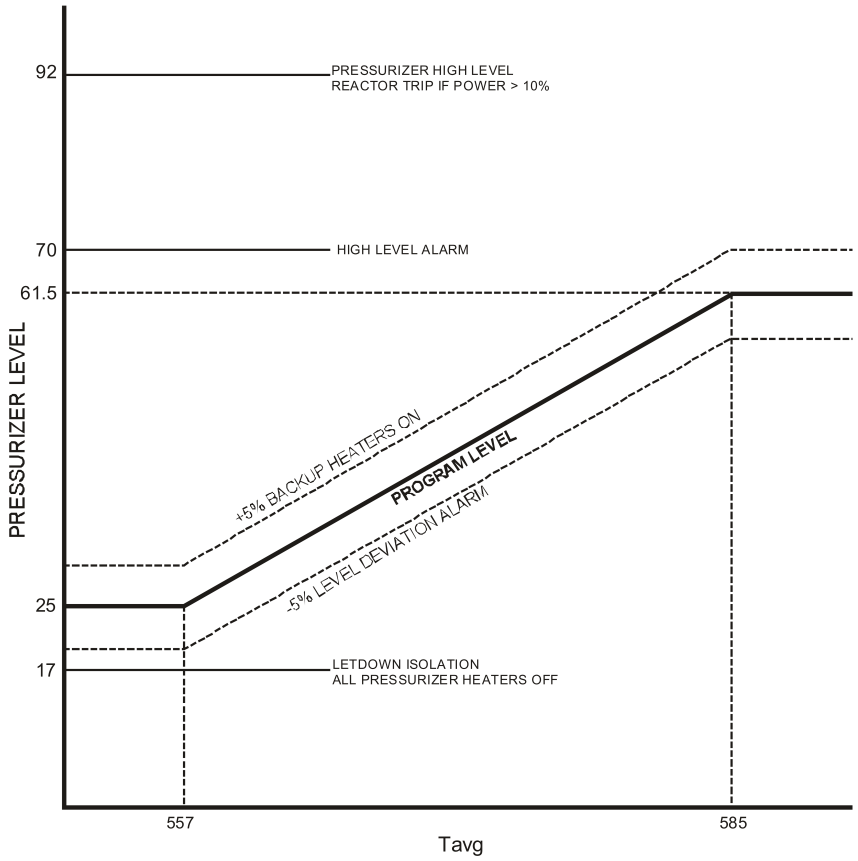

Figure 6.7: *Pressurizer level control set-points (Source: U.S. NRC [1])*

- **Rod control**

  One function of the rod control system is to control the neutron flux through the insertion/withdrawal of the control rods. Since the control rods are manufactured from one or several neutron-absorbing materials, their insertion/withdrawal into the core will produce a decrease/increase of reactivity that will cause a power decrease/increase if the reactor is critical and it is operating at power. The control

rod system regulates the position of the control rods by using a set of grippers and coils. Their actuation is driven by the demand signals either from the automatic control system or by the manual system driven by the operator.

When the system is in automatic mode, the rods are inserted/withdrawn as a function of the rod speed demand (the system does not regulate the rods position, only their speed). The system is designed to follow the average temperature program shown if Figure 6.8 by regulating the reactor power.

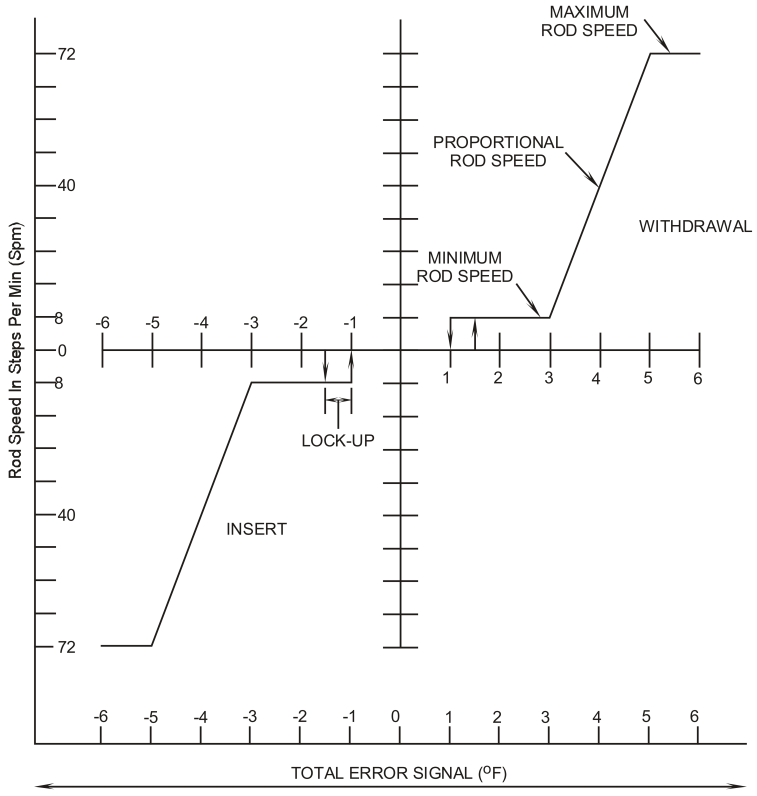

Figure 6.8: *Control rods speed program (Source: U.S. NRC [1])*

As shown in Figure 6.9, the rod speed demand program depends on the error between the reference temperature (proportional to turbine power) and the average temperature (difference between inlet/outlet vessel temperature) compensated by a set of compensating functions to improve the response of the system. The rod control system is modelled in the RELAP5 model in detail, allowing for the manual or automatic control of the system.

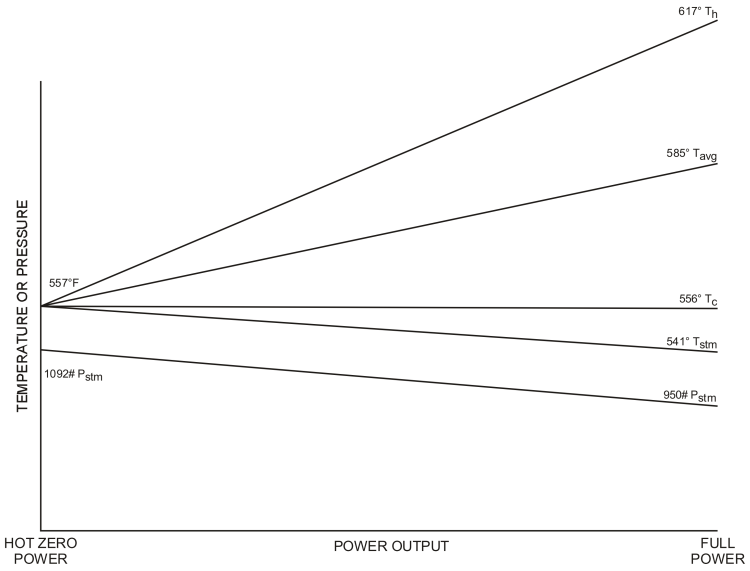

Figure 6.9: *RCS temperature control program (Source: U.S. NRC [1])*

- **Main feedwater control**

  The MFW system regulates the amount of subcooled water that is injected into the SGs, in order to maintain the narrow range level at 50%. The error level signal is compensated by the difference between steam and water massflows. The control system then actuates the main feedwater valves, which regulate the massflow supplied from the main feedwater pumps.

- **Turbine control**

  The turbine power is considered proportional to the steam flow injected into the high-pressure turbine. The steam flow is controlled by a set of valves that receive signals from the control system. The control system can work in automatic mode, where the steam massflow rate is regulated to maintain the turbine power, or in manual mode, where the valve's position depends on manual operator actuation.

  The turbine power is measured through pressure in the high-pressure turbine impulse chamber to provide a signal to the control rods system. In the RELAP5 model, the turbine is modelled as a time-dependent volume, and the turbine power is calculated proportionally from the steam flow value through the control valve.

6.1.1.5 Reactor protection system

The RPS trips the reactor when an automatic trip setpoint is reached, in addition to the manual reactor trip actuated by the operator. Automatic reactor trips have the function of protecting the core in case of deviations from critical safety-related parameters. The reactor trip signal causes the control rod system breakers to open, de-energizing all control rod coils and causing the insertion of all control rods driven by gravity.

The reactor trip delay is a relevant parameter in the safety analyses. It consists of the sum of the control rods insertion time plus the trip signal generation delay. The control rods insertion time is limited by the TS of the NPPs and set to 1.56 seconds, considered from the moment that the de-energization of the control rod coils starts until the moment the control rods are fully inserted. The trip signal generation delay is considered from the moment that the process parameter exceeds the trip setpoint until the trip signal is produced by the RPS, and it is set to 2.0 seconds.

Both cases of interest (described in Section 1.3) are terminated by the automatic reactor trip. For each case the main reactor trip has been defined, considering that is the first reactor trip setpoint to be exceeded. For each case study the reactor trip, the trip setpoint, and the time delay are:

Case	Reactor trip	Set-point	Trip delay
RCP	Low RCS flow	90% of the RCS flow	2.0 s
PORV	Low pressurizer pressure	12,85 MPa	2.0 s

Table 6.3: *Reactor trips considered in PORV and RCP cases*

6.1.2 Adapted RELAP5 plant model to SIC method

The original RELAP5 plant model has been adapted to match the requirements of the SIC scheme presented in Chapter 1. The changes made to the original model fall into three main categories: core section, point kinetics model and control variables. As a consequence of removing the core section, some of the information sent from these

components to the point kinetics model and some control systems need to be adapted to the new model, since these components no longer exist in the adapted model.

- **Core section adaptation**

  The core (containing the hydrodynamic volumes, their connections and the heat structures) has been substituted by two sets of time-dependant volumes (137 and 138) and two sets of single volumes (136 and 139) connected to volumes 112 and 140 respectively (see Figure 6.10). The original junction properties between volumes 112 and 140 and 120-123 have been preserved (junctions 255 and 259).

  This substitution is coherent with the semi-implicit coupling approach described in Section 3.2. The core bypass, connecting the inlet and outlet of the core, volumes 112 and 140, and represented by volume 130, has been unaltered from the RELAP5 original model.

- **Point kinetics model adaptation**

  In the adapted model, the point kinetics model used in the original model is kept by adapting some of the variables. In the first place, the reactor power is obtained from the point kinetics model, and instead of being applied to the RELAP5 core heat structures, it is sent to CTF, where it is imposed on the fuel rods, as described in Section 6.2. In the second place, all parameters affecting reactivity through MTC and FTC are maintained, as well as all the control-related parameters (control rods modelling and boron concentration)

  The point kinetics model of the original RELAP5 model uses three parameters related to the core components to obtain the changes in reactivity caused by the change in the core conditions: liquid temperature, liquid density and boron concentration. The first two variables are read in the user-defined multiple locations and the reactivity is computed by applying input deck reactivity tables with the averaged values. The third variable is obtained by a user-defined control variable that ponderates the boron concentration with the volume of each hydrodynamic volume in the core.

  In the adapted model the liquid temperature, liquid density and boron concentration are sent from CTF to the RELAP5 point kinetics model. Since the parameters can

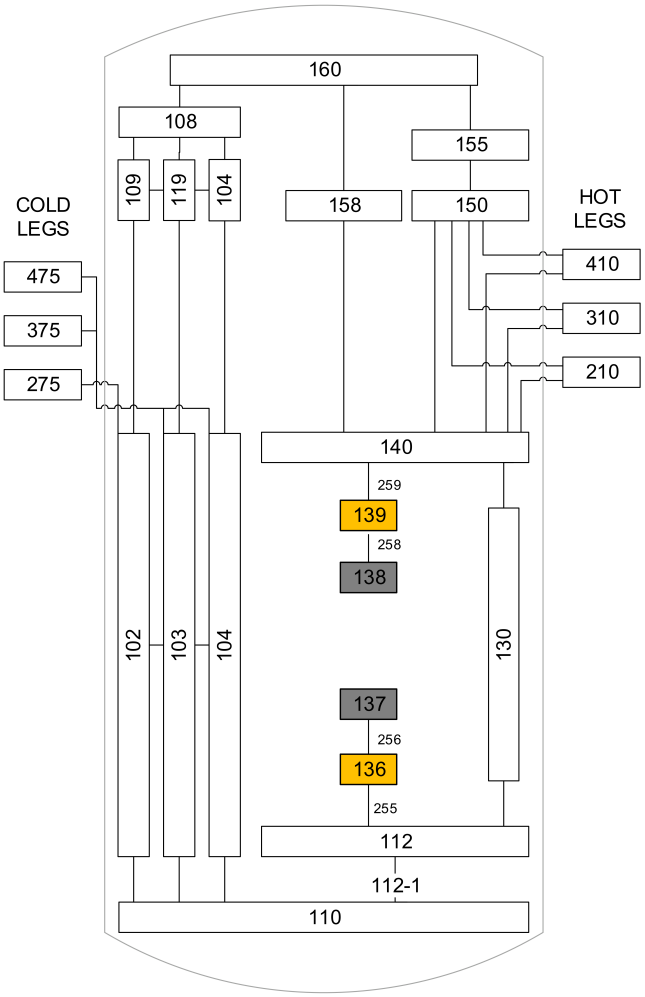

Figure 6.10: *Adapted RELAP5 model vessel nodalization*

be obtained for every node for each channel of the CTF core model, they need to be averaged. The solution has been to obtain the average from the core inlet and outlet values averaged with mass flow rates.

6.2 CTF core model description

A CTF core model has been developed using the same reference data as the RELAP5 core model described in Section 6.1, including the core and fuel elements geometry, as well as the power distribution within the core. The same CTF core model is used in both OLC and SIC methods, and since the CTF-RELAP5 code is running on a single thread,

a compromise between results precision and calculational cost has been taken.

One option is to take advantage of the possibility of CTF's capability of modelling a full core at the sub-channel level, which results in a model with 50868 channels for a core with 157 fuel arrays of 17x17 fuel rods. Another option allowed by CTF is to model the core at the assembly level, by averaging power for each fuel bundle and assigning one single channel per fuel bundle. While the first option's precision is high, it is impractical due to the computational cost and available resources. The main disadvantage of the second option is that it does not use the full CTF capabilities to obtain detailed results of the region of interest in the core.

The final solution has been to develop a hybrid model, first by building a core model at the assembly level and a fuel array model at the sub-channel level, and second, by substituting the assembly in which the results are expected to be more restrictive with the sub-channel fuel array model. The next sections describe the assembly, the sub-channel model and the process of substitution to obtain the hybrid model.

6.2.1 CTF assembly model

The CTF assembly-level core model has been developed by using the same reference material as the RELAP5 core model. The model is built in 3 sections: lower and upper sections with a single channel with one axial node each, and a central section with 157 channels with 11 axial nodes. The reason for building a model with 3 sections is to take advantage of a recent improvement of CTF, which consisted of removing a limitation of 6 connections per channel. This way, the CTF pressure matrix adaptation for the SIC method is performed only for 2 volumes since the coupling volumes are limited to one volume at the core inlet and one volume at the core outlet.

Figures 6.11 and 6.3 show the radial distribution of the 157 assemblies and the axial nodalization for the central core section. The axial nodes in the central section are connected by transverse connections between channels, to account for the crossflows between fuel elements. The spacer grids are located at the elevations shown in Figure 6.3. In the assembly model, the power radial power distribution is considered uniform

within the fuel elements, and each element has the average power factor referenced in Figure 6.11. The axial power distribution is the same for all fuel elements, as shown in Figure 6.5, where the average profile shown is multiplied by each radial power factor for each fuel element.

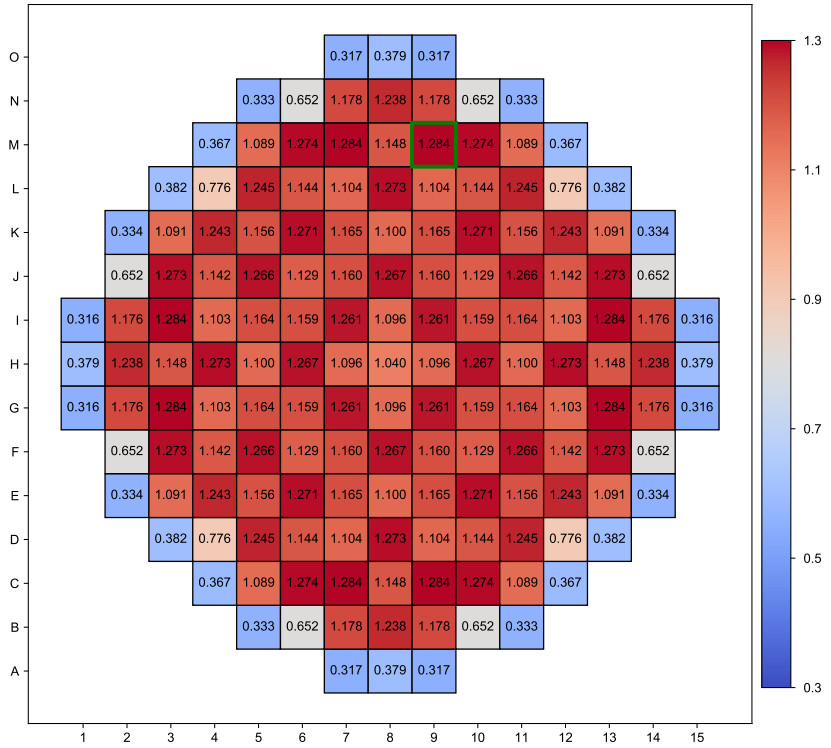

Figure 6.11: *Assembly model average power factors*

6.2.2 CTF sub-channel model

An entire fuel element has been modelled at the sub-channel level to take advantage of the CTF sub-channel features. The geometry parameters are the same as in the RELAP5 model, as shown in Table 6.1. The fuel bundle modelled is a 17 x 17 rods array with 264 fuel rods, 24 guide tubes and 1 instrumentation tube at the centre location of the fuel bundle, as shown in Figure 6.12. The axial geometry is identical to the assembly model, and the sub-channel model also incorporates transverse connections and spacer grids.

The original RELAP5 core reference data does not include the power distribution within the fuel bundle as required by CTF, so it has been taken from Reference [104], in which the same reference data was used to build a coupled model for TRACE and

PARCS codes. The axial and radial power distributions are shown respectively in Figures 6.5 and 6.12.

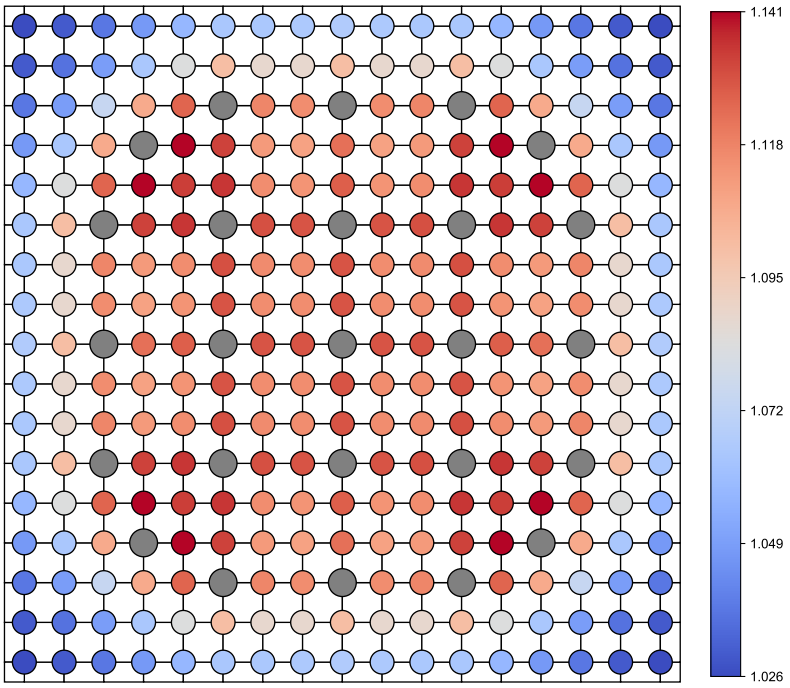

Figure 6.12: *Sub-channel model rod power factors*

6.2.3 Hybrid core model

A hybrid model between the assembly level approach (a single CTF channel models an entire fuel element) and the sub-channel approach (each sub-channel of a fuel element is modelled by a CTF sub-channel) has been developed. The two main reasons for using a hybrid model are obtaining detailed results at the sub-channel level and significantly decreasing the computational time.

First, the two models have been developed (see Sections 6.2.1 and 6.2.2). Second, a Python tool to integrate the sub-channel model into the assembly level model has been programmed. And third, the base case calculations described in Chapter 1 have been run using the assembly level model, where the most restrictive location in terms of MDNBR has been identified in location M-9 (see Figure 6.11).

The hybrid model has been generated then by integrating the assembly level model in position M-9 of the assembly level model, with a power factor of 1.284. The model consists of 3 sections, the top and bottom sections consist of one single node, and the middle section consists of 480 channels (156 at the assembly level and 324 at the sub-channel level), divided into 11 axial nodes with transverse connections. Figure 6.13 Shows the axial and radial node distribution for the hybrid model, and Figure 6.14 shows a 3-D representation of the hybrid model.

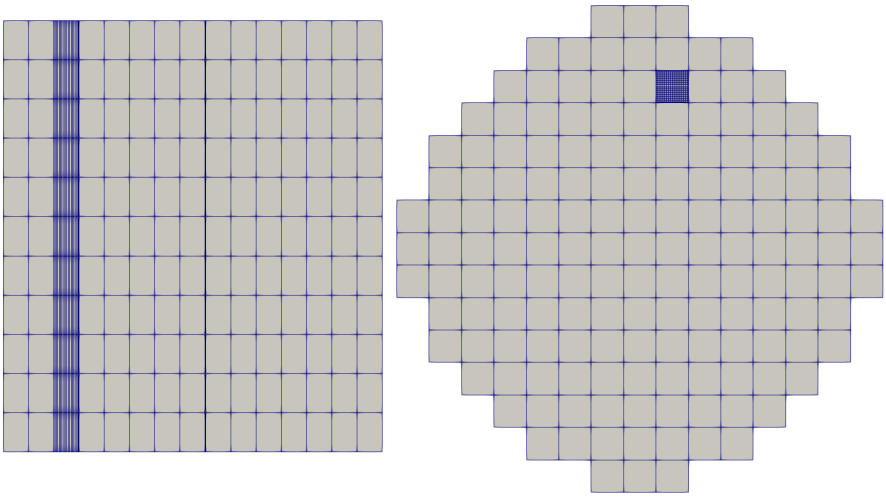

Figure 6.13: *Hybrid model nodalization axial and radial views*

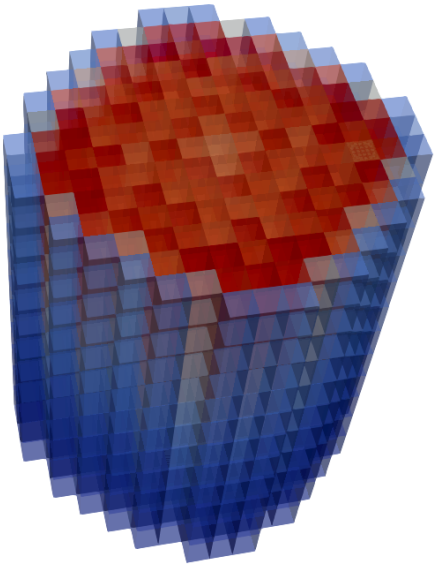

Figure 6.14: *Hybrid model 3-D view*

CHAPTER 7

SIC AND OLC METHODS COMPARISON

This chapter contains:

- A description of the cases execution process
- A comparison of the steady state and base case calculations
- A discussion of the sensitivity analysis results
- A discussion of the BEPU results and the comparison between the SIC and OLC methods

7.1 Input generation and results extraction

In this section, the input decks generation process is explained, as well as some considerations on the cases execution and the results extraction. The generation of the input decks for both codes is closely related to the type of calculations performed in each step of the study. The steps for performing SIC and OLC methods comparisons on the selected cases are: First, qualitative comparisons are carried out for the selected base cases. Second, sensitivity analyses are performed to evaluate the influence of the input parameters on results for both coupling methods. Third, the comparison between the coupling methods is expanded with the application of the BEPU analysis.

7.1.1 Input decks generation and execution of cases

The input decks have been generated for each type of calculation: base case, sensitivity analysis and BEPU analysis. Once the input decks are generated for the base cases, then the input decks for sensitivity analysis and BEPU analysis are obtained by modifying only the relevant parameters, mostly related to the uncertain parameters and the BCs. This process has been carried out with Python scripts due to a large number of input decks to generate (base cases: 4, sensitivity analysis: 384 and BEPU analysis: 372).

The execution of the cases follows a specific scheme depending on the coupling method to apply (SIC or OLC methods). While RELAP5 allows for restart calculations (the ability to store a model calculation state to use as the starting point for other calculations), in CTF this option is not implemented. In both coupling methods, the RELAP5 plant conditions depend on the BCs, and some parameters, such as the SGs or pressurizer levels are highly dependent on the plant controls actuation, needing a considerable amount of time to obtain stable values.

The calculations performed in the sensitivity and BEPU analysis require then specific steady-state conditions, as some of the defined uncertain parameters are related to the initial plant conditions at the moment the transient starts. In order to obtain relatively short stabilization periods and less computational cost, some automated modifications of

the input decks have been performed. The plant parameters related to the steady-state conditions with input deck modifications are described:

- **RCS pressure**

  The RCS pressure is controlled by the control elements installed in the pressurizer, as described in Section 1.1.3. For each case in the RELAP5 model, the pressure setpoint is modified, as well as the initialization pressure for all RCS volumes. In CTF the model is also initialized at the setpoint pressure.

- **Core power**

  The core power is regulated by the rod control system as a function of the turbine power and the derivative of the reactor power. In steady-state conditions, the derivative of the reactor power is neglected. In this case, the reactor power level is imposed by modifying the turbine load setpoint, so the turbine control system reaches the setpoint power and the rod control system adapts the reactor power to the turbine power.

- **Mass flow rate**

  The core mass flow rate is controlled by regulating the RCPs speed. Since the mass flow rate variations from the base case are relatively small, the RCPs speed is considered proportional to the mass flow rate. Due to the mass flow rate change, the core temperature conditions are also modified, and the rod control system consequently regulates the reactor power.

- **Pressurizer level**

  The pressurizer level is controlled by the CVCS control elements, as described in Section 1.1.3. Since the pressurizer level is the plant parameter that takes more time to stabilize, in parallel to modifying the level setpoint for the level control system, the initialization of the pressurizer hydrodynamic volumes has been automated to obtain the desired pressurizer level by imposing particular void fraction values across the pressurizer axial levels.

7.1.2 Results extraction

CTF and RELAP5 codes provide a large amount of available data obtained from their output decks. In the case of CTF, the 3-D model produces results for each node and every fuel rod surface. In the case of RELAP5, a large amount of volume and junctions data is extracted, as well as other available parameters from specific system components.

In all cases, for comparison purposes between the coupling methods, data has been extracted from equivalent locations (core and system). No data has been used from the RELAP5 core heat structures neither for the case of the OLC model nor the SIC model (in this case the core has been removed from RELAP5 model), since in both cases the relevant results are obtained from the CTF models. In consequence, no data is being compared between different codes, only between the same code but applying different coupling methods (SIC and OLC).

Figures 7.1 and 7.2 show an example of a representation of the available results of the core at the assembly and sub-channel levels, consisting of a slice of the upper node of the hybrid CTF core model, showing the liquid coolant temperatures and the fuel clad surface temperatures at steady-state conditions.

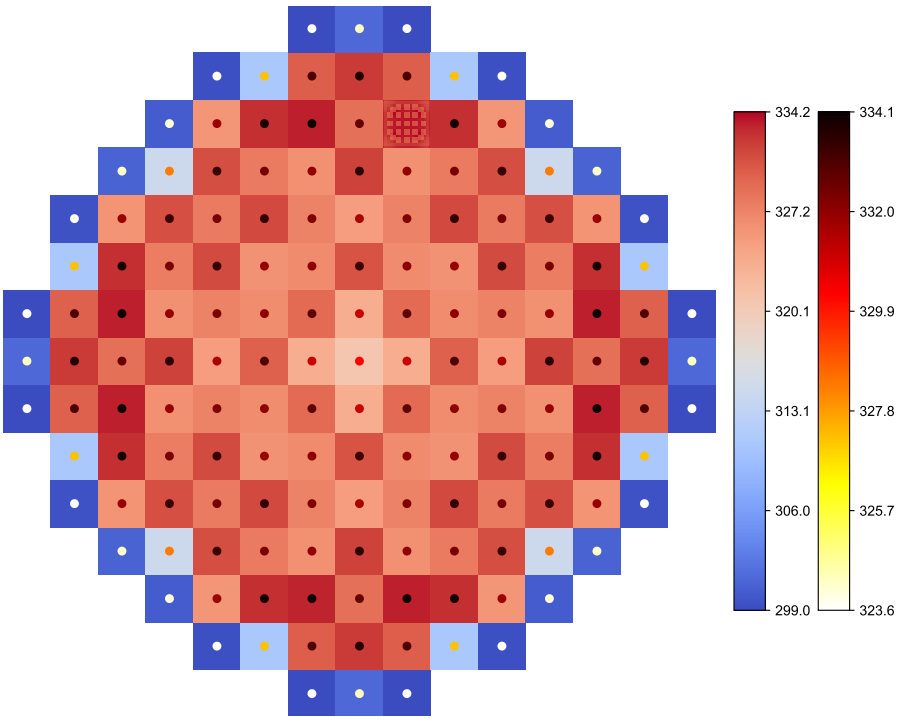

Figure 7.1: *CTF hybrid model liquid and clad outlet temperatures distribution - core, left legend: liquid temperature, right legend: fuel clad surface temperature*

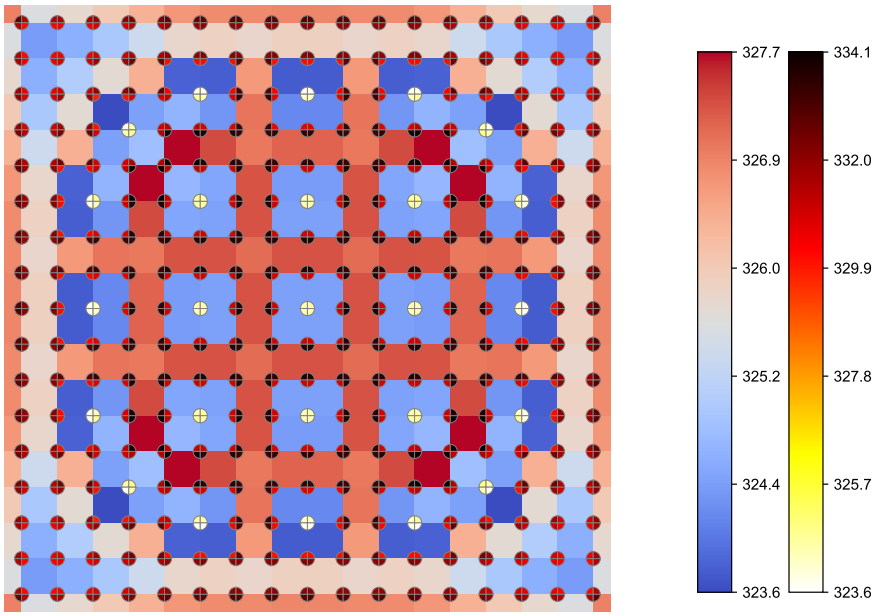

Figure 7.2: *CTF hybrid model liquid and clad outlet temperatures distribution - fuel element, left legend: liquid temperature, right legend: fuel clad surface temperature*

7.2 SIC and OLC steady states calculations

The steady-state calculations are obtained as described in the previous section, either for the base cases or for the cases needed for sensitivity and BEPU analyses. The sets of input parameters used for the generation of the sensitivity and BEPU cases are identical for both SIC and OLC coupling methods.

The process of obtaining the adapted RELAP5 plant model from the original RELAP5 plant model, as described in Section 6.1.2, consists of a substitution of the reactor core with a set of time-dependent volumes and junctions. In order to compare calculations with both coupling methods, a comparison of the steady-state conditions between the original and the adapted RELAP5 plant model is performed.

Tables 7.1 and 7.2 show the differences of the steady-state main parameters for the original and the adapted model. The absolute error between the variables is also provided. The comparison shows that the errors are acceptable, with the higher absolute errors in both tables being related to the secondary systems, such as SG narrow range levels or steam flows. These errors are considered acceptable since they have a small effect on the case results.

Parameter	Unit	Original Model	SIC Model	error
Nuclear Power	%	100.0	100.0	0.0%
Turbine Power	%	100.0	100.0	0.0%
Pressurizer Pressure	MPa	15.49	15.52	0.2%
Pressurizer Level	%	53.20	53.26	0.1%
Reference Temperature	K	580.05	579.95	0.0%
Average Temperature	K	580.05	579.49	0.1%
Cold Leg Temperature Loop 1	K	561.18	560.86	0.1%
Cold Leg Temperature Loop 2	K	560.92	560.86	0.0%
Cold Leg Temperature Loop 3	K	561.04	560.85	0.0%
Hot Leg Temperature Loop 1	K	599.10	598.12	0.2%
Hot Leg Temperature Loop 2	K	599.10	598.12	0.2%

Parameter	Unit	Original Model	SIC Model	error
Hot Leg Temperature Loop 3	K	599.06	598.12	0.2%
SG1 Pressure	MPa	6.56	6.56	0.0%
SG2 Pressure	MPa	6.53	6.56	0.5%
SG3 Pressure	MPa	6.54	6.56	0.2%
Feed Water Flow SG1	kg/s	546.04	545.81	0.0%
Feed Water Flow SG2	kg/s	549.36	546.03	0.6%
Feed Water Flow SG3	kg/s	546.81	548.88	0.4%
Steam Flow SG1	kg/s	546.04	544.56	0.3%
Steam Flow SG2	kg/s	549.37	545.90	0.6%
Steam Flow SG3	kg/s	546.82	544.72	0.4%
Narrow Range Level SG1	%	50.60	50.02	1.2%
Narrow Range Level SG2	%	50.60	50.11	1.0%
Narrow Range Level SG3	%	50.60	50.35	0.5%
RCS loop 1 Mass Flow	kg/s	4526.25	4546.13	0.4%
RCS loop 2 Mass Flow	kg/s	4530.46	4540.80	0.2%
RCS loop 3 Mass Flow	kg/s	4527.14	4539.13	0.3%

Table 7.1: *Steady-state parameters (original RELAP5 Model and RELAP5-CTF SIC Model)*

Parameter	Unit	Original Model	OLC Model	error
Nuclear Power	%	100.0	100.0	0.0%
Turbine Power	%	100.0	100.0	0.0%
Pressurizer Pressure	MPa	15.49	15.51	0.2%
Pressurizer Level	%	53.29	53.27	0.1%
Reference Temperature	K	580.05	580.05	0.0%
Average Temperature	K	580.05	580.07	0.0%
Cold Leg Temperature Loop 1	K	561.18	561.20	0.0%
Cold Leg Temperature Loop 2	K	560.92	561.20	0.0%
Cold Leg Temperature Loop 3	K	561.04	561.19	0.0%
Hot Leg Temperature Loop 1	K	599.10	598.95	0.0%

Parameter	Unit	Original Model	OLC Model	error
Hot Leg Temperature Loop 2	K	599.10	598.95	0.0%
Hot Leg Temperature Loop 3	K	599.06	598.92	0.0%
SG1 Pressure	MPa	6.56	6.56	0.0%
SG2 Pressure	MPa	6.53	6.56	0.5%
SG3 Pressure	MPa	6.54	6.56	0.2%
Feed Water Flow SG1	kg/s	546.04	545.15	0.2%
Feed Water Flow SG2	kg/s	549.36	545.38	0.7%
Feed Water Flow SG3	kg/s	546.81	548.23	0.3%
Steam Flow SG1	kg/s	546.04	545.23	0.1%
Steam Flow SG2	kg/s	549.37	545.02	0.8%
Steam Flow SG3	kg/s	546.82	544.11	0.5%
Narrow Range Level SG1	%	50.60	50.33	0.5%
Narrow Range Level SG2	%	50.60	50.13	0.9%
Narrow Range Level SG3	%	50.60	50.64	0.1%
RCS loop 1 Mass Flow	kg/s	4526.25	4543.63	0.4%
RCS loop 2 Mass Flow	kg/s	4530.46	4545.00	0.3%
RCS loop 3 Mass Flow	kg/s	4527.14	4543.15	0.4%

Table 7.2: *Steady-state parameters (original RELAP5 Model and RELAP5-CTF OLC Model)*

7.3 Base case calculations

The base cases are obtained by assigning the central values of the uncertain parameters considered in Section 4.2.3 for the RCP trip and PORV opening cases, resulting in a single run for each case. In this section, the base case calculations are described, and the results obtained by applying the SIC and OLC methods are compared. A specific set of general assumptions have been imposed on each case, with the purpose of maximising the effect of the plant response to the acceptance criteria to analyze (MDNBR).

In the attempt to maximise the outcome (more limiting MDNBR), there is no intention to assimilate the cases to licensing calculations but to obtain realistic limiting cases with the purpose of analysing the coupling methodologies. Also, no branching of the cases has been considered in order to keep the number of runs limited. The same assumptions have been made for both SIC and OLC methods. Table 7.3 shows the model assumptions related to the availability of the control systems for each case.

	RCP	PORV
Reactor trip	Low RCS flow	Low RCS pressure
Turbine trip	Caused by reactor trip	Caused by reactor trip
RCP trip due to LOOP	Enabled	Disabled
Control rods movement	Disabled	Disabled
CVCS level control	Disabled	Disabled
Pressurizer PORV	Enabled	Fail open
Pressurizer Heaters	Disabled	Disabled
Pressurizer Spray	Enabled	Enabled
Turbine control	Enabled	Enabled
Feedwater control	Disabled	Disabled

Table 7.3: *Calculations BC and plant systems considerations*

Figures from 7.5 to 7.13 show the comparison of the main parameters for the SIC and OLC coupling methods: the pressurizer pressure, the RCS mass flow rate, the reactor and turbine power, the core inlet and outlet normalized temperatures, the pressurizer

level, the SG pressure, the MDNBR and the maximum cladding temperature (MCT) at the core location of the highest clad temperature reached in the core.

Also, the following parameters obtained at the location (surface) where the MDNBR occurs are included: the heat flux, the critical heat flux, the void fraction, and the clad temperature. In addition, the PORV opening case includes the PORV mass flow rate trend. In both cases, the core inlet and outlet normalized temperatures are obtained by subtracting the steady-state values from each time trend.

All results have been extracted from the same volumes/junctions from the CTF or RELAP5 models, in some cases processed to obtain the relevant data, such as averaged values or normalized values. This implies that there is no data from different codes being compared, using the same physical models to produce results on both couplings with the objective to isolate the coupling effects.

7.3.1 RCP trip base case (SIC and OLC methods)

The RCP trip case consists of a complete loss of forced flow due to the RCPs trip, as described in Section 1.3. The RCPs trip can be produced by a loss of off-site power, which causes the under-voltage RCP motor trip protection to open the breakers for all RCPs. The main effect of the RCPs trip is an immediate coast-down of the RCS forced flow that occurs until the natural circulation starts as a consequence of the SGs depressurization. Figure 7.3 shows that there is a good agreement between the SIC and OLC method mass flow rate trend, measured at the inlet of the CTF core model.

Prior to reaching the reactor trip due to low RCS flow in one of 3 loops (90% of nominal mass flow rate), the mass flow rate reduction at practically nominal power causes the RCS coolant to heat up due to two effects: on one hand, a reduced flow through the core at nearly constant nominal power causes the coolant temperature to rise at the reactor outlet, and on the other hand, the reduced RCS mass flow rate at the RCS side of the SGs causes a reduced cooling due to the lower heat exchange rate at the SGs tubes.

The two effects contribute to the RCS temperature increase (as shown in Figure 7.4).

The temperatures, extracted from the CTF model (inlet/outlet), correspond to the liquid temperatures since no relevant amount of steam is expected to be present at the core outlet. The time trend shows that the SIC and OLC cases are in good agreement, but since the coolant temperature is an important contributor to the CHF correlation, it is important to note the following differences: while the outlet temperature is slightly higher at the peak for the SIC case, the inlet temperature presents a higher value in the OLC case at the end of the transient.

The increase of the RCS temperature causes an expansion of the RCS coolant, which produces a pressure peak that is ended by the reactor trip and a consequential temperature decrease. Figure 7.5 shows the inlet/outlet pressures for SIC and OLC methods, where some pressure oscillations can be observed, having a greater amplitude for the case of the OLC method and in consequence producing a higher pressure peak.

The evolution of the reactor and turbine power is shown in Figure 7.6, where the reactor power decreases due to the effect of the FTC and the MTC as a consequence of the temperature increase in both fuel and moderator. During this short period, the turbine control system maintains the turbine power constant. At 2.8 s, the reactor signal is reached and it causes the reactor and turbine to trip. The effective reactor trip is delayed as described in Chapter 6, while for the turbine no delay is considered. The reactor and turbine powers present the same evolution in both SIC and OLC methods.

Figure 7.7 shows the evolution of the pressurizer level. The level first increases as a consequence of the expansion of the RCS coolant caused by the temperature increase and decreases after the reactor trip. Some discrepancy between the SIC and OLC method is observed, with a difference lower than 0.4 m at the peak level. Figure 7.8 shows the evolution of the steam generator pressure. The pressure is maintained constant until the turbine trip occurs, causing a sudden decrease in the steam flow generation and a pressure increase. SIC and OLC methods present consistent values.

Table 7.4 shows the main scalar calculation results related to MDNBR. The MDNBR results for each coupling method are 2.679 (SIC method) and 2.699 (OLC method). The MDNBR occurs in both cases shortly after the effective reactor trips, when the control

rods insertion begins, indicating that the condition leading to the degradation of core cooling due to low mass flow rate at power is terminated by the reactor trip.

The following scalar calculation results are obtained at the same time and location in the core when the MDNBR occurs: HF, CHF, void fraction and clad surface temperature. In addition, the MCT in any location of the core is displayed, being slightly higher than the clad temperature at the MDNBR location and time.

Parameter	Unit	SIC	OLC
MDNBR time	s	3.95	4.00
Effective reactor trip time	s	3.60	3.61
MDNBR	-	2.679	2.699
MDNBR channel	-	174	174
MDNBR node	-	10	10
HF (MDNBR)	kW/m^2	995.2	1012.2
CHF (MDNBR)	kW/m^2	2666.7	2732.2
Clad temperature (MDNBR)	K	674.57	675.25
Void fraction (MDNBR)	-	0.063	0.49
Max clad temperature	K	674.65	675.48
Max clad temperature channel	-	174.0	174.0
Max clad temperature node	-	10.0	10.0

Table 7.4: *RCP trip case parameters*

The CHF, obtained by using the W-3 correlation, is slightly lower in the case of the SIC method (Figure 7.9 shows the evolution of the HF and CHF at the core location where the MDNBR occurs), while the HF is equal in both methods. This is translated into a lower MDNBR in case of the SIC method, with a 0.74% difference (see Figure 7.10).

Figure 7.11 shows the void fraction at the location of the MDNBR. It can be observed that the SIC method predicts a higher production of steam. Figures 7.12 and 7.13 show the clad temperature at the MDNBR location and the MCT in any location of the core. In both cases the OLC method predicts a higher clad temperature, having a difference of 0.68 K and 0.6 K at the peak respectively.

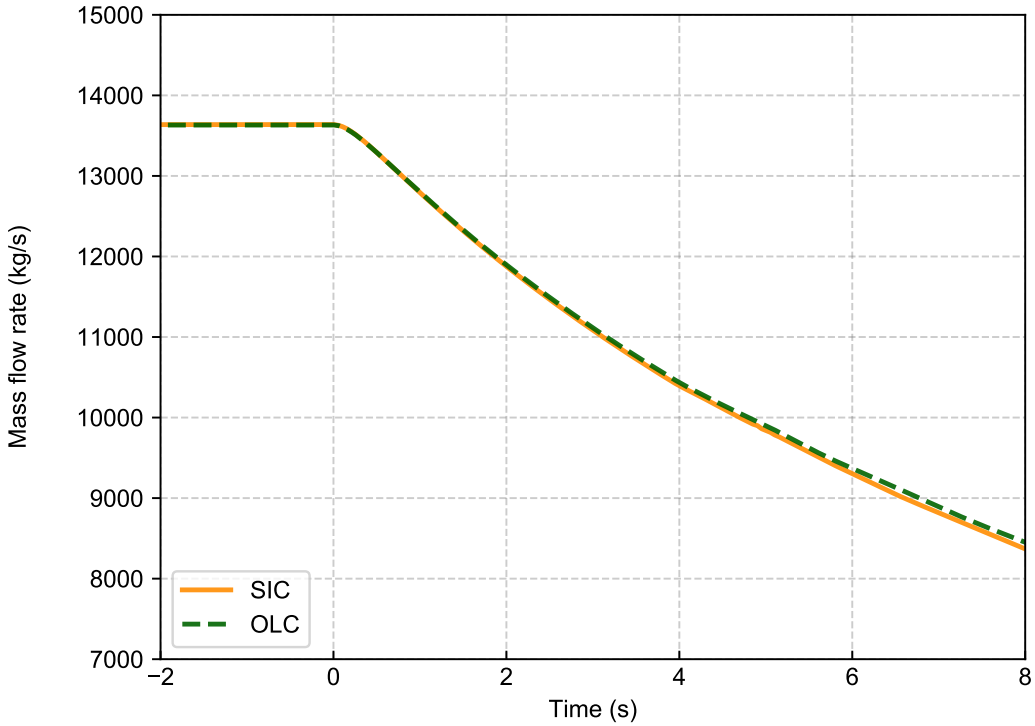

Figure 7.3: *RCP trip - Core mass flow rate*

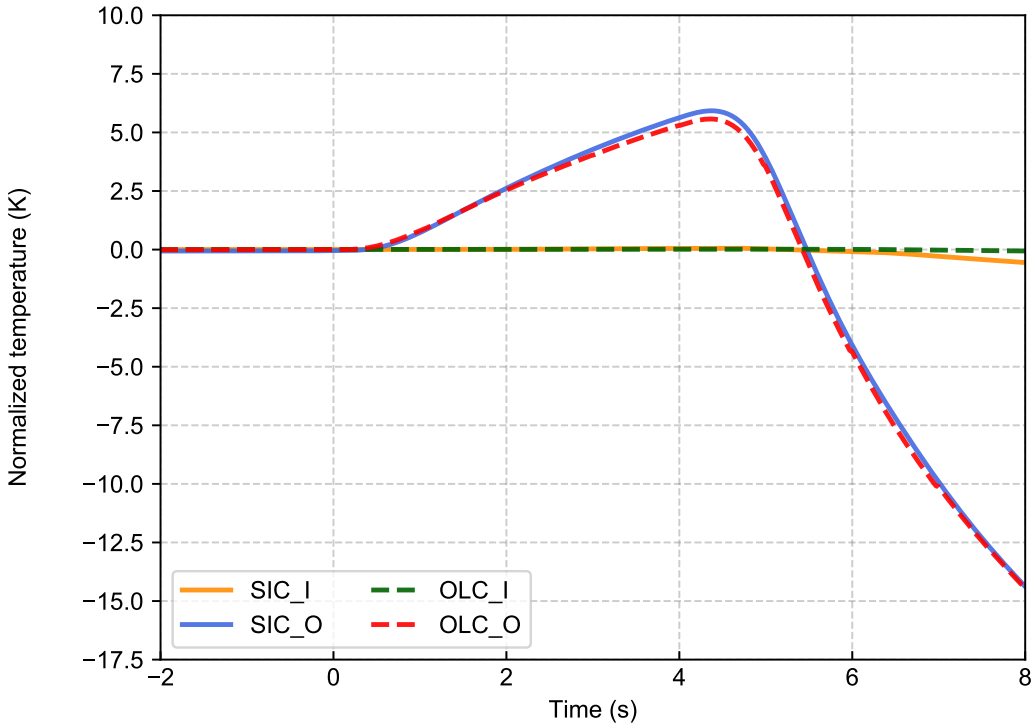

Figure 7.4: *RCP trip - Normalized inlet/outlet temperatures*

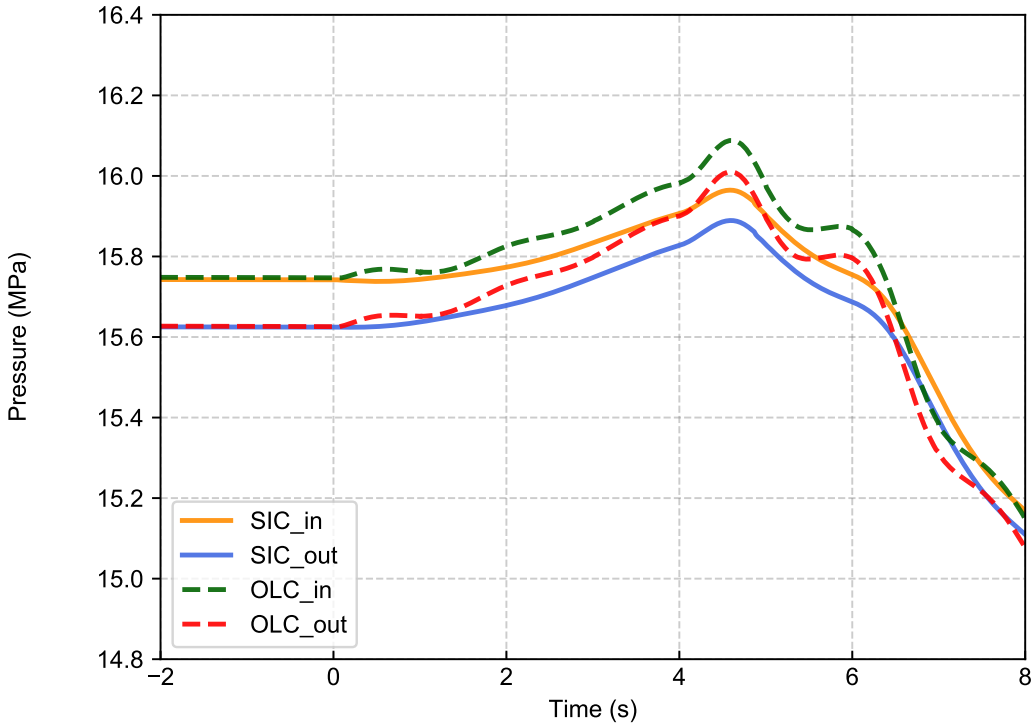

Figure 7.5: *RCP trip - Inlet/outlet core pressure*

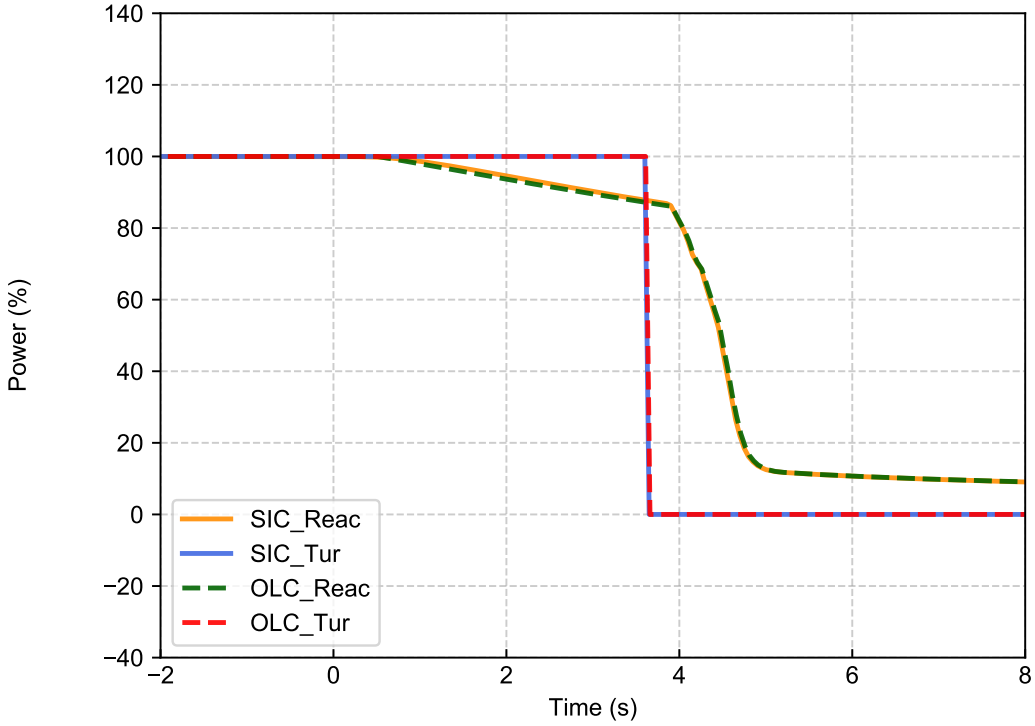

Figure 7.6: *RCP trip - Reactor/turbine power*

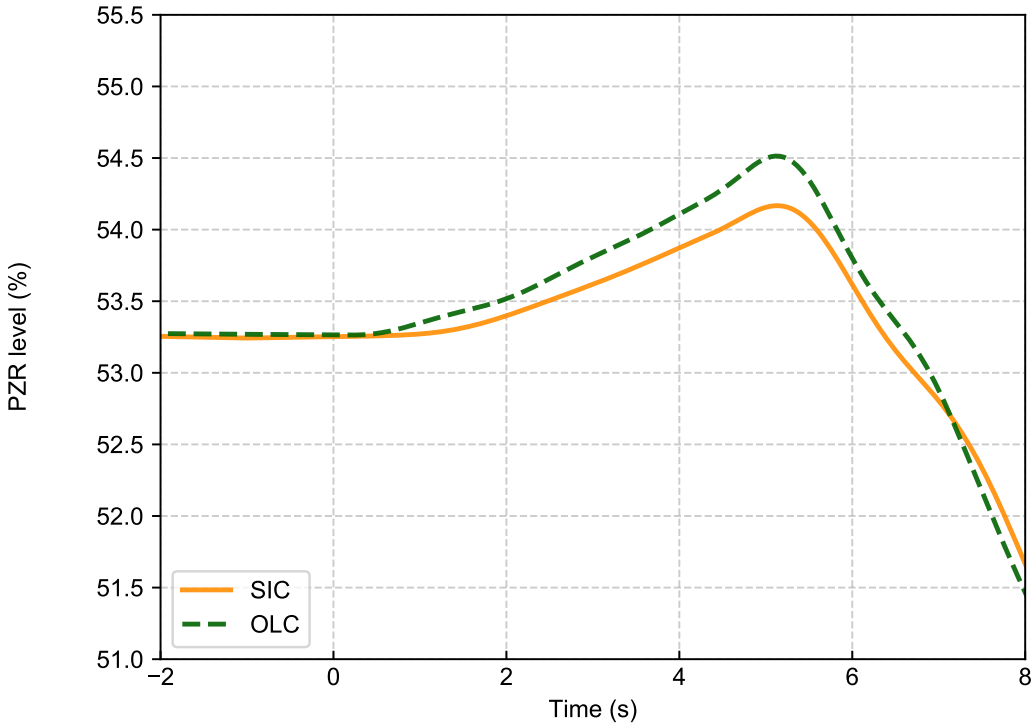

Figure 7.7: *RCP trip - Pressurizer level*

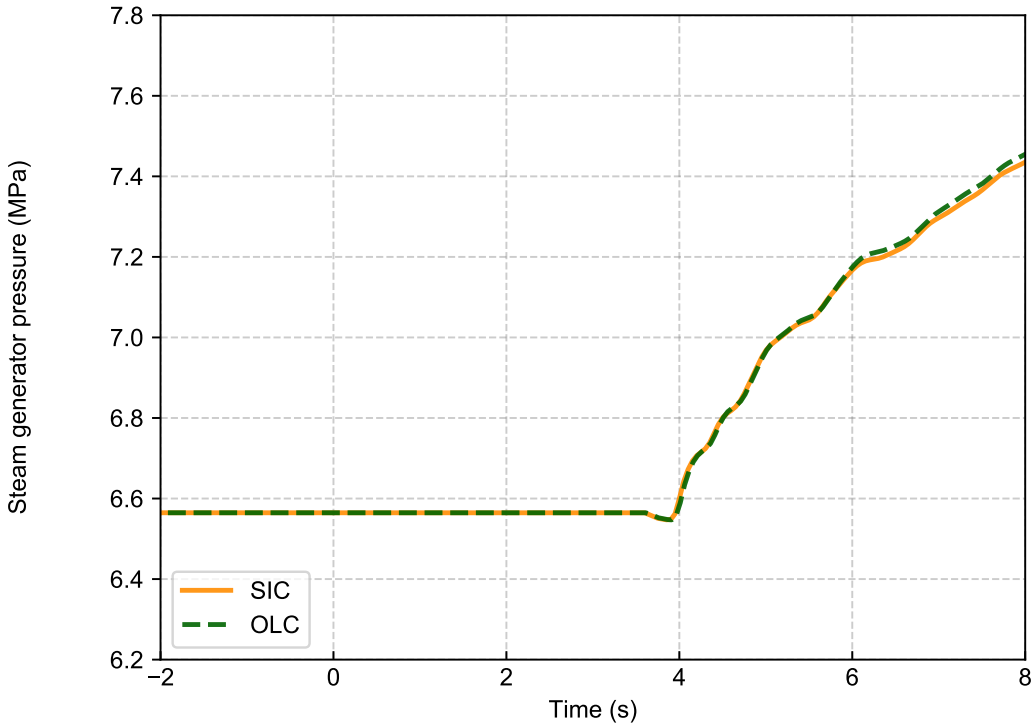

Figure 7.8: *RCP trip - Steam generators pressure*

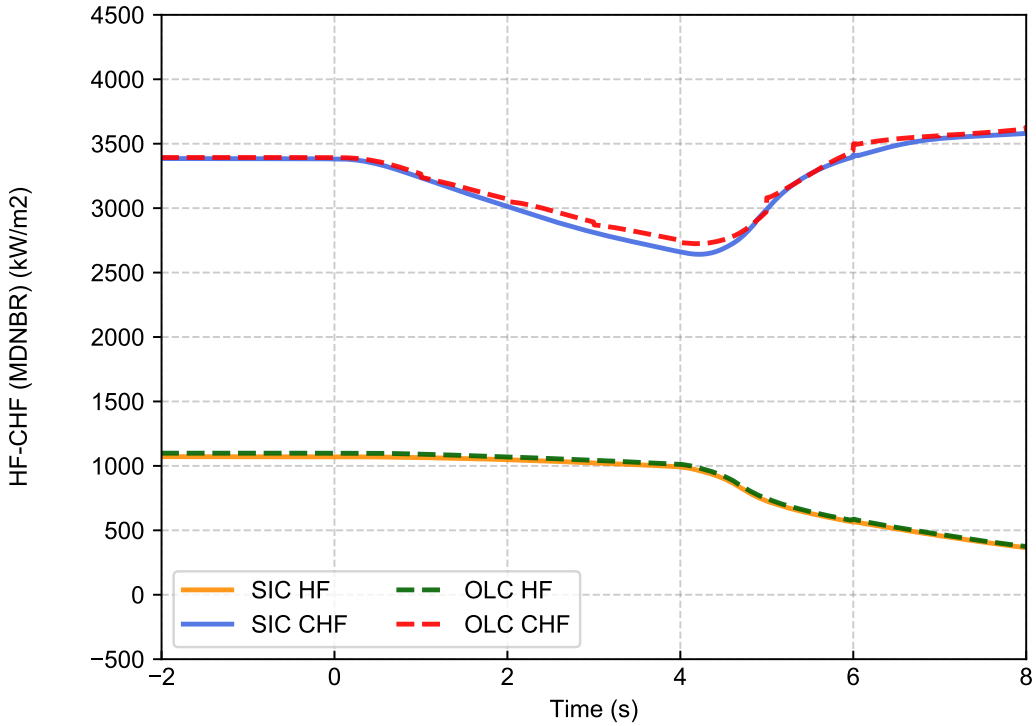

Figure 7.9: *RCP trip - HF, CHF (MDNBR)*

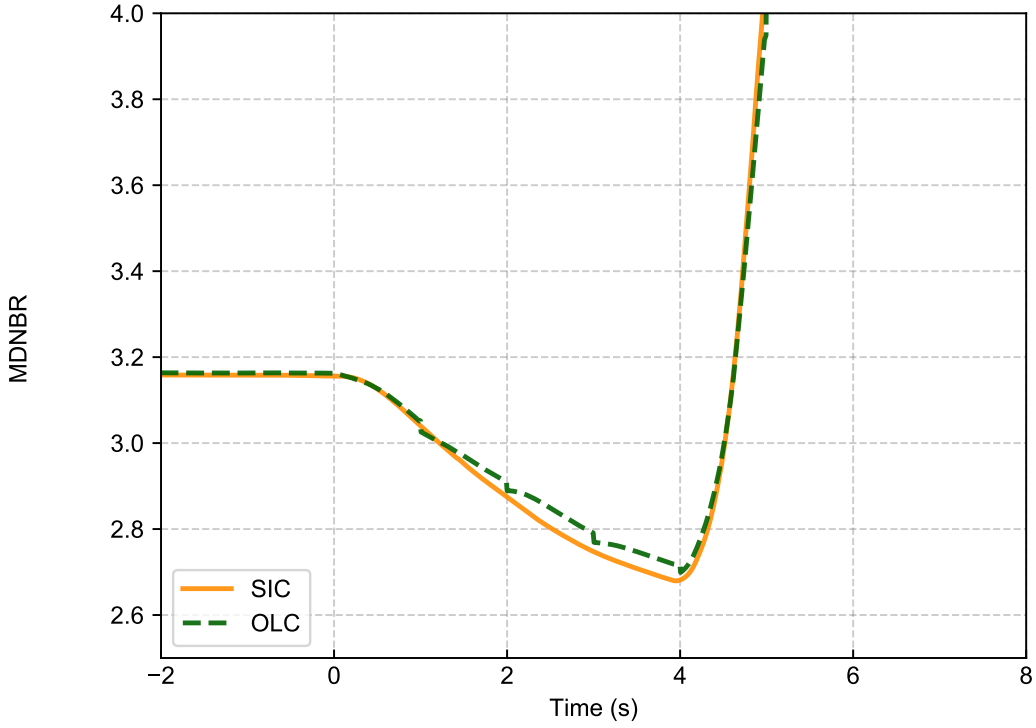

Figure 7.10: *RCP trip - MDNBR*

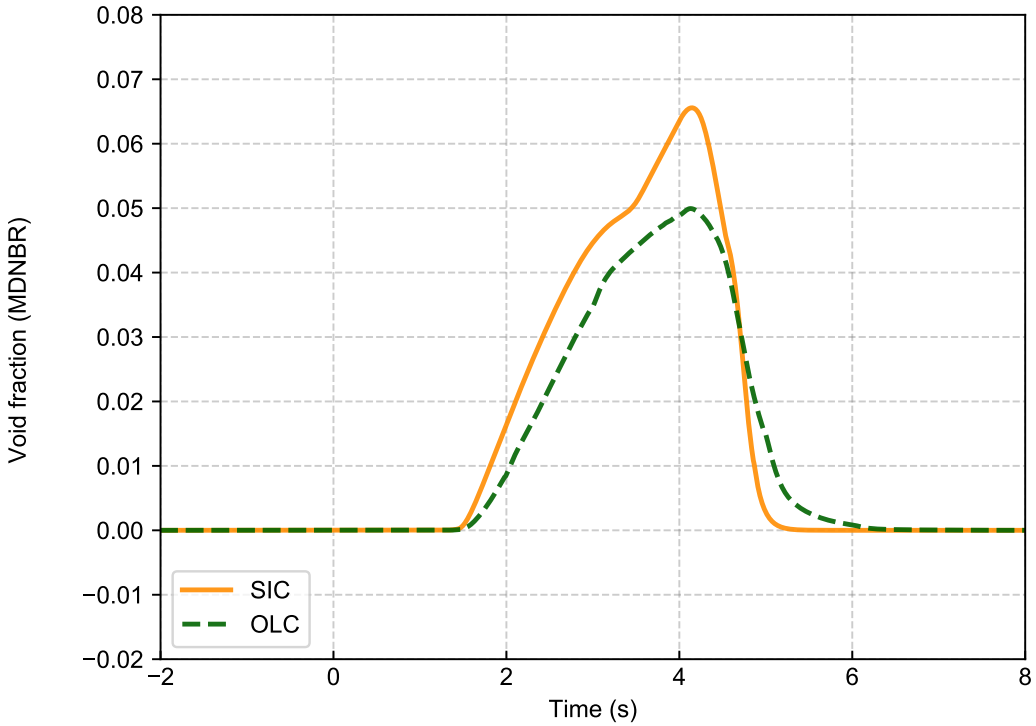

Figure 7.11: *RCP trip - Void fraction (MDNBR)*

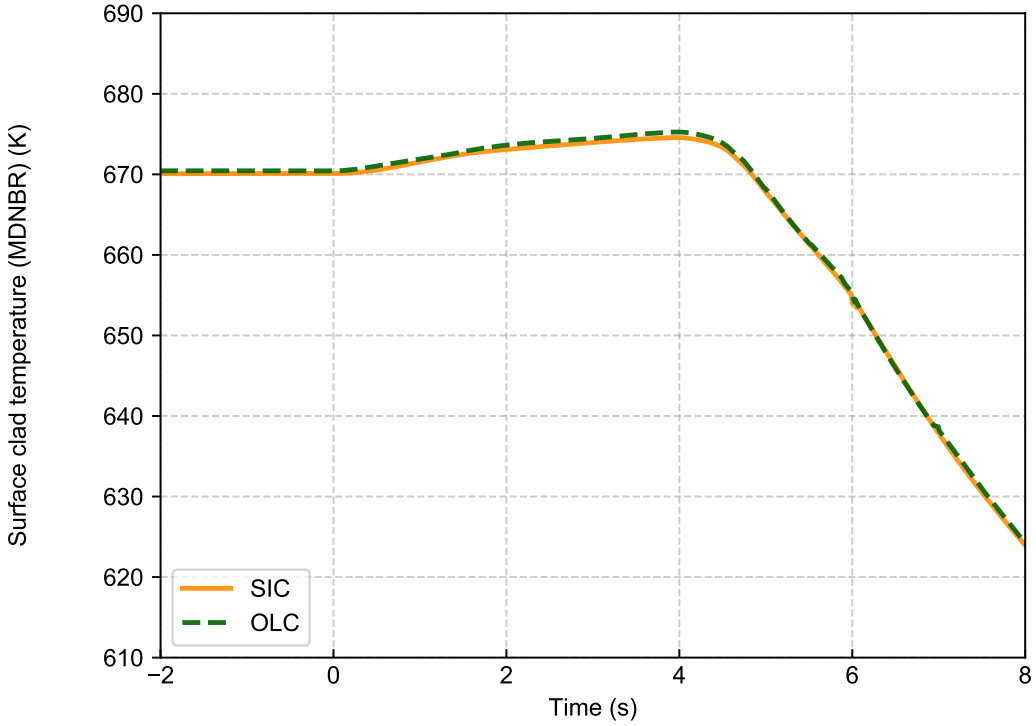

Figure 7.12: *RCP trip - Surface clad temperature (MDNBR)*

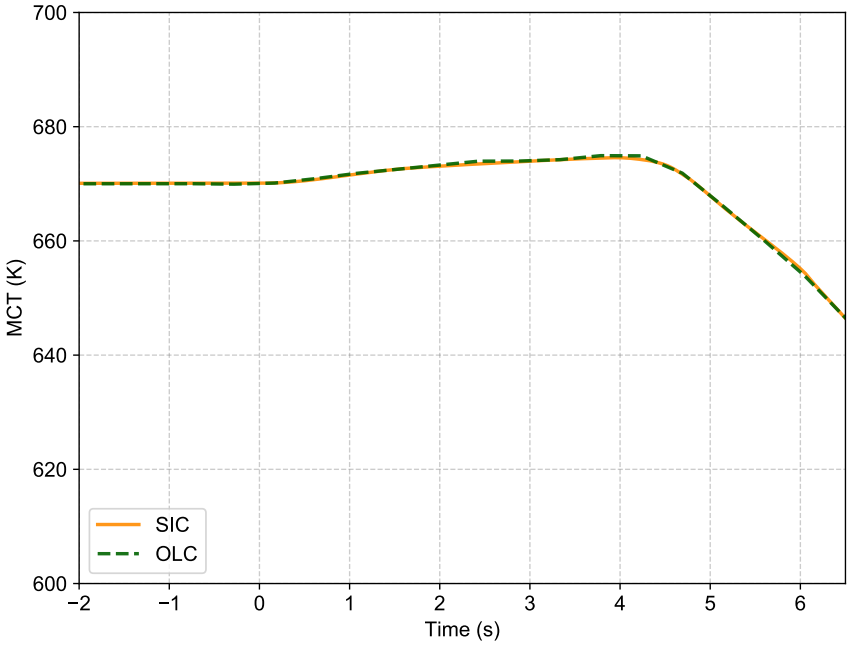

Figure 7.13: *RCP trip - MCT*

As stated before, some boundary parameters do not match between system and sub-channel codes when performing OLC calculations. This is the case of the inlet pressure and outlet temperature for the OLC scheme applied. Figure 7.14 shows the differences in the BCs for the OLC case, where it can be seen that the inlet pressure and outlet temperature do not match between RELAP5 and CTF, showing small differences for both parameters.

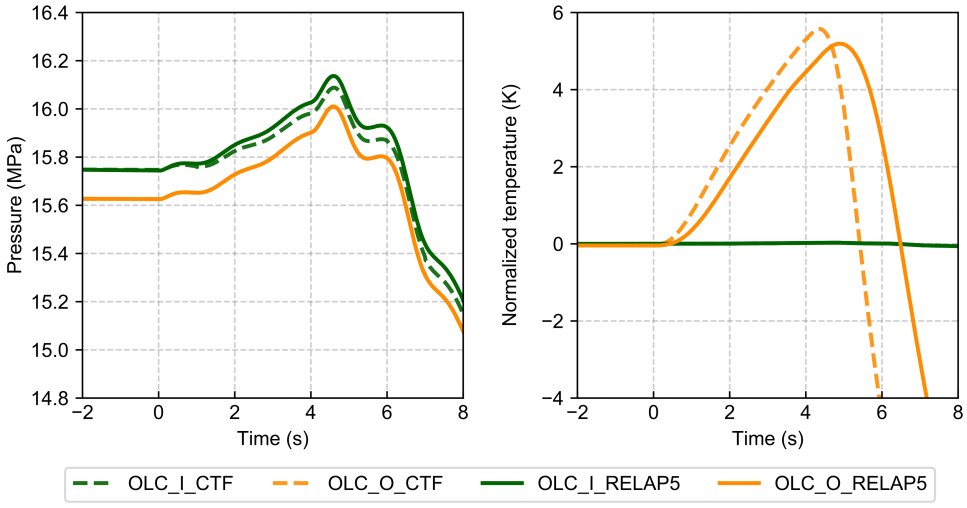

Figure 7.14: BC comparison for OLC scheme RCP and PORV base cases

7.3.2 PORV opening base case (SIC and OLC methods)

The PORV case consists of a failure of one of the pressurizer PORV valves, as described in Section 1.3. The failure of the valve can be mechanical or electrical, causing the valve to fail open and to remain in this position throughout the transient. The main effect of the PORV opening is a continuous pressure decrease, as the pressurizer steam inventory leaks through the valve to the pressurizer relief tank. The PORV massflow and the pressure decrease at the core is shown respectively in Figures 7.15 and 7.17, where a good agreement can be observed between the SIC and OLC method calculations.

The core mass flow rate (shown in Figure 7.17), remains practically constant while the RCS depressurizes. Due to this RCS depressurization, a small reactor power decrease is observed due to the moderator density feedback, while the turbine power is constant until the reactor trip occurs (see Figure 7.18). The reduced power causes a moderated RCS temperature decrease (see Figure 7.19).

Figure 7.20 shows the evolution of the steam generator pressure. The pressure is maintained constant until the turbine trip occurs, causing a sudden decrease in the steam flow generation and a pressure increase in a similar manner as in the RCS case. The evolution of the main parameters presents consistent values between the SIC and OLC methods, with the exception of the pressurizer level (see Figure 7.21), which presents minor differences, with the highest deviation being of 3% level difference at the moment of the reactor trip.

Table 7.5 shows the main scalar calculation results related to MDNBR. The MDNBR results for each coupling method are 2.754 (SIC method) and 2.646 (OLC method). The MDNBR occurs in both cases also shortly after the effective reactor trips, when the control rods insertion begins, indicating that the condition leading to the degradation of core cooling due to the RCS pressure decrease at power is terminated by the reactor trip.

As in the RCP case the following scalar calculation results are obtained at the same time and location in the core when the MDNBR occurs: HF, CHF, void fraction and clad surface temperature. In this case, the MCT in any location of the core is practically

equivalent to the clad temperature at the MDNBR location and time.

Parameter	Unit	SIC	OLC
MDNBR time	s	31.66	31.61
Effective reactor trip time	s	31.35	31.31
MDNBR	-	2.754	2.646
MDNBR channel	-	174	174
MDNBR node	-	10	10
HF (MDNBR)	kW/m^2	1029.0	1061.0
CHF (MDNBR)	kW/m^2	2835.0	2807.1
Clad temperature (MDNBR)	K	658.27	658.75
Void fraction (MDNBR)	-	0.054	0.066
Max clad temperature	K	658.41	658.75
Max clad temperature channel	-	174.0	174.0
Max clad temperature node	K	10.0	10.0

Table 7.5: *PORV opening case parameters*

The CHF, also obtained by using the W-3 correlation, is slightly lower in the case of the OLC method (see Figure 7.22), while the HF is slightly higher than in the case of the SIC method. This causes the MDNBR to be lower in the case of the OLC method, with a 3.92% difference (see Figure 7.23). The void fraction at the location of the MDNBR is shown in Figure 7.24, where it can be seen that there is a similar void fraction difference to the one observed in the RCP case. Figures 7.25 and 7.26 show the clad temperatures. In this case, the clad temperatures present similar values for the SIC and OLC methods, with a difference of 0.48 K and 0.34 K at the peak respectively.

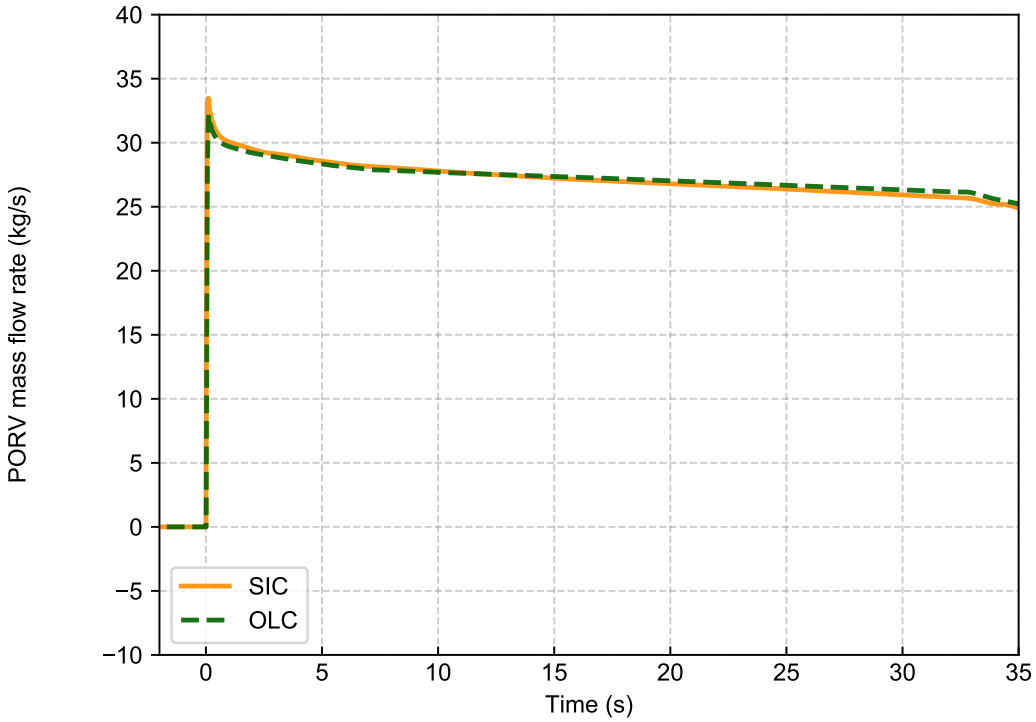

Figure 7.15: *PORV opening - Core mass flow rate*

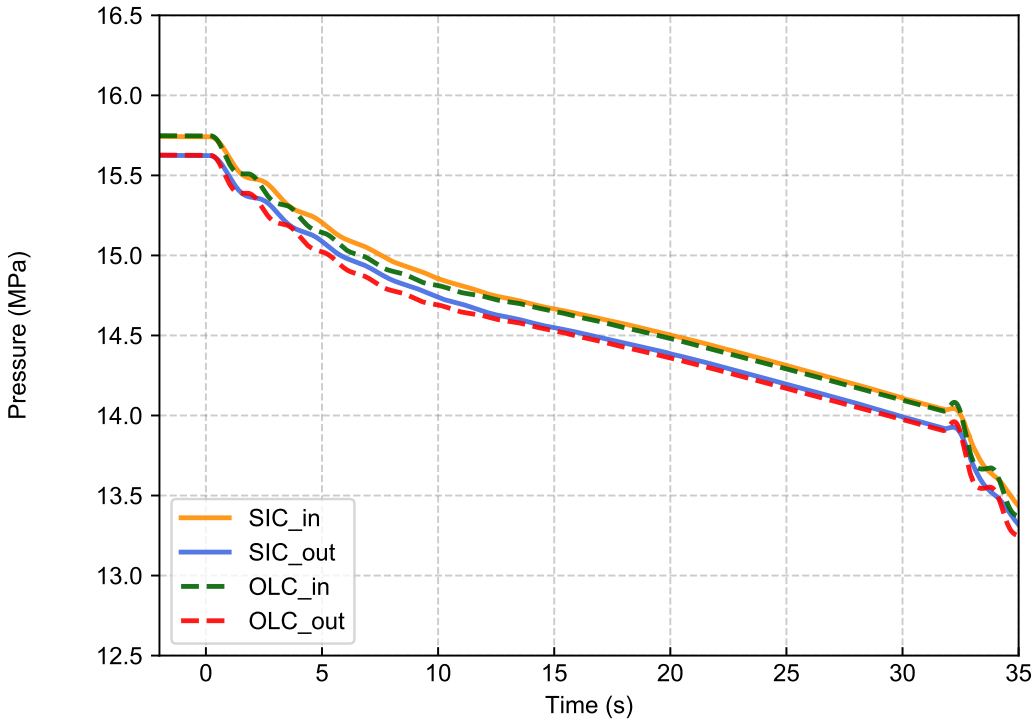

Figure 7.16: *PORV opening - Inlet/outlet core pressure*

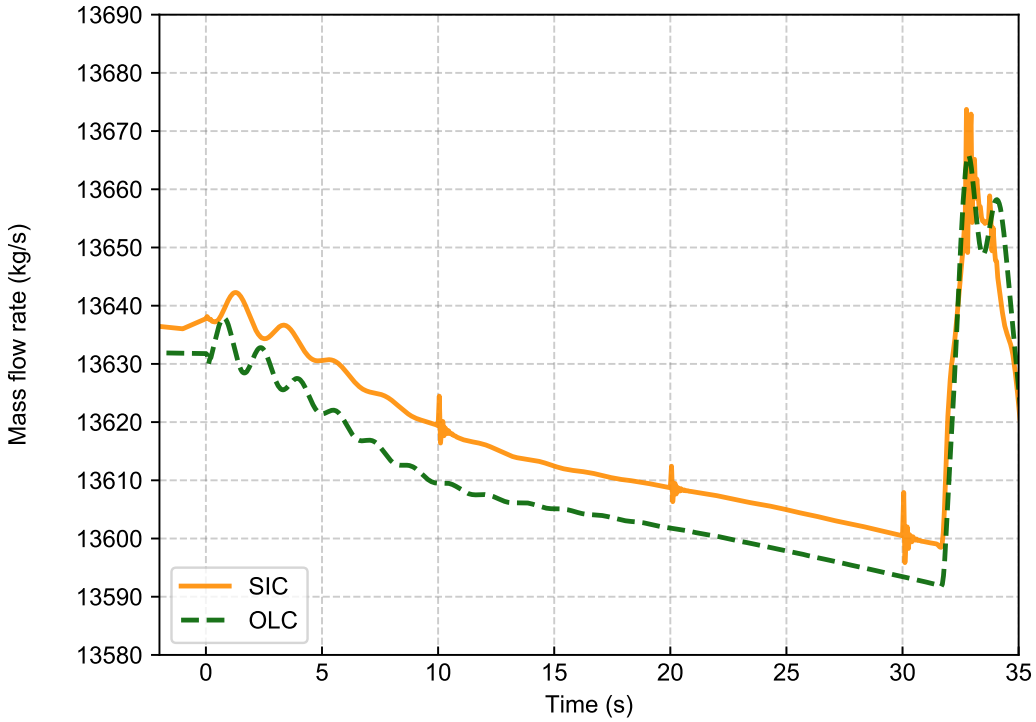

Figure 7.17: *PORV opening - PORV mass flow rate*

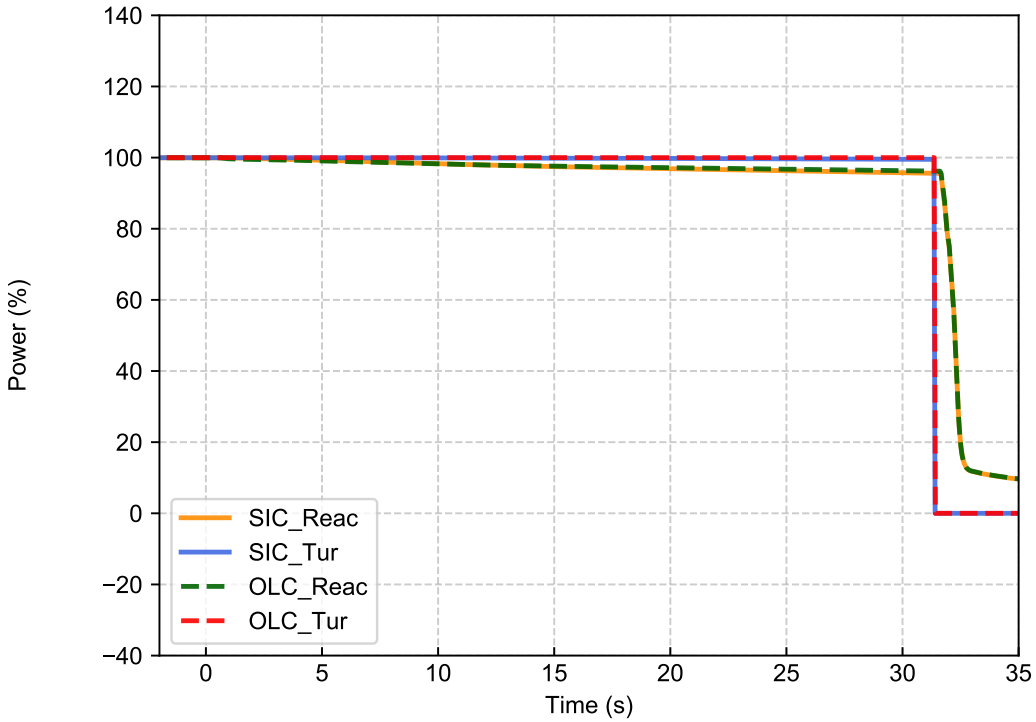

Figure 7.18: *PORV opening - Reactor/turbine power*

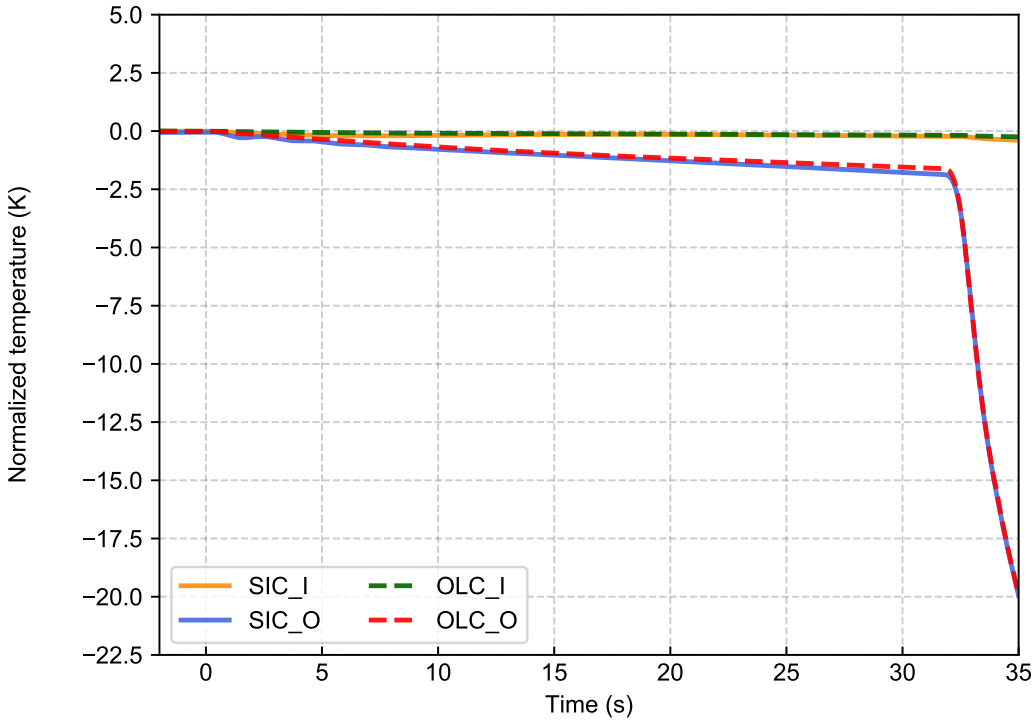

Figure 7.19: *PORV opening - Normalized inlet/outlet temperatures*

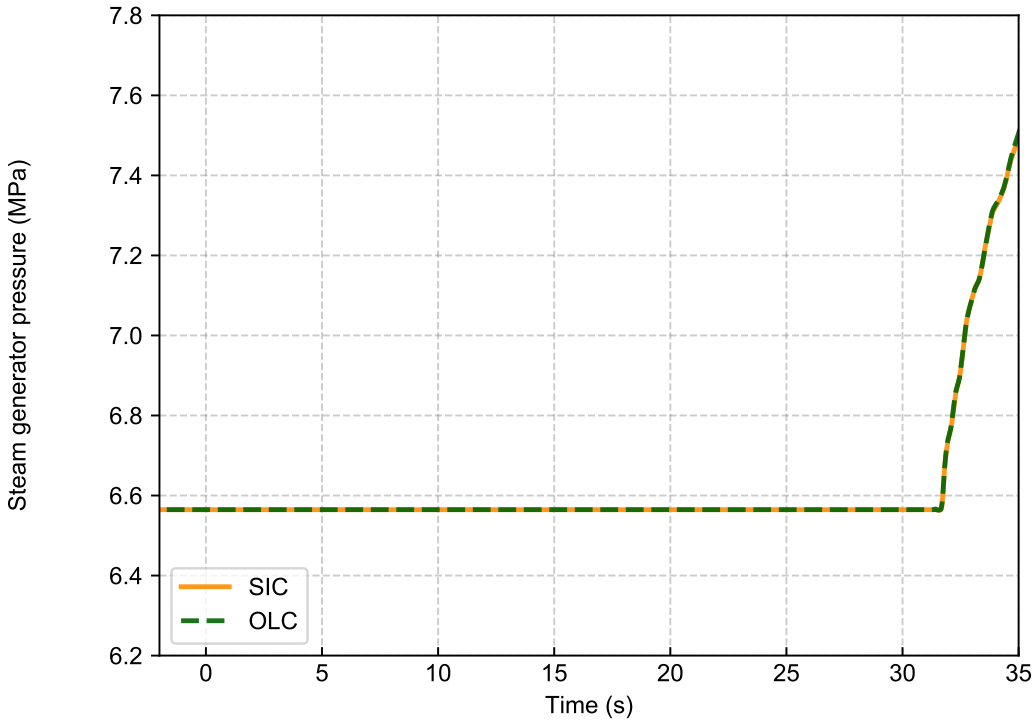

Figure 7.20: *PORV opening - Steam generators pressure*

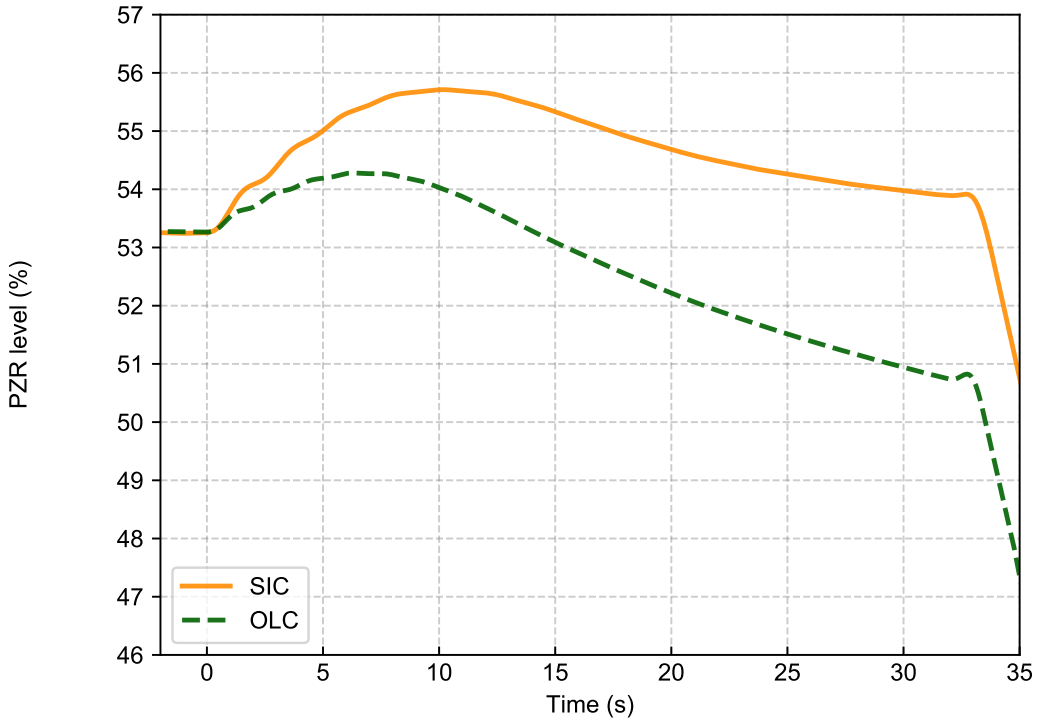

Figure 7.21: *PORV opening - Pressurizer level*

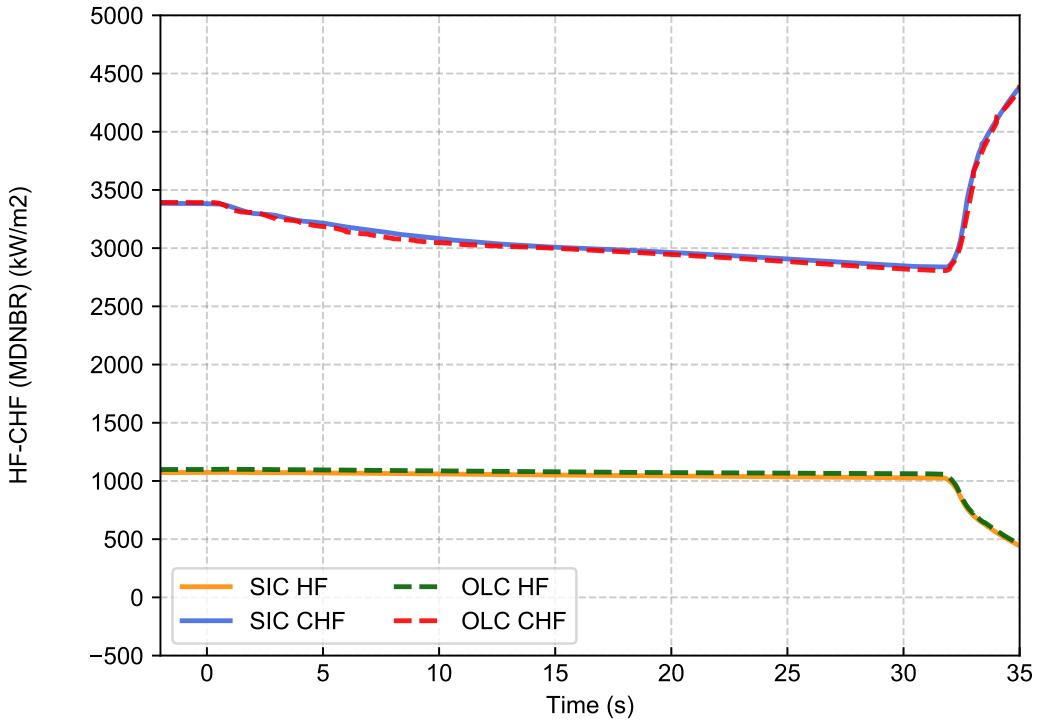

Figure 7.22: *PORV opening - HF, CHF (MDNBR)*

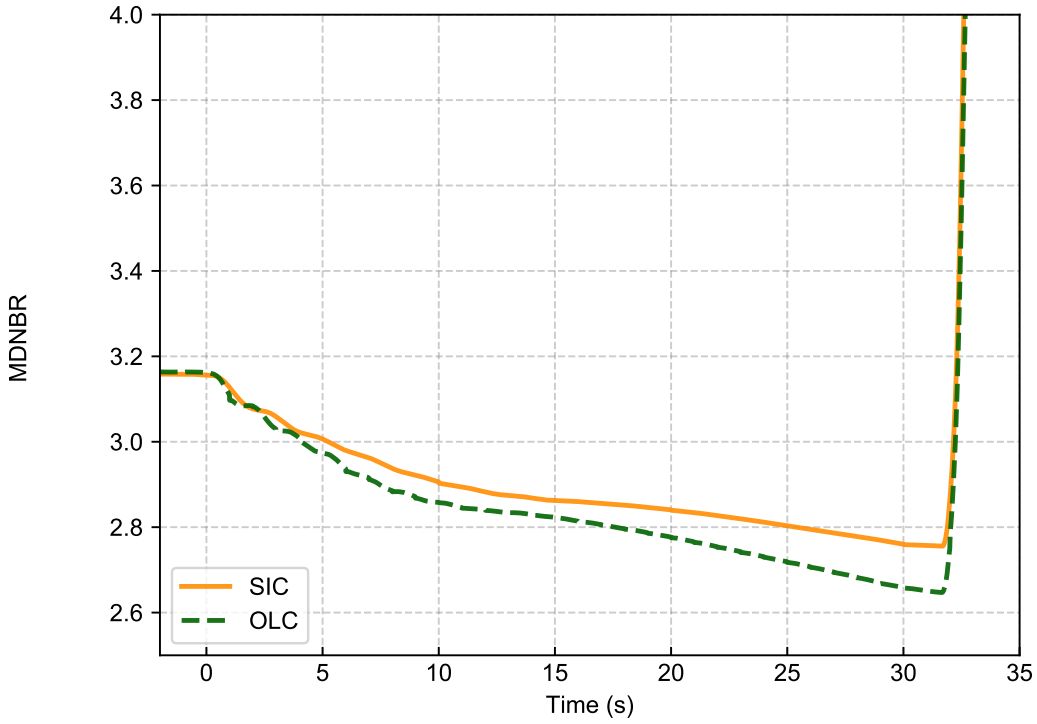

Figure 7.23: *PORV opening - MDNBR*

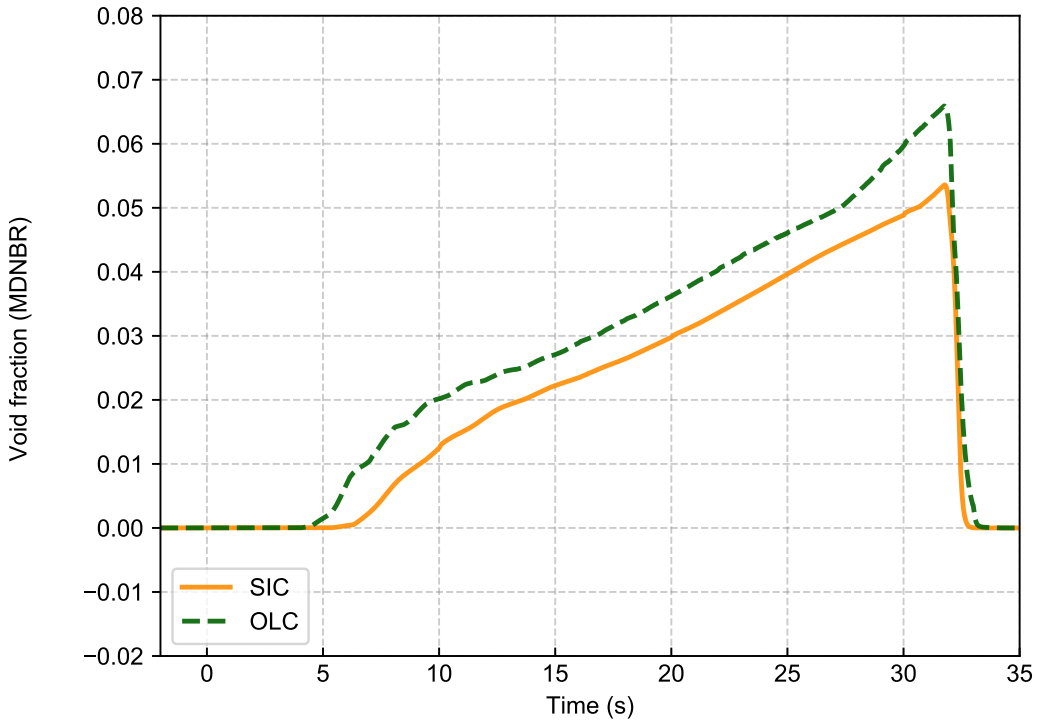

Figure 7.24: *PORV opening - Void fraction (MDNBR)*

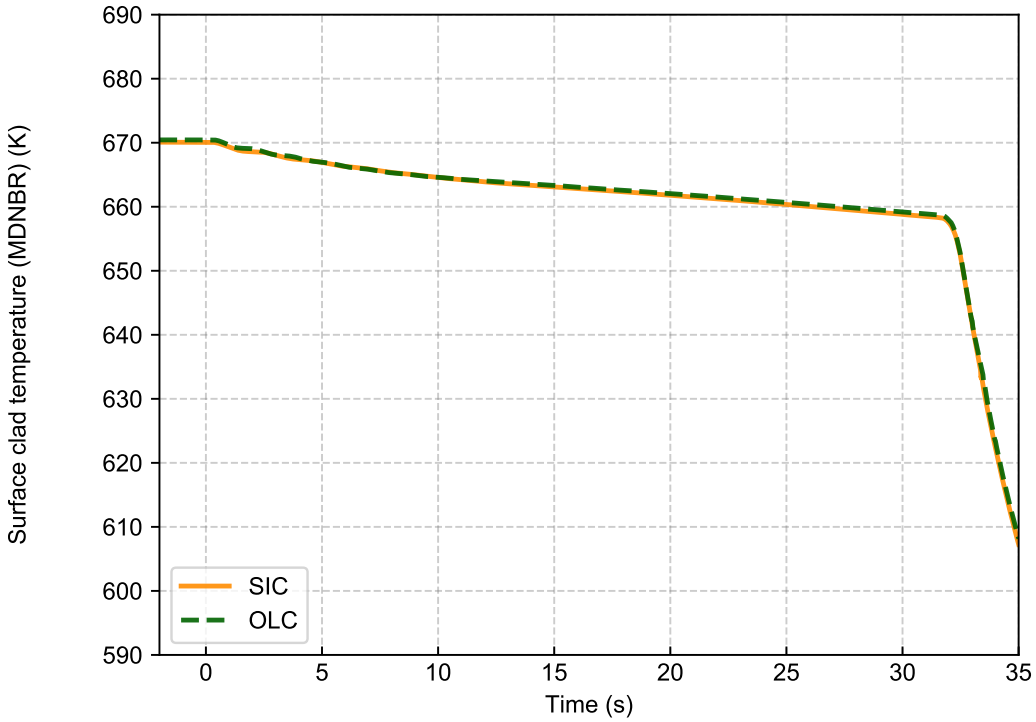

Figure 7.25: *PORV opening - Surface clad temperature (MDNBR)*

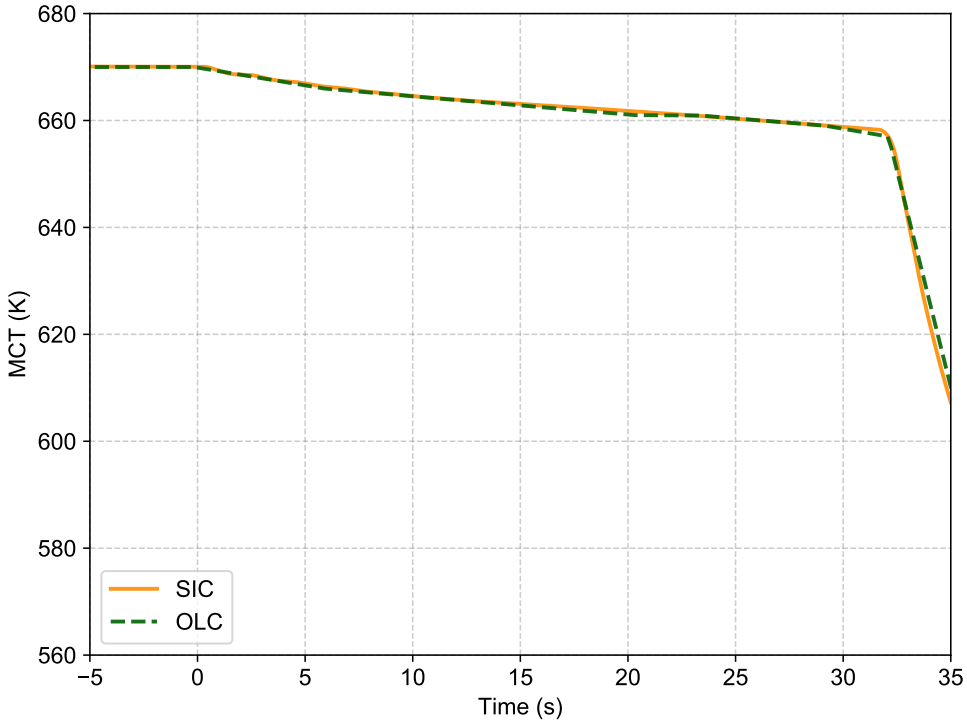

Figure 7.26: *PORV opening - MCT*

Figure 7.27 shows the differences in the BCs for the OLC case, where it can be seen that while no inlet pressure differences can be observed, the outlet temperatures do not match between RELAP5 and CTF, showing a small difference for this parameter.

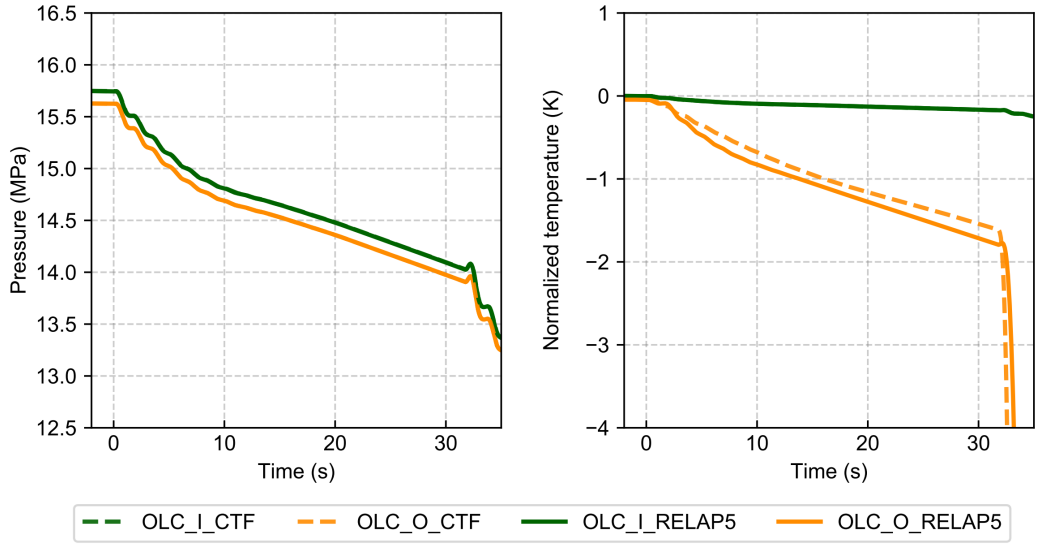

Figure 7.27: BC comparison for OLC scheme RCP and PORV base cases

7.4 Sensitivity analysis results

As described in Chapter 4, a set of uncertain CTF and RELAP5 input parameters have been considered (as presented in Table 4.2 in Section 4.2.3). Table 4.2 includes the nominal values (NV), corresponding to the values of the uncertain parameters considered in the base case calculations, and their uncertainty ranges (UR). The uniform distribution has been considered for all uncertain parameters PDFs.

Prior to the BEPU analysis, a sensitivity comparison has been carried out to cover the entire uncertainty range for each parameter and to evaluate the influence of the input parameters on results for both coupling SIC and OLC methods. For the sensitivity analysis, the base cases and 6 additional cases have been run for each coupling method; 3 in the upper and 3 in the lower uncertainty ranges for each parameter (evenly distributed). The sensitivity has been evaluated by varying a single uncertain parameter with the following set of values:

$$[NV - UR, NV - \frac{2}{3}UR, NV - \frac{1}{3}UR, NV, NV + \frac{1}{3}UR, NV + \frac{2}{3}UR, NV + UR] \quad (7.1)$$

Figures 7.28 to 7.29 show the normalized MDNBR with respect to the base case values for each uncertain parameter and the sensitivity range considered.

7.4.1 RCP trip sensitivity analysis comparison

In the RCP case, the slope of the trends is in all cases equivalent with some exceptions. The highest variation of the MDNBR due to the uncertain parameters variation is observed to occur in parameters 1, 2, 3, 5 and 8, the first 3 being the main RCS parameters (pressure, power and mass flow rate) which can be directly related to DNBR, and parameters 5 and 8 being relevant parameters in this specific transient (reactor trip time and gap HTC) since this transient occurs in a brief period of time.

On the contrary, in parameters 11, 13, 14 and 15, no effect on the MDNBR is observed, since the differences presented are statistical rather than physical. Also, parame-

ters 1, 3, 4 and 5 present differences in the slope of the curves between the SIC and OLC methods. This indicates that the effect of modifying the uncertain parameter is different for the SIC and OLC methods. In any case, the maximum differences observed at the limit of the ranges considered are less than 1.5%. Parameter 7 (pumps moment of inertia) is the only parameter with a change of the slope for the case of the OLC method. While the upper values of the range present the same linearity for the SIC and OLC methods, in the lower range the OLC method predicts higher MDNBR values than the SIC method, with a maximum difference of 1.6% at the limit of the lower range.

7.4.2 PORV opening sensitivity analysis comparison

In the PORV case, a general consistent agreement is also observed between the MDNBR response, except for parameter 3 (mass flow rate). In this case, there is a change of slope for the SIC method, and the extreme cases present differences between OLC and SIC methods (1.4% and 1.2% at the limits of the range considered). For parameters 7, 8, 11, 13, 14, 15, 16 and 17 there is no effect on the MDNBR for the sensitivities considered. Parameters 1, 5, and 10 present a difference in the curves' slope between SIC and OLC methods. The highest variation of the MDNBR is observed in parameters 1, 2 and 3, being the main RCS parameters (pressure, power and mass flow rate).

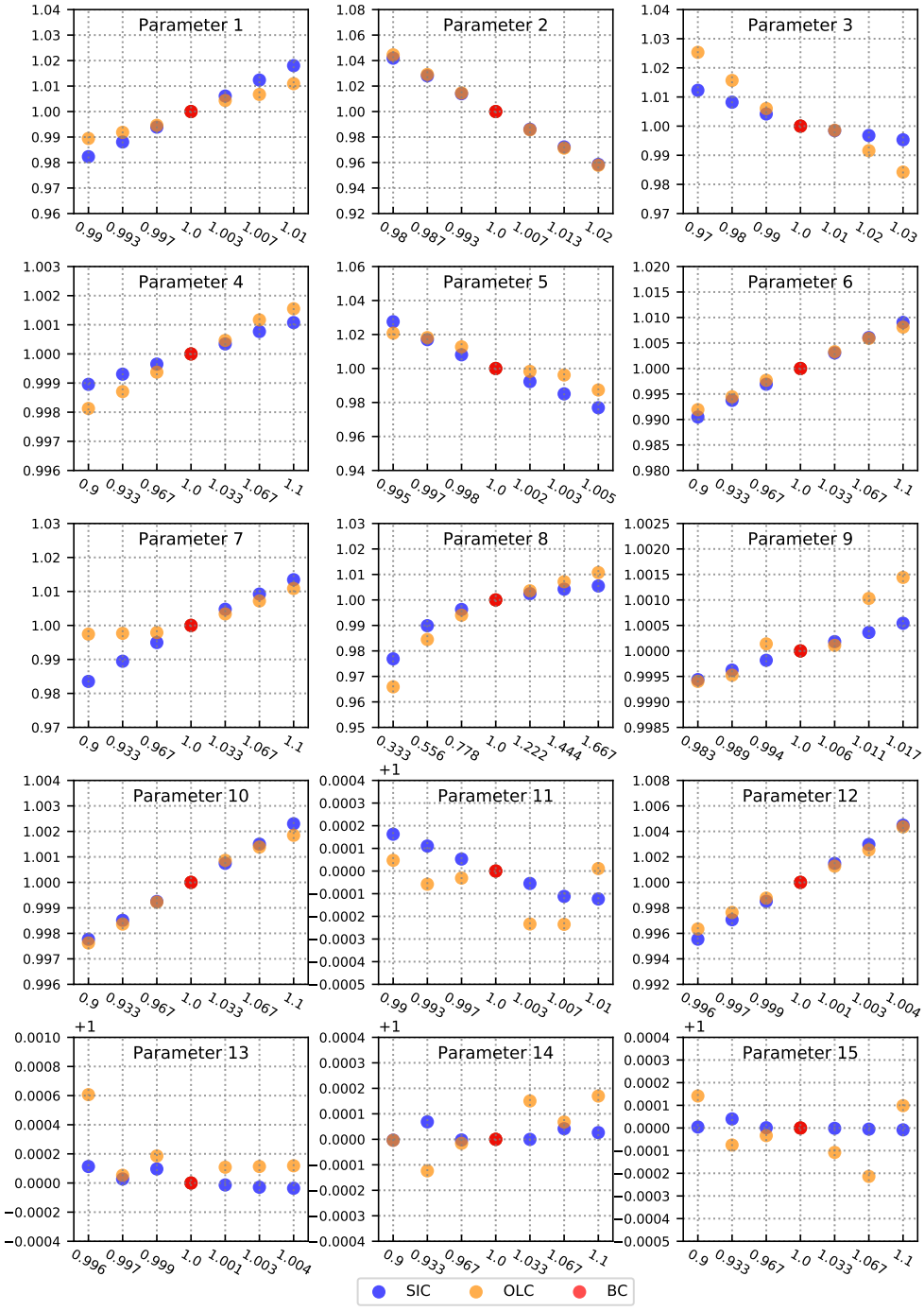

Figure 7.28: *RCP trip - MDNBR sensitivities*

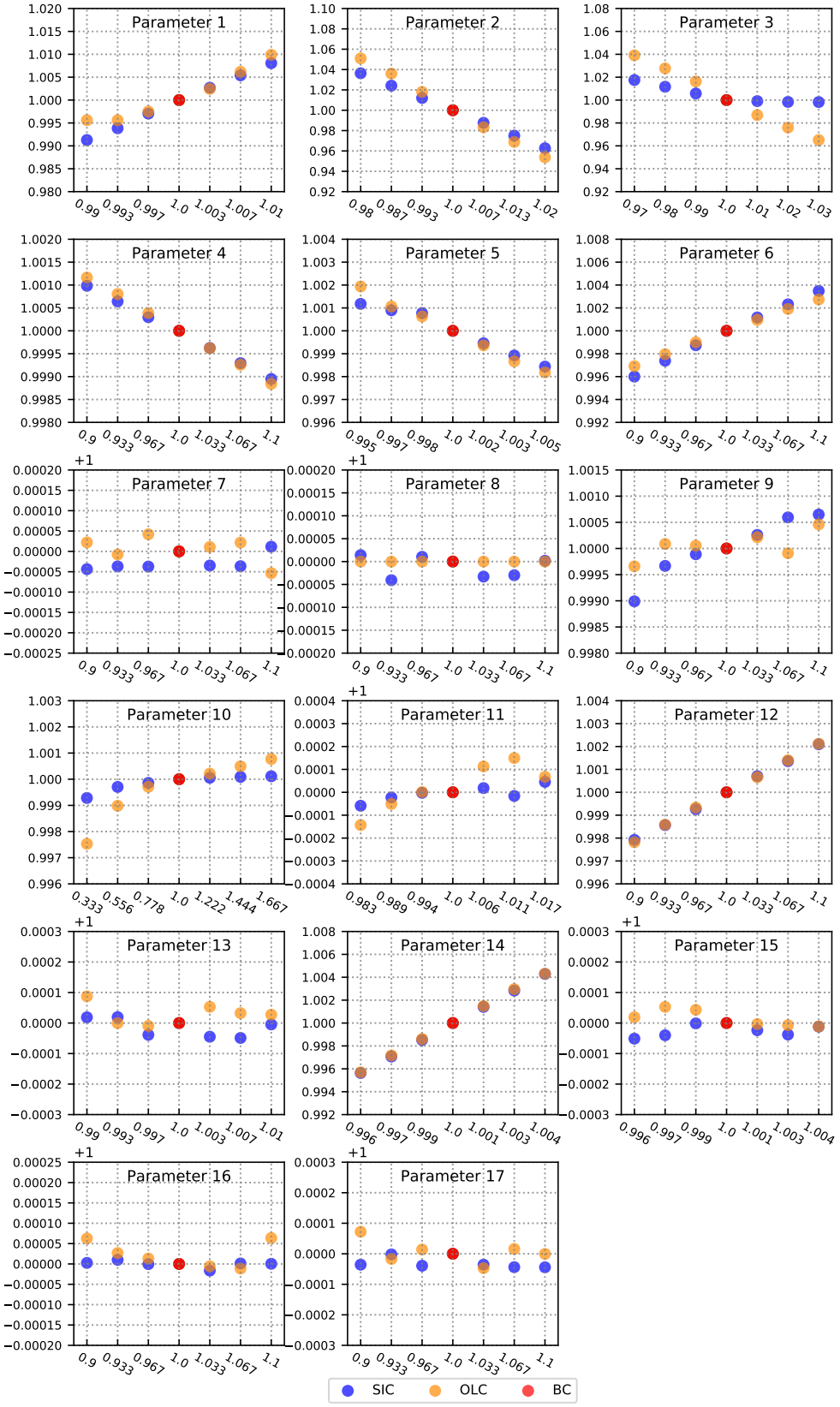

Figure 7.29: *PORV opening - MDNBR sensitivities*

7.5 BEPU analysis results

Two BEPU analyses have been performed using the method described in Chapter 4. The main FOM considered is MDNBR, while additional FOM have been considered (HF, CHF, clad temperature and void fraction at the core location of MDNBR and MCT). Two sets of uncertain parameters, one for each one of the cases, RCP and PORV, have been generated using data provided in Table 4.2. Each set, applied to both SIC and OLC methods calculations, consists of 93 random generated combinations of the uncertain parameters to feed the CTF and RELAP5 input decks.

The BEPU results are shown in a variety of plots to provide a basis for the BEPU comparison. First, the FOM bands of all parameters for the SIC and OLC methods are plotted simultaneously. Second, the FOM distributions are displayed, where the median, 25th and 75th percentiles are marked. Finally, Spearman's rank correlation coefficients for the defined FOM and uncertain parameters have been obtained, as well as the correlations between the errors of the BCs between RELAP5 and CTF codes and the MDNBR for the OLC method.

7.5.1 RCP trip BEPU analysis comparison

The BEPU results for the RCP trip case are presented in Table 7.6, where the MDNBR base case and lower band minimum values for SIC and OLC coupling methods are displayed. As explained in Chapter 4, by using the one-sided second-order Wilks' formula, with 95% of coverage and 95% confidence (95/95), and executing 93 runs, it is allowed to discard the case with the most limiting (minimum) value for the MDNBR.

The values of the other FOM are also displayed for the 2nd most restrictive case of the MDNBR. It is important to note that in this case, the base case (BC) value (SIC: 2.679, OLC: 2.699) and the lower band 2nd minimum value (LB2M) from the SIC and OLC methods (SIC: 2.532, OLC: 2.567) present a good degree of consistency, and the deviation of the LB2M values from the base case values is similar in SIC and OLC methods.

Parameter	Unit	SIC BC	SIC LB2M	OLC BC	OLC LB2M
MDNBR	-	2.679	2.532	2.699	2.567
HF (MDNBR)	kW/m2	995.2	978.9	1012.2	2 76.2
CHF (MDNBR)	kW/m2	2666.7	2478.6	2 732.2	2505.9
VF (MDNBR)	-	0.063	0.105	0.049	0.068
Surf. temp. (MDNBR)	K	674.5	673.8	675.2	675.0

Table 7.6: *BEPU RCP case results: MDNBR and related parameters base case values (BC), lower band 2nd minimum values (LB2M).*

Theoretically, Wilks' formula can only be applied to make assumptions on one scalar, in this case, the 2nd minimum value for the MDNBR throughout the transient. In this chapter, the MDNBR and other FOM bands are included to provide only qualitative information. Figures 7.30 to 7.34 show the BEPU FOM bands for the RCP case in SIC and OLC methods. It can be noticed that the minimum MDNBR values and the bands present general consistency between the coupling methods. The void fraction bands (Figure 7.32) present differences already seen in the base cases, producing a higher broadening of the uncertainty bands for the case of the SIC method.

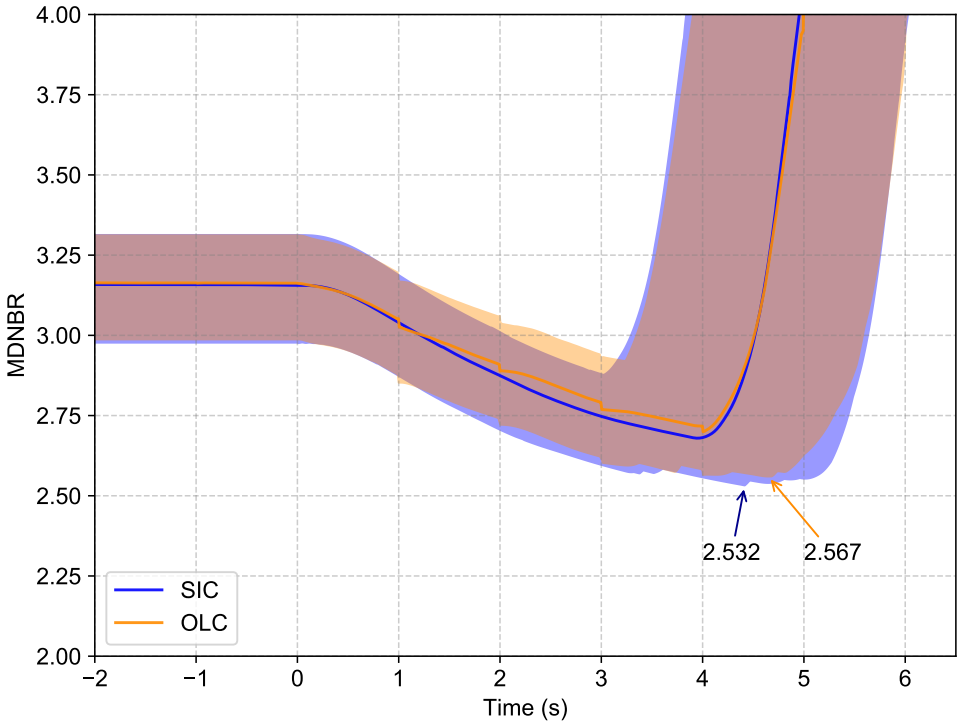

Figure 7.30: *RCP trip - MDNBR bands*

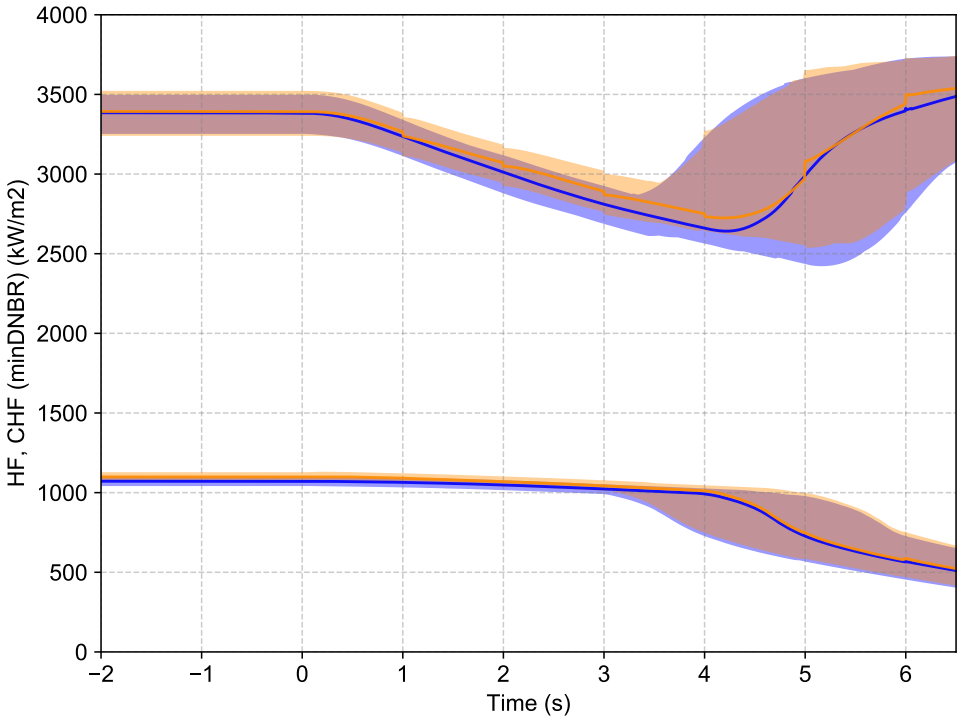

Figure 7.31: *RCP trip - HF, CHF (MDNBR) bands*

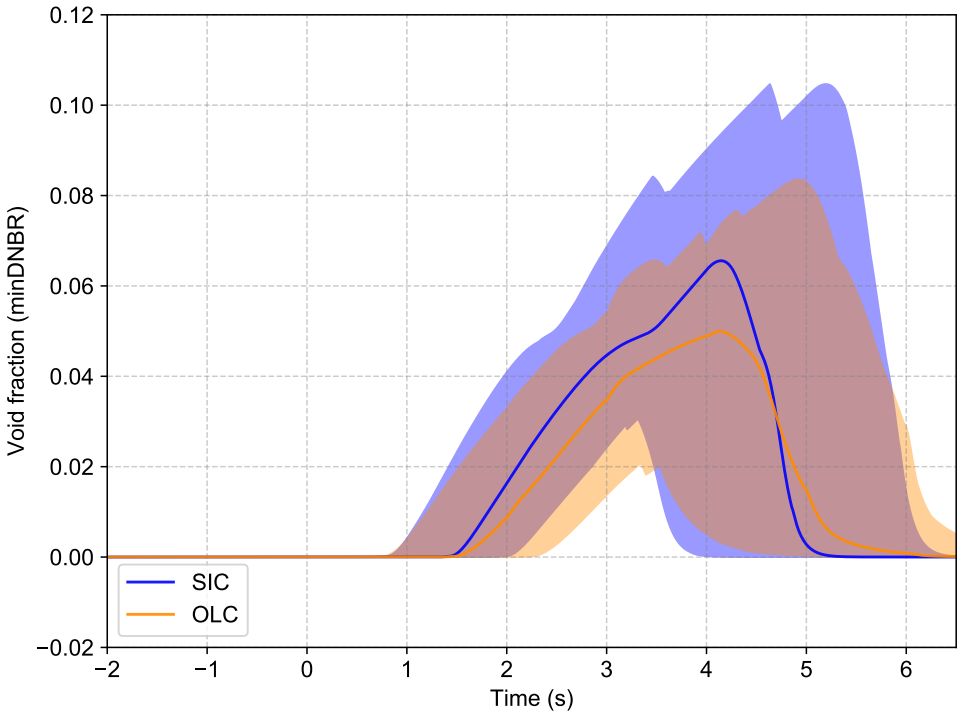

Figure 7.32: *RCP trip - Void fraction (MDNBR) bands*

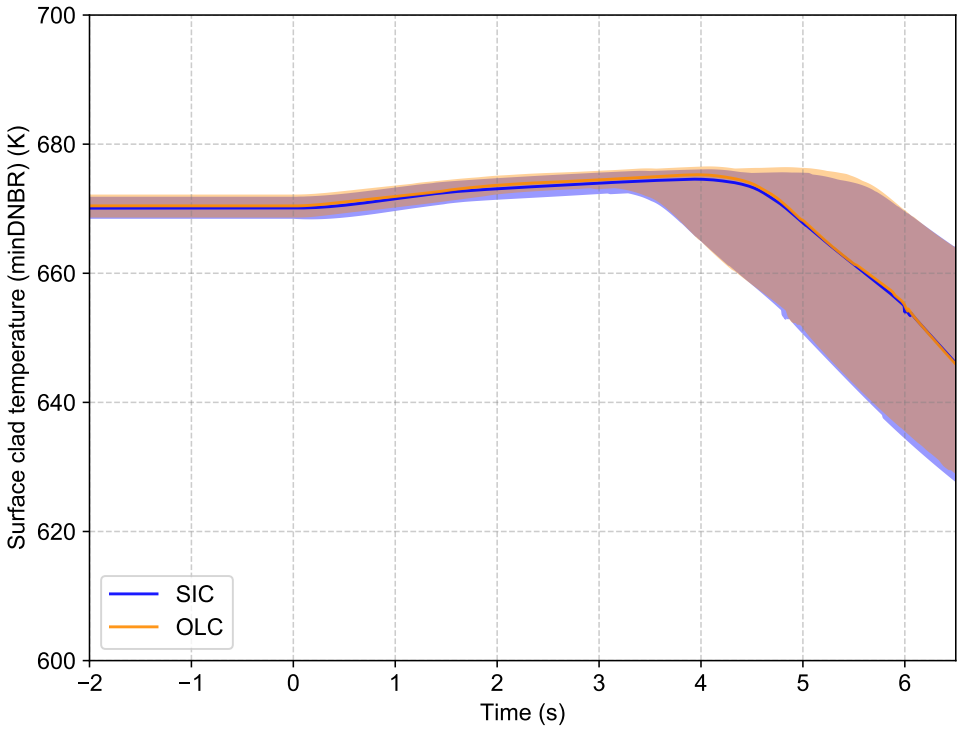

Figure 7.33: *RCP trip - Surface clad temperature (MDNBR) bands*

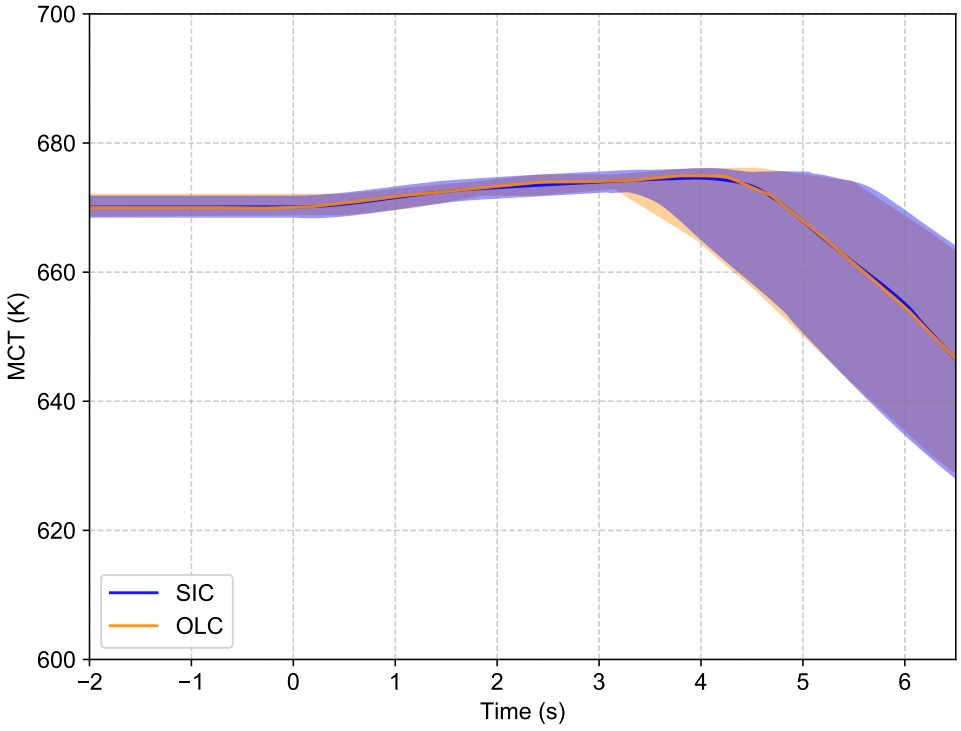

Figure 7.34: *RCP trip - MCT bands*

The results of the cases run in the BEPU analysis for the RCP case are compared for the SIC and OLC coupling methods. Figure 7.35 shows the FOM dispersion plots of the MDNBR, its related parameters and the MCT. The density of the results for the OLC method is shown on the left side and the right side shows the distribution of results of the SIC method. The discontinuous lines represent the 25th, 50th and 75th percentiles. The red and green values represent the base cases for OLC and SIC methods, respectively. It should be taken into account that observing similar distributions of the FOMs is an additional indicator to judge the acceptability of different calculations (in this case for coupling method comparisons) as a further step to the base case and sensitivity comparisons.

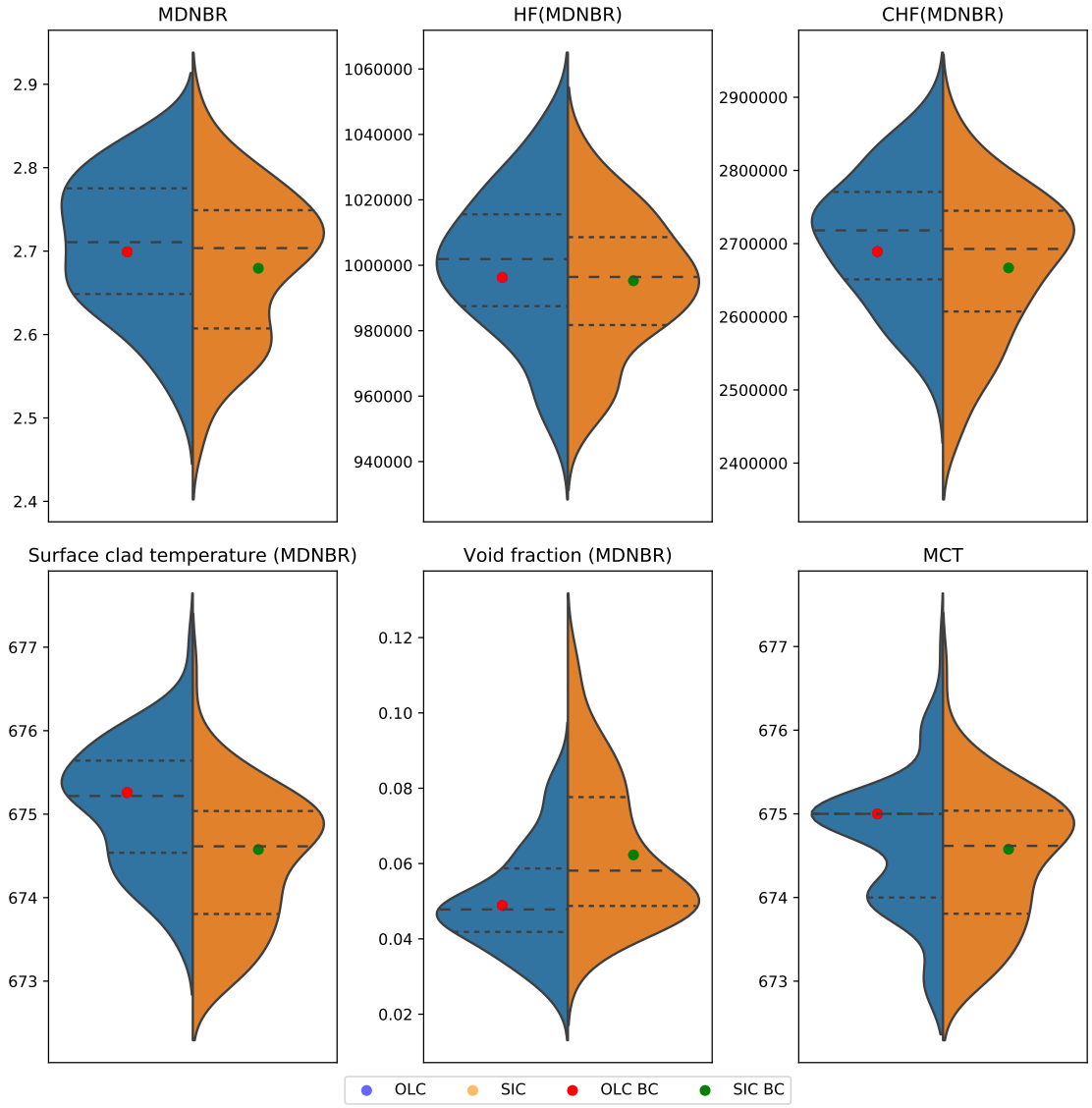

Figure 7.35: *RCP trip - FOM distributions and base case values*

Figure 7.35 shows that the RCP case presents in general similar distribution values of the FOM considered. It is important to note that the HF and CHF distributions are practically equivalent between the SIC and OLC methods. Clad temperatures at the MDNBR location present also similar distribution considering the difference already present in the base cases. On the contrary, both the void fraction and the MCT present an equivalent distribution despite the differences in the base case values.

Figures 7.36 and 7.37 show the Spearman's rank correlation coefficients for the defined FOM for the SIC and OLC methods. Spearman's rank-order correlation has been chosen in order to capture the monotonic relationships between the defined FOM and the uncertain input parameters (#1 to #15).

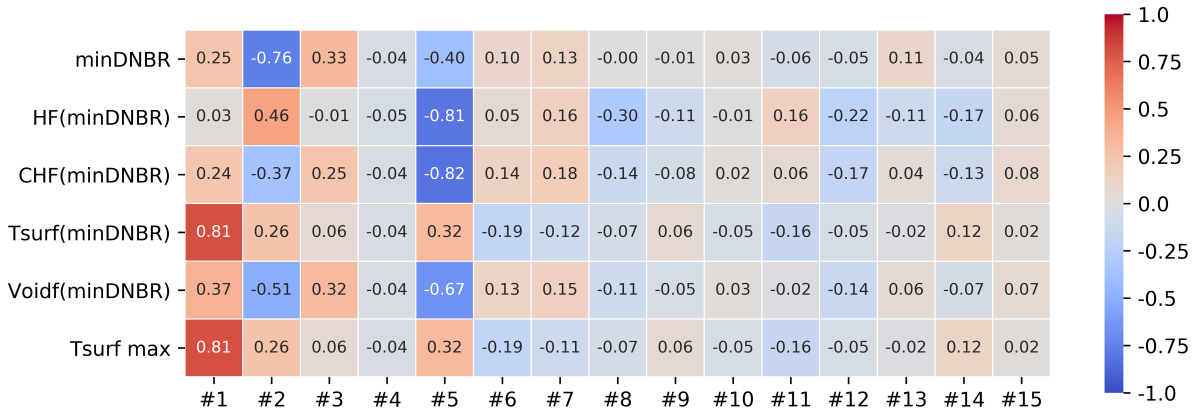

Figure 7.36: *RCP trip - Spearman's rank correlation coefficients SIC method*

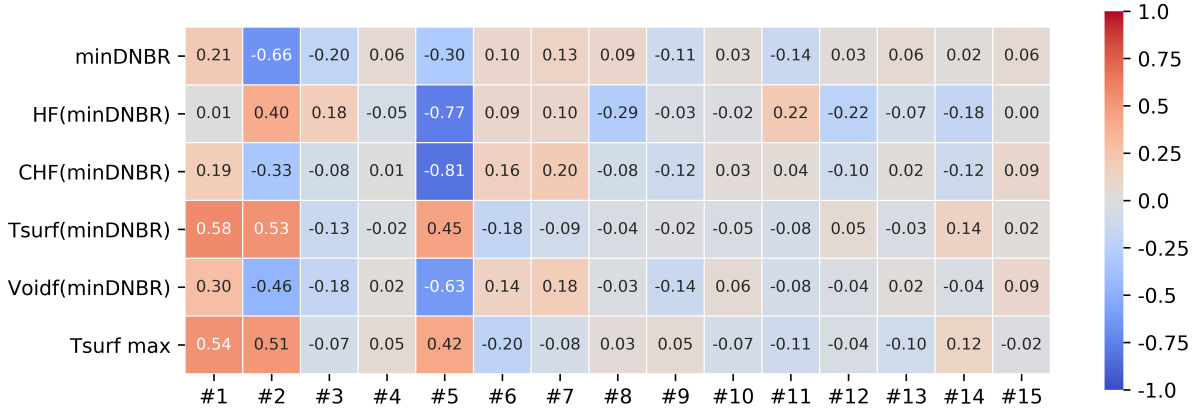

Figure 7.37: *RCP trip - Spearman's rank correlation coefficients OLC method*

In the RCP case, for both SIC and OLC methods, results show that the main contributors to MDNBR are the RCS pressure (#1), the core power (#2), the core mass flow rate (#3) and the reactor trip time (#5), all of them being system parameters (RELAP5 model). With the exception of the core mass flow rate (#3), the correlation coefficients are consistent with the sensitivity analysis. Also, the correlation coefficients are similar between the coupling methods, being stronger in the case of the SIC method.

The correlation coefficient of the core mass flow rate (#3) for the SIC method presents a value of 0.33, while the OLC method is -0.20. This difference indicates that while the sensitivity analysis shows a positive correlation between the core mass flow rate and MDNBR in the SIC method, the BEPU analysis shows otherwise. This can be caused by the effect of the change of the core mass flow rate to the other relevant plant parameters with high contribution to DNBR during the transient, even though before the transient those parameters were normalized to their nominal values. The fact that this effect is not observed for the OLC method may indicate that the dependence between the main plant parameters and results is not fully taken into account by this coupling method.

The other FOM also present a similar degree of correlation between the coupling methods. HF, CHF and void fraction are mainly correlated to the core power (#2) and reactor trip time (#5). Clad temperatures (maximum and MDNBR location) are also correlated in both methods to the same uncertain parameters: RCS pressure (#1), the core power (#2) and the reactor trip time (#5). The similarity of the FOM correlations between the coupling methods indicates that the transmission of uncertainties from the system domain to the core domain occurs similarly for the SIC and OLC methods.

7.5.2 PORV opening BEPU analysis comparison

The BEPU results for the PORV opening case are presented in Table 7.7. The LB2M values (SIC: 2.654, OLC: 2.495) are consistent with the difference observed in the base cases (SIC: 2.754, OLC: 2.646). MDNBR shows different values between both coupling methods mainly due to the differences in the calculation of the CHF, affected by many parameters as explained in Section 2.

Parameter	Unit	SIC BC	SIC LB2M	OLC BC	OLC LB2M
MDNBR	-	2.754	2.654	2.646	2.495
HF (MDNBR)	kW/m2	1029.0	1044.1	1061.0	2 075.9
CHF (MDNBR)	kW/m2	2835.0	2771.1	2807.1	2 684.4
VF (MDNBR)	-	0.054	0.069	0.066	0.098
Surf. temp. (MDNBR)	K	658.2	658.6	658.7	659.5

Table 7.7: *BEPU RCP case results: MDNBR and related parameters base case values (BC), lower band 2nd minimum values (LB2M).*

Figures 7.38 to 7.42 show the BEPU FOM bands for the PORV case in SIC and OLC methods. The bands present consistent values between the methods, with the exception of the MDNBR (Figure 7.38), CHF (Figure 7.39) and void fraction (Figure 7.40). In the case of MDNBR and CHF, the deviation is produced by the differences in the base cases, but in this case, the OLC band is wider than the SIC band and includes the less restrictive values of the SIC method (upper band).

The deviation of the CHF can be observed in Figure 7.39, which consists of a broader CHF band in the OLC method. This effect can be also observed in the void fraction (Figure 7.40), where the differences associated with the base case differences are combined with broader bands in the case of the OLC method. In the case of the clad temperatures (Figures 7.41 and 7.42), a time shift of the bands is observed, that is increased from the point that the reactor trip occurs.

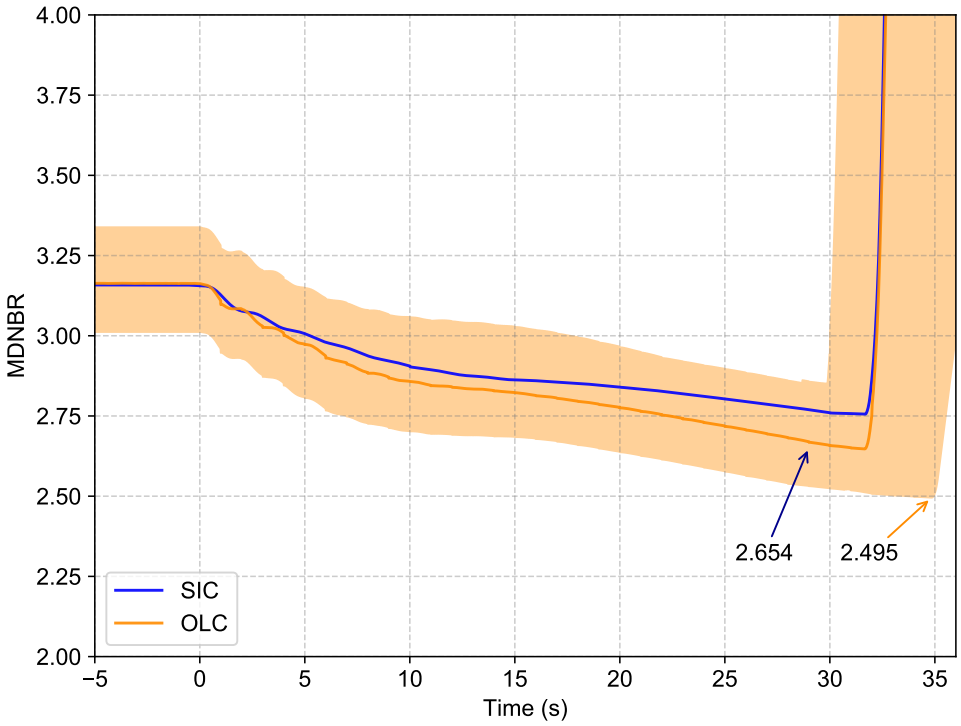

Figure 7.38: *PORV opening - MDNBR bands*

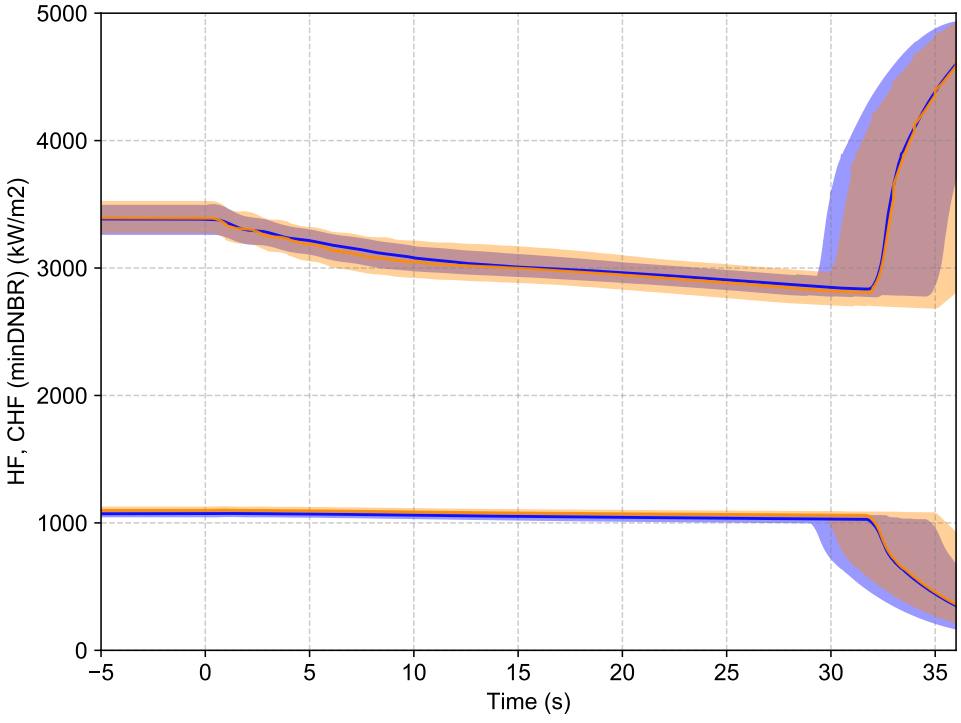

Figure 7.39: *PORV opening - HF, CHF (MDNBR) bands*

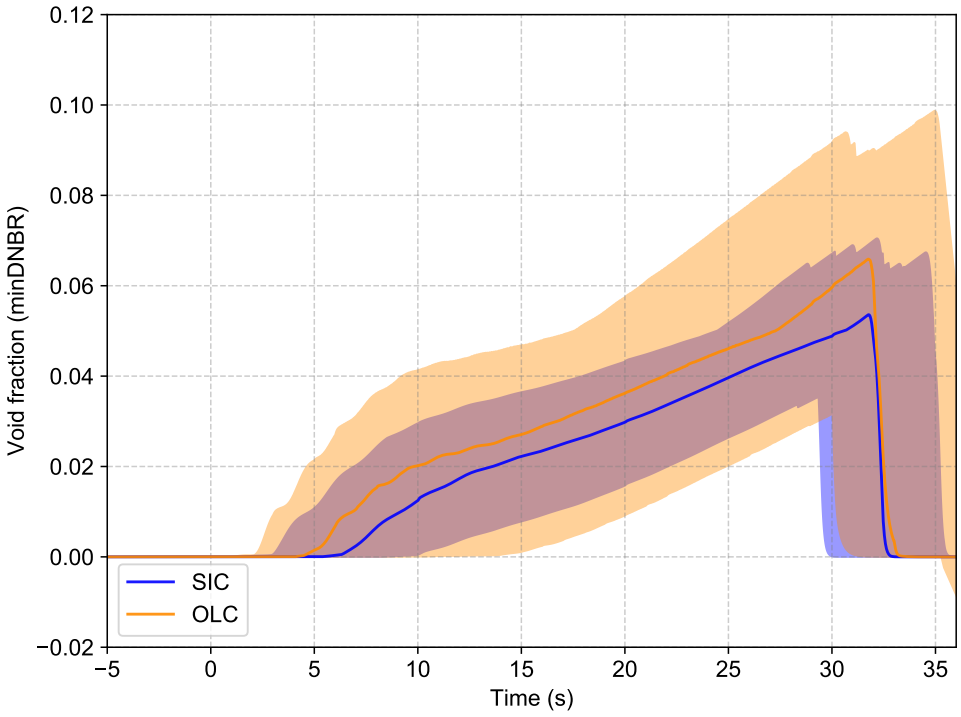

Figure 7.40: *PORV opening - Void fraction (MDNBR) bands*

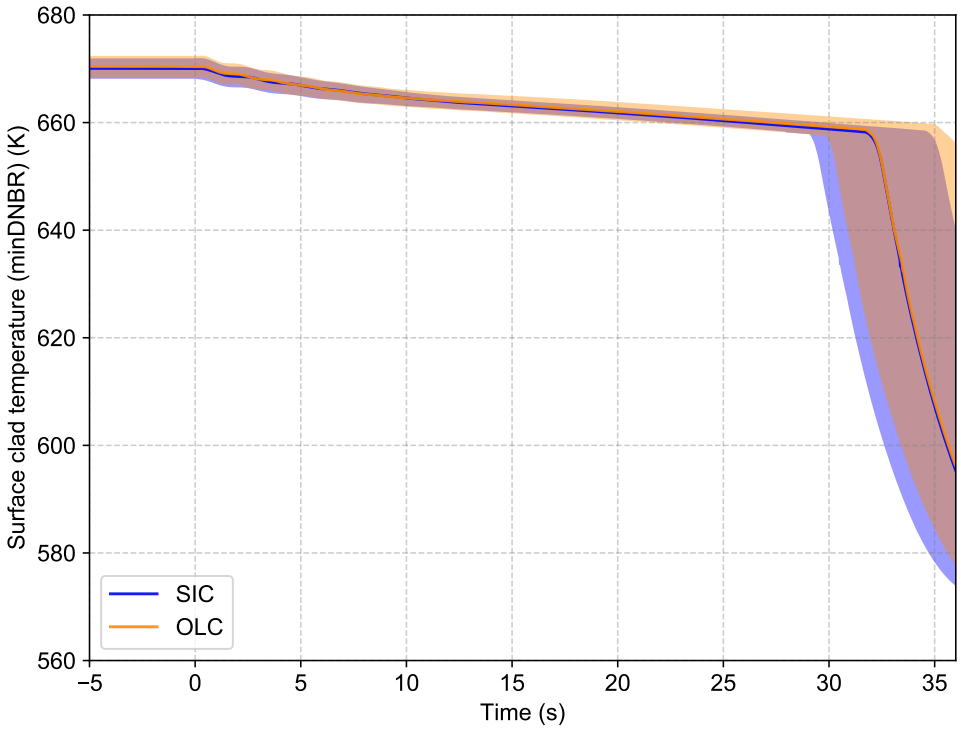

Figure 7.41: *PORV opening - Surface clad temperature (MDNBR) bands*

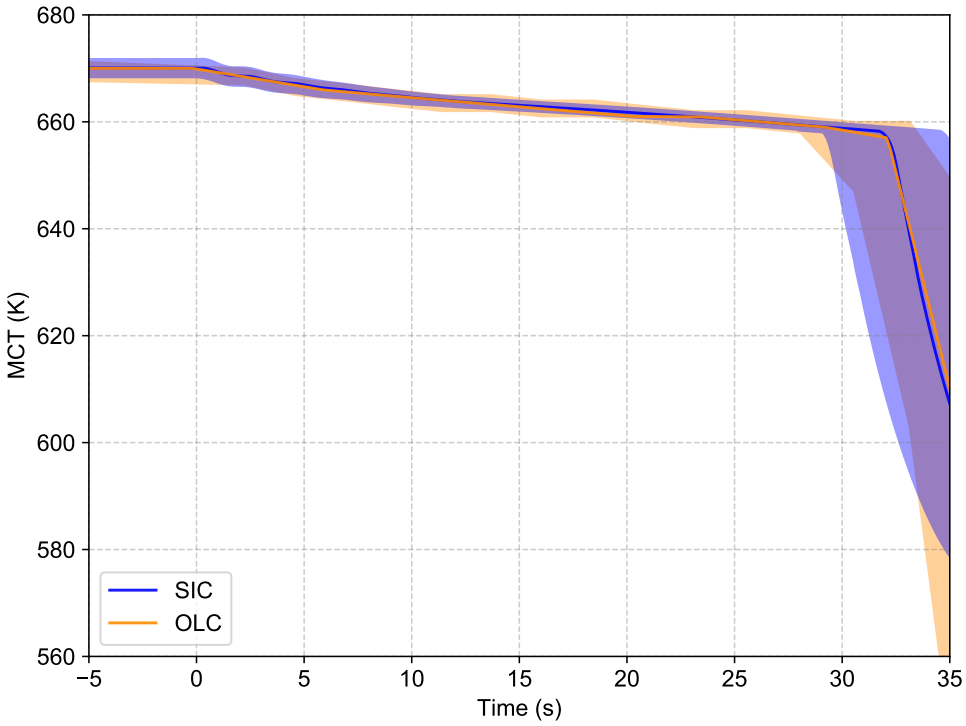

Figure 7.42: *PORV opening - MCT bands*

The plots of the dispersion of the FOM for each coupling method are shown in Figure 7.43. In the PORV case, the FOM distributions are unequal, partially as a result of the differences between the base cases described in Section 7.3. In the first place, it can be seen that the differences in the base case CHF values are directly extrapolated to the MDNBR since the distribution shape of both FOM is equivalent. This can be explained by the similar base case values and similar distribution of the HF FOM. This confirms that the action of analyzing the differences in the FOM distributions provides more tools to analyze the effects of the FOM on results.

Also, CHF and MDNBR distributions for the OLC method present a broader dispersion of results than the SIC method, possibly indicating that the differences between methods are not only a direct consequence of the base case differences but of the coupling method itself. Clad temperature and void fraction present both different base case values and different dispersion of results, having a lower dispersion in the case of the SIC method, as can be seen for all FOM considered. The MCT distributions present a good agreement, in this case, being an independent result from the MDNBR and its related parameters.

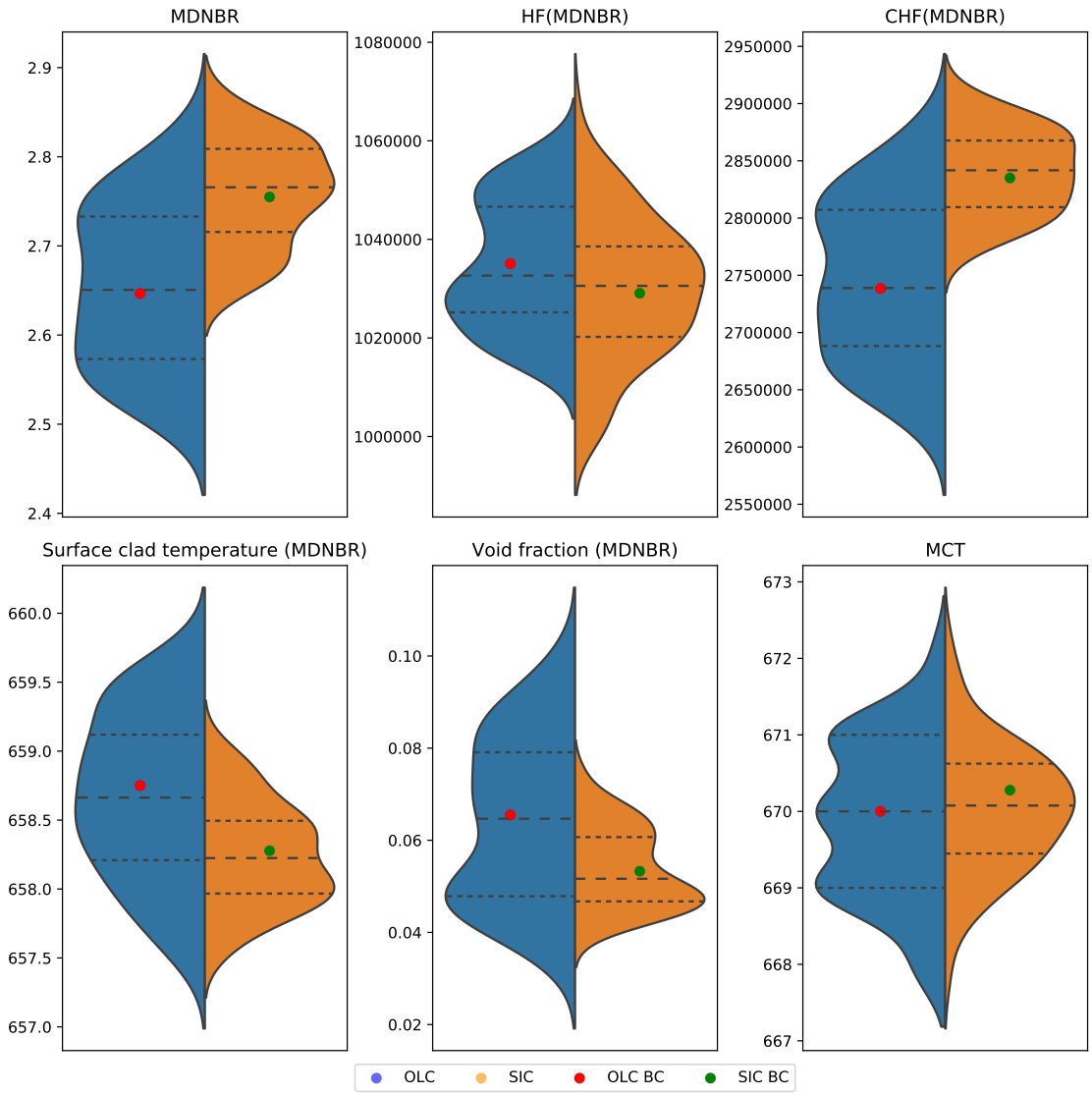

Figure 7.43: *PORV opening - FOM distributions and base case values*

Figures 7.44 and 7.45 show the Spearman's rank correlation coefficients for the defined FOM for the PORV case. In this case, the main contributors to the MDNBR are the core power (#1) and the core mass flow rate (#3), with a lower contribution of the reactor trip time delay (#5) and the MTC factor (#6), in agreement with the sensitivity analysis. The pressurizer valve discharge coefficient and the pressurizer level are not correlated to any FOM because they have an influence only on the time when the reactor trips (low pressurizer pressure). It is relevant to notice that at this time event the FOM values are very similar.

In this case, for the rest of FOM considered, there is not always a clear similarity between SIC and OLC methods, having in some cases relevant differences. While the core power similarly correlates to most of the FOM, the core mass flow rate correlates with most of the FOM with significant differences between the coupling methods. Reactor trip time delay and MTC factor both present a similar correlation for SIC and OLC methods.

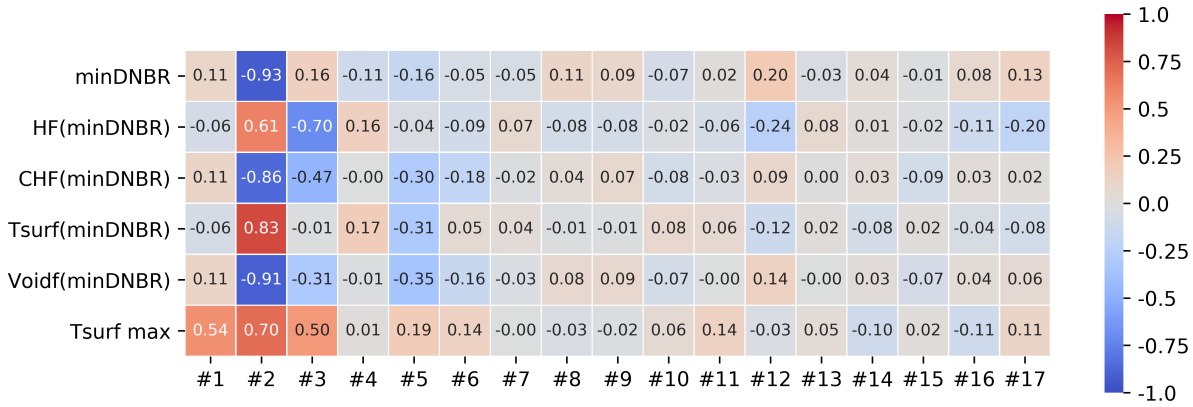

Figure 7.44: *PORV opening - Spearman's rank correlation coefficients SIC method*

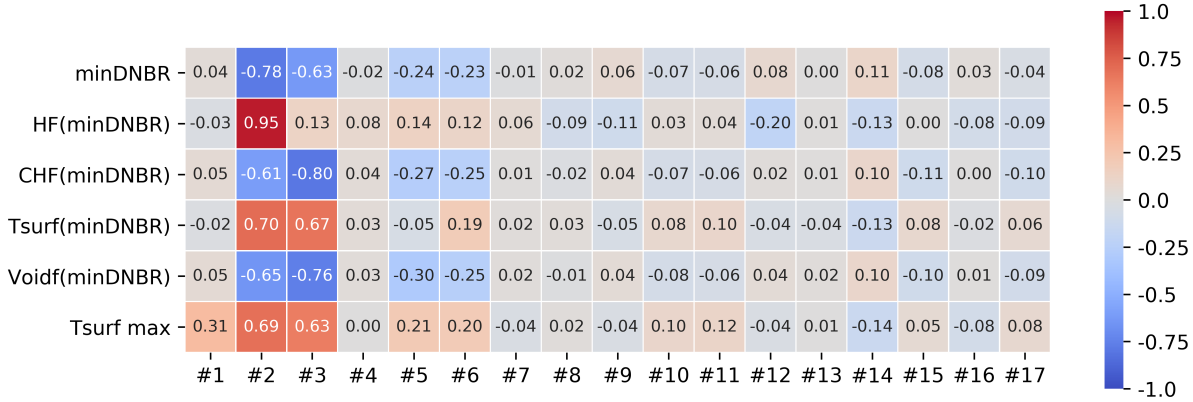

Figure 7.45: *PORV opening - Spearman's rank correlation coefficients OLC method*

7.5.3 MDNBR and boundary conditions correlation

A further step has been taken to analyze the differences in the results of the SIC and OLC coupling methods in relation to the BCs applied to the CTF core model. When comparing the BEPU analysis results of the OLC method, the BCs present inconsistencies by definition. While the outlet pressure and the inlet mass flow and temperature are imposed, the

inlet pressure and outlet temperature do not match between CTF and RELAP5 (as seen in Figures 7.14 and 7.27). This occurs because these values depend exclusively on the CTF calculation.

Therefore, Spearman's rank correlation coefficients have been obtained (see Figures 7.46a and 7.46b) in order to evaluate the possible correlation between the SIC and OLC methods MDNBR and related parameters differences (the differences of the MDNBR and its related parameters between the SIC and OLC methods) and the differences in the inlet pressures and outlet temperatures between the CTF and RELAP codes.

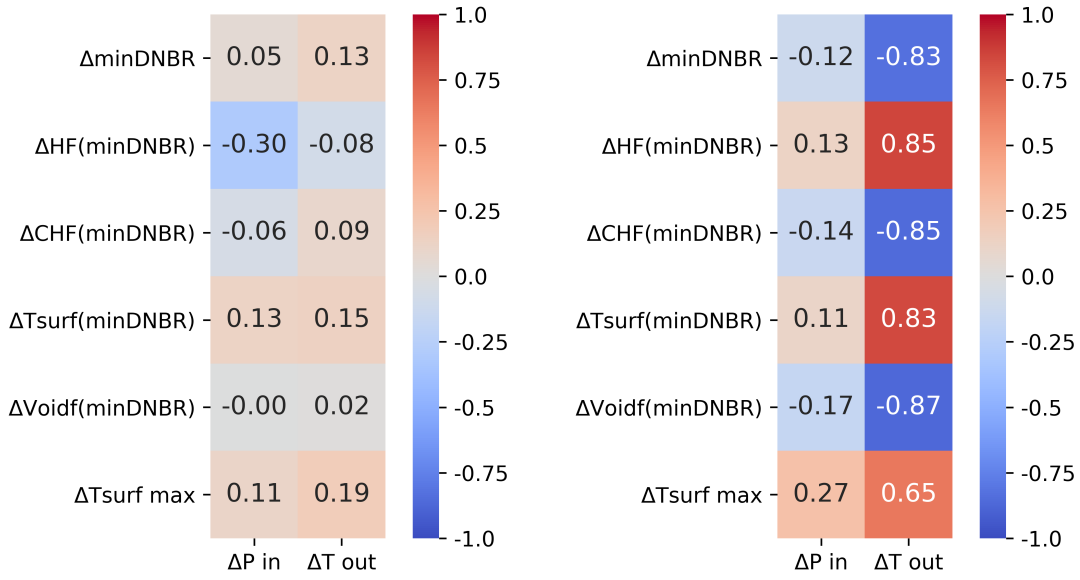

(a) *RCP trip* (b) *PORV opening*

Figure 7.46: *FOMs error between SIC and OLC methods correlation to BC errors in the OLC method*

In the RCP case, Figure 7.46a shows no relevant correlation between the BC difference and most of the FOM, with the exception of the error corresponding to the HF (-0.30), being coherent with the analysis of the FOM distributions previously described. This indicates that the differences in the BC (inlet pressure and outlet temperature) when performing a calculation using the OLC method, do not introduce significant deviations in results as a consequence of the coupling method.

On the other hand, in the PORV case, while there is no practically any relevant cor-

relation between the inlet pressure difference and most of the difference in the FOMs, with the exception of the error corresponding to MCT (0.27), there are strong correlations between the temperature differences at the core outlet and all the FOM differences. This indicates that the previously noted differences between SIC and OLC methods in the FOM distributions and Spearman's rank correlation coefficients are caused by differences in the BC, and are implicit in the selection of the coupling method.

CHAPTER 8

CONCLUSIONS

This chapter contains:

- The conclusions on the development of the CTF-RELAP5 codes coupling
- The conclusions on the application of the CTF-RELAP5 codes coupling
- The conclusions on the BEPU comparison between coupling methods

8.1 General considerations

Coupling TH system codes with TH sub-channel codes provides the capability of increased detail modelling in system transients with an impact on the core parameters such as the MDNBR. The differences among standard practices when coupling TH-TH codes have been assessed by evaluating the influence of model uncertainties for different coupling methods in multi-scale simulations. This evaluation has been complemented by applying a BEPU analysis by using the same sets of uncertain parameter values for the different coupling methods.

CTF and RELAP5 have been coupled using two coupling methods: on one hand, the SIC method has been applied, obtaining a tool that provides the capability of having equal convected quantities across the coupling junctions and equal properties at the coupling volumes while maintaining the mass and energy balance in the system. On the other hand, the OLC method has been used by extracting the RELAP5 model BC values and imposing them on CTF; by this method, not all BC are consistent between codes, for the present study and the coupling schemes used, the BCs that are not consistent are inlet pressure and outlet enthalpy.

The comparison of the coupling methods has been carried out by selecting two transients related to RCS mass flow rate decrease and pressure decrease:

- The trip of the three RCPs
- The opening of a pressurizer PORV valve

Firstly, a qualitative comparison has been carried out for the PORV opening and RCP trip cases, defining the different FOMs that are considered of interest. Secondly, the uncertain parameters and the related PDFs have been defined, and sensitivity analyses have been performed using the defined uncertain parameters. Finally, a BEPU analysis has been carried out for the selected uncertain parameters and the defined FOM. After performing the BEPU analysis, the differences between the coupling methods have been correlated to the differences between BCs for the OLC method.

This chapter describes the conclusions derived from the present work. The conclusions related to the coupled code developed and its application are presented, as well as the conclusions related to the results of the BEPU analysis comparison between coupling methods.

8.2 Conclusions on the development and the application of the CTF-RELAP5 coupled code

The coupling of CTF and RELAP5 has been carried out first by implementing the semi-implicit coupling methodology developed by W.L. Weaver [29]. It has taken a great effort in programming since substantial modifications in both source codes were necessary to execute the intra-step information exchange and the addition of the coupling boundaries and volumes to the time advancement schemes. Also, a large amount of code programming has been needed in order to manage the advancement of the program and writing results. The OLC method, on the other hand, has been performed using the standalone version of the codes, thus needing less programming work. In this case, the management of input/output data and the code execution has been managed by using Python scripts.

The nodalization used by RELAP5 was previously developed, but an adaptation process has been carried out for the case of the SIC method, as described in Chapter 6. The CTF hybrid model has been developed to match the core modeled in the RELAP5 model. A Python script has been developed to build the hybrid model by placing the sub-channel portion of the model in the desired position substituting a fuel array with the necessary detail.

With respect to the calculations, it is worth noting that because CTF does not have the capability of restarting a calculation, the step of obtaining the steady states as a function of the uncertain parameters has been challenging, considering that parameters affecting the model such as mass flow rates, power, pressure and pressurizer level with associated control systems were required to be adjusted. This added the necessity to compare the steady states for both coupling methods (SIC and OLC) for all sensitivity cases to check that the cases for which the uncertain parameters were affecting the initial conditions

were consistent.

The coupling code developed in this work permits obtaining detailed results of the fuel response to failures or malfunctions of system-related components, without the need to impose sometimes not consistent BCs. The use of a coupled hybrid CTF model helps decrease the computational effort while maintaining the ability to model an entire fuel element at the sub-channel level. On the other hand, the coupled code presents some issues that could be solved in the future:

- The code is strongly related to the particular nodalization of the core model (CTF) since the number of sections, channels and nodes of the model determines the formulation for the expansion and solution of the CTF pressure matrix. Considering this, in order to couple other models (nodalizations) using this code would require further development of the code.
- CTF-RELAP5 has only been tested for the liquid phase and in one direction, so for instance, the code would not be able to reproduce most of the LOCA-related phenomena where two-phase and backward flows are expected. However, it is worth recalling that CTF is mostly used in safety analysis to predict the fuel response in most cases when the flow enters the core from the bottom (no reverse flow) and in subcooled conditions.
- In terms of code verification, the oscillations observed in the verification process would require additional work to analyze their origin and to assess the numerical stability of the code over a broader set of test runs and different models to find possible solutions.

8.3 Conclusions on the SIC and OLC methods comparison by BEPU analysis

Results on the base case, sensitivity and BEPU comparisons have been carried out between the SIC and OLC coupling methods and described in Subsections 7.5.1 and 7.5.2 respectively. The first method for performing the BEPU comparison is the qualitative com-

parison of Spearman's rank correlation coefficients between the defined FOM and the uncertain input parameters for the two coupling methods. Spearman's rank correlation coefficients are considered a measure of the contribution of each uncertain parameter to the FOM. In order to verify that the use of Spearman's rank correlation coefficients is adequate, the scatter plots of MDNBR versus each uncertain parameter were generated and no non-monotonic relationships were observed. The second method is a qualitative comparison of the BEPU FOM distributions. Finally, the differences in results between the coupling methods are evaluated by correlating the FOM to the differences in BC values.

The comparison of the two coupling approaches by means of BEPU calculations shows that using BEPU analyses, some additional parameters to compare multi-scale coupled calculations are available. Among them, the most relevant is the comparison of the distribution of the different FOMs, the comparison of the Spearman's rank correlation coefficients and the more traditional comparison of the FOM uncertainty bands.

For the RCP case, the results are in good agreement for the considered FOM related to MDNBR (Spearman's rank correlation coefficients and distributions). On the contrary, for the PORV case, there is a significant difference in the evaluation of FOM, this is confirmed by observing the MDNBR distribution differences in Figure 7.43. This can be explained by the difference in BC values for the OLC method. This suggests that non-imposed BC values for OLC methods is an important issue to take into account when using OLC methods for system-dependent transients that are extended in time, being in this case more conservative than SIC methods. In both cases, the MCT (independent from the MDNBR and its related parameters) presents consistent base-case results for both coupling methods and similar distributions for the BEPU calculations.

After the calculations and the performed comparisons, it has been confirmed that the uncertainty of sub-channel code results (in this case for MDNBR) presents a strong influence on parameters related to the BCs. In the two cases run, RCP trip and PORV opening, there is a strong influence on the parameters that determine the BCs: pressure, mass flow rate and power. It can be stated then that BEPU analysis can be considered an additional tool for evaluating the impact of the coupling methods on results.

In this work, the coupling methods and the assumptions when coupling CTF and RELAP5 codes were selected based on the fact that they are often used by the industry and researchers. Since some coupling assumptions can differ depending on the specific decisions taken by the analyst, the results may not be applicable to the coupling schemes mentioned in all cases. Anyhow, the conclusion that the difference in results between the coupling methods can be associated with the coupling method is relevant.

Additionally, for reasons related to the transit times of the coolant through the RCS loops, the difference in results is higher for transients that occur longer in time, because the error between the inherent inconsistent BCs related to the coupling method can be accumulated over time. It can be described as a good practice to evaluate the differences of the inconsistent BCs when using off-line coupling schemes.

8.4 Proposal for further work

This Subsection provides a proposal on potential subjects to be further developed related to the programming of the CTF-RELAP5 coupled code and the coupling methods comparison using BEPU methodologies.

8.4.1 CTF-RELAP5 coupled code

On the coupling of CTF and RELAP5 using the SIC method, some further development is considered to be needed in terms of extending the verification process and increasing the capability of the coupled code. In relation to the first subject, further verification would be required in terms of testing the code against more restrictive conditions on the change of relevant boundary parameters. Also, a study of the pressure change across the coupling boundaries and sensitivity analysis of the time-step size of the codes would be required.

In relation to the second subject, some limitations would require further development and verification, such as the ability of the coupled code to manage two-phase flow mixtures at the coupling boundaries. This, in particular, would permit the modelling of higher condition events such as LOCA or RCP stuck rotor events. Also, this coupled code is

limited in some cases to the particularities of the models used, since some additional work would be needed to obtain a model-independent coupling scheme.

The coupled code is designed for models having two coupling volumes, one for the core inlet and one for the outlet. This decision was taken for two main reasons: first, the fact that a single node at the inlet/outlet is an advantage when modifying the CTF pressure matrix. If the pressure matrix expansion had to be performed with multiple or a variable number of coupling boundaries, finding the coupling coefficients previously described would be highly challenging. The second reason is related to the limited capabilities of RELAP5 to reproduce heterogeneous conditions at the core inlet. CTF is capable of defining a very detailed inlet mass-flow distribution, but since RELAP5 is not able to provide it, a single node has been placed to provide a coupling volume instead (in this case the lower plenum is modelled with RELAP5, not CTF).

The selection of the cases is based on the requirement to avoid substantial inlet flow distribution asymmetries at the core inlet (symmetrical case) since the modelling of a complex geometry like the lower plenum with RELAP5 trying to reproduce a 3-D component is not appropriate. A CFD code would be needed to obtain appropriate results. As reported by Reference [18]: *"According to the results of the literature survey, the asymmetry of the core flow rate is strongly influenced by the real geometry. Therefore, the CFD analysis should be used to model the actual geometry"*.

The last point would be the possibility of coupling CTF with a neutronics code that takes into account the core local conditions to provide the ability to model transients with asymmetric neutron flux profiles, and those depending on the thermal-hydraulic local conditions. In this case, the coupling would require less programming effort, since it is a coupling related to multi-physics instead of multi-scale. Also, extended literature is available on the subject.

8.4.2 Coupling methods comparison

The comparison between coupling methods by applying BEPU methods has proven useful for these particular cases, helping to identify the dependence of results on the BCs

deviations. It should be taken into account that finding similar distributions of the FOM is an additional indicator to judge the acceptability of different calculations (in this case for coupling method comparisons) as a further step to the base case and sensitivity comparisons. It would be useful to compare this dependence in other cases in which the core limiting conditions are determined by system failures with asymmetries in the neutron flux profile, such as MSLB accidents.

Previous works, such as the OECD/NRC BFBT benchmark [105], aimed to reduce the uncertainties in steady-state calculations for different scales of TH calculations. In this benchmark, the comparisons were performed by applying BEPU analysis to coupled calculations for TH-NK codes against experimental data, obtained from full-scale mock-up experiments that reproduce boiling water reactors (BWR) conditions [51]. The use of BEPU analysis could be extended to assess not only the coupled codes but the differences in results from different coupling scheme methods also for multi-physics problems.

BIBLIOGRAPHY

[1] Westinghouse Electric Company, “Westinghouse Technology Manual (ML20057E160),” tech. rep., U.S. Nuclear Regulatory Commission, 2020.

[2] International Atomic Energy Agency, “Guidebook on the Introduction of Nuclear Power,” Tech. Rep. 217, International Atomic Energy Agency, Vienna, 1982.

[3] M. Schneider, J. Hazemann, A. Ahmad, T. Katsuta, M. V. Ramana, A. Froggatt, L. Author, B. Wealer, and J. Kang, “The World Nuclear Industry Status Report 2020,” Tech. Rep. September, 2020.

[4] U.S. Nuclear Regulatory Comission, “Standard Format and Content of Safety Analysis Report for Nuclear Power Plants LWR Edition (RG 1.70 Rev. 3),” Tech. Rep. , 1978.

[5] Autorité de Sûreté Nucléaire, “Harmonisation of nuclear safety: international initiatives,” tech. rep., ASN, 2006.

[6] International Atomic Energy Agency, “IAEA Safety Standards,” tech. rep., https://www.iaea.org/resources/safety-standards. IAEA.

[7] International Atomic Energy Agency, “Deterministic Safety Analysis for Nuclear Power Plants - IAEA SSG-2 Revision 1,” 2019.

[8] U.S. Nuclear Regulatory Comission, “U.S. Nuclear Regulatory Commission Regulations: Title 10, Code of Federal Regulations,” 2010.

[9] American Nuclear Society, “Nuclear Safety Criteria for the Design of Stationary Pressurized Water Reactor Plants,” *ANSI Standards*, no. ANS-51.1/N18.2-1973, 1973.

[10] International Atomic Energy Agency, “Safety margins of operating reactors,” Tech. Rep. IAEA-TECDOC-1332, 2003.

[11] International Atomic Energy Agency, “Best Estimate Safety Analysis for Nuclear Power Plants: Uncertainty Evaluation,” tech. rep., IAEA, 2008.

[12] F. D’Auria, *Thermal Hydraulics in Water-Cooled Nuclear Reactors*. Woodhead Publishing, 2017.

[13] F. D’Auria, C. Camargo, N. Muellner, M. Lanfredini, and O. Mazzantini, “The simulation of IC in accident analyses of nuclear power plants,” *Nuclear Engineering and Design*, vol. 250, pp. 656–663, 2012.

[14] Information Systems Laboratories, “RELAP5 MOD3.3 Code Manual Volume I: Code Structure, System Models, and Solution Methods,” tech. rep., Information Systems Laboratories, 2010.

[15] Idaho National Laboratory, “RELAP5-3D Code Manual, Volume I: Code Structure, System Models and Solution Methods,” tech. rep., INL, 2012.

[16] M. N. Avramova and R. K. Salko, “CTF Theory Manual,” tech. rep., Reactor Dynamics and Fuel Modeling Group (RDFMG), 2016.

[17] D. Bestion, “The difficult challenge of a two-phase CFD modelling for all flow regimes,” *Nuclear Engineering and Design*, vol. 279, pp. 116–125, nov 2014.

[18] I. S. Lee, D. H. Yoon, Y. S. Bang, T. H. Kim, and Y. C. Kim, “Assessment of realistic departure from nucleate boiling ratio (Dnbr) considering uncertainty quantification of core flow asymmetry,” *Energies*, vol. 14, no. 5, 2021.

[19] U.S. Nuclear Regulatory Commission, “SRP Standard Review Plan for the Review of Safety Analysis Reports for Nuclear Power Plants: LWR Edition,” tech. rep., U.S. NRC, 2018.

[20] W. Beck, P. Blanpain, T. Fuketa, A. Gorzel, Z. Hozer, K. Kamimura, and R. Rehacek, “Nuclear Fuel Safety Criteria Technical Review,” tech. rep., OECD-NEA, 2012.

[21] U.S. Nuclear Regulatory Comission, “NUREG-0800 15.3.1: Loss of Forced Reactor Coolant Flow Including Trip of Pump Motor and Flow Controller Malfunctions,” tech. rep., NRC, 2007.

[22] U.S. Nuclear Regulatory Comission, “NUREG-0800 15.6.1: Inadvertent Opening of a PWR Pressurizer Pressure Relief Valve or a BWR Pressure Relief Valve,” tech. rep., 2007.

[23] International Atomic Energy Agency, “Use and Development of Coupled Computer Codes for the Analysis of Accidents at Nuclear Power Plants,” tech. rep., IAEA, 2007.

[24] B. L. Smith, U. Bieder, E. Graffard, M. Heitsch, M. Henriksson, T. Höhne, E. Komen, J. Mahaffy, F. Moretti, T. Morii, P. Mühlbauer, U. Rohde, M. Scheuerer, C.-H. Song, and G. Zigh, “Assessment of Computational Fluid Dynamics (CFD) for Nuclear Reactor Safety Problems,” Tech. Rep. January, OECD/NEA, 2008.

[25] M. J. Thurgood, J. M. Kelly, T. E. Guidotti, R. J. Kohrt, and K. R. Crowell, “COBRA/TRAC-A Thermal-Hydraulics Code for Transient Analysis of Nuclear Reactor Vessels and Primary Coolant Systems. Equations and Constitutive Models,” *NUREG/CR-3046*, vol. 1, p. 196, 1983.

[26] J. J. Jeong, S. K. Sim, and S. Y. Lee, “Development and Assessment of the COBRA/RELAP5 Code,” *Journal of Nuclear Science and Technology*, vol. 34, no. 11, pp. 1087–1098, 1997.

[27] S. Y. Lee, J. J. Jeong, and S.-H. Kim, “COBRA/RELAP5; A merged version of the COBRA-TF and RELAP5/MOD3 codes,” *Nuclear Technology*, pp. 177–187, 1992.

[28] J. J. Jeong, K. S. Ha, B. D. Chung, and W. J. Lee, "A Multi-Dimensional Thermal-Hydraulic System Analysis Code, MARS 1.3.1," *Journal of the Korean Nuclear Society*, 1999.

[29] W. L. Weaver, E. T. Tomlinson, and D. L. Aumiller, "A generic semi-implicit coupling methodology for use in RELAP5-3D," *Nuclear Engineering and Design*, vol. 211, no. 1, pp. 13–26, 2002.

[30] A. Geist, A. Beguelin, J. Dongarra, W. Jiang, R. Manchek, and V. Sunderam, "PVM 3 User Guide," Tech. Rep. 12187, ORNL, 1993.

[31] W. L. Weaver, "An Executive Program For Use With RELAP5-3D ©," tech. rep., INEEL, 2001.

[32] M. D. Soler-Martínez, "Semi-implicit thermal-hydraulic coupling of advanced subchannel and system codes for pressurized water reactor transient applications," *Master of Science Thesis (The Pennsylvania State University, Department of Mechanical and Nuclear Engineering)*, 2011.

[33] J. Jiménez, V. Di Marcello, V. Sanchez Espinoza, and Y. Perin, "Application of the ATHLET/COBRA-TF thermal-hydraulics coupled code to the analysis of BWR ATWS," *Nuclear Engineering and Design*, vol. 321, pp. 318–327, 2017.

[34] A. Abarca, *Desarrollo y verificación de una plataforma multifísica de altas prestaciones para Análisis de Seguridad en Ingeniería Nuclear*. PhD thesis, Universitat Politecnica de Valencia (UPV), 2017.

[35] R. M. Al-Chalabi, P. J. Turinsky, F. X. Faure, H. N. Sarsour, and P. R. Engrand, "NESTLE: A nodal kinetics code," Transactions of the American Nuclear Society, 1993.

[36] A. Wysocki, R. Salko, and I. Arshavsky, "Coupling of CTF and RELAP5-3D Within an Enhanced Fidelity Nuclear Power Plant Simulator," in *International Topical Meeting on Nuclear Reactor Thermal Hydraulics (NURETH-19)*, pp. 1–16, 2022.

[37] U.S. Nuclear Regulatory Comission, "Regulatory Guide 1.203, Transient and accident analysis methods," no. December, pp. 1–20, 2005.

[38] O. Mazzantini, G. Galassi, and F. D'Auria, "Reprint of The role of nuclear thermal-hydraulics in the licensing of Atucha-II: The LBLOCA," *Nuclear Engineering and Design*, no. 354, 2019.

[39] M. R. Galetti, "Regulatory scenario for the acceptance of uncertainty analysis methodologies for the LB-LOCA and the Brazilian approach," *Science and Technology of Nuclear Installations*, vol. 2008, 2007.

[40] F. D'Auria and O. Mazzantini, "The Best-Estimate Plus Uncertainty (BEPU) challenge in the licensing of current generation of reactors," *International Conference on Nuclear Engineering, Proceedings, ICONE*, vol. 4, no. 1, pp. 15–23, 2012.

[41] F. D'Auria, C. Camargo, and O. Mazzantini, "The Best Estimate Plus Uncertainty (BEPU) approach in licensing of current nuclear reactors," *Nuclear Engineering and Design*, vol. 248, pp. 317–328, jul 2012.

[42] M. Panicker, "Licensing and Regulatory Requirements for Best Estimate Plus Uncertainty Applications," in *ANS Best Estimate Plus Uncertainty International Conference (BEPU 2018)*, vol. 46, p. 11, 2018.

[43] U.S. Nuclear Regulatory Comission, "Standard Technical Specifications Westinghouse Plants (NUREG-1431)," tech. rep., U.S. NRC, 2004.

[44] N. Boyack, B.E. and Duffey, Romney and Griffith, P. and Katsma, K.R. and Lellouche, G.S. and Levy, S. and Rohatgi, Upendar and Wilson, G.E. and Wulff, Wolfgang and Zuber, "Quantifying reactor safety margins: Part 1: An overview of the code scaling, applicability, and uncertainty evaluation methodology," *Nuclear Engineering and Design*, vol. 119, pp. 1–15, 1990.

[45] J. Sauvage, S. Laroche, *Validation of the Deterministic Realistic Method Applied to CATHARE on LB LOCA Experiments*. No. 39, American Society of Mechanical Engineers - ASME, 2002.

[46] H. Glaeser, "GRS method for uncertainty and sensitivity evaluation of code results and applications," *Science and Technology of Nuclear Installations*, 2008.

[47] B. Boyack, R. Duffey, P. Griffith, G. Lellouche, U. Rohatgi, G. Wilson, W. Wulff, and N. Zuber, "Quantifying Reactor Safety Margins: Application of Code Scaling, Applicability, and Uncertainty Evaluation Methodology to a Large-Break, Loss-of-Coolant Accident," *NUREG/CR-5249*, 1989.

[48] Committee on the Safety of Nuclear Installations, "Report on the Uncertainty Methods Study," tech. rep., CSNI, 1998.

[49] F. D'Auria, N. Debrecin, and G. M. Galassi, "Outline of the uncertainty methodology based on accuracy extrapolation," *Nuclear Technology*, vol. 109, no. 1, pp. 21–38, 1994.

[50] F. D'Auria, "CIAU Method for Uncertainty Evaluation," in *Exploratory meeting of experts on BE calculations and uncertainty analysis*, (Aix-en-Provence), 2002.

[51] M. Avramova, K. Ivanov, T. Kozlowski, I. Pasichnyk, W. Zwermann, K. Velkov, E. Royer, A. Yamaji, and J. Gulliford, "Multi-physics and multi-scale benchmarking and uncertainty quantification within OECD/NEA framework," *Annals of Nuclear Energy*, vol. 84, pp. 178–196, 2015.

[52] K. Ivanov, M. Avramova, C. Schneidesh, A. Boulore, and E. Royer, "Uncertainty Analysis in Modelling for Light Water Reactors Consistent Approach for Multi-scale Modelling," in *Proceedings of ANS Best Estimate Plus Uncertainty International Conference*, (Lucca), 2018.

[53] M. Avramova, A. Abarca, J. Hou, and K. Ivanov, "Innovations in Multi-Physics Methods Development, Validation, and Uncertainty Quantification," *Journal of Nuclear Engineering*, vol. 2, no. 1, pp. 44–56, 2021.

[54] N. W. Porter, M. N. Avramova, and V. A. Mousseau, "Uncertainty quantification study of CTF for the OECD/NEA LWR uncertainty analysis in modeling benchmark," *Nuclear Science and Engineering*, vol. 190, no. 3, pp. 271–286, 2018.

[55] N. Porter, M. Avramova, and K. Ivanov, "Uncertainty and sensitivity analysis of COBRA-TF for the OECD LWR UAM benchmark using Dakota," *International Topical Meeting on Nuclear Reactor Thermal Hydraulics 2015, NURETH 2015*, vol. 6, pp. 4894–4906, 2015.

[56] C. S. Brown, H. Zhang, V. Kucukboyaci, and Y. Sung, "Best estimate plus uncertainty analysis of departure from nucleate boiling limiting case with CASL core simulator VERA-CS in response to PWR main steam line break event," *Nuclear Engineering and Design*, vol. 309, pp. 8–22, dec 2016.

[57] M. Avramova, "Developments in thermal-hydraulic sub-channel modeling for whole core multi-physics simulations," *Nuclear Engineering and Design*, vol. 358, no. October 2019, pp. 110–387, 2020.

[58] R. K. Salko, T. S. Blyth, and C. A. Dances, *CTF User's Manual*. U.S. DOE - CASL, 2016.

[59] R. K. Salko and M. Avramova, *CTF Pre-processor User's Manual*. NCSU Reactor Dynamics and Fuel Management Group (RDFMG), 2020.

[60] S. Patankar, *Numerical heat transfer and fluid flow: Computational methods in mechanics and thermal science*. McGraw-Hill Book Company, 1980.

[61] L. S. Tong, "Prediction of departure from nucleate boiling for an axially non-uniform heat flux distribution," *Journal of Nuclear Energy*, vol. 21, no. 3, pp. 241–248, 1967.

[62] L. Tong, "Boiling crisis and critical heat flux," tech. rep., Westinghouse Electric Corp., Pittsburgh, Pa., 1972.

[63] N. E. Todreas and M. S. Kazimi, *Nuclear Systems I: Thermal Hydraulic Fundamentals*. Taylor and Francis, 1990.

[64] Information Systems Laboratories, "RELAP5 MOD3.3 Code Manual Volume II: Appendix A Input Requeriments," tech. rep., Information Systems Laboratories, 2010.

[65] V. H. Ransom, "Course A - Numerical Modeling of Two-phase Flows for Presentation at Ecole d'Ete d'Analyse Numerique," tech. rep., U.S. Department of Energy, 1989.

[66] F. Franceschini, A. Godfrey, S. Stimpson, T. Evans, B. Collins, J. Gehin, J. Turner, A. Graham, and T. Downar, "AP1000 PWR Startup Core Modeling and Simulation with VERA-CS (ANFM V)," in *Advances in Nuclear Fuel Management V*, (Hilton Head), 2015.

[67] E. Davidson, M. Baird, B. Collins, and T. Pandya, "VERA-Grizzly Ex-Core Calculations : Watts Bar Unit 1 Cycles 1-2," tech. rep., Oak Ridge National Laboratory, 2021.

[68] F. Reventós, L. Batet, C. Llopis, C. Pretel, M. Salvat, and I. Sol, "Advanced qualification process of ANAV NPP integral dynamic models for supporting plant operation and control," *Nuclear Engineering and Design*, vol. 237, pp. 54–63, jan 2007.

[69] R. Ashley, M. El-Shanawany, F. Eltawila, and F. D'Auria, "Good Practices for User Effect Reduction," tech. rep., OECD-NEA, 1998.

[70] International Atomic Energy Agency, "Accident Analysis for Nuclear Power Plants with Pressurized Water Reactors," *Safety Reports*, no. 30, p. 65, 2003.

[71] V. M. Martínez-Quiroga, *Scaling-up methodology, a systematical procedure for qualifying NPP nodalizations. Application to the OECD/NEA ROSA-2 and PKL-2 Counterpart test*. PhD thesis, UPC - Universitat Politecnica de Catalunya, 2014.

[72] V. Martínez-Quiroga, J. Freixa, and F. Reventós, "PVST, a tool to assess the Power to Volume scaling distortions associated to code simulations," *Nuclear Engineering and Design*, vol. 332, pp. 173–185, 2018.

[73] C. Pretel, L. Batet, A. Cuadra, A. Machado, G. S. José, I. Sol, and F. Reventós, "Qualifying, validating and documenting a thermal-hydraulic code input deck," in *Advanced Thermal-hydraulic and Neutronic Codes: Current and Future Applications*, vol. 2, (Barcelona), pp. 239–250, 2001.

[74] F. Reventós and C. Llopis, "Benefits of Using Integral Plant Models in Utilities Availability and Safety Issues," in *Advanced Thermal-hydraulic and Neutronic Codes: Current and Future Applications*, (Barcelona), pp. 158–170, OECD-NEA, 2001.

[75] F. Reventós, C. Llopis, C. Pretel, J. Posada, and P. Moreno, "Improving NPP availability using thermalhydraulic integral plant models. Assessment and application of turbine run-back scenarios," in *9th International Conference on Nuclear Engineering (ICONE9)*, (Nice), 2001.

[76] C. Llopis, J. Pérez, and R. Mendizábal, "Assessment of RELAP5/MOD2 Against a Turbine Trip From 100% Power in the Vandellos II Nuclear Power Plant," Tech. Rep. July, U.S. Nuclear Regulatory Commission, 1993.

[77] C. Llopis, J. Pérez, and R. Mendizábal, "Assessment of RELAP5/MOD2 Against a Main Feedwater Turbopump Trip Transient in the Vandellos II Nuclear Power Plant," Tech. Rep. July, U.S. Nuclear Regulatory Commission, 1993.

[78] J. Posada, F. Reventós, J. Sanchez-Baptista, A. Pérez-Navas, and P. Moreno, "Study of Transients Related to .AMSAC Actuation, Sensitivity Analysis," Tech. Rep. November 1998, U.S. Nuclear Regulatory Commission, 1998.

[79] F. Reventós, J. Baptista, A. P. Navas, and P. Moreno, "Assessment and application of blackout transients at Ascó nuclear power plant with RELAP5/mod2," tech. rep., U.S. Nuclear Regulatory Comission, 1993.

[80] F. Reventós, J. Baptista, A. P. Navas, and P. Moreno, "International Agreement Report Assessment of a Pressurizer Spray Valve Faulty Opening Transient at Ascó Nuclear Power Plant," tech. rep., U.S. Nuclear Regulatory Comission, 1993.

[81] F. H. Harlow and A. A. Amsden, "Numerical calculation of almost incompressible flow," *Journal of Computational Physics*, vol. 3, pp. 80–93, aug 1968.

[82] D. R. Liles and W. H. Reed, "A semi-implicit method for two-phase fluid dynamics," *Journal of Computational Physics*, vol. 26, pp. 390–407, mar 1978.

[83] D. L. Aumiller, E. T. Tomlinson, and W. L. Weaver, "An integrated RELAP5-3D and multiphase CFD code system utilizing a semi-implicit coupling technique," *Nuclear Engineering and Design*, vol. 216, no. 1-3, pp. 77–87, 2002.

[84] M. Casamor, M. N. Avramova, F. Reventós, and J. Freixa, "Offline And Semi-implicit Coupling Comparisons in DNB Transients," in *Spring CAMP Meeting. València, Spain, 29-31 May 2019*, no. May, (Valencia, Spain), 2019.

[85] Y. Périn, *Development of a Multi-Physics, Multi-Scale simulation tool for LWR safety analysis*. PhD thesis, TECHNISCHE UNIVERSITÄT MÜNCHEN, Lehrstuhl für Nukleartechnik, 2016.

[86] S. S. Wilks, "Determination of Sample Sizes for Setting Tolerance Limits," *The Annals of Mathematical Statistics*, vol. 12, no. 1, pp. 91–96, 1941.

[87] S. S. Wilks, "Statistical prediction with special reference to the problem of tolerance limits," *The Annals of Mathematical Statistics*, pp. 400–409, 1942.

[88] A. Guba, M. Makai, and L. Pál, "Statistical aspects of best estimate method," *Reliability Engineering and System Safety*, vol. 80, no. 3, pp. 217–232, 2003.

[89] H. E. Robbins, "On the Measure of a Random Set," *The Annals of Mathematical Statistics*, vol. 15, no. 1, pp. 70–74, 1944.

[90] N. W. Porter, "Wilks' formula applied to computational tools: A practical discussion and verification," *Annals of Nuclear Energy*, vol. 133, pp. 129–137, 2019.

[91] X. Wu, Z. Xie, F. Alsafadi, and T. Kozlowski, "A comprehensive survey of inverse uncertainty quantification of physical model parameters in nuclear system thermal-hydraulics codes," *Nuclear Engineering and Design*, vol. 384, p. 111460, dec 2021.

[92] J. Freixa, E. de Alfonso, and F. Reventós, "Testing methodologies for quantifying physical models uncertainties. A comparative exercise using CIRCE and IPREM (FFTBM)," *Nuclear Engineering and Design*, vol. 305, pp. 653–665, aug 2016.

[93] R. Mendizábal, E. de Alfonso, J. Freixa, and F. Reventós, "Post-BEMUSE Reflood Model Input Uncertainty Methods (PREMIUM) Benchmark: Final Report (NEA-CSNI-R–2016-18)," no. August, 2017.

[94] J. Baccou, J. Zhang, P. Fillion, G. Damblin, A. Petruzzi, R. Mendizábal, F. Reventós, T. Skorek, M. Couplet, B. Iooss, J. Baccou, J. Zhang, P. Fillion, G. Damblin, A. Petruzzi, J. Zhang, P. Fillion, G. Damblin, R. Mendizábal, F. Reventós, and T. Skorek, "SAPIUM : a generic framework for a practical and transparent quantification of thermal hydraulic code model input uncertainty," pp. 0–23, 2021.

[95] J. Freixa, R. Mendizábal, V. Martínez-quiroga, M. Casamor, F. Reventós, and M. Sánchez-Perea, "On the validation of BEPU methodologies through the simulation of integral experiments : Application to the PKL test facility," *Nuclear Engineering and Design*, vol. 379, no. January, 2021.

[96] C. S. Brown and H. Zhang, "Uncertainty quantification and sensitivity analysis with CASL Core Simulator VERA-CS," *Annals of Nuclear Energy*, vol. 95, pp. 188–201, 2016.

[97] M. D. Soler-Martínez, "Documentation of Coupling COBRA-TF with RELAP-3D Using PVM Environment," tech. rep., The Pennsylvania State University, 2011.

[98] V. Kucukboyaci, Y. Sung, and R. Salko, "COBRA-TF parallelization and application to PWR reactor core subchannel DNB analysis," *Mathematics and Computations, Supercomputing in Nuclear Applications and Monte Carlo International Conference, M and C+SNA+MC 2015*, vol. 3, no. April, pp. 2376–2393, 2015.

[99] F. Reventós, L. Batet, C. Llopis, C. Pretel, and I. Sol, "Thermal-hydraulics analysis tasks for ANAV NPPs in support of plant operation and control," *Science and Technology of Nuclear Installations*, vol. 2008, no. June 2014, 2008.

[100] J. Freixa, V. Martínez-Quiroga, and F. Reventós, "Core Exit temperature response during an SBLOCA event in the ASCó NPP," *International Topical Meeting on Nuclear Reactor Thermal Hydraulics 2015, NURETH 2015*, vol. 1, no. September, pp. 217–230, 2015.

[101] R. Pericas, K. Ivanov, F. Reventós, and L. Batet, "Code improvement and model validation for Ascó-II Nuclear Power Plant model using a coupled 3D neutron kinetics/thermal-hydraulic code," *Annals of Nuclear Energy*, vol. 87, pp. 366–374, 2016.

[102] J. Freixa, V. Martínez-Quiroga, and F. Reventós, "Qualification of a full plant nodalization for the prediction of the core exit temperature through a scaling methodology," *Nuclear Engineering and Design*, vol. 308, pp. 115–132, 2016.

[103] American Nuclear Society, "ANSI /ANS 5.1-1979 Decay Heat Power in Light Water Reactors," tech. rep., American Nuclear Society, 1979.

[104] R. Pericas, *Contribution to the validation of best estimate plus uncertainties coupled codes for the analysis of NK-TH nuclear transients*. PhD thesis, Universitat Politecnica de Catalunya. Physics and Nuclear Engineering Deparment, 2015.

[105] B. Neykov, F. Aydogan, L. Hochreiter, K. Ivanov, and M. Martin, *NUPEC BWR Full-size Fine-mesh Bundle Test (BFBT) Benchmark Volume I: Specifications*. No. 6212, NEA NRC, 2006.